SPECIAL PUBLICATION 508

U.S. DEPARTMENT OF COMMERCE / National Bureau of Standards

Applications of Closed-Cycle Cryocoolers to Small Superconducting Devices

Applications of Closed-Cycle Cryocoolers to Small Superconducting Devices

Proceedings of a Conference Held at the
National Bureau of Standards,
Boulder, Colorado

October 3-4, 1977

Edited by

James E. Zimmerman and Thomas M. Flynn

Cryogenics Division
Institute for Basic Standards
National Bureau of Standards
Boulder, Colorado 80303

Sponsored by

National Bureau of Standards

and

Office of Naval Research
Arlington, Virginia 22217

U.S. DEPARTMENT OF COMMERCE, Juanita M. Kreps, Secretary

Dr. Sidney Harman, Under Secretary

Jordan J. Baruch, Assistant Secretary for Science and Technology

NATIONAL BUREAU OF STANDARDS, Ernest Ambler, Director

Issued April 1978

Library of Congress Catalog Card Number: 78-606017

National Bureau of Standards Special Publication 508
Nat. Bur. Stand. (U.S.) Spec. Publ. 508, 238 pages (Apr. 1978)
CODEN: XNBSAV

U.S. GOVERNMENT PRINTING OFFICE
WASHINGTON: 1978

For sale by the Superintendent of Documents, U.S. Government Printing Office, Washington, D.C. 20434
Stock No 003-003-01910-1 Price $4.25
(Add 25 percent additional for other than U.S. mailing).

ABSTRACT

This document contains the proceedings of a meeting of specialists in small superconducting devices and in small cryogenic refrigerators. Industry, Government, and academia were represented at the meeting held at the National Bureau of Standards (NBS) on October 3 and 4, 1977. The purpose of the meeting was to define the refrigerator requirements for small superconducting devices and to determine if small cryogenic refrigerators that are produced in relatively large quantities can be adapted or developed to replace liquid helium as the cooling medium for the superconducting devices. Because the focus was on small superconducting devices, the discussion was primarily limited to refrigerators with capacities from zero up to a watt or two in the temperature range of 2 to 20 K. The meeting was jointly sponsored by the Office of Naval Research (ONR) and NBS.

Key words: Cryocoolers; Refrigeration; Superconducting devices.

Library of Congress Catalog Card Number: 78-606017

National Bureau of Standards Special Publication 508
Nat. Bur. Stand. (U.S.) Spec. Publ. 508, 238 pages (Apr. 1978)
CODEN: XNBSAV

U.S. GOVERNMENT PRINTING OFFICE
WASHINGTON: 1978

For sale by the Superintendent of Documents, U.S. Government Printing Office, Washington, D.C. 20434
Stock No 003-003-01910-1 Price $4.25
(Add 25 percent additional for other than U.S. mailing).

ABSTRACT

This document contains the proceedings of a meeting of specialists in small superconducting devices and in small cryogenic refrigerators. Industry, Government, and academia were represented at the meeting held at the National Bureau of Standards (NBS) on October 3 and 4, 1977. The purpose of the meeting was to define the refrigerator requirements for small superconducting devices and to determine if small cryogenic refrigerators that are produced in relatively large quantities can be adapted or developed to replace liquid helium as the cooling medium for the superconducting devices. Because the focus was on small superconducting devices, the discussion was primarily limited to refrigerators with capacities from zero up to a watt or two in the temperature range of 2 to 20 K. The meeting was jointly sponsored by the Office of Naval Research (ONR) and NBS.

Key words: Cryocoolers; Refrigeration; Superconducting devices.

TABLE OF CONTENTS

TABLE OF CONTENTS, continued

DISCLAIMER

Papers by non-NBS authors have not been reviewed or edited by NBS. Therefore, the National Bureau of Standards accepts no responsibility for comments or recommendations contained therein.

INTRODUCTORY REMARKS AND SUMMARY

Richard Brandt
Office of Naval Research
Pasadena, California 91106

Arnold Silver
Aerospace Corporation
Los Angeles, California 90009

James Zimmerman
National Bureau of Standards
Boulder, Colorado 80203

INTRODUCTORY REMARKS AND SUMMARY

R. Brandt, A. Silver and J. Zimmerman

This document contains the proceedings of a meeting of specialists in small superconducting devices and in small cryogenic refrigerators. Industry, Government, and academia were represented at the meeting held at the National Bureau of Standards (NBS) on October 3 and 4, 1977. The purpose of the meeting was to define the refrigerator requirements for small superconducting devices and to determine if small cryogenic refrigerators that are produced in relatively large quantities can be adapted or developed to replace liquid helium as the cooling medium for the superconducting devices. Because the focus was on small superconducting devices, the discussion was primarily limited to refrigerators with capacities from zero up to a watt or two in the temperature range of 2 to 20 K. The meeting was jointly sponsored by the Office of Naval Research (ONR) and NBS, and was organized by Edgar Edelsack of ONR (who for personal reasons was unable to attend), Professor Little of Stanford University, and Tom Flynn, Ray Radebaugh and Jim Zimmerman of NBS.

Superconducting devices are finding applications in many areas, including biomedical research, geophysical measurements, metrology, electromagnetic radiation detection, digital signal processing and computing. The customary way to provide the required low-temperature environment is to immerse the device in a bath of liquid helium. This procedure has many advantages; in particular, the liquid helium bath is mechanically and magnetically quiet, thermally stable even with large heat loads, and not subject to mechanical breakdown, whereas existing cryogenic refrigerators suffer from many of these problems. Furthermore, liquid helium is readily available commercially and is relatively inexpensive in the present supply/demand situation. For these reasons, considerable efforts have been made to optimize the design of liquid helium dewars for specific applications. This approach is satisfactory at present while the various application possibilities are being explored. However, if superconductive instruments are ever to have widespread use, it will be necessary to incorporate cryocoolers which can be operated by ordinary technicians rather than cryogenic specialists.

The papers contained herein cover a broad range of technologies, from classical refrigeration techniques at one extreme, to recent exotic applications of superconductivity such as magnetic measurements of earth conductivity and of human brain activity at the other. It was precisely the purpose of the meeting to bring together those of such diverse interests. It is hoped that face-to-face encounters between the users and the producers of low temperature will stimulate thought and development of small superconducting and other cryogenic instrumentation which can be put into operation by the simple expedient of throwing a switch.

Since the facilities available for the meeting did not permit an open invitation to everyone who might have wished to attend, it is the purpose of this document to make available to a wider audience most of what was discussed. It contains most of the papers that were presented orally at the meeting, as well as a paper by Holdeman and Chang, not presented at the meeting, describing recent development of a simplified Josephson dc voltage standard. Papers not included (no manuscripts having been submitted) are one by Durenec on a miniature ultra-quiet dual-reciprocating compressor for small cryocoolers, one by Goodkind on his notable work with a gravimeter (mentioned briefly by Stanley in his paper), one by Goree on the use of small cryocoolers to extend the operating time of liquid helium dewars, and others.

The list of superconducting and other practical small cryogenic devices discussed here is far from complete. There is virtually no mention of mm-wave superconducting paramps and mixers, bolometers, super-Schottky diodes, nor a variety of devices for precise dc and rf metrology [1,2,3,4]. The refrigeration power required by all such devices is modest, and their potential usefulness would be enormously enhanced by cleverly-designed and integrated refrigeration systems that are easy and economical for non-specialists to operate and maintain.

Most cryocooler development over the past decade has occurred in response to distinct, large-quantity needs, resulting in the manufacture and sale of hundreds of units. Two notable examples, discussed by Longsworth, Chellis and others, are cryocoolers for infrared detectors and for low-noise microwave receivers. In the first case, cooling to either 77 K or 20 K is required, depending on the detector material, while a temperature of 4.5 K is used for the traveling-wave maser amplifiers. Typical refrigeration capacities of commercial units range from a few watts to tens of watts at 77 K and 20 K and a watt or so at 4 K. To maintain temperatures below about 6 K, a Joule-Thomson stage is added to the cold end of a helium temperature refrigerator such as a Stirling or Gifford-McMahon machine as described in several papers. The reliability of these relatively large (compared to the needs of most superconducting devices) cryocoolers is very good, with mean times between failures measured in thousands of hours. The reliability is not good enough for space applications, however. For this reason, among others, liquid cryogens will be used in the forthcoming space experiment described by Vorreiter and McCreight. Further information on space requirements are discussed by Mason and Tward.

A Joule-Thomson stage adds considerably to the cost and complexity of the refrigeration system. Papers by Radebaugh and by Steyert discuss electrocaloric and magnetocaloric processes as possible alternatives. The former, although attractive in principle, is not a viable process at present because a material with suitable electric polarizability has not been discovered. Magnetic cooling, on the other hand, is eminently practical in the low temperature range with possible extension to rather high temperatures. It is clear that very little effort has been made to date to satisfy the specific refrigeration requirements of small superconducting devices. An exception is the work reported by Zimmerman and Radebaugh in which a Nb SQUID is being operated at 8.5 K in a very-low-power 4-stage Stirling cryocooler.

The papers by Edrich and by Hartwig describe the use of commercial cryocoolers to operate superconducting devices; these are examples where (to quote Professor Little's words out of context) the cryocoolers may be grossly mismatched to the devices.

An interesting proposal is made by W. Little concerning the use of microminiature Joule-Thomson (JT) coolers for superconducting devices. He has derived a set of scaling laws which show that the open JT system can be miniaturized and still yield acceptable amounts of refrigeration with reasonable supplies of high pressure gas. The JT system has many attractive features including a short cool-down time, estimated to be 25 seconds, which is far less time than required by most closed-cycle mechanical refrigerators.

One of the highlights of the meeting is the optimistic view of high-T_c superconductors by Beasley, who suggests that development of clean and precise fabrication methods may lead to very good devices operating in the 10-20 K range. Realization of this prospect would greatly reduce the cost and complexity of the requisite cryocooler. This is not to say that lower temperatures will not be necessary or desirable for many applications.

The final session of the meeting was a panel discussion, with input from the audience, on where the technology should go from here. Panel members were Professor Little (Chairman), Longsworth, Gifford, Higa, Hartwig, Nisenoff, and Zimmerman. No general consensus was reached on how commercial quantities of small cryogenic refrigerators could be produced to replace helium as the cooling medium for small superconducting devices. A major reason for this is the large diversity of refrigerator requirements and configurations. Even in the application of closed-cycle cryocoolers to SQUID's there is a significant spectrum of requirements.

Perhaps the most pervasive feature of the free-for-all discussion was the enthusiasm of those suggesting that the time of cryocoolers for small devices has arrived, countered by the conservatism of the industry representatives pointing out that one needs a reasonable expectation of a profitable market.

There appears to be no major <u>technical</u> obstacle to satisfying the various user needs for the cryogenic refrigerator, however elimination of vibration, magnetic disturbance, and temperature variations does pose a challenge. Except for the use of liquid helium and the SQUID-cryocooler program at NBS-Boulder, no solution is at hand or in the offing. Similarly there is no likelihood of a near term, space qualified, closed-cycle cryocooler. Approaches which could be undertaken for small superconducting devices, given funding, are use of a Stirling or Gifford-McMahon cycle to 10-20 K, followed by either small Joule-Thomson or magnetic systems. Addition of the last stage adds significantly to the cost.

On the subject of appropriate research and development effort, a number of people felt that geophysical magnetometers should be selected as a trial system for incorporation of a closed-cycle refrigerator because of the large perceived market, even though the demands on isolation from vibrational and magnetic noise are severe. Others felt that biomedical gradiometers would be a better choice because the availability of a simply operated and maintained instrument is needed to encourage its widespread use in the biomedical community.

It was clear from the discussion that an overall systems approach to small superconducting devices has rarely been used and is really needed to optimize system performance and define refrigerator requirements more precisely. It was also felt that there is a strong need for innovation and that research on new refrigeration concepts should be encouraged.

REFERENCES

[1] P.L. Richards, "Superconducting Devices for Millimeter and Submillimeter Wavelengths," p 323 in Superconducting Quantum Interference Devices and Applications, Hahlbohm and Lübbig, eds., de Gruyter, Berlin (1977).

[2] J. Clarke, et al., "Superconducting Tunnel-Junction Bolometers," Rev. Phys. Appl. 9, 69 (1974).

[3] M. McColl, et al., "The Super-Schottky Microwave Mixer," IEEE Trans. on Magnetics MAG-13, 221 (1977).

[4] R. Kamper, "Superconducting Devices for Metrology and Standards," Chap. 5 in Superconductor Applications, Schwartz and Foner, eds., Plenum, New York (1977).

REFRIGERATION FUNDAMENTALS: A VIEW TOWARD NEW REFRIGERATION SYSTEMS *

Ray Radebaugh
Cryogenics Division
National Bureau of Standards
Boulder, Colorado 80303

ABSTRACT

It is pointed out in this paper that most of the refrigeration techniques used today which are applicable to superconducting devices were conceived over 100 years ago. The paper emphasizes the need to look for new refrigeration systems if great strides in reliability, size and cost are to be made. To stimulate this search, thermodynamic fundamentals and refrigeration cycles applicable to any refrigeration system are discussed. Since refrigeration power of a system is proportional to its available entropy, a comparison of entropies for various systems is made. These systems include such things as electrons, phonons, spins, electric dipoles, mixtures, reversible cells, as well as more familiar gas-liquid-solid systems. The merits of various refrigeration systems are discussed in context with this entropy comparison. Finally, approaches to eliminate some of the troublesome mechanical parts in gas-liquid systems are discussed.

REFRIGERATION FUNDAMENTALS:
A VIEW TOWARD NEW REFRIGERATION SYSTEMS

INTRODUCTION

In a paper of this sort it would seem reasonable to review the basic thermodynamics behind refrigeration, to discuss the various refrigeration cycles now in use and to compare them in some manner to aid the user in selecting the best refrigeration scheme for his application. Since many readers will be experts in refrigeration, such an approach is followed only to a limited extent. The emphasis of the paper will be on a search for new refrigeration methods.

In spite of great scientific strides over the last century, the refrigeration principles used today are, for the most part, the same as those used for the last century. These principles were refined between the period of the first liquefaction of air in 1877 by Cailletet and by Pictet and the first liquefaction of helium by Onnes in 1908. The mechanical work required for these gas systems presents difficult engineering problems. However, considerable engineering progress has been made since that time so that such cryogenic refrigerators or liquefiers have moved from the category of laboratory devices to industrial machines. Still further engineering strides are needed to make such refrigerators sufficiently reliable, inexpensive, and efficient to be used regularly for cooling small superconducting devices.

The emphasis of this paper will be to encourage the reader to think of new approaches to refrigeration. If the new refrigeration system is inherently more simple than present day gas systems, then less engineering effort is needed to make the system competitive. A technique of entropy comparison will be discussed in some detail. The comparison allows one to quickly assess the refrigeration potential of a new system and to develop some feel for how to look for a new system. A brief comparison of present day gas-liquid cycles will be made so that those not already expert in refrigeration will have a sufficient background to understand the papers on refrigeration techniques given at this conference.

THERMODYNAMIC CONSIDERATIONS

Refrigeration means that some heat, Q, is absorbed at a temperature below ambient. It should be realized that this Q may be due entirely to the heat leak from ambient. Such will be the case in refrigeration of some small superconducting devices which dissipate nanowatts of power. The absorption of Q at some low T is the desirable part of a total refrigeration cycle. Unfortunately the first and second laws of thermodynamics tell us that this process does not come to us free. How much we pay for such refrigeration can be determined only by considering the rest of the refrigeration cycle. At some point in the cycle heat is given off at ambient temperature. Also, the second law of thermodynamics requires that work be done to the system to supply the refrigeration.

Though it is not obvious to the laboratory user of liquid helium, the rest of the cycle still needs to be considered. The liquid helium in a dewar is part of a discontinuous flow of the working fluid to a separate location from some other part of the cycle. The cost and availability of the helium is determined by the efficiency and reliability of that part of the cycle. When the boil-off gas is vented to the atmosphere instead of returned to the compressor, the cycle is not completed but the process is often called an open cycle. Though often convenient for laboratory use, the discontinuous supply of refrigerant in a dewar can be troublesome for use in remote locations and for use where the expertise does not exist to transfer liquid from a discontinuous supply. In those cases it is better to provide a continuous supply of refrigeration, which means that the rest of the cycle must be considered as an integral part of the refrigeration process. The refrigerant system, e.g., helium, then undergoes a complete cycle so the term closed-cycle refrigeration is used to describe the process.

Ideal Refrigeration Cycles

The path used in any refrigeration cycle can be drawn in a temperature-entropy plane, or T-S diagram. Figure 1 shows one such cycle known as the Carnot cycle. The amount of

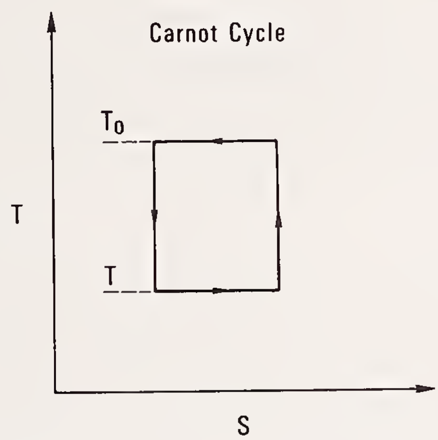

Figure 1. Temperature-entropy diagram for the Carnot cycle.

heat absorbed at the temperature T is related to the entropy change by

$$dQ \leq TdS. \qquad (1)$$

If the process is done reversibly, the heat absorbed is:

$$dQ_{rev} = TdS. \qquad (2)$$

According to this equation, the heat Q absorbed at the temperature T will be the area under the line at T in Fig. 1. The heat Q_0 given off at T_0 is the area under that line. It is assumed that all the steps in going around the cycle in Fig. 1 are reversible. Because the two isotherms are connected by adiabatic lines, i.e., constant entropy, no heat crosses the system boundary during these processes. According to the first law of thermodynamics the total amount of work required to complete the cycle is:

$$W = Q_0 - Q. \tag{3}$$

This work is represented by the enclosed area shown in Fig. 1. From Eqs. (2) and (3) we may write:

$$W = T_0\Delta S - T\Delta S = \Delta S(T_0 - T). \tag{4}$$

The efficiency of any refrigeration process is defined by $\eta = Q/W$. From Eqs. (2) and (4) the efficiency of the Carnot cycle becomes:

$$\eta_c = T/(T_0 - T), \tag{5}$$

where η_c is called the Carnot efficiency and represents the highest possible efficiency for a cycle operating between T and T_0. Any real cycle will have irreversibilities which lead to a lower efficiency.

The Carnot cycle is difficult to carry out in practice partly because a very high generalized force (e.g., pressure in a gas-liquid system) is required to reach the upper left corner of the cycle in Fig. 1. That problem can be overcome by shifting the ambient part of the cycle to the right. Figures 2(a) and 2(b) show two examples of such altered

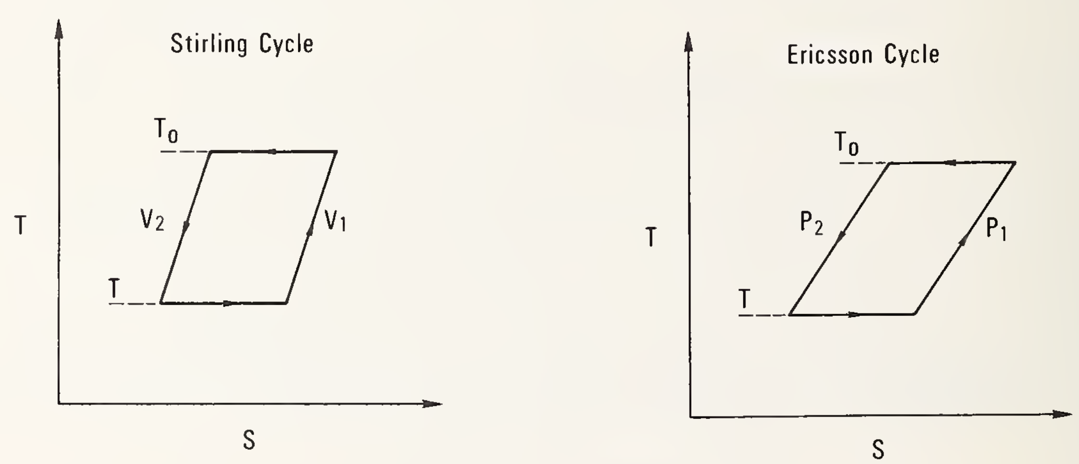

Figure 2(a)　　　Figure 2(b)

Figure 2. Temperature-entropy diagrams for the (a) Stirling cycle and (b) the Ericsson cycle.

cycles. The particular ones shown in these figures can be approximated in practice if the cycle times are long. The names given to these cycles are after the persons who first built working engines following such cycles. Though the cycle direction is reversed for a refrigerator, it is still customary to use the same name for the refrigeration cycle.

In Fig. 2(a) the isotherms at T and T_0 are connected by constant volume processes (constant displacement in a general system). Such an ideal thermodynamic-cycle is known as the Stirling cycle. In 1816 Robert Stirling [1], a minister of the Church of Scotland, devised the practical means of approximating the cycle shown in Fig. 2(a), but the direction was reversed to produce a power cycle. In 1874 the Scottish engineer Alexander Kirk [2] published his work on a refrigerator utilizing the Stirling cycle in reverse. His refrigerator reached about 214 K with air as the working system operating between about 1 and 2 atmospheres pressure. The refrigerator was the same in many details to modern Stirling-cycle refrigerators and even had a conical displacer representing the limit of an infinite number of stages. No doubt his temperature was limited by the relatively poor insulation provided by sawdust, but then Dewar did not introduce vacuum insulation until 1893. Understandably the name Kirk is used sometimes with such refrigerators, but in keeping with present practice, the name Stirling will be used in this paper even when referring to the refrigeration cycle. It should be kept in mind that the Stirling cycle as defined by a path in a T-S diagram is not limited to a gas system undergoing pressure-volume variations. Any material whose entropy can be changed can serve as the working substance.

In Fig. 2(b) the isotherms at T and T_0 are connected by constant pressure lines (constant generalized force). In about 1826 the Swedish inventor John Ericsson [3] devised an air engine which approximated the reverse of the cycle shown in Fig. 2(b). Thus Ericsson cycle is the name associated with the ideal cycle shown in Fig. 2(b), whether it be for an engine or refrigerator. Actually, there is no limit to the number of ways which the two isotherms can be connected, but the simple ones shown in Figs. 1, 2(a) and 2(b) are particularly significant. In a later section other specific cycles commonly used in liquid-gas systems will be discussed. It is emphasized again that any material can serve as the working substance for these cycles.

A special case of the Ericsson cycle which has a separate name is the vapor-compression cycle. We mention this cycle here because it, too, may be used with any system, and not just a gas-liquid system. The difference between this and the Ericsson cycle considered previously is that the vapor-compression cycle utilizes the phase equilibrium between an ordered and disordered phase, e.g., liquid-gas. The T-S diagram for the vapor-compression cycle is shown in Fig. 3. The two isotherms are connected by constant pressure lines

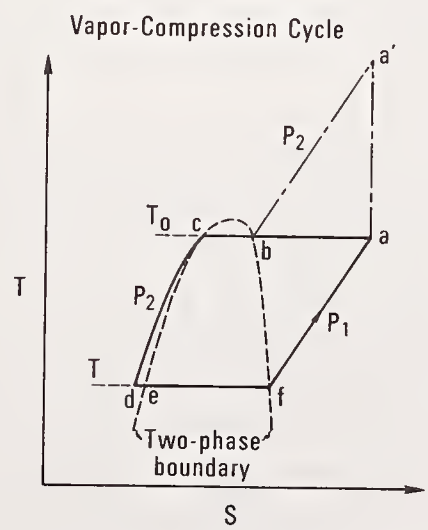

Figure 3. Temperature-entropy diagram of the vapor-compression cycle, which operates across a phase boundary.

(constant generalized force) as for the Ericsson cycle, except that these constant pressure lines cross the phase equilibrium portion of the system. In most cases the pressure reduction in the ordered phase (from point d to point e in Fig. 3) need not be done reversibly since the entropy change in that step is small compared with the entropy change during the phase change. Thus, in a gas-liquid system, a throttle valve is used to reduce the pressure in the liquid instead of a more complex liquid turbine. In practice the compression process may follow the adiabatic path (step a to a') instead of the more desirable isothermal path (step a to b).

Unlike the adiabatic paths in the Carnot cycle, the entropy is changed during the constant volume or constant pressure processes shown in Figs. 2(a), 2(b), and 3. Thus, heat must be transferred at a varying temperature. For a reversible heat transfer this heat is given by:

$$Q_e = \int TdS \ , \tag{6}$$

where the integral is along one of the lines between T and T_0 or vice versa. Such heat is simply the area under each V = constant or P = constant curve. The system absorbs heat in going from T to T_0 and gives off heat in going from T_0 to T. In an ideal system the two lines are parallel so that the two heat transfers are equal. In practice this heat transfer is handled by placing a heat exchanger between the two lines. A practical heat exchanger, however, is a source of irreversibilities. In the Carnot cycle no heat exchanger is required because the processes are adiabatic.

The amount of work required in the Stirling, Ericsson, and vapor-compression cycles is given by Eq. (3). For Q the same as in the Carnot cycle, Q_0 will also be the same as in the Carnot cycle when the system is ideal, i.e., both the constant pressure and constant volume lines are parallel. The work, given by the area enclosed, is also the same as for the Carnot cycle. It then follows that the efficiencies of the ideal Stirling and Ericsson cycles are the same as that of the Carnot cycle, given by Eq. (5). The efficiency of the vapor-compression cycle will be equal to or less than the Carnot efficiency. If the average slope of the line from d to c in Fig. 3 is equal to that from f to a, the efficiency will be the same as the Carnot efficiency. The slope of the line depends on the system used.

All of the preceeding cycles operated between two fixed temperature levels, T and T_0. In situations where the heat leak from the surroundings dominates any internal heat generation, as is usually the case with small superconducting devices, then it becomes more advantageous to absorb heat over a range of temperatures. If, in the Ericsson cycle, the isothermal process at T is replaced by an adiabatic process, then refrigeration is available over the temperature range of T' to T as shown in Fig. 4, by the path from d to d'. The enclosed area of the cycle and, therefore, the work required, is larger than that of the Ericsson cycle. The heat absorbed, which is equal to the area under the curve from d to d', is less than that of the Ericsson cycle (area under c to d'). The efficiency of the cycle is less than the Ericsson cycle; but on the other hand, refrigeration is provided at a lower temperature. A fairer comparison is to say that we want to absorb the same amount of heat as does the Ericsson cycle, e.g., the heat leak from the surroundings. This is accomplished

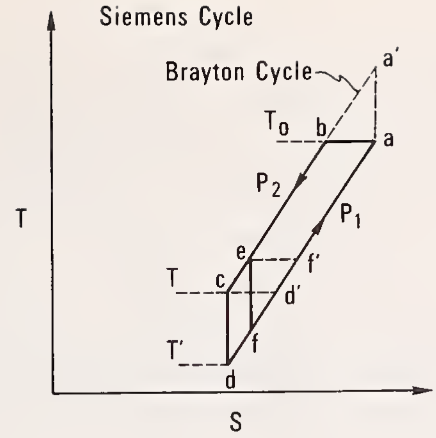

Figure 4. Temperature-entropy diagram of the Siemens and Brayton cycles.

by starting the adiabatic process at a higher temperature, from point e in Fig. 4. The area under the curve from f to f' is now the same as that under c to d'. The total work for the cycle is also the same as the Ericsson cycle, and thus the efficiency is the same. The important point to realize is that the lowest temperature reached is less than that of the Ericsson cycle. In addition, less heat needs to be transferred in the heat exchanger. These advantages are realized only when heat is absorbed over a range of temperatures. In 1857 Charles Siemens received a patent for a machine approximating this cycle and so his name is often given for this cycle [2]. If the isothermal process at T_0 is also made into an adiabatic process, the cycle is known as the Brayton cycle. The Siemens cycle is sometimes called the modified Brayton cycle. If both isotherms in the Stirling cycle are replaced by adiabatics, then the cycle becomes the Otto cycle. With high-speed operation practical Stirling-cycle refrigerators may approximate the ideal Otto cycle.

There are two ways in which a system, or working substance, can be made to go around a cycle in a T-S diagram. The first is the time domain. In this case the system remains physically stationary and is connected to the reservoirs at T and T_0 by heat switches which open and close at the appropriate time. A generalized force does work on the system or receives work from the system at the appropriate time to carry out the cycle. The advantage is that some systems then require no moving parts. Obviously, refrigeration occurs only intermittently in this time-domain operation. The use of rapid cycle times, or two equal systems operating 180° out of phase, eliminates this problem. The other mode of cycle operation is in the physical domain. In this case the working substance moves to different locations for the various parts of the cycle in the T-S diagram. This is particularly easy to do with a liquid or gas system and has the advantage of continuous refrigeration. However, solid systems also can go around the cycle in the physical domain by placing the material on a rotating wheel. Unfortunately, it is sometimes difficult for the solid system to interact with the generalized force during a part of the cycle. The physical mode of operation does not always imply that there will be moving mechanical parts, as we shall see later for thermoelectric refrigeration. Besides the two modes of cycle operation discussed above, it is possible to combine the two, as is done in the gas Stirling cycle. Certain combinations can make it difficult to show the cycle on a T-S diagram and to analyze it.

Interaction of Force With System

So far we have discussed complete cycles and the net work required to complete the cycle in terms of the heat Q absorbed at a temperature T. Nothing has been said about how the work is accomplished and what is the maximum Q or W a system is capable of absorbing in one cycle. For a fixed Q in each cycle, the refrigeration power is directly proportional to the molar flow rate around the cycle or to the number of moles of refrigerant times the cycle frequency. Each system will have a characteristic minimum cycle time, below which extraneous heating effects become comparable to the refrigeration power. The extraneous heating effects may come from such things as pressure drops, eddy currents, joule heating, etc. The maximum refrigeration power per mole of working substance will be the product of the maximum cycle frequency and the maximum heat absorption capacity of the substance in one cycle. We shall now consider the maximum heat absorption capacity per cycle in more detail.

Equations (1) and (2) show that the heat absorption capability of a substance is a maximum when the process is reversible. In addition, these equations show that when a system absorbs heat at a constant temperature, the entropy of the system increases. The system then goes from a relatively ordered state with low entropy to a disordered state with higher entropy. For the case of boiling liquid helium, heat is absorbed reversibly as the system goes from the ordered liquid state to the disordered gaseous state. For an isothermal process the reversible heat absorption capacity of a system with n moles is given by

$$Q_{rev} = nT(S_d - S_o), \tag{7}$$

where S_d is the molar entropy in the disordered state and S_o is the molar entropy in the ordered state. A system with good potential for refrigeration would have a relatively large value of $S_d - S_o$. Such a requirement implies S_d must always be large. The maximum heat absorption capability of various systems can be compared by viewing curves of entropy vs temperature for the various systems.

Before making such a comparison, we first need to discuss how a generalized force acting on the system can lower its entropy to S_o or to permit the entropy to change from S_o to S_d in a reversible manner. It is this generalized force acting on the system which carries out the necessary work to complete the cycle. In a closed cycle the first law of thermodynamics relates via Eq. (3) the net work required to the heat transferred. It should be noted that during part of the refrigeration cycle the system may do work on the surroundings. In a closed cycle the state of the system or the energy of the system is never considered. When only part of the cycle is considered, the system undergoes a change in state. The most important part of the cycle we wish to consider is the absorption of heat at some low temperature. For a closed system where there is no mass flow (a cycle operating in the time domain) the heat absorption from the first law of thermodynamics is given by:

$$dQ = dU + dW_c , \tag{8}$$

where U is the internal energy of the system and W_c is the work done to the surroundings by the closed system. When there is mass flow, as in an open system (a cycle operating in the physical domain), the first law of thermodynamics gives:

$$dQ = dH + dW_o , \tag{9}$$

where H is the enthalpy and W_o is the work done to the surroundings by the open system. For a reversible process the entropy change is related to the heat absorption by Eq. (2) and thus to the work by Eqs. (8) and (9). Such a relationship is written as

$$dQ_{rev} = TdS = dU + dW_c \tag{10}$$

$$dQ_{rev} = TdS = dH + dW_o . \tag{11}$$

Also for a reversible process the work terms become:

$$dW_c = FdX \tag{12}$$

$$dW_o = XdF , \tag{13}$$

where F is a generalized force (intensive variable) which can bring about a generalized displacement X (extensive variable). The enthalpy is given by

$$H = U + FX . \tag{14}$$

Some examples of generalized forces and their associated generalized displacements are given in Table 1. The reader is encouraged to think of other examples not listed here. The negative sign for some of the forces is necessary to give the right sign in Eqs. (10-14).

Equations (10) and (11) show that the entropy can be changed by either of the following: (i) $dW = 0$, in which case a change in internal energy or enthalpy is responsible for the entropy change or, or (ii) $dW \neq 0$, in which case the system does reversible work on the surroundings. However, a large work term does not always imply a large entropy change because sometimes the work term may be dominated by a change in internal energy or enthalpy which occurs at the same time work is done. Case (i) occurs when the disordered and ordered states are in equilibrium with each other at the temperature T. Boiling liquid helium is a classical example. A magnetic material at the transition from the ferromagnetic to paramagnetic states is another example. This case of phase equilibrium is an especially attractive means of refrigeration because of the simplicity of no work. The refrigerant can be separated a considerable distance from the rest of the cycle. The disadvantage is that the refrigeration can occur at only one temperature, unless the generalized force is varied to shift the temperature of phase equilibrium. There are usually practical and intrinsic limits as to how far the phase-equilibrium temperature can be shifted. The advantage of case (ii) is that phase equilibrium is not required, which means that the system may work over a wide

TABLE 1.

Examples of Generalized Forces and Their Associated Generalized Displacements in Thermodynamic Systems

F (force)	X (displacement)
Pressure, P (N/m^2)	Volume, V (m^3)
Tension, $-\tau$ (N)	Length, L (m)
Surface tension, $-\sigma$ (N/m)	Surface, A (m^2)
Magnetic field, -H (A/m)	Magnetic moment*, $\mu_o m$ (Wb•m)
Electric field, -E (V/m)	Dipole moment*, p (C•m)
Electric potential, $-\varepsilon$ (V)	Charge, Z (C)
Centrifugal potential, $-r^2\omega^2/2(m^2/s^2)$	Mass, M
Chemical potential, $-\mu$ (J/mol)	Moles, n

* m = $\mathcal{M}$V, where $\mathcal{M}$ is the magnetization and V is the volume.
p = $\mathcal{P}$V, where $\mathcal{P}$ is the polarization.

range of temperatures. The disadvantage of case (ii) is that a means must be provided for the system, which is at the low temperature T, to interact and do work on the surroundings. In case (ii) only one phase exists, but its entropy can be changed by the action of the generalized force.

Table 2 lists several systems which have ordered and disordered phases in equilibrium. The use of these two phases permit refrigeration in the manner of (i). The temperature of the phase equilibrium can be altered by the force shown in the third column in Table 2. It is also this force which can be used to change the entropy of the disordered phase and achieve refrigeration in the manner of (ii). Some of the systems, e.g., liquid-gas, have sharp transitions whereas others are more broad. The question mark in the force column for some systems means that the best generalized force to act on such a system is uncertain. Again the reader is encouraged to extend the list of systems given in this table. In some cases an ordered phase of one system may still have a high entropy relative to the ordered phase of another system because of some other internal disorder. An example is a solid, which is ordered relative to a liquid on a molecular basis, but which can still be magnetically disordered.

There are also some systems where a force acting on one phase changes the entropy, but an appropriate second phase does not seem to exist at any temperature unless a more microscopic view is taken. Consider the case of tension on a wire. The tension tries to disorder the system, hence increase the entropy [not obvious from Eqs. (10 and 12)], but what is the phase which it is trying to approach -- a liquid? Or is it a gas phase? On a microscopic basis the excitations in the solid are phonons, which when excited represent a disorder in the system. A tension on a wire reduces the density of the solid, which causes more phonons to be excited at the same temperature. This will be discussed in more detail later.

TABLE 2.

Ordered and Disordered Phases of Some Systems and the Generalized Force Necessary to Change the Equilibrium Temperature of the Entropy S_d

System		Generalized Force
Disordered Phase	Ordered Phase	
gas	liquid	pressure, P
liquid	solid	pressure, P
paramagnet	(anti-)ferromagnet	magnetic field, H
paraelectric	(anti-)ferroelectric	electric field, E
normal metal	superconductor	magnetic field, H
Fermi gas	Fermi liquid	Fermi pressure or density, n
surface film	bulk liquid	surface tension, σ
interstitial atoms	martensite	tension, τ
flexible polymer	crystalline polymer	tension, τ
disordered β brass	ordered β brass	?
uniform solution	precipitate	pressure, P, 2 concentration, x
molecular rotation	rotational order	?
$Zn + CuSO_4$	$Cu + ZnSO_4$	electric potential, E
dilute solution	concentrated solution	chemical potential, μ, or concentration, x

For some of the systems shown in Table 2, the effect of increasing the generalized force is to decrease the entropy. In that case it is clear that when dealing with one phase it should be the disordered phase. The maximum entropy change the force can produce is just equal to the absolute entropy of the disordered phase. The force can do no better than to completely order the system and give it zero entropy. For some systems shown in Table 2, an increasing force can increase the entropy of the ordered phase. Examples are the antiferromagnet, antiferroelectric, and superconductor. The effect of the increasing field is to lower the transition temperature. At any given temperature a field is reached where the ordered phase transforms to the disordered phase. Any further increase in field decreases the entropy. A field always decreases the entropy of paramagnets and paraelectrics but has a negligible effect on normal electrons. Thus, we can say that in these cases where the field increases the entropy of the disordered phase, the entropy can increase to a value no greater than the entropy of the associated disordered phase.

ENTROPIES AND REFRIGERATION PRINCIPLES OF VARIOUS SYSTEMS

As stated in the previous section, the maximum refrigeration power of any refrigeration system is proportional to the temperature times the maximum possible entropy change at that temperature. Thus, the merit of any system can be evaluated roughly but quickly by a comparison of its entropy curve with those of well-established refrigeration systems. To evaluate the entropy of a given system, we make use of the second TdS equation (derived in any textbook on thermodynamics):

$$TdS = C_F dT - T\left(\frac{\partial X}{\partial T}\right)_F dF \ . \tag{15}$$

In this equation C_F is the heat capacity of the system at a constant generalized force. The entropy at (T, F) can be evaluated by integrating Eq. (15) from (0, 0) to T, F) by any convenient path. Figure 5 shows the two easiest paths. As shown in this figure, the entropy

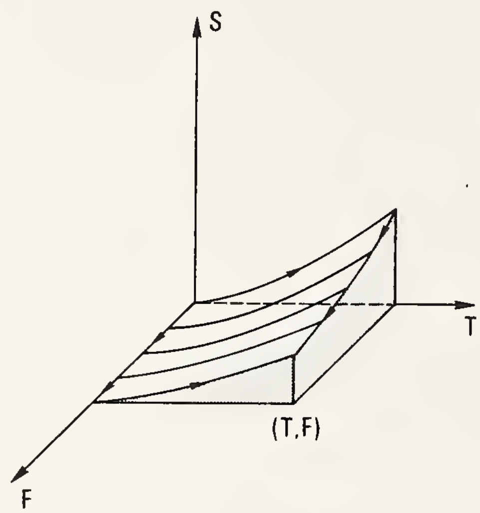

Figure 5. Integration paths for evaluating entropy at specified values of temperature and generalized force.

is zero at T = 0 for any F. This follows from the third law of thermodynamics for any system which does not have any frozen-in disorder at T = 0. The third law then requires that $(\partial X/\partial T)_F = 0$ at T = 0. The entropy determinations rely on specific heat measurements from temperatures near absolute zero to the temperature T. Specific heat measurements as a function of T for various F allow the entropy to be evaluated for different F. Otherwise specific heat measurements at F = 0 combined with measurements of $(\partial X/\partial T)_F$ vs F at various T can be used to find S(T,F). A peak in the specific heat of a system is a very desirable feature for refrigeration since it indicates a change in phase and a large change in entropy. Whether any practical force can change the entropy is another question. The value of $(\partial X/\partial T)_F$ gives an indication of the size of F required to change the entropy, as is evident from Eq. (15).

Figures 6 through 9 show entropy as a function of temperature for many systems. The entropies are divided by the gas constant R = 8.3143 J/mol K to make them dimensionless. Notice that these figures show S as a function of T instead of vice versa, as was done for the thermodynamic cycles shown in Figs. 1 to 4.

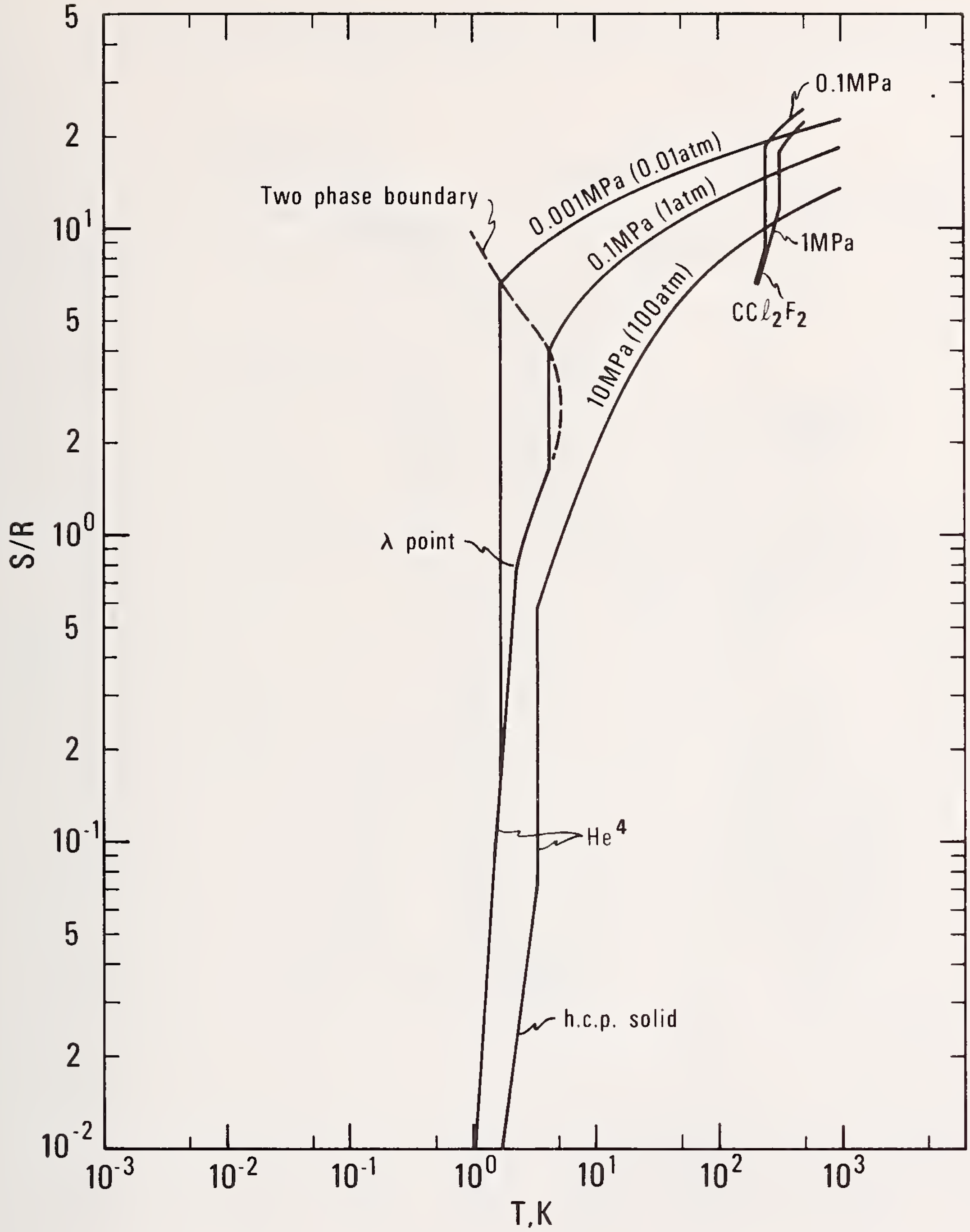

Figure 6. Reduced entropy as a function of temperature for helium and CCl_2F_2 at different pressures.

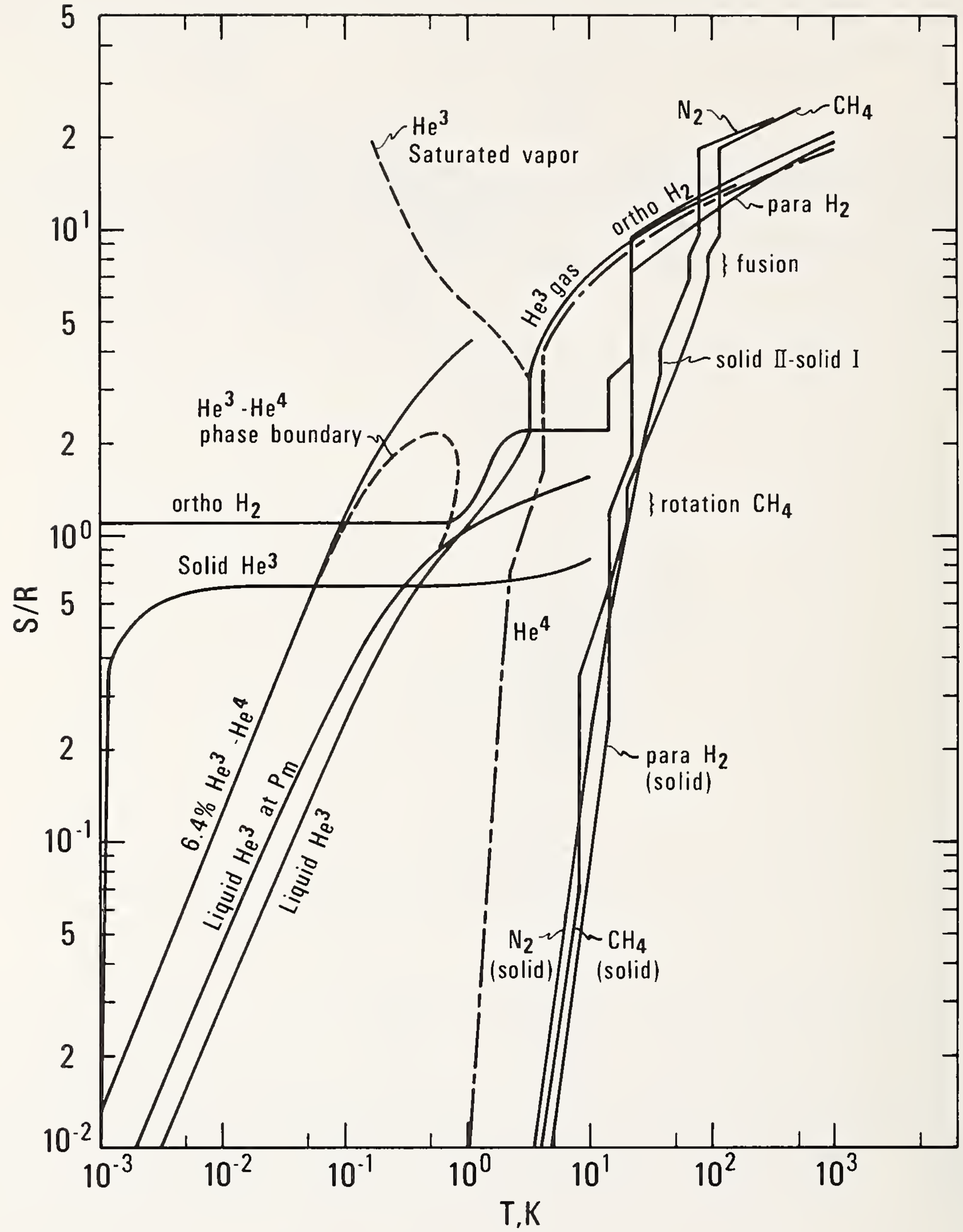

Figure 7. Reduced entropy as a function of temperature for several gas-liquid-solid systems.

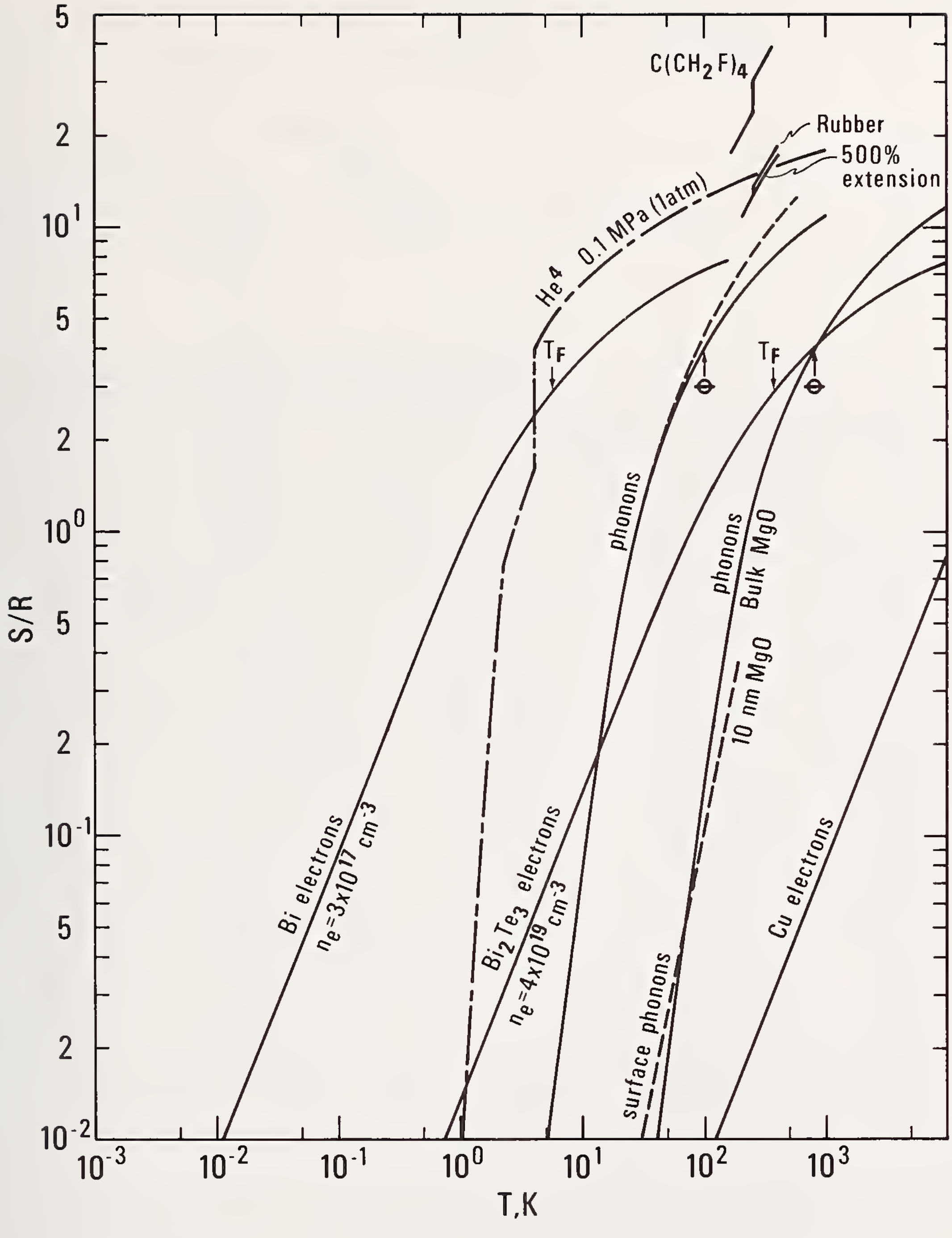

Figure 8. Reduced entropy as a function of temperature for solid systems.

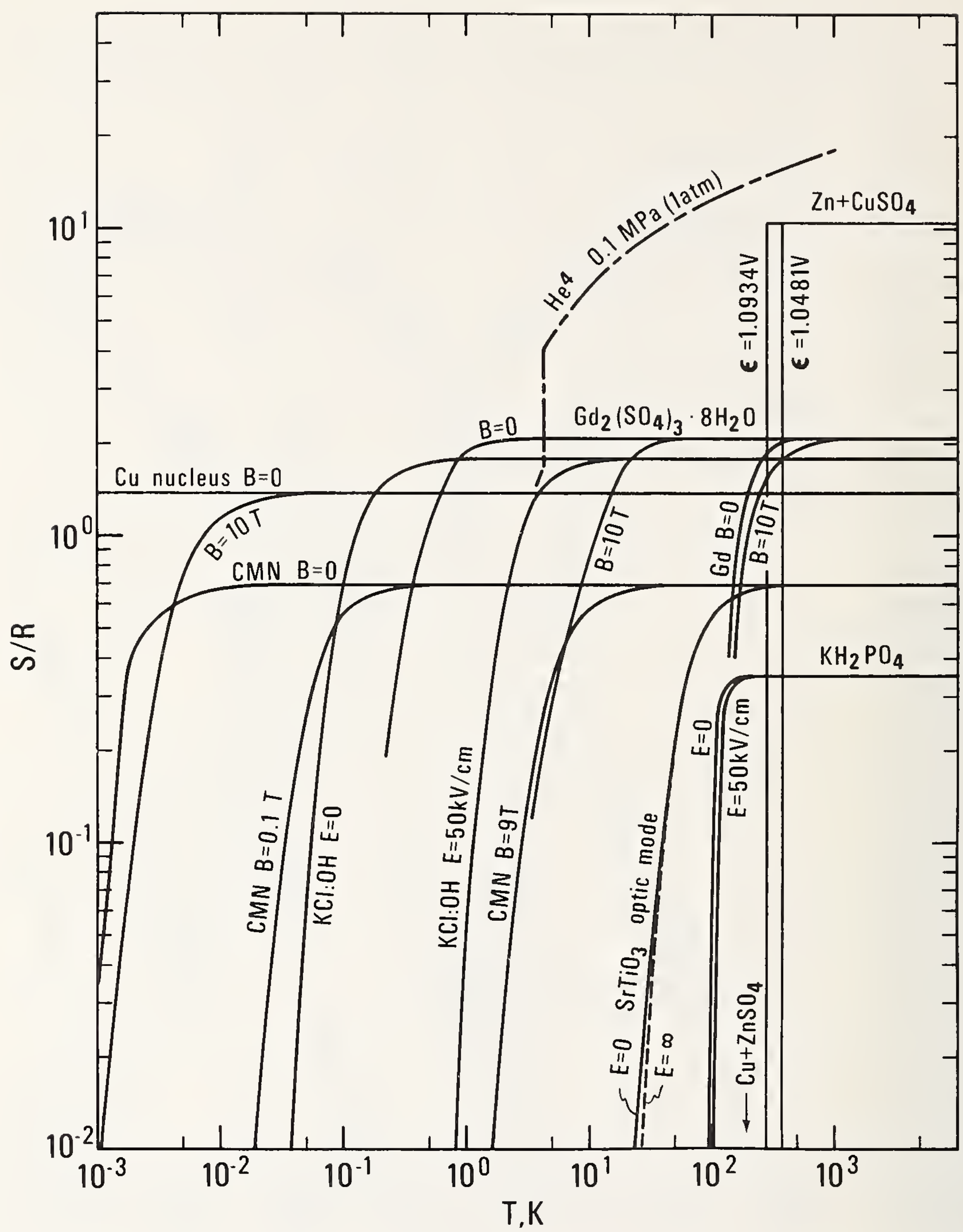

Figure 9. Reduced entropy as a function of temperature for magnetic, dielectric, and electrolytic systems.

Helium-4 and CCl_2F_2

Figure 6 shows the entropy of He^4 in the gas, liquid and solid phases.[4,5] This system is by far the most common refrigerant for use with superconductors. Its entropy in the gas phase is very high and remains in this disordered phase down to temperatures below superconducting transition temperatures. For a gas system Eq. (15) becomes

$$TdS = C_p dT - T(\partial V/\partial T)_p dP \ . \tag{16}$$

The isothermal entropy change in an ideal gas is then given by

$$\Delta S/R = \ell n\left(P_1/P_2\right) \ , \tag{17}$$

where P_1 and P_2 are the initial and final pressure. Thus, even pressure ratios of 10 can give a $\Delta S/R$ of 2.3. In comparison with other systems at low temperatures this entropy change is high and shows why helium is such an important refrigerant. Figure 6 shows how the entropy drops significantly from the gas phase to the liquid phase. As discussed previously, this entropy difference in the phase equilibrium region is very useful. At lower temperatures the entropy of the liquid drops suddenly at the superfluid transition temperature (λ point) due to a quantum ordering process. Another type of order takes place when sufficient pressure is applied to solidify the helium. As seen in the figure, the entropy change associated with melting is small compared with vaporization and thus, would not be very useful for refrigeration. Refrigeration at 1.8 K could be accomplished by using a porous plug to separate the superfluid component from the normal component. Heat is then absorbed by raising the entropy of the superfluid fraction from zero to about $S/R = 0.2$ (the value for liquid He^4 at 1.8 K. This change is small compared with the change in S/R of about 6 for vaporizing the liquid at 1.8 K. This disadvantage could be offset by the ad vantage of a much smaller molar volume in the liquid state compared with the gas phase at 0.001 MPa (0.01 atm). In fact, the rapidly increasing molar volume in the gas phase as the temperature is reduced places a lower limit of the order of 1 K for refrigeration with He^4. In this case the limit occurs because the molar flow rate is severely restricted by the large molar volume.

Also shown in Fig. 6 is the entropy [6] of the common refrigerant, dichlorodifluoromethane, CCl_2F_2. The absolute entropy is uncertain, but the values shown are reasonable. The important thing to observe is the entropy change during vaporization. This system is shown in comparison with He^4 to point out its advantage when working over a small temperature span near room temperature. This system is commonly used in household refrigerators and air conditioners, and the pressures used are typically those shown in Fig. 6. The cycle used is the vapor-compression cycle discussed previously and shown in Fig. 3. Notice that at 315 K only 1 MPa (10 atm) is required to liquefy the system. After being cooled in a heat exchanger to about 245 K the liquid is expanded to 0.1 MPa (1 atm) and evaporated. During the evaporation the entropy changes by $\Delta S/R = 9.8$. A similar entropy change in He^4 at that temperature would require a pressure ratio of 10^4 compared with 10 for CCl_2F_2. This comparison points out the ease of changing the entropy of a system just above the ordering temperature. Thus it is clear that a He^4 refrigeration system would require a much higher molar flow rate or pressure ratio to achieve the same refrigeration power as a CCl_2F_2 vapor-compression system. If that were done, it is obvious that inefficiencies in the He^4 system would be higher. The curves shown in Fig. 6 then tells us immediately that a Stirling-cycle refrigerator using He^4 or some other ideal gas would not be as efficient or useful as a CCl_2F_2 refrigerator for use near room temperature. The same conclusion is reached by Nesselmann [7] using more detailed calculations on actual cycles.

Other Gas-Liquid Solid Systems

Figure 7 shows the reduced entropy of several other systems which exist in the gas phase at room temperature. Helium 4 at 0.1 MPa (1 atm) is also shown for comparison purposes. The absolute entropy of solid and liquid N_2 is based on the work of Giauque and Clayton [8] and the liquid-gas values of Strobridge [9] are added to this. There is an entropy change associated with a structural change in the solid at 35.6 K, as well as the entropy change with fusion. This transition is one in which a generalized force has little effect, except possibly pressure.

The entropy of methane, CH_4, is taken from several sources [10-12]. In the solid phase there is a cooperative rotational ordering at 20.4 K which results in a sudden drop in entropy below that temperature. A similar but less-studied transition occurs at about 8 K. Again, these transitions are ones that we have little control over by the use of some generalized force. The transition temperatures are determined primarily by the molecular moment of inertia, which cannot be changed much by external forces. Thus these transitions are of little use for refrigeration unless we can find some "handle" to change the moment of inertia. In addition, the entropy changes associated with them are rather small.

The hydrogen molecule can take on two modifications due to the relative orientations of the two nuclear spins. The name orthohydrogen is used for the form with the spins in the same direction and the term parahydrogen is used for the form with the spins in the opposite directions. Since parahydrogen has no net spin, it has the lowest energy state. Thus at 0 K, equilibrium hydrogen will be 100% parahydrogen. The high-temperature equilibrium concentration is 75% orthohydrogen, which is closely approached at room temperature. As shown in Fig. 7, there is a difference in entropy between parahydrogen [13,14] and orthohydrogen [15]. The drop in entropy of orthohydrogen below about 1.6 K is due to a splitting of the lowest rotational energy state by internal electric field gradients on the nuclear quadrapole moment. Because of the entropy difference between ortho- and para-hydrogen, it is tempting to think of some external force which could change the equilibrium concentration at some temperature. Practical levels of electric field gradients or magnetic fields would have only a minor effect on the equilibrium concentration, though further studies may be useful.

Helium 3 is a very useful refrigerant for temperatures below 1 K. Because the nucleus has a spin of 1/2, it follows Fermi-Dirac statistics. The main feature of a Fermi fluid is that ordering into lower energy states is a gradual process. For instance, compare the entropy of liquid He^3 with that of liquid He^4. In Fig. 7 the liquid and gas entropy for temperatures above 1.5 K are from the work of Gibbons, et al. [16] and Daunt [17]. The work of Radebaugh [18] is used for temperatures below 1.5 K and for He^3-He^4 mixtures. Solid entropies are taken from the book by Betts [19] and the publication of Dugdale and Franck [20]

Because the He^3 entropy falls off so slowly as the temperature is reduced it has enough entropy for refrigeration over a temperature range from 10^{-3} to 1 K, a wider range than any other system. The entropy of the saturated vapor can be used for reaching temperatures of about 0.3 K. The He^3 density becomes too small to reach any lower temperature with the gas phase.

The entropy of solid He^3 remains at the high value of $S/R = \ln 2$ until the nuclear spins order magnetically at about 1.2 mK. At the solid-liquid equilibrium pressures the liquid entropy is changed from that at atmospheric pressure to that shown in Fig. 7. Still there is a considerable entropy change between the liquid and solid for temperatures below about 0.1 K. Application of pressure to solidify the He^3 then becomes a useful refrigeration technique for the range 1 mK to 0.1 K. This technique is known as Pomeranchuk refrigeration, based on a proposal in 1950. Details of this refrigeration technique are well described in the two books [19,21] on millikelvin techniques. Practical use of Pomeranchuk refrigeration has occurred only since 1965. This refrigerator operates in the time domain where the refrigerant is stationary and heat switches are used. So far only a heat switch between the high temperature reservoir at about 30-50 mK has been used, which limits it to single cycle operation rather than continuous operation.

If He^4 is added to He^3, the He^4 acts to separate the He^3 atoms and to make them behave more like an ideal gas. Because the entropy of He^4 itself is so small below 1 K, it contributes nothing to the entropy of the solution. Because of its gas-like behavior, the entropy of the He^3 in solution with He^4 is higher per mole of He^3 than that of liquid He^3. This is shown in Fig. 7 by the curve for 6.4% He^3 in He^4. In 1951 H. London first proposed the use of He^3-He^4 mixtures for refrigeration [21]. At that time the existence of phase equilibrium in He^3-He^4 mixtures was not known, so it was thought that some generalized force was needed to interact with the system to bring about a reversible dilution of the He^3. It was discovered about four years later that the He^3-He^4 mixtures phase separated and that at temperatures below about 50 mK the maximum He^3 concentration in the dilute phase was 6.4%. Any excess He^3 floats on top of the mixture in the form of nearly pure He^3. The thermodynamics of the mixtures are described in detail elsewhere [18]. This phase separation meant that pure He^3 could be diluted reversibly to 6.4% in a manner very much like evaporation of a liquid. Since the dilution could be done without doing external work, the process would be much simpler than if phase separation did not occur. In 1965 the first successful dilution refrigerator was built and now these have become off-the-shelf items for continuous temperatures down to 10 mK. Continuous temperatures of 2 mK have been reached recently [22]. The operating temperature span of 2 mK to 1 K for the dilution refrigerator is considerably larger than any other refrigerator when one considers temperature on a logarithmic scale.

Figure 10 shows a schematic of the dilution refrigerator. Detailed explanations are given elsewhere [19,21], but a brief account is given here because it has much to contribute toward a fundamental understanding of refrigeration. Heat is absorbed in the mixing chamber during the dilution process. The reversible refrigeration power is given by [18]

$$\dot{Q} = (82\ \mathrm{J/mol\cdot K^2})\dot{n}T^2 \tag{18}$$

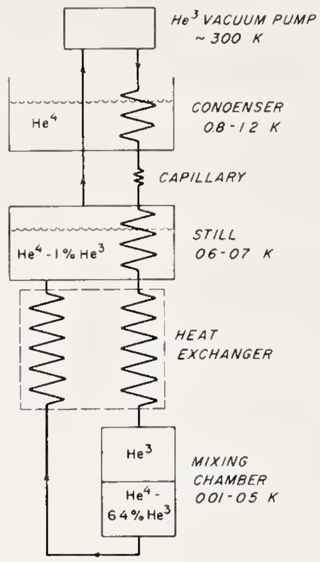

Figure 10. A schematic diagram of the He^3-He^4 dilution refrigerator.

where $\dot{n}$ is the molar flow rate ($\dot{n} = 10^{-3}$ to 10^{-5} mol/s for typical dilution refrigerators). Dilution occurs because He^3 is continuously removed from the dilute solution at another location, the still. A heater holds the still at a temperature of about 0.6 - 0.7 K. Because the vapor pressure of He^3 is much higher than He^4, the gas phase above the liquid in the still is about 98% He^3. The vapor pressure at 0.6 - 0.7 K is also high enough to achieve reasonable molar circulation rates. A vacuum pump is used to recirculate the He^3. A pumped He^4 bath at about 1.2 K is used to re-liquefy the He^3. The He^4 in the system essentially remains stationary as the He^3 diffuses through it from the mixing chamber to the still. In passing through the heat exchanger the cold dilute He^3 cools the incoming pure He^3. The lower temperature limit depends on the efficiency of the heat exchanger. The driving pressure for the diffusion of He^3 through the He^4 is the osmotic pressure of He^3 in He^4, which in this case is the Fermi gas pressure of the He^3 at a density equal to 6.4% He^3. This pressure is about 2.3 KPa (17 torr) even down to 0 K. At equilibrium this osmotic pressure is constant from the mixing chamber to the still. Because of this relatively high pressure it is possible to get reasonable flow rates through an efficient heat exchanger without a significant pressure drop. This high osmotic pressure is the reason the dilution refrigerator works down to such a low temperature, whereas the He^3 refrigerator does not. Even though the entropy in the dilute phase of He^3 is not as high as pure He^3 gas, the He^3 density remains high enough in the dilute phase to be easily circulated. The thermodynamic cycle used in the dilution refrigerator is essentially the vapor-compression cycle shown in Fig. 3. The existence of a solution on the low-pressure side from the mixer to the still means that the relevant pressure or generalized force there is the chemical potential or osmotic pressure. Because He^3 is continuously pumped around the cycle, we say the cycle operates in the physical domain.

Solid Systems

Figure 8 shows the entropy of several solid materials. In the previous figure we saw that the relatively slow ordering in Fermi-fluid He^3 was useful for providing refrigeration over a wide temperature range below 1 K. Helium 3 is a nuclear Fermi fluid, but now we consider a much lighter Fermi fluid -- electrons in a metal, semimetal, or semiconductor. The Fermi temperature of a system of spin 1/2 particles is given by:

$$T_F = \frac{\hbar(3\pi^2 n)^{2/3}}{2km^*} \tag{19}$$

where n is the density of particles, k is Boltzmann's constant, and m* is the effective mass of the particle. The Fermi temperature is the approximate temperature below which ordering begins to take place. The specific heat and entropy of a Fermi gas are linear in T much below T_F whereas the specific heat approaches the constant value (3/2)R above T_F. Using the mass of the He^3 nucleus in Eq (19) gives T_F on the order of 1 K for He^3. The much lighter mass of electrons results in a T_F of about 6×10^4 K for electrons in most metals, such as copper. At room temperature or below these electrons are ordered quite well, as suggested by the low entropy. Additional ordering of the electrons can occur when they pair via virtual phonons to become superconducting. The entropy would then drop off very rapidly below the transition temperature. Similar behavior occurs in liquid He^3 when it becomes a superfluid below 2.7 mK.

The usefulness of these entropy curves becomes clear when they are used to evaluate the potential for cooling via magnetization of superconductors. Application of a magnetic field to a superconductor will drive it into the normal state. Because the entropy of normal electrons is higher than that of the superconducting state, heat will be absorbed. However, S/R at 10 K for normal electrons is only about 10^{-3}, much too small for useful refrigeration.

According to Eq. (19) the Fermi temperature can be lowered by reducing the concentration of electrons. The resultant entropy per mole of electrons is thus increased at a given temperature. Figure 8 shows how this reduced density gives higher electron entropies [23] to the semiconductor Bi_2Te_3 and semimetal Bi. It is clear that heat will be absorbed if electrons go from a normal metal (or superconductor) to Bi_2Te_3 or Bi. This can be done by joining the two materials and passing an electric current through the junction. The heat absorbed is known as the Peltier heat, and the technique of utilizing this effect is called thermoelectric refrigeration. A voltage source (ε) provides the power necessary (εI) to drive the electrons around the cycle. The electrons return to the metal from Bi or Bi_2Te_3 at the other junction. This process gives off heat. The similarity to the dilution refrigerator is evident, but in this case it is electron dilution which produces refrigeration. A current of 10 A gives an electron flow rate of 10^{-4}mol/s, which is a typical He^3 flow rate in dilution refrigerators.

The He^3-He^4 dilution refrigerator is a powerful and successful refrigerator for temperatures down to 2 mK. Why isn't the thermoelectric refrigerator equally successful in a higher temperature range? To answer that question we need to consider several points. First, consider the case of a metal or semimetal with a molar electron density of 6.4% per mole of metal or semimetal, which is the same as the He^3 concentration in the dilute side of a dilution refrigerator. The entropy curve would be increased over that of the Cu electrons by the same amount as the He^3-He^4 curve is above the pure He^3 curve. At a lower practical limit of about 5 mK for a dilution refrigerator the dilute He^3 entropy is about $S/R = 6 \times 10^{-2}$. For a similarly dilute electron system a value of 6×10^{-2} for S/R occurs at 200 K, which is about the lowest practical temperature for thermoelectric refrigeration [24]. The lowest temperature achieved to date is 159 K [25]. In practice n- and p-type Bi_2Te_3 are most often used for the two materials. The electron entropy in p-type Bi_2Te_3 is somewhat less than that of a metal. In n-type Bi_2Te_3 the electrons are diluted to the point of $n = 4 \times 10^{19} cm^{-3}$. The entropy per mole of electrons is then quite high at 100 K but the low density makes it difficult to obtain a reasonable electron flow rate, i.e., the electrical resistance becomes high. A figure of merit for a material for thermoelectric refrigeration is given by [23]

$$Z = \alpha^2\sigma/k \ , \tag{20}$$

where α is the thermoelectric power, or Seebeck coefficient, σ is the electrical conductivity, and k is the thermal conductivity. The electronic part of the Seebeck coefficient is simply proportional to the electron entropy and is given by

$$\alpha = (8.6 \times 10^{-5} \ V/K)S/R \tag{21}$$

For the case where α, σ and k do not vary much with temperature, the maximum temperature drop is given by [23]

$$(T_h - T_c)/T_c = \frac{1}{2} ZT_c \ . \tag{22}$$

Larger temperature drops can be achieved by staging. The highest values of Z are about $3 \times 10^{-3} K^{-1}$ between 100 and 300 K for the Bi_2Te_3 materials [23,25]. A factor of ten improvement would be a significant breakthrough, but the prospects for it are not good [23,24], though there is no thermodynamic upper limit for Z.

The presence of phonons in the thermoelectric materials is both a disadvantage and an advantage. The disadvantage is that the phonons transport considerable heat from the hot junction to the cold junction and provide resistance to the flow of electrons. The advantage is that as the electrons collide with the phonons, the phonons are dragged along with the electrons in what is called the phonon-drag effect. The reason that this is good is because the phonons then contribute their entropy to the flow process. As seen in Fig. 8 the phonon entropy can be quite high, especially for a material with a low Debye temperature, Θ. The phonon-drag effect often dominates the Seebeck coefficient of pure metals in the 5-50 K temperature range. Optimization of the phonon-drag effect could be useful to enhance α for temperatures below 200 K. The presence of spins from magnetic impurities can give rise to a similar effect known as spin-drag [26]. In a particular type of electron-spin scattering, the electrons may drag along the relatively high spin entropy. (See Fig. 9). This effect deserves further study for enhancement of the figure of merit.

A problem with the drag effects is that they also contribute to the electrical resistivity. A more desirable way of increasing the figure of merit is to increase the effective mass of the electrons and thus reduce the Fermi temperature according to Eq. (19). A distortion of the Fermi surface causes such an enhanced effective mass. An effective mass of at least 100 electron masses may be necessary to give a high enough figure of merit. This high effective mass must occur with high values of electron density. The figure of merit can be increased sometimes by the application of a magnetic field. In anisotropic crystals magnetic enhancement of the thermoelectric figure of merit up to $11 \times 10^{-3} K^{-1}$ in bismuth-antimony has been achieved [25] at 80 K, with a field of 0.13 T. A low temperature of 128 K has been reached with a combined thermoelectric-magnetothermoelectric refrigerator [25].

The magnetothermoelectric effect discussed above should not be confused with thermomagnetic effects. In the latter a magnetic field is placed at right angles to the current flow, which then gives rise to a temperature gradient perpendicular to both the current flow and the magnetic field. In essence, the magnetic field deflects the faster, higher energy electrons more than the slower ones. The lower energy electrons tend to go to one side of the sample and can absorb heat. The effect is even greater when both electrons and holes are present. In that case an electron hole pair is created on the cold side (an entropy increase) and driven toward the hot side where the excess pairs are annihilated (an entropy decrease). This thermomagnetic effect is called the Ettingshausen effect after the Austrian botanist and geologist who discovered it in 1887 [23]. Thermomagnetic refrigeration is better than thermoelectric refrigeration for temperatures below about 150 - 200 K. Combining the two could give temperatures on the order of 70 K [24]. Because efficiencies of such systems are so low, these devices are useful only for cooling small devices with little power dissipation. Cooling of small superconducting devices would be an ideal application if high enough figures of merit could be achieved to reach a temperature on the order of 10 K.

The two curves shown in Fig. 8 for the phonon entropy represent the approximate upper and lower limits for most solids. The upper curve is for a solid with a Debye temperature Θ of 100 K whereas the lower curve is for MgO, which has Θ = 800 K. The dashed line rising above the solid line for the Θ = 100 K curve shows a typical deviation from the ideal Debye behavior. Previously we discussed how phonon-drag effects in the thermoelectric effect utilize some of the phonon entropy for cooling. Other methods of utilizing this entropy may be available. In analogy to thermoelectric refrigeration or the dilution refrigerator, cooling should occur at a junction between two solids as phonons pass from the high Θ solid to the low Θ solid. A suitable driving mechanism is not obvious. Electronic or ultrasonic means may exist to drive the phonons across the junction. Considerable problems may exist because of phonon reflections at the junction.

Refrigeration with a force acting on a single solid is possible if Θ can be changed by the force. The Debye temperature of a solid can be given by

$$\Theta = (\hbar/k)c(18\pi^2 n)^{1/3} , \qquad (23)$$

where c is the sound velocity and n is the atomic density. Because of the high short-range forces in a crystal, pressure has only a small effect on n and on c, and thus on Θ. The small effect of pressure on the entropy is seen from Eq. (15), which for this system becomes

$$TdS = C_p dT - T(\partial V/\partial T)_p\, dP \, . \tag{24}$$

The term $(\partial V/\partial T)_p$ is just the thermal expansion. Some solid hydrocarbons (low Θ) may have values for $(1/V)(\partial V/\partial T)_p$ of $6 \times 10^{-4} K^{-1}$ at room temperature. Because an ideal gas has the value $3.4 \times 10^{-3} K^{-1}$ for $(1/V)(\partial V/\partial T)_p$ at room temperature, it is clear that the refrigeration power of the solid hydrocarbon will be 18% as much as that for an equal volume of gas. For 10 MPa (100 atm) $\Delta S/R$ for the hydrocarbon may be about 10^{-1} at 300 K. The effect will drop off like T^3 at lower temperatures. Because of the high specific heat of hydrocarbons, a 10 MPa pressure change will change the temperature by only 1 - 2 K at 300 K.

For a linear system of the same material $(1/L)(\partial L/\partial T)_\tau$ will be about 1/3 of the volumetric thermal expansion coefficient. The entropy change and cooling effects for the same volume of material and for a stress equal to 10 MPa will thus be 1/3 as large as for the case of pressure on a volume. A 10 MPa stress will cool the material somewhat less than 1 K at 300 K. An interesting exception is the case of vulcanized rubber, such as an ordinary rubber band. This high-polymer consists of long chains, which in the relaxed state can be twisted at random in many different ways, i.e., a disordered state. That leads to a high entropy in the relaxed state. As the rubber is stretched, one configuration of the molecular chains becomes preferable and so the entropy of the chain approaches zero according to the relationship

$$S = R \ln m \, , \tag{25}$$

where m is the number of micro-configurations. Figure 8 shows the entropy of natural rubber for both a relaxed state and for a 500% elongation. These entropies include the normal phonon entropy in addition to the configurational entropy. Unlike the case of a normal solid, which has only the phonon entropy, stretching a rubber band reduces the entropy. For a 500% isothermal elongation the entropy is reduced by an amount $\Delta S/R \simeq 0.8$. The temperature increases during elongation by about 8 K at room temperature if adiabatic conditions are maintained [27]. According to the second TdS equation, Eq. (15), the linear thermal expansion coefficient under tension must be large and negative to give the required entropy change. That behavior is indeed the case for rubber.

The entropy change in rubber is sufficiently large to utilize it for a motor [28], although it may be useful only for demonstration purposes. Another interesting demonstration would be to use a separate motor to drive the previously mentioned motor [28] in reverse and obtain refrigeration. Figure 11 is a sketch of such an arrangement which could give a maximum temperature reduction of about 8 K. The demonstration is useful in showing how a solid material can be made to go through a refrigeration cycle in the physical domain and provide continuous refrigeration. The type of cycle that this system goes through is actually rather inefficient and is not quite like any of those discussed earlier. The cycle followed is the Stirling cycle (constant length paths) except in the sketch of Fig. 11 no provision exists for heat transfer between the two constant length paths in the cycle. Hence, the refrigeration power is reduced because of the additional heat load of cooling the rubber bands from T_0 to

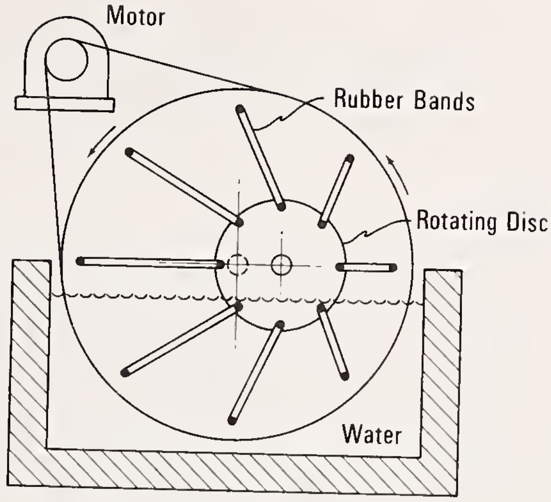

RUBBER BAND REFRIGERATOR

Figure 11. A schematic of a rubber band refrigerator based on a scheme for a rubber band motor. The small disc rotates along with the larger disc but on a different center.

T. If a heat transfer mechanism were provided (a moving oil layer on top of the water bath), the demonstration refrigerator could possibly freeze water.

Another material which can be used in the same way as rubber is 55-NITINOL [29]. This alloy (55% Ni - 45% Ti) has an unusual martensitic transition at about 50° C, but this temperature can be varied by changing the concentration. This alloy has a memory in the sense that a sample deformed below the transition temperature will revert back to its original shape when heated above the transition temperature. The material can exert considerable force in reverting to the original shape. The entropy of the high temperature disordered phase is reduced by applying a tensile force. A sufficiently high force can drive the material into the ordered phase. The entropy change between the two phases is on the order of $\Delta S/R = 0.5$, comparable to that of rubber. The material has been considered for use as a motor in the manner described for the rubber band motor previously.

A solid material with a very high entropy change during a solid-solid transition at about 245 K is pentaerythrityl fluoride [30], $C(CH_2F)_4$. The entropy change of $\Delta S/R = 6.4$ would have considerable practical significance if it could be controlled by a reasonable force. Because it may be a rotational ordering transition [30], such a reasonable force may not exist.

All of the entropies discussed so far have been for bulk samples. In very small dimensions (nm sizes) the finite energy level spacing of phonons or electrons will bring about an entropy decrease compared with bulk values. However, the surface phonons or electrons will then tend to dominate the total entropy of the material. The entropy of surface phonons or electrons will be higher than for bulk behavior since they are less ordered. Figure 8 shows an example of the entropy for surface phonons in 10 nm particles of MgO. This entropy dominates the bulk entropy of MgO only below about 50 K. Other two-dimensional systems such as adsorbed gases can have higher entropies than the ordered bulk phase. An adsorbed gas is also an ordered phase which can exist at temperatures much higher than the critical point of the bulk liquid. Such surface behavior could be useful for refrigeration.

Magnetic and Electric Systems

Figure 9 shows other sources of entropy useful for refrigeration, particularly magnetic systems. The entropy of the disordered-paramagnetic phase can be quite high. In addition this disordered phase in some cases can exist down to very low temperatures before ordering to a ferromagnetic or antiferromagnetic phase takes place and the entropy is removed. The nucleus has a small magnetic moment and hence a low ordering temperature. The entropy of the copper nucleus is shown in Fig. 9 for the case of an applied magnetic field of 0 and 10 T. Ordering for B = 0 takes place at about 10^{-7} - 10^{-6} K. Thus adiabatic demagnetization from about 5 mK and 10 T will result in a nuclear temperature of about 10^{-6} K. This method has been used to cool other materials (copper electrons or liquid He^3) to temperatures of about 0.5 mK.

Magnetic moments of electron spin systems are much higher which means that ordering temperatures are higher. For a magnetic system the entropy in the disordered phase is given by:

$$S/R = \ell n(2s + 1) \,, \tag{26}$$

where (2s + 1) is the number of possible orientations of the magnetic dipole of spin s. The three electronic magnetic systems shown in Fig. 9 are $Ce_2Mg_3(NO_3)_{12} \cdot 24\ H_2O$ (CMN), $Gd_2(SO_4)_3 \cdot 8H$ and pure Gd. Values of s for these systems are 1/2, 7/2 and 7/2 respectively. The ordering temperature for these three systems covers the range from about 10^{-3} K to room temperature. The material $Gd_2(SO_4)_3 \cdot 8H_2O$ has an entropy of S/R = 2.1 which is easily removed by a field of 10 T at 4 K. Because it is a solid with a resulting low molar volume, it may prove to be competitive with helium for refrigeration in the 4 K temperature range. The system could use the Carnot cycle with time domain operation by using heat switches such as beryllium magneto-resistive types [31]. Such a refrigerator would have no moving mechanical parts. Stirling- or Ericsson-cycle operation may also be used by placing the material on a rotating wheel. More details about the use of $Gd_2(SO_4)_3 \cdot 8H_2O$ and similar materials for refrigeration at 4 K is given by Steyert [32].

CMN has been used for refrigeration down to 1 mK for many years. The idea of adiabatic demagnetization originated in the mid-1930's and was used until the dilution refrigerator took over most of the refrigeration tasks for the millikelvin temperature range. The entropy for CMN shown in Fig. 9 is based on the recent work of Giauque, et al. [33]. Magnetic refrigeration around room temperature utilizing gadolinium has recently been proposed by Brown [34 The entropy can be changed by about $\Delta S/R = 0.3$ with a 10 T field at room temperature. We point out here that the entropies shown in Fig. 9 do not include the phonon entropies of these solids. The specific heat associated with this additional entropy can be large at room temperature and act as a heat load on the refrigeration cycle. Figure 9 shows how a field of

10 T has less and less effect on the magnetic entropy of a system as the temperature increases. This is due to the tendency of the phonons to disorder the magnetic spins. Carnot cycle operation with Gd would be limited to temperature differences less than 10 K. Ericsson cycle operation would follow the B = 0 and 10 T curves down to much lower temperatures so that larger temperature differences can be provided with that cycle or the Stirling cycle. The high phonon specific heat places a severe requirement on the heat exchangers for such cycles.

As was mentioned earlier, a magnetic field will increase the entropy of an antiferromagnet until a transition to the paramagnetic phase occurs at some high field. Thus, at low fields cooling takes place during adiabatic magnetization. The maximum entropy change will always be less than the entropy of the paramagnetic phase in zero field. Since paramagnetic systems exist which have transitions at nearly any desired temperature, it is usually best to use them just above the transition instead of an antiferromagnet below the transition.

The magnetic systems just discussed have an electrical analog. Dielectric materials may have a high electric dipole entropy in the disordered, paraelectric state, but lose the entropy when the material orders at some low T to a ferro- or antiferroelectric state. The entropy [35] of potassium dihydrogen phosphate, KH_2PO_4, in electric fields of 0 and 50 kV/cm are shown in Fig. 9. The transition temperature of 122 K is the lowest of any of the order-disorder type of ferroelectric materials. These materials are analogous to the magnetic materials in the sense that they have permanent electric dipoles above and below the transition temperature. Lower transition temperatures are possible in dilute systems such as KCℓ doped with OH^- dipoles. As shown by the entropy curves [36] for KCl:OH in Fig. 9, ordering can be made as low as 0.1 K. The entropies shown here are on the basis of one mole of OH dipoles, but the concentration of these is only about 3×10^{18} cm^{-3}. Attempts to raise the concentration and provide a greater refrigeration power usually result in a clustering of the dipoles and hence a loss of their entropy. Further material studies may be useful in this area.

Another type of ferroelectric or antiferroelectric ordering can take place in some materials. This is known as a displacive transition and is described in more detail in a paper by Radebaugh [37]. In these cases there is no permanent dipole above the transition temperature. The entropy in the disordered phase is due to the optic mode, which can be shifted by an electric field. The optic mode entropy of $SrTiO_3$ is shown for electric fields of 0 and ∞ [38]. As discussed in another paper [37], these entropy changes in the displacive materials are too small to be of much practical significance.

Chemical Systems

We conclude our discussion of various systems with galvanic, or reversible, cells [39]. Reversible chemical reactions take place in such cells at a certain temperature, depending on the cell voltage. In the example shown in Fig. 9, the reaction

$$Cu + ZnSO_4 \rightarrow Zn + CuSO_4 \qquad (27)$$

takes place at 273 K with a cell voltage of $\varepsilon = 1.0934$ V. With a cell voltage of 1.0481 V the reaction takes place at 373 K. In the plot of Fig. 9 the entropy of Cu + $ZnSO_4$ is taken as 0 and that of Zn + $CuSO_4$ is just the entropy increase of the reaction. A refrigeration cycle is possible by allowing the battery to discharge reversibly at room temperature and give off heat as the entropy is reduced. Heat can then be absorbed at a lower temperature during the reversible charging of the battery. In some systems the charging and discharging steps are reversed. In those cases, e.g., the ordinary lead-acid battery, heat is absorbed during discharging so that it then serves as a "storage battery" for refrigeration as well as power. The first law of thermodynamics is not violated since it takes more work to charge the battery at a higher temperature. The galvanic cell has not been considered for refrigeration as far as this author knows. The rather high entropy changes possible in these systems make it appear attractive. One possible hindrance to their practicality is the Joule heat losses which accompany current flow. Another is the slowing down of chemical reactions at low temperatures. Further studies of such systems may be useful.

How Much Entropy Is Enough?

Figures 6-9 show the entropies of many systems -- some commonly used for refrigeration and others never considered for refrigeration. Other workers may wish to consider other systems not shown here. A question important to both funding agencies and reserachers is "how large should the entropy of some new system be before it has the potential for practicality?" There are two ways to approach this question. One way is to look at the entropy of the disordered state for existing practical systems. Generally, these entropies (S/R) lie in the range from about 10^{-1} at 1 mK to about 10 at 100 K. A straight line can be drawn between these points in the log-log plots of Figs. 6-9. This line represents the general range of S/R for present systems. If any new system has a molar flow rate or cycle time comparable to these systems then the entropy of the disordered phase in the new system should probably not be less than 1/10 that of the line discussed above. One point to consider is that for liquid or solid systems the higher density may permit more compact refrigerators if it is possible to transfer the same amount of heat in a more compact heat exchanger.

A second approach to determine a reasonable value of $\Delta S/R$ for a system is to consider how much entropy is required to cool itself. For a temperature change of ΔT small compared with T, the relation

$$\frac{\Delta T}{T} = \frac{\Delta S/R}{C/R} \tag{28}$$

is valid, where C is the specific heat. In order to overcome inefficiencies of practical heat exchangers, $\Delta T/T$ should be at least 2×10^{-2} near room temperature. At room temperature C/R for most materials will be at least 3. From Eq. (28) an entropy of $\Delta S/R = 6 \times 10^{-2}$ would be needed to cool the sample. In order to have enough entropy left for refrigeration, a minimum value of $\Delta S/R \simeq 0.1$ seems reasonable at room temperature. At 10 K the specific heat of materials may range from $C/R \simeq 10^{-2}$ to 10^{-1}. Since heat transfer may be more of a problem at 10 K, $\Delta T/T$ whould probably be at least 10^{-1}. Thus at 10 K a minimum value of $\Delta S/R \simeq 10^{-2}$ is required when a provision for some useful entropy is included. The specific heat of most active materials does not decrease much below $C/R \simeq 10^{-2}$ for temperatures down to 10^{-3} K. From this argument the minimum $\Delta S/R$ needed for a practical refrigerator is 10^{-2} from 1 mK to 10 K. From 10 K to room temperature the value should rise up to about 10^{-1}. The previous argument gave somewhat higher values. The region between these two limits is shown in Fig. 12. This band represents the lower limit of $\Delta S/R$ necessary for any new system to be a practical refrigerator.

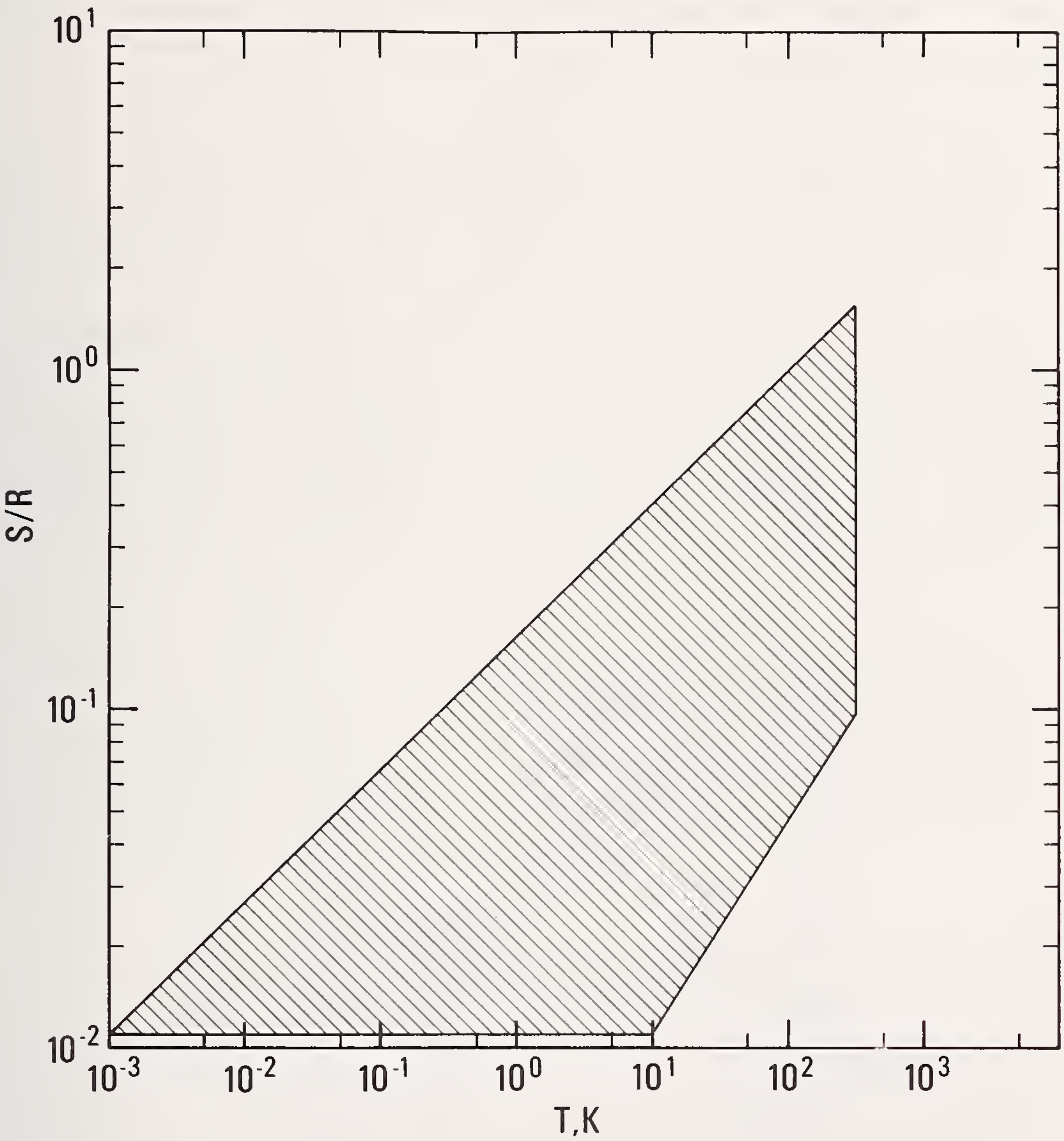

Figure 12. The region in a reduced entropy which represents the miminum change of entropy for a system in order for that system to be a practical refrigerator.

GAS-LIQUID SYSTEMS

Because of the success and wide-spread use of gas-liquid systems, we consider them in [illegible]re detail here. It is these systems which provide nearly all of the refrigeration needs [illegible] temperatures from 1 - 300 K. The entropies of such systems are high in the disordered [illegible]ate and so such systems have high efficiencies. These methods have been in use for a [illegible]tury or more and so the engineering aspects of such systems are quite sophisticated.

Several practical cycles exist which closely follow the ideal thermodynamic cycles discussed earlier. Since many of these cycles are commonly used and referred to in the literature, we discuss some of these here.

The vapor compression cycle was discussed earlier and shown in Fig. 3. In that case expansion of the liquid phase from a pressure of P_2 to P_1 occurs. The expansion is usually done with a throttle valve or capillary. In systems using the permanent gases it is not possible to liquefy the gas at room temperature because the critical temperature is below room temperature. A cascade system has been used but the use of many fluids leads to a complex system.

Hampson Cycle

An expansion valve can also be used with the gas phase as an inlet but the expansion process is not so efficient. This expansion process, known as a Joule-Thomson expansion, is a constant enthalpy process, and so no heat is absorbed. Such a process follows a path somewhere between an isotherm and an isentrope on a T-S diagram if the temperature is below the inversion temperature for the gas. Otherwise the gas heats upon expansion. If the expansion process in the Brayton cycle (Fig. 4) is replaced by a Joule-Thomson expansion, the cycle is referred to as the Hampson cycle or the Joule-Thomson cycle. This cycle is shown schematically in Fig. 13(a). The Linde cycle is essentially the same except that two

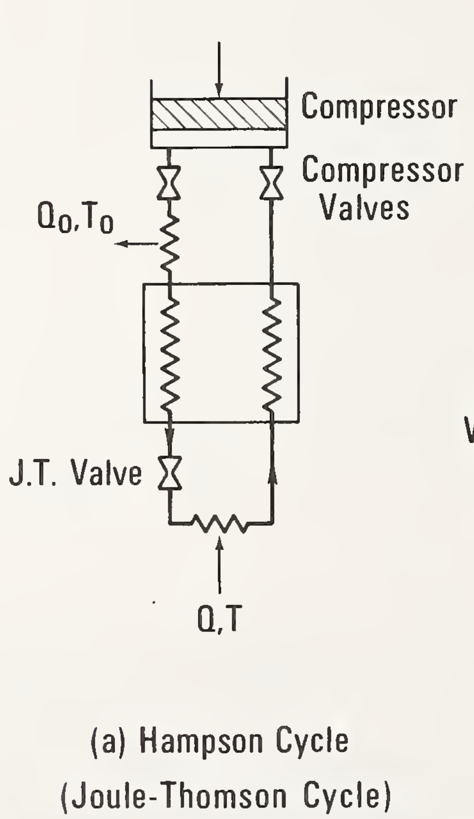

Figure 13. (a) A schematic of the Hampson cycle which uses a Joule-Thomson valve and a counterflow heat exchanger. Heat Q is absorbed at the low temperature T and Q_0 is given off at room temperature T_0. The work input is W_0. (b) A schematic of the Claude cycle in which an expander with cold valves does work W.

pressures and two Joule-Thomson expansions are used to improve efficiency. For nitrogen a temperature of 77 K can be reached with a single-stage Hampson cycle or Joule-Thomson expansion since the inversion temperature of nitrogen is above room temperature. Hydrogen and helium stages can be added below the nitrogen stage to reach 4 K. Nitrogen-hydrogen systems are commonly used for cooling infrared detectors [40]. These devices are usually made in miniature sizes (a few mm diameter by a few cm long) and have cool-down times of a few seconds. Bottled high-pressure gas is usually used with these systems. These are attractive for cooling of small superconducting devices since there are no moving mechanical parts and little vibrational or magnetic noise. Little [41] discusses scaling laws for miniature Joule-Thomson systems. Ejectors [42] can be used in conjunction with a Joule-Thomson valve to allow a lower temperature stage to be added which can reach temperatures below the normal boiling point of the liquid.

Claude Cycle

A combination of the Brayton cycle (Fig. 4) for an upper stage and a Joule-Thomson expansion for a lower stage is called the Claude cycle, Fig. 13(b). Several stages of expansion engines may be used. This cycle was first used in 1902 [2], and is now commonly used for liquefying helium. The Collins helium liquefiers use this cycle. Because this cycle uses expansion engines (rotary or reciprocating), it performs a reversible adiabatic expansion and thus it is more efficient than the Hampson cycle. Table 3 compares [43] the actual efficiency of several types of refrigerators for a temperature of 20 K. The reciprocating expansion engines in the Claude cycle require inlet and outlet valves at the low temperature, hence the system is mechanically complex. In 1912 Heylandt patented [2] a design for a reciprocating expansion engine which had a long nonconducting piston and room-temperature seals. Low-temperature valves are eliminated when expansion turbines are used but these are not efficient in small-size refrigerators.

TABLE 3. Comparison of Efficiencies for Actual Refrigeration Cycles with 1 W at 20 K

Cycle	η/η_c
Stirling	0.030
Gifford-McMahon	0.013
Brayton	0.011
Hampson (Joule-Thomson)	0.007

Solvay Cycle

In 1887 Solvay [2] was issued a patent for a gas refrigeration machine which did not have the problem of low-temperature valves. Also, instead of a counter-flow heat exchanger, he used a regenerative heat exchanger in the Brayton cycle. Warm high-pressure gas passed from the valve through the regenerator to the expansion engine. The regenerator was actually the annular gap between the piston and cylinder. After expanding in the engine and doing work, the cold gas passed through the regenerator and out the exit valve. The Solvay cycle, shown in Fig. 14(a) is well suited to small refrigerators [44].

Stirling Cycle

As mentioned early in this paper, Kirk in 1874 first used the Stirling cycle for refrigeration. Fig. 14(b) gives a schematic of such a refrigerator and Table 3 shows its relative efficiency, which is the highest of all refrigerators. This refrigerator also uses a regenerative heat exchanger but unlike the Solvay cycle, no valves are required. In the Stirling-cycle refrigerator the piston and displacer must be synchronous and 90° out of phase. This connection is represented by the dashed line between the compressor and displacer in Fig. 14(b). Negligible force is required to move the displacer since it only displaces gas back-and-forth between the high- and low-temperature ends. The gas volume in the regenerator should be small compared with the total gas volume. The piston delivers the work of compression and also receives the work of expansion. Since no valves are required, this cycle is very simple and well suited to small refrigerators for superconductors. With a three-stage displacer temperatures as low as 7.8 K have been obtained [45]. Zimmerman and Radebaugh [46] discuss the use of this refrigerator for cooling a SQUID. In that refrigerator the regenerator is just the gap between the displacer and the walls. It should be pointed out here that in high-speed operation of the Stirling-cycle refrigerator, isothermal compression and expansion do not occur. Thus the actual thermodynamic cycle followed by such refrigerators is more like the Otto cycle instead of the ideal Stirling-cycle. It would seem less confusing to use the name Kirk cycle to refer to the mechanical means of approximating this cycle and Stirling cycle to refer to the ideal thermodynamic cycle. Unfortunately the name Stirling cycle seems to be in widespread use for the mechanical cycle as well. The Stirling cycle can also be carried out by using two pistons operating 90° out of phase, instead of a piston and a displacer.

Gifford-McMahon Cycle

In 1959 Gifford and McMahon [47] described another cycle which used regenerative heat exchangers and a displacer. Unlike the Stirling-cycle refrigerator, room-temperature valves are used to separate the displacer from the compressor. Figure 14(c) shows a schematic of the Gifford-McMahon refrigerator. In this refrigerator expansion of the gas in the cold chamber is a free expansion through the exit valve. No external work is done by the expansion, but it does do work on the gas leaving the system. The enthalpy and temperature of the gas leaving the system is thus raised. The gas left in the cold space expands adiabatically, if done fast, just as in the Stirling cycle. Unlike the Stirling cycle, the work from expansion is not recovered and its efficiency is lower. (See Table 3). It is difficult to show the Gifford-McMahon on a single T-S diagram because different portions of the gas follow different curves [48]. The general shape is similar to the Brayton cycle for high-speed operation and the Ericsson cycle in the more ideal low-speed operation. The difference between the Gifford-McMahon refrigerator and the Solvay refrigerator is that in the Solvay refrigerator work is extracted from the expanding gas, whereas in the Gifford-McMahon refrigerator work is not extracted. The cycle sometimes referred to as the work Gifford-McMahon

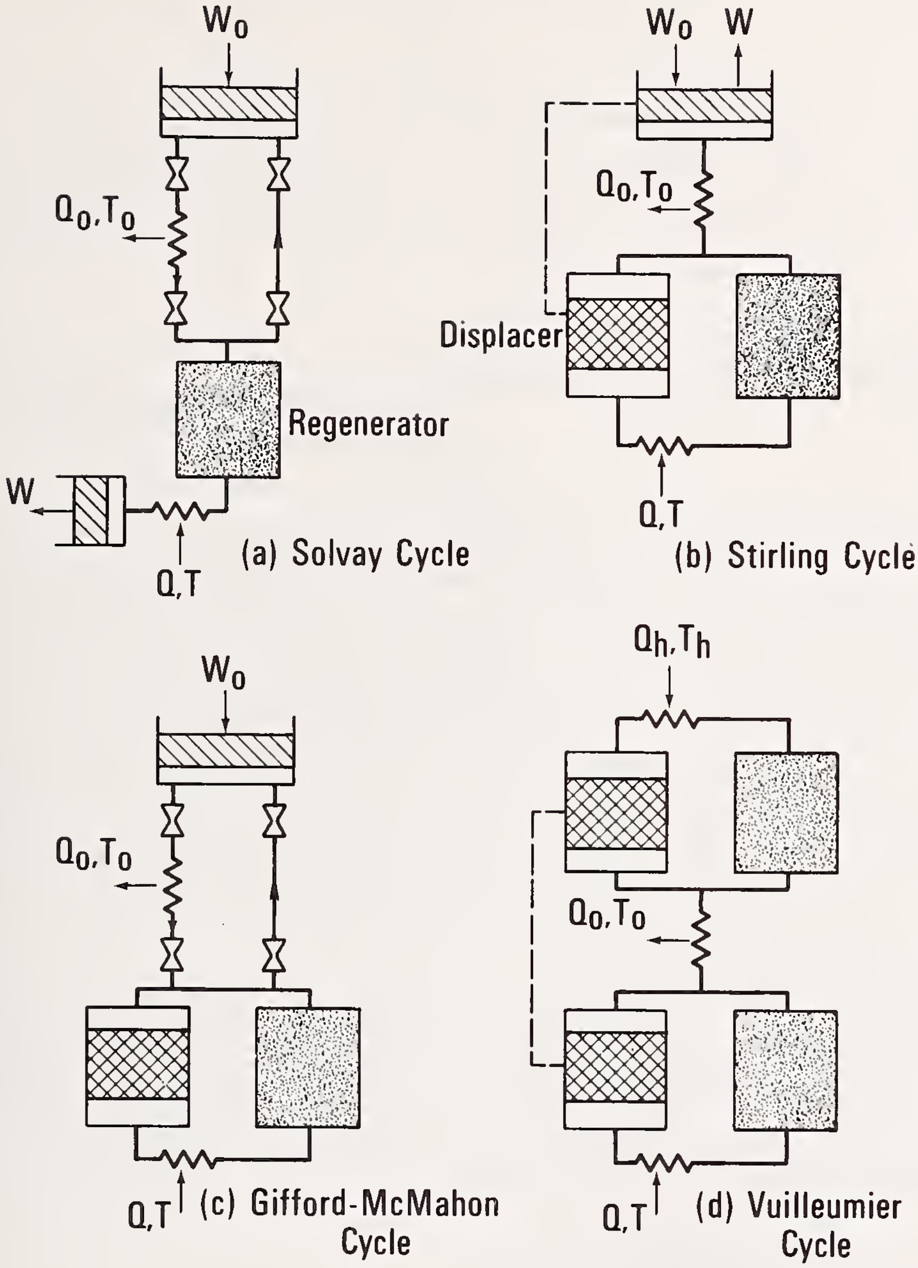

Figure 14 (a) A schematic of the Solvay cycle which uses an expander, warm valves, and a regenerative heat exchanger. (b) A schematic of the Stirling cycle in which a displacer operates synchronously with the piston. The piston does work W_0 to compress the gas and receives work W during the expansion. (c) A schematic of the Gifford-McMahon cycle which has a displacer and room-temperature valves. (d) A schematic of the Vuilleumier cycle which uses a thermal compressor comprised of a displacer and regenerator with a high-temperature heat source. The high- and low-temperature displacers operate synchronously.

cycle is the same as the Solvay cycle described previously. One advantage of the Gifford-McMahon refrigerator is that high-speed oil-lubricated compressors can be used with a low-speed displacer. Such refrigerators have relatively long MTBF and are well suited to small sizes. With a three-stage displacer temperatures of 6.5 K have been obtained [49]. The addition of a Joule-Thomson stage on the bottom end permits temperatures of 4.2 K to be reached. By so doing, the complexity and cost are increased, but Higa [50] shows that reliability is still good.

Vuilleumier Cycle

The efficiency of refrigerators for cooling small superconducting devices is not very important. Instead, reliability, size and cost are the important engineering aspects which are considered. Some of the practical cycles discussed above eliminate the low temperature expansion engines to achieve better reliability. The mechanical compressor can also be eliminated as is done in the Vuilleumier cycle [51], (VM cycle) patented in 1918. This cycle is like the Stirling-cycle refrigerator except that the mechanical compressor is replaced by a thermal compressor, see Fig. 14(d). A thermal compressor is simply a displacer moving between the hot (600° C) end of a cylinder and the room-temperature end. The cold and hot displacers are the only moving parts and the forces on them are small. The disadvantage is that pressure ratios are limited to relatively small values, but that may effect only the efficiency. The Vuilleumier cycle is discussed in more detail [52] in other places. Temperatures as low as 6.1 K have been reached with this method [52], which is the lowest for any regenerative refrigerator.

Another step in the elimination of moving parts would be to eliminate the crankshaft which moves the displacers in the Vuilleumier cycle. The displacers could oscillate in a resonance fashion with no mechanical connections. Stirling engines have been developed which operate with no crankshaft. These are called free-piston Stirling engines [1,53]. To the author's knowledge no free-piston Vuilleumier refrigerators have been built.

Other Means for Eliminating Mechanical Parts

Crankshafts for reciprocating compressors and expanders can be eliminated by using linear-drive motors. When the pistons are also rotated by a rotating field, a gas-bearing effect is produced that eliminates wear from metallic contact of piston and cylinder. This rotary-reciprocating concept for compressors and expanders is being utilized [54] in a Brayton-cycle refrigerator for a predicted temperature of about 10 K. The cost of precision machining for the components is high but the potential for long life is good. The same rotary-reciprocating concepts could be used in other cycles, such as the Stirling cycle [55].

The old ammonia-gas refrigerators replaced a mechanical compressor with a thermal compressor. In these refrigerators ammonia was absorbed in water at room temperature and then the solution was pumped to a high temperature section where the ammonia gas was driven off at high pressure. The process did require a liquid pump, but these are more efficient than a gas compressor. An absorption compressor using $LaNi_5$-hydride has been described [56] for use with a hydrogen refrigerator operating near 20 K. Other gases can be pumped and thermally compressed by using gas adsorption on zeolites. Details of such adsorption pumping are given by Hartwig [57].

Gifford and Longsworth [58] devised a method known as pulse tube refrigeration in which there are no moving low-temperature parts. In this method gas is pulsed in and out of a tube closed at the other end at a rate of about 30 - 200 pulses per minute. The gas passes through a regenerator before entering the pulse tube. Refrigeration occurs at the inlet to the tube and heat is rejected at the other end, which is closed. Two or three stages are required [59] to reach 80 K, and it seems unlikely that a temperature as low as 10 K can be reached with this method. An advantage over the Hampson cycle is that pressures are much lower, thus a simpler compressor is required.

SUMMARY

The purpose of this paper has been to show how the thermodynamic principles of refrigeration can be applied to a wide spectrum of systems other than gas-liquid systems. The discussion of refrigeration with different systems has been on a unified basis to facilitate comparisons. It has been shown how entropy comparisons can be an aid to a search for new refrigeration systems. Emphasis is placed on new refrigeration systems since they could lead to large changes in cost and reliability. A separate section on gas-liquid systems has been included to show how engineering progress has brought such systems to a sophisticated state and to bring the reader up to date on the progress in these systems. New areas of engineering research in eliminating moving parts has been discussed.

Use of the Josephson junction and other small superconducting devices may well become one of the biggest applications of cryogenics. Progress in refrigeration and in the mating of the device and refrigerator should keep pace with the device development. In the long run the device will sell only as part of a system, and the system can be no better than the weakest link. To insure that refrigeration is not the weak link, an effort to develop new systems for the long run, in parallel with engineering efforts on present gas-liquid systems, may be the best approach.

REFERENCES

1. G. Walker, Stirling-Cycle Machines, Clarendon Press, Oxford (1973).
2. S.C. Collins and R.L. Cannaday, Expansion Machines for Low Temperature Processes, Oxford University Press, Oxford (1958).
3. J. Ericsson, see Encyclopedia Americana, Vol. 10, New York (1972) p 547.
4. R.D. McCarty, NBS Tech. Note 631 (1972).
5. J. Wilks, The Properties of Liquid and Solid Helium, Clarendon Press, Oxford (1967).
6. G.J. Van Wylen and R.E. Sonntag, Fundamentals of Classical Thermodynamics, John Wiley and Sons, New York (1965) p 590.
7. K. Nesselmann, Chem. Ing. Tech. 29, 198 (1957).
8. W.F. Giauque and J.O. Clayton, J. Am. Chem. Soc. 55, 4875 (1933).
9. T.R. Strobridge, NBS Tech. Note 129 (1962).
10. R.D. Goodwin, NBSIR 73-342 (1973).
11. A. Frank and K. Clusius, Z. Physik. Chem. B36, 291 (1937).
12. J.H. Colwell, E.K. Gill and J.A. Morrison, J. Chem. Phys. 36, 2223 (1962).
13. V.J. Johnson, WADD Tech Tech. Report 60-56, Part I, 1960.
14. R.D. McCarty NASA SP-3089 (1975).
15. H.W. Woolley, R.B. Scott and F.G. Brickwedde, J. Res. Nat. Bur. Std. 41, 379 (1948).
16. R.M. Gibbons and D.I. Nathan, AFML-TR-67-175 (1967); R.M. Gibbons and C. McKinley, Adv. Cry. Eng. 13, 375 (1968).
17. J.G. Daunt, Cryogenics 10, 473 (1970).
18. R. Radebaugh, NBS Tech. Note 362 (1967).
19. D.S. Betts, Refrigeration and Thermometry Below One Kelvin, Sussex University Press (1976).
20. J.S. Dugdale and J.P. Franck, Phil. Trans. R. Soc. 257, 1 (1964).
21. O.V. Lounasmaa, Experimental Principles and Methods Below 1 K, Academic Press, London, (1974).
22. G. Frossati, H. Godfrin, B. Hébral, G. Schumacker, D. Thoulouze, Int'l Symposium on Physics at Ultralow Temperatures, Japan, 1977 (to be published).
23. H.J. Goldsmid, Thermoelectric Refrigeration, Plenum Press, New York (1964).
24. J.E. McCormick and J.B. Brauer, Adv. Cry. Eng. 10A, 493 (1965).
25. W.M. Yim and R.D. Rosi, Solid-State Electron. 15, 1121 (1972); W.M. Yim and A. Amith, Solid-State Electron. 15, 1141 (1972).
26. D.K.C. MacDonald, Thermoelectricity: An Introduction to the Principles, John Wiley & Sons, New York (1962) p 84.
27. L.R.G. Treloar, The Physics of Rubber Elasticity, Clarendon Press, Oxford (1958).
28. C.L. Stong, Sci. Am. 224, 118 (April 1971).
29. C.M. Jackson, H.J. Wagner and R.J. Wasilewski, NASA-SP5110 (1972).
30. E.F. Westrum, Jr., Pure Appl. Chem. 2, 241 (1961).
31. R. Radebaugh, J. Low. Temp. Phys. 27, 91 (1977).

32. W.A. Steyert, This Conference; W.P. Pratt, Jr., S.S. Rosenblum, W.A. Steyert and J.A. Barclay, Cryogenics 17, 689 (1977).
33. W.F. Giauque, R.A. Fisher, E.W. Hornung and G.E. Brodale, J. Chem. Phys. 58, 2621 (1973); R.A. Fisher, E.W. Hornung, G.E. Brodale and W.F. Giauque, J. Chem. Phys. 58 5584 (1973).
34. G.V. Brown, J. Appl. Phys. 47, 3673 (1973).
35. F. Jona and G. Shirane, Ferroelectric Crystals, MacMillan, New York (1962), p 251; H. Baumgartner, Helv. Phys. Acta 23, 651 (1950).
36. I.W. Shepherd, J. Phys. Chem. Solids, 28, 2027 (1967).
37. R. Radebaugh, This Conference.
38. R. Radebaugh, J.D. Siegwarth, W.N. Lawless and A.J. Morrow, NBSIR 76-847 (1977).
39. M.W. Zemansky, Heat and Thermodynamics, 4th Ed., McGraw-Hill, New York (1957), p 292.
40. S.W. Stephens, Infrared Phys. 8, 25 (1968).
41. W.A. Little, This Conference.
42. J.A. Rietdijk, in: Liquid Helium Technology Pergamon Press, London, (1966) p 241; D.E. Daney, P.M. McConnell and T.R. Strobridge, Adv. Cry. Eng. 18, 476 (1973).
43. H.L. Jensen, T.C. Nast and A.P.M. Glassford, in: Applications of Cryogenic Technology, Vol. 4, XYZYX Information Corp. (1972) p 384.
44. R.C. Longsworth, Adv. Cry. Eng. 16, 195 (1970).
45. A. Daniels and F.K. du Pré, Adv. Cry. Eng. 16 178 (1970).
46. J.E. Zimmerman and R. Radebaugh, This Conference.
47. H.O. McMahon and W.E. Gifford, Adv. Cry. Eng. 5, 354 (1960).
48. W.E. Gifford, Adv. Cry. Eng. 11, 152 (1966).
49. R.W. Stuart, B.M. Cohen and W.H. Hartwig, Adv. Cry. Eng. 15, 428 (1970).
50. W.H. Higa, This Conference.
51. Vuilleumier, U.S. Patent 1,275,507 (1918).
52. T.T. Rule and E.B. Qvale, Adv. Cry. Eng. 14 343 (1969); B.L. Renyer, in: Closed Cycle Cryogenic Cooler Technology and Applications, AFFDL-TR-73-149, Vol. 1 (1973) p 147; R.D. Doody, Tech. Report AFFDL-TR-75-108 (1975).
53. W. Beale, W. Holmes, S. Lewis and E. Cheng, Paper 730647, SAE Automotive Engineering Congress, June 1973.
54. C.A. Schulte, A.A. Fowle, T.P. Heuchling and R.E. Kronauer, Adv. Cry. Eng. 10A, 477 (1965); R.W. Breckenridge, Jr., in Closed Cycle Cryogenic Cooler Technology and Applications, AFFDL-TR-73-149, Vol. 1 (1973) p 355.
55. R.W. Breckenridge, Jr., private communication (1977).
56. H.H. van Mal and A. Mijnheer, 4th Int'l Cry. Eng. Conf. (1972).
57. W. H. Hartwig, This Conference.
58. W.E. Gifford and R.C. Longsworth, Adv. Cry. Eng. 11, 171 (1966); 10B, 69 (1965).
59. R.A. Lechner and R.A. Ackermann, Adv. Cry. Eng. 18, 467 (1973).

Concepts for Cooling Small Superconducting Devices Using Closed-Cycle Regenerative Refrigerators

Ralph C. Longsworth
Air Products and Chemicals, Inc.
Allentown, Pennsylvania

The use of regenerative type refrigerators to cool small superconducting devices requires solving the following problems:

. difficulty of cooling below 10K
. isolation of the refrigerator vibration
. cooling by conduction rather than liquid or gas
. maintaining constant temperature

Air Products and Chemicals, Inc. as a manufacturer of small regenerative type cryocoolers, JT coolers, helium transfer cryostats, and small helium liquefiers which are sold for use in laboratory research, has had appreciable experience in solving many of these problems. This paper describes some of the concepts that have been developed which include:

. three stage regenerator type cryocoolers for 7K operation
. 4.2K JT loop attached to 10K cryocooler
. refrigerated helium dewars with low boiloff rates
. flexible low loss helium transfer lines
. convective gas heat transfer to isolate vibration
. temperature cycle attenuators
. automatic temperature controllers.

In addition, the characteristics of the Air Products' modified Solvay cycle cryogenic refrigerator are described.

Key words: Helium dewar; JT loop, regenerative cryocooler; temperature control; three stages; two stages; vibration isolation.

1. Introduction

Most of the research work done to date on superconducting devices has utilized liquid helium as a refrigerant. Liquid helium has the characteristics of providing a constant temperature independent of heat load at its boiling temperature of about 4.2K, and an absence of vibration. Good heat transfer is obtained by immersing the object being cooled directly in the liquid or surrounding it with cold gas. Flexibility of orientation and portability are possible by using small light weight dewars that can hold enough liquid helium to operate for several hours or days.

In order to reduce the operating cost and eliminate the need for handling liquid helium, closed-cycle refrigeration will be required as superconducting devices move from the research laboratory to commercial applications. Claude cycle refrigerator/liquefiers are most commonly used for producing the liquid helium used today and some small units built by Air Products and Chemicals, Inc. are in use as Maser coolers [1]; however, most of the small closed-cycle cryogenic coolers presently in use are of the regenerative type operating on cycles related to the Stirling or Solvay cycles. They are used for applications above 10K, because they have proven to be most economical and reliable for long term operation.

When closed-cycle regenerative type refrigerators are used, then one must consider the following:

. operation at temperatures above 4.2K
. temperature control (short and long term)
. refrigerator vibration
. heat transfer mechanism to refrigerator
. size of refrigerator
. need for electrical power and heat rejection

Many of these problems have been addressed in adapting regenerative cryocoolers to a wide range of applications. The concepts that have been employed in solving these problems are described in this paper. These concepts can be considered to be the building blocks that are presently available to utilize regenerative cryocoolers in cooling new small superconducting devices. The paper also describes the characteristics of the refrigerators manufactured by Air Products and Chemicals, Inc.

2. Two Stage Displex^R Refrigerator

Figure 1 is a photograph of the CS-202 Displex refrigerator [2] which consists of the expander, separate compressor, and interconnecting gas and electrical lines. The helium compressor is a modified oil lubricated air conditioning compressor with an oil removal system which includes an adsorber.

The expander, which is shown disassembled in Figure 2, produces refrigeration by a modified Solvay cycle. It consists of a two-stage displacer with regenerator heat exchangers packed inside the displacer body. Pressure cycling is set by a rotary valve disc which sets the cycle rate at 144 rpm on 60 cycle power. Piston motion is controlled by a pneumatic dash pot which also dissipates the work energy produced in the refrigeration cycle. It is the lack of mechanical linkages that enables long life and high reliability to be achieved. The cycle timing is such that the unit runs smoothly and is quiet; however, the reciprocating inertia of the piston must be considered in applications that are extremely sensitive to vibration. Recommended maintenance consists of changing the expander piston seals and valve disc, and compressor adsorber at 9,000 hour intervals.

Figure 3 is a curve showing the cooling capacity of the CS-202 refrigerator. If the refrigerator is operating in a vacuum with no heat load, the first stage will operate at about 35 K and the second stage at just under 10 K. The rated capacity of the unit is two watts at 20 K plus seven watts at 77 K. As the curve shows, there is a slight influence of the first stage heat load on the second stage temperature for first stage temperatures below 80 K. Temperatures above 80 K cause a significant reduction in second stage performance.

Two larger refrigerators are also presently available. The CS-208L has a capacity of ten watts at 20 K and the CS-227 has a capacity of fifty watts at 20 K. It is possible to operate a multiplicity of small expanders with one of the larger compressors.

3. Minimum Temperature of Regenerative Type Refrigerator

Work on reducing the minimum temperature of regenerative type refrigerators has followed several paths. Work on optimizing the design of a conventional lead shot regenerator and the cold end heat exchanger was pursued by Gifford [3] which resulted in a temperature of 6.8K being achieved on a two stage Gifford-McMahon unit.

Several efforts have been directed at improving the thermal storage capacity of the regenerator matrix. The use of rare earth materials has been studied by Moore [4]. Fleming [5] considered using helium adsorbed on charcoal, stored in small glass spheres, and stored in a surrounding cylinder. The third concept was tried on a Gifford-McMahon unit which operated at 7.6K vs. 7.7K with standard lead shot.

The most successful efforts to reduce the minimum temperature have consisted of adding a third stage of expansion. Stuart et. al. [6] reported a temperature of 6.5K in a Gifford -McMahon cycle unit. Daniels and duPre [7] reported on testing of a three stage Stirling cycle unit with three different regenerator materials. A temperature of 9.0K was reached with a conventional lead regenerator, 8.5K was reached with charcoal, and 7.8K was reached with europium sulfide. Daniels and DuPre expressed the opinion that the higher pressure ratio at which the Gifford-McMahon (and Solvay) cycle units typically operate compared with Stirling cycle units accounts for their lower temperatures. Cowans [8] built a three stage Vuilleumier Cycle refrigerator with a stored helium regenerator; however, internal leaks prevented successful operation.

There has been essentially no commercial market to date for small 7K refrigerators; thus it is premature to say which if any of the approaches that have been tried is best.

Certainly there is room for improvement in terms of minimum temperature and efficiency. It is unlikely that the efficiency of regenerative type refrigerators near their minimum temperature will be as good as Brayton cycle machines; thus their use will be limited to applications that require less than a few watts at temperatures below 10K.

4. 4.3K JT Loop

Figure 4 is a flow sheet of the Model CS-308 presently being built by Air Products and Chemicals, Inc. which shows a helium JT (Joule-Thomson) loop which is precooled by a CS-208L expander that produces 10W @ 20K plus 30W @ 77K. In addition to providing refrigeration at 4.3K, it has the advantage of having a stream of cold gas which can be used to transport the refrigeration that is available at each temperature level to remote points where it can intercept heat leak. This feature can also be used to separate the refrigerator from the object being cooled by transferring the cold gas through a flexible vacuum jacketed transfer line, thus helping to isolate the vibration inherent in the refrigerator.

The compressor that supplies gas to the cold end is a multi cylinder oil lubricated air conditioning compressor. One cylinder compresses the JT return flow from 15 psia to 75 psia where it joins the return from the expander to be compressed to 275 psia.

The Jet Propulsion Laboratory has been operating 1 watt 4.3K systems similar to this for more than ten years with a very good record of reliability. It is hoped that W. Higa, who is scheduled to attend this meeting, will give an updated report on their experience.

5. Other Cold Stages

Other methods of bridging the gap from the 15K temperature level where regenerative type coolers have reasonable efficiency to 4.2K that have been or are being tried are Simon Cooling and Dielectric refrigeration. Gifford et. al. [9] reported on a Simon expansion device used with a Gifford-McMahon cycle refrigerator that produced about .25 L of liquid helium after precooling gas at about 2,500 psi to less than 12K. This produces liquid in batches, but presumably a dual system could provide continuous refrigeration. From a manufacturing standpoint it does not appear as attractive as the JT loop because of the switching mechanisms required and because another high pressure stage of compression is required.

Development of a Dielectric cold stage was initiated by Lawless [10] and work continues today at Los Alamos. It is hoped that W. A. Steyert will give a report on this work during the present meeting.

6. Refrigerated Helium Dewar

Figure 5 is a schematic drawing showing a two stage Displex refrigerator mounted on a helium dewar to reduce the boiloff rate [11]. A dewar similar to this but with a warm bore tube extending all the way through and having the refrigerator direct mounted was built and tested. With six 30 Ga instrument leads in one of the neck tubes the boiloff rate was 10.1 ml liquid/hr. When the wires were removed the boiloff rate dropped to 3.8 ml liquid/hr, which enabled the customer to operate for more than ten months before adding more liquid helium.

During the test program it was demonstrated that the expander piston could be removed from the cold cylinder, serviced, and reinstalled without warming the piston. A total of 50 ml of liquid helium vented as a result.

This concept is most attractive for applications where there is no heat generated at 4.2K and where there are no lead wires to the liquid helium. If the heat loss at 4.2K is more than a few mw, then the boiloff rate of helium is high enough that the sensible heat intercepts heat leak and the refrigerator is not needed.

In addition to providing a constant temperature bath, the liquid helium dewar has the advantage of having an inventory of stored refrigeration. If a cold stage is added to a regenerative machine such as a JT loop that is cold enough to recondense the helium, then one can combine the advantages of liquid helium with those of a closed-cycle refrigerator and, at the same time, have built in a high degree of reliability.

7. Vibration Isolation

Some low temperature devices are sensitive to the vibration of regenerative coolers which all have reciprocating displacers. Figure 6 is a photograph of a Heli-Tran[R] refrigerator unit which has a flexible helium transfer line [12], [13]. By having part of the helium stream make a return pass through the transfer line to intercept heat leak, it is possible to maintain 4.2K with less than 1 L/hr liquid helium consumption. The technologies of this transfer line can be used to transfer refrigeration in a closed-cycle cooler and, at the same time, provide vibration isolation.

A second concept for isolating vibration is shown in Figures 5 and 7. The unit shown in Figure 7 has been successfully used to conduct Mossbauer experiments at 10K. The principal that is employed is to mount the refrigerator on a separate base from the cryostat and thermally couple the two with a cold helium gas convective circulation loop [14]. There is a loss of about 25% of the refrigeration produced with a modest sized heat exchange loop.

Figure 8 is a drawing of a gas well cooled by a two stage Displex refrigerator which is used with a Faraday balance. The cold gas provides good heat transfer while keeping the object being cooled both mechanically and electrically isolated from the refrigerator.

8. Temperature Control

Temperature fluctuations in a regenerative cycle cooler are both short term and long term. The short term cycle corresponds to the reciprocating rate of the expander, 144 rpm on 60 Hz and 120 rpm for 50 Hz power for the Displex refrigerator. The low specific heats of the refrigerator materials at 10K result in a temperature change of about 1K each cycle at the refrigerator cold tip. Long term temperature changes are due to changes in heat load, ambient temperature, and wear of the refrigerator. Experience has shown that refrigerator wear results in temperature changes of several tenths of a degree within recommended maintenance intervals.

Two adapters have been developed to reduce short term temperature cycle. A one inch long rod of pure lead attenuates the fluctuation at 10K by a factor of 10. This has the desirable characteristic of having a very high thermal conductivity, but it has the disadvantage of adding 30 minutes to the cooldown time of the refrigerator. The second adapter that has been developed is multiple layers of indium and mylar. This is compact and has a relatively small thermal mass. It reduces the short term temperature cycle at 10K to about .005K, but one pays the penalty of losing half the refrigeration that is produced at temperature between 10K and 20K.

Control of temperature over a long period of time requires an active temperature controller. Most commonly used is one which employs Au .07% Fe vs. Kp thermocouple and has a 24 hour stability rating of $\pm$ 0.2K. For more precise requirements silicone diode sensors are commonly used in conjunction with a controller that has a 24 hour stability of $\pm$ .02K.

For applications which use the JT loop, the temperature can be controlled by regulating the vapor pressure. A controller of this type with vacuum as an absolute pressure reference has been successfully employed to maintain a stability of $\pm$ .01K at 3.9K to 4.2K in the small Claude cycle Maser coolers built by Air Products and Chemicals, Inc. [1].

9. Summary

The task of matching a refrigeration system with a given application starts with understanding the requirements of the application and the characteristics of available refrigeration systems. It is hoped that this paper will help potential users of closed-cycle regenerative coolers to generate a list of requirements and, at the same time, suggest the concepts that are presently available to solve certain problems.

In the long run the best refrigeration system for a given application is the one that meets performance and reliability requirements at minimum capital and operating cost.

10. References

[1] Zeitz, K., and Meier, R. N., The evolution of helium refrigerators at Air Products and Chemicals, Inc., Low Temperature Refrigeration, p. 219 (Boston Technical Publishers, Inc., Cambridge, MA, 1967).

[2] Longsworth, R. C., A modified Solvay-cycle cryogenic refrigerator, Advances in Cryogenic Engineering, 16, p.195 (Plenum Press, N.Y., 1971).

[3] Gifford, W. E., Low temperature refrigerator design optimization, Tech Report AFFDL-TR-70-158 (Wright-Patterson AFB, Ohio, 1970).

[4] Moore, R. W., Jr., An investigation of thermal regenerators for the 4 to 20K temperature range, Tech Report AFFDL-TR-70-64 (Wright-Patterson AFB, Ohio, 1970).

[5] Fleming, R. B., Regenerators in cryogenic refrigerators, Tech Report AFFDL-TR-68-143 (Wright-Patterson AFB, Ohio, 1968).

[6] Stuart, R. W., Cohen, B. M., and Hartwig, W. H., Operation and application of a three-stage closed-cycle regenerative refrigerator in the 6.5K region, Advances in Cryogenic Engineering 15, p. 428 (Plenum Press, N.Y., 1970).

[7] Daniels, A., and du Pre, F. K., Triple-expansion Stirling-cycle refrigerator, Advances in Cryogenic Engineering 16, p. 178 (Plenum Press, N.Y., 1971).

[8] Cowans, K. W., 5K Vuilleumier cryogenic refrigerator, Tech Report AFFDL-TR-72-10 (Wright-Patterson AFB, Ohio, 1972).

[9] Gifford, W. E., Kadaikkal, N., and Acharya, A., Simon helium liquifaction method using a refrigerator and thermal valve, Advances in Cryogenic Engineering 15, p. 422 (Plenum Press, N.Y., 1970).

[10] Lawless, W. N., Dielectric cooling technology: 15-4.2K, Tech Report AFFDL-TR-73-149 1, p. 147 (Wright-Patterson AFB, Ohio, 1973).

[11] Longsworth, R. C., Application of a 20K refrigerator to reducing boiloff rate of a liquid helium dewar (Proceedings of the Fifth International Cryogenic Engineering Conference, Kyoto, p. 390, IPS Science & Technology Press, London, 1974).

[12] Kadi, F. J., Longsworth, R. C., and Meier, R. N., Flexible cryogenic liquid transfer system and support means therefor (U. S. Patent 3,706,208).

[13] Longsworth, R. C., Liquid cryogen transfer system (U. S. Patent 3,696,627).

[14] Longsworth, R. C., Vibration-free refrigeration transfer (U. S. Patent 3,894,403, 1975).

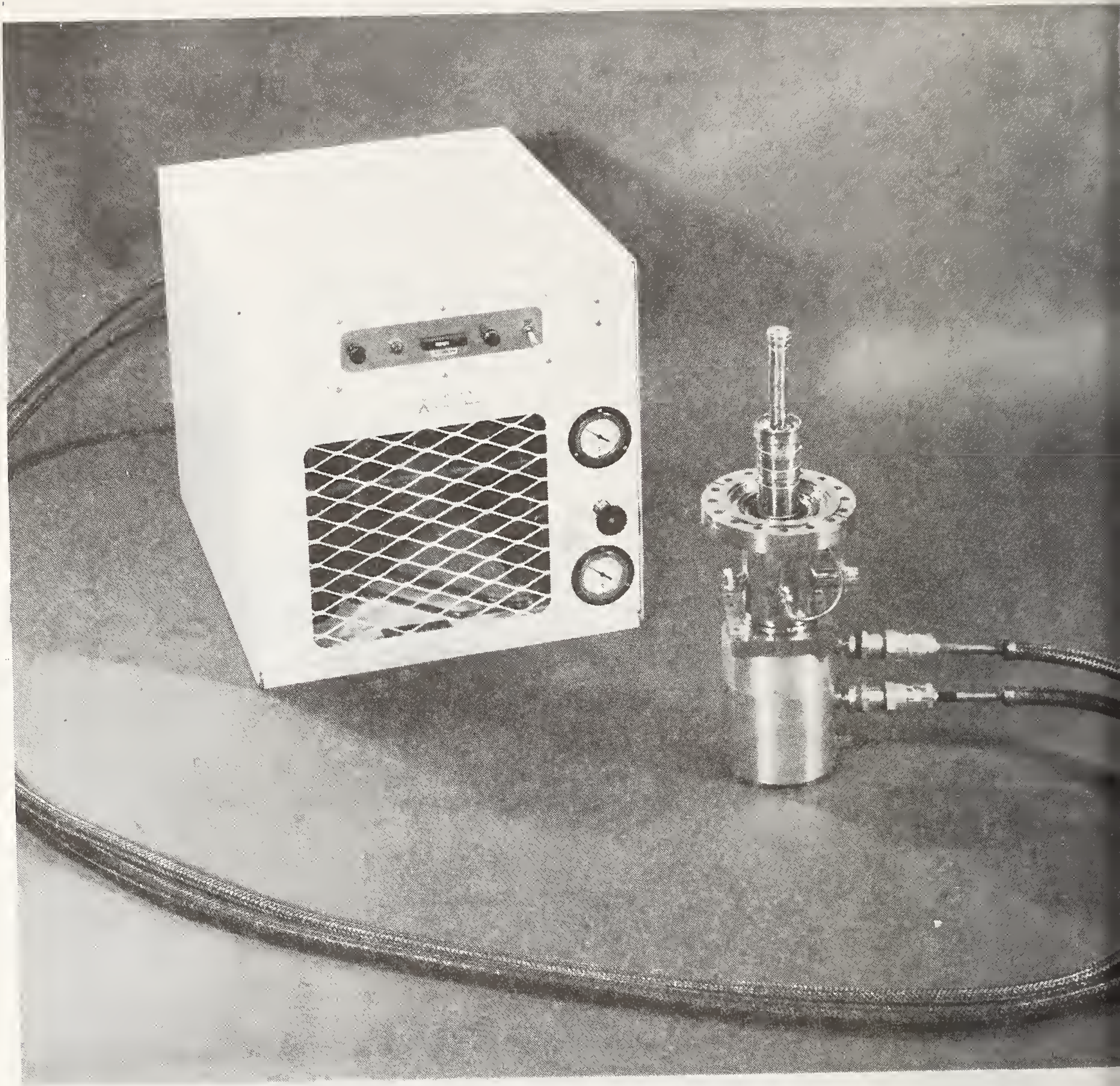

Figure 1. CS202 Displex Refrigerator

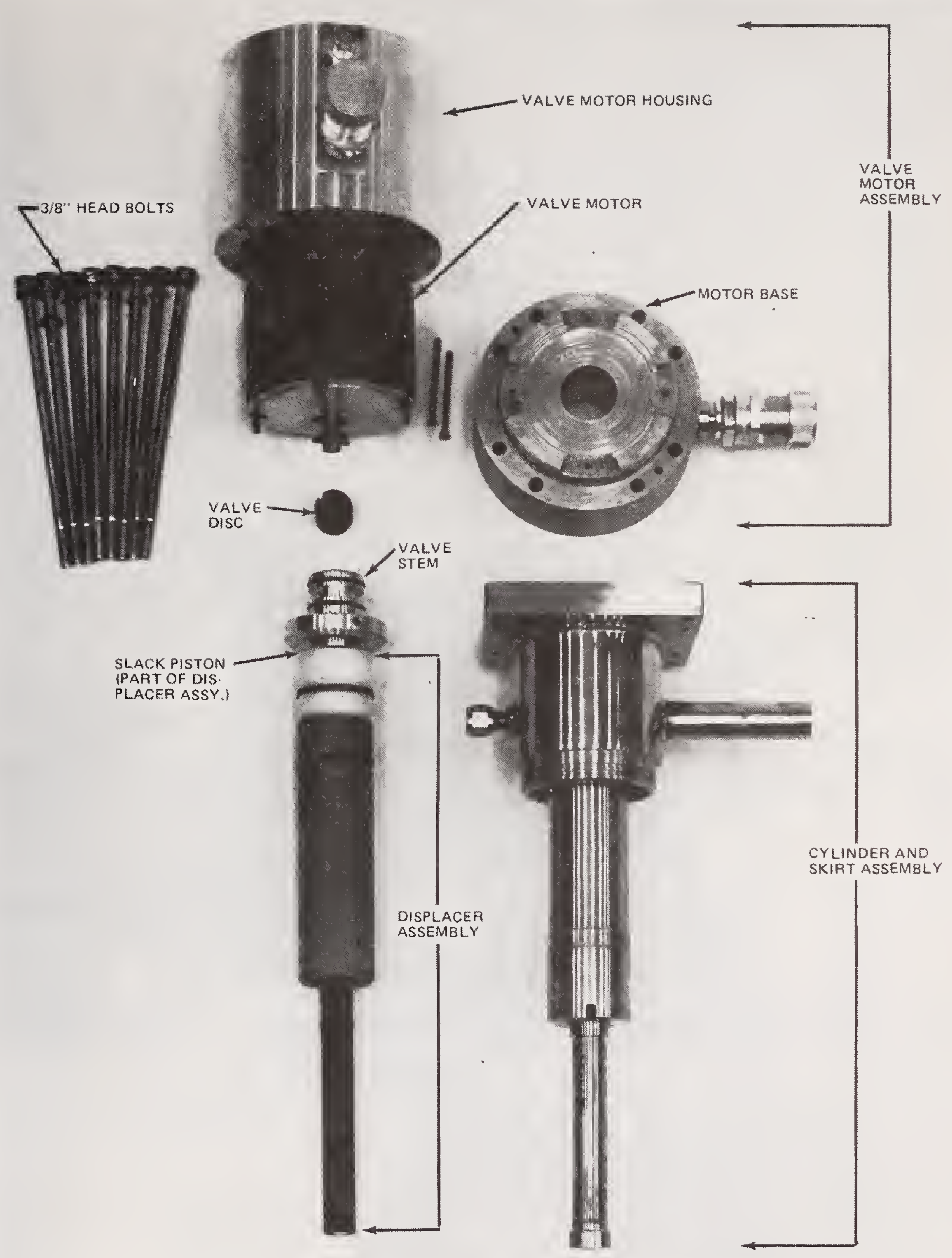

Figure 2. CS202 Expander Components

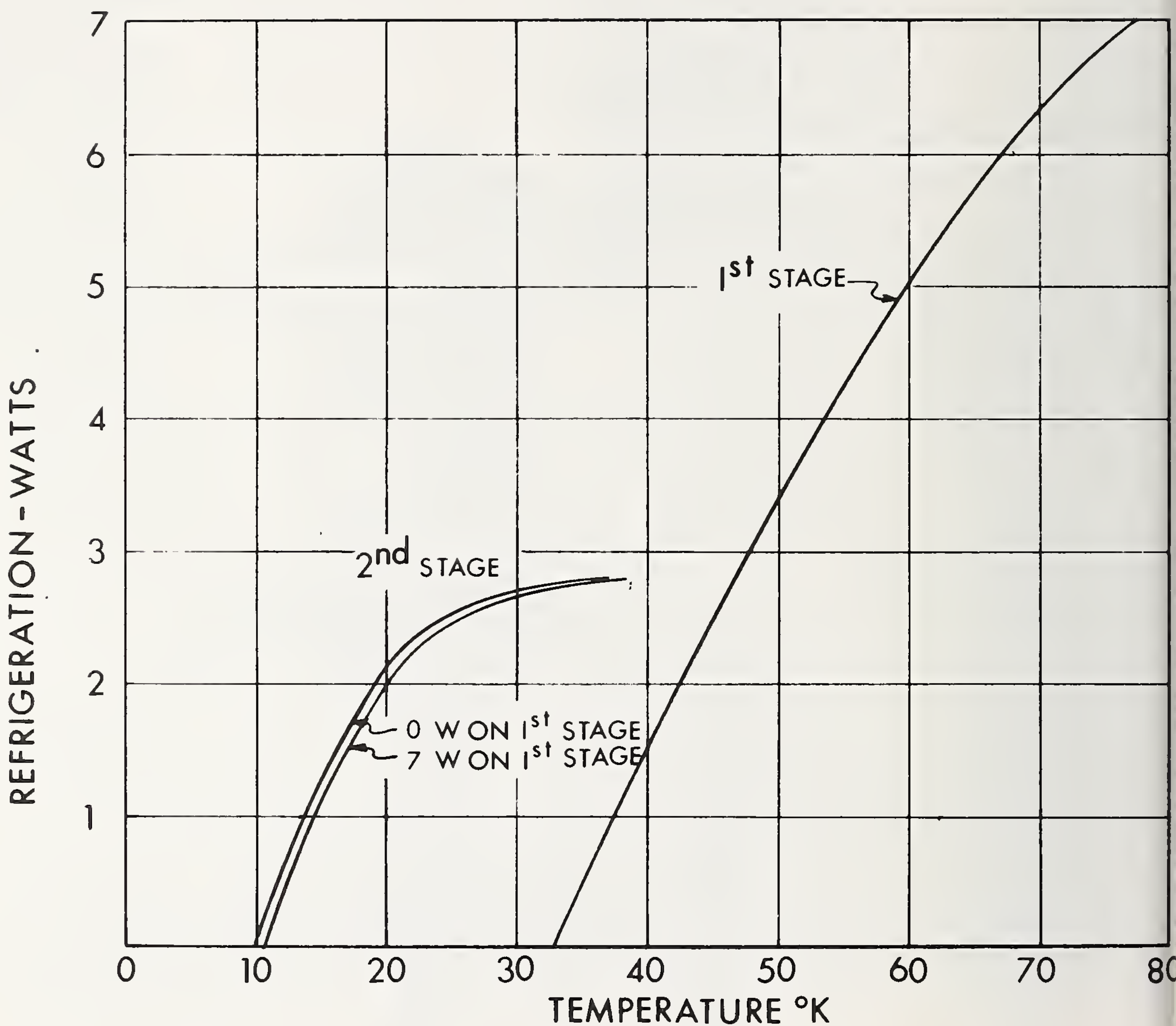

Figure 3. CS202 Refrigeration Capacity Vs Temperature.

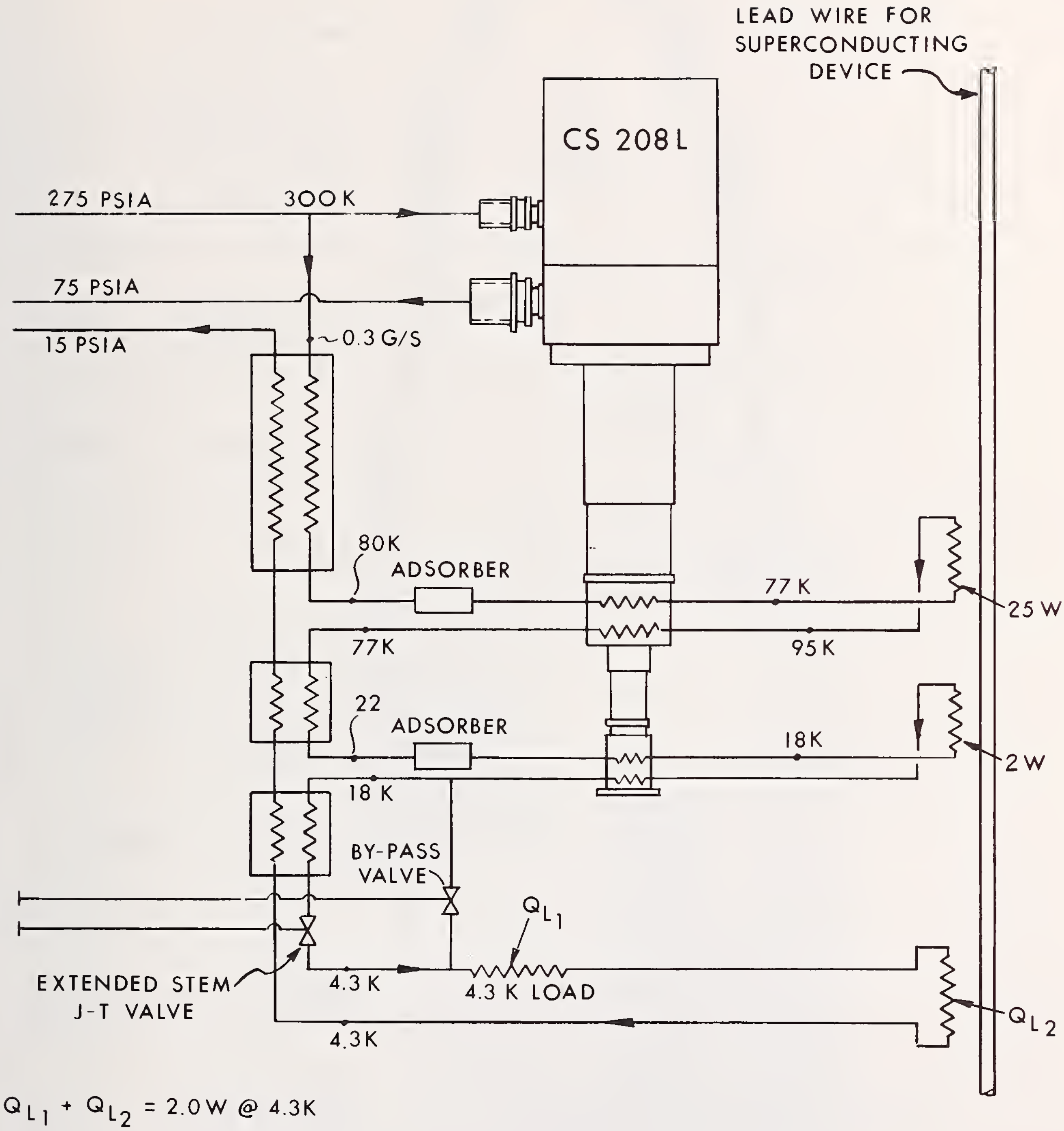

Figure 4. Flow Schematic of Two-Stage Displex Refrigerator with 4.3 K. JT Loop, Model CS-308

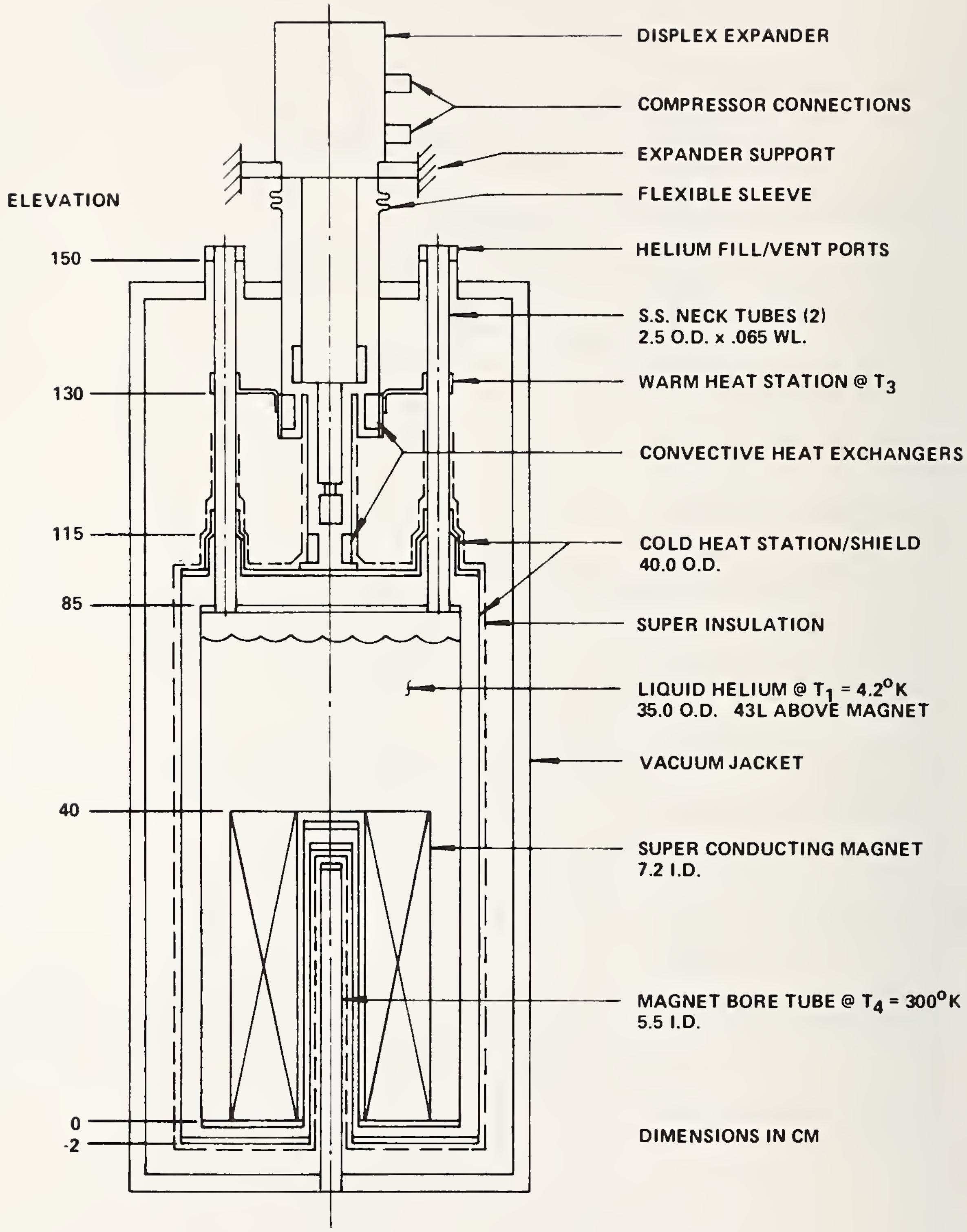

Figure 5. Helium Dewar with Displex Refrigerator to Reduce Boiloff Rate

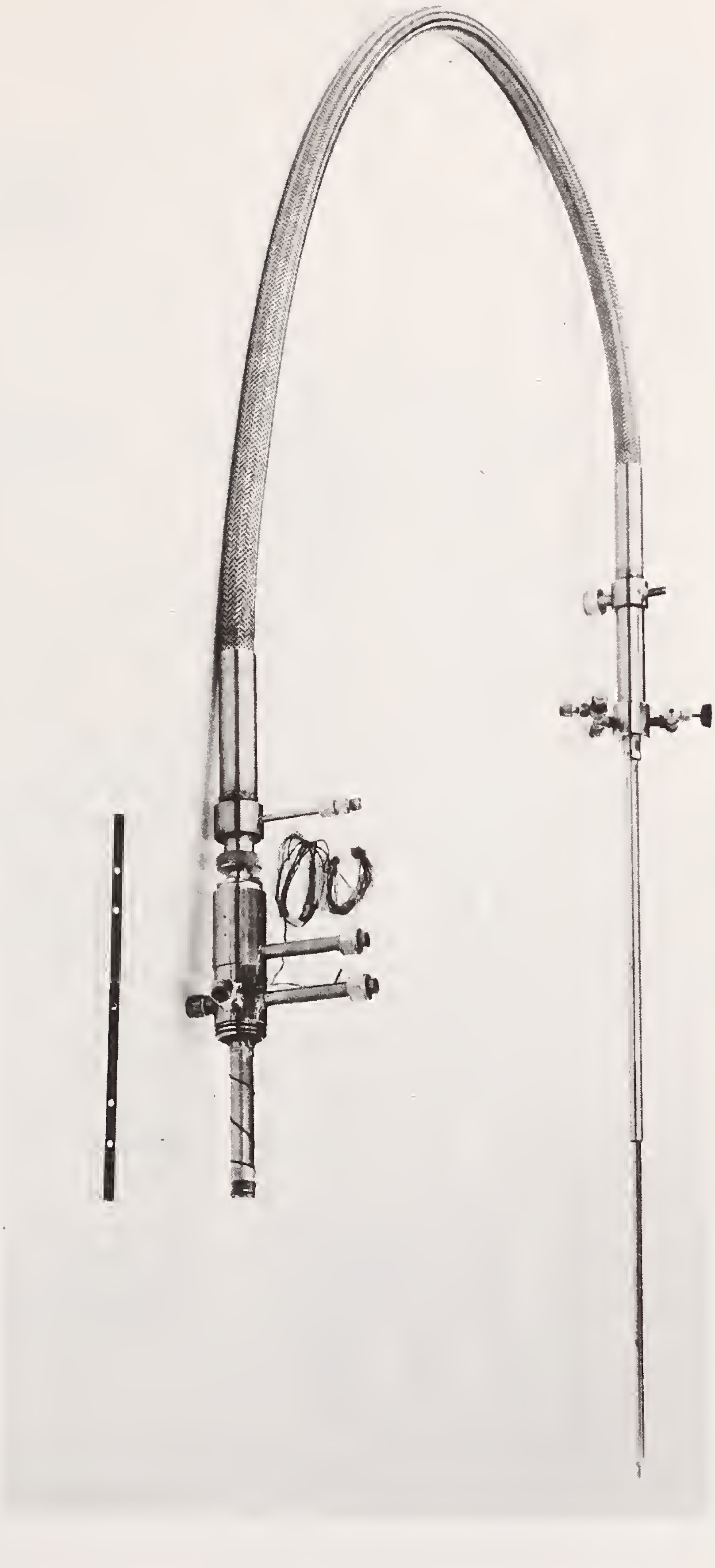

Figure 6. Heli-Tran Refrigerator Employing Flexible Helium Transfer Line

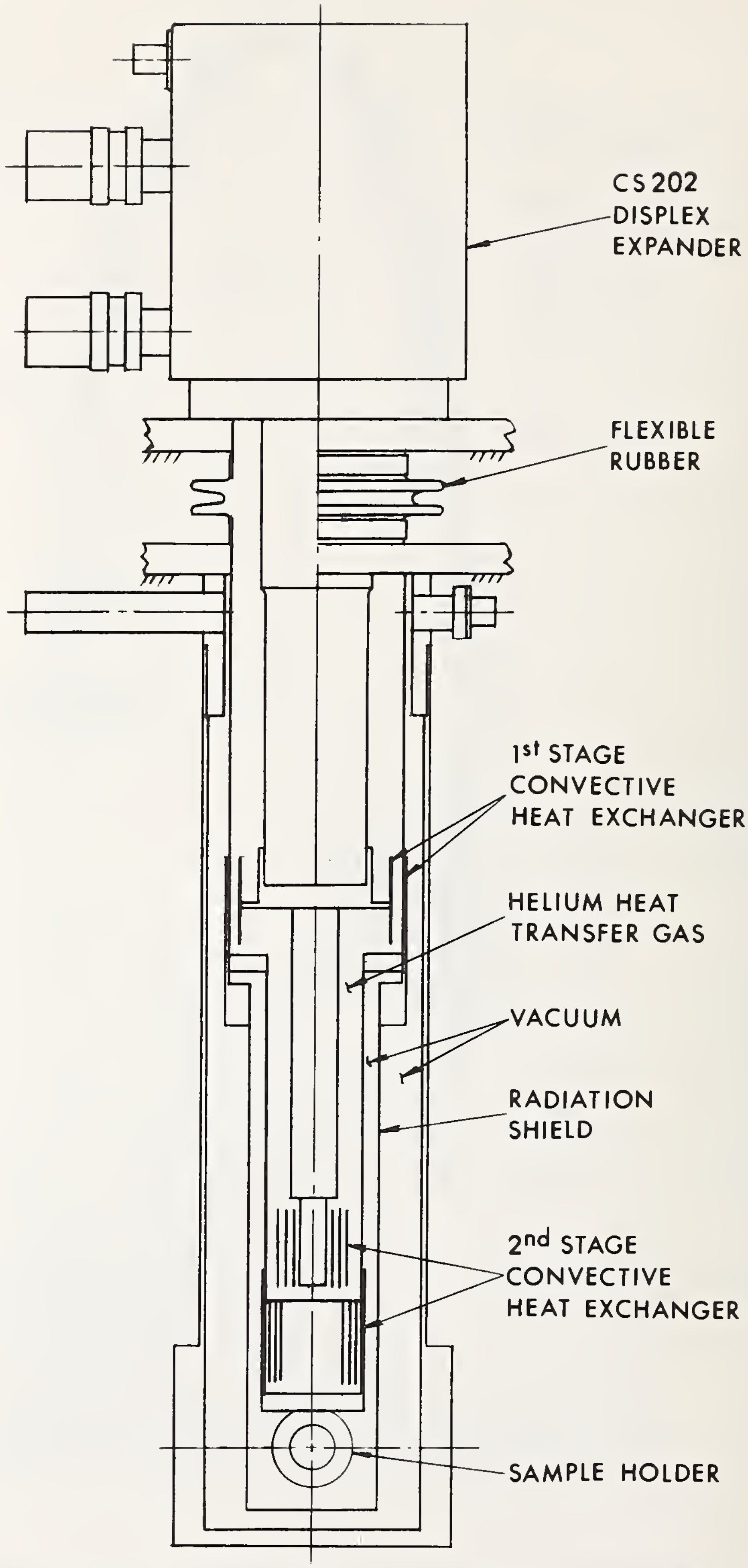

Figure 7. Model DMX-20 Interface for Mossbauer Spectroscopy Employing Cold Gas Convection for Vibration Isolation

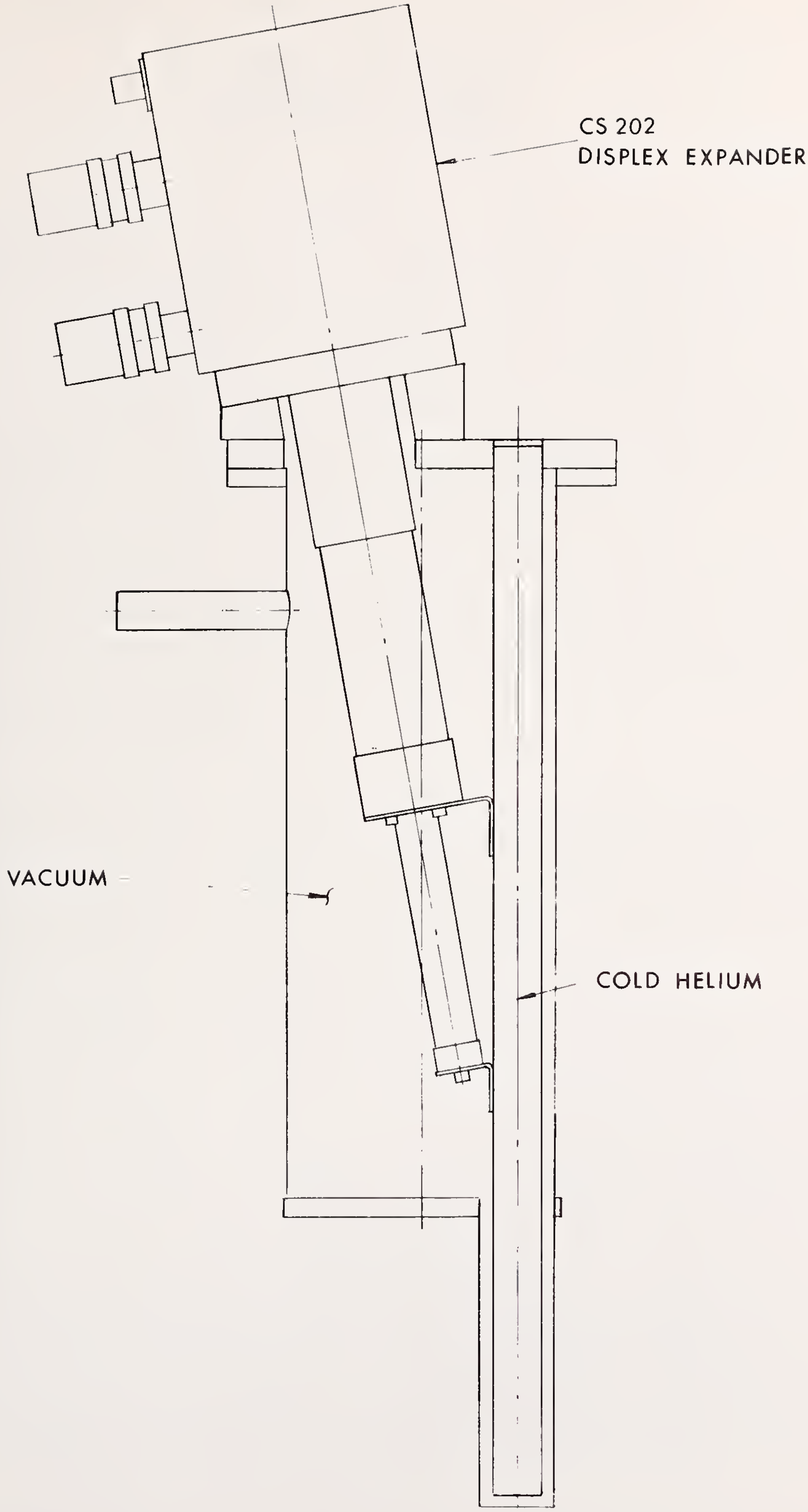

Figure 8. Cold Gas Well Cooled by Displex Refrigerator for Faraday Balance

Operation of a SQUID in a Very Low-Power Cryocooler *

J.E. Zimmerman and Ray Radebaugh
Cryogenics Division
National Bureau of Standards
Boulder, Colorado 80303

Abstract

A point-contact Nb SQUID has been operated a total of several hundred hours at a temperature of about 8.5 K in a low-power Stirling cryocooler with a four-stage displacer. The system requires the order of 15 W of mechanical drive power. Except for the drive motor, the entire unit is non-magnetic, and the displacer and cold cylinder are made of non-conducting plastics, to minimize ferromagnetic and eddy-current fields, which would interfere with the operation of the SQUID when used as a magnetometer. With the system operating in the earth's field B_e, an ac interfering signal of about 10^{-5} B_e (i.e., $\sim 10^{-9}$ T) at the SQUID was seen at the 1 Hz operating frequency of the cryocooler. This signal was probably caused by rotation of the SQUID in the earth's field due to pressure flexing of the cold cylinder, although magnetic impurities in the moving parts would also contribute. Measurements of the complete self-generated interference spectrum, and experiments aimed at reducing interference to levels of 10^{-12} T and below are in progress.

We have previously published an essentially theoretical discussion of the operation of a very-low-power superconducting device, such as a SQUID, in a closed-cycle cryogenic refrigerator (cryocooler) [1,2]. It was pointed out that the refrigeration capacity required for the devices themselves is negligible, and the capacity required to cool the electrical leads is small. On the other hand, a SQUID magnetometer, in particular, places a rigorous upper limit on the allowable level of magnetic and mechanical interference.

It is assumed, of course, that all of the major heat loads (room temperature radiation, and heat flow along electrical leads and support members, for example) are intercepted and pumped out at one or more higher-temperature refrigeration points, rather than at the cold end. In fact, in most small-device applications, it would seem that the refrigeration requirement at the cold end is almost incidental, if the heat loads at the higher-temperature points are handled efficiently. Obvious though this point is, cryocoolers are very often described in terms of cold-end refrigeration capacity only.

In liquid-helium cryostats, higher-temperature refrigeration is provided by the helium vapor, whose total refrigeration capacity, uniformly distributed in temperature, is about 70 times that of the evaporating liquid itself. In a cryocooler one has the opportunity, in principle, of optimizing the distribution of refrigeration at several points between ambient and low temperature regions. Furthermore, a cryocooler is required to cool only the device

---

* Contribution of the National Bureau of Standards, not subject to copyright.
Supported in part by the Naval Electronics System Command.

itself and not a large liquid reservoir. Thus, for two reasons, estimates of refrigeration requirements based on experience with liquid-helium cryostats may be quite conservative.

Since there is a pervasive casual tendency to specify cryocoolers only by their refrigeration capacity at cold end, it may be useful to illustrate this point with a hypothetical, but fairly typical, example. A one-liter plastic liquid-helium cryostat with a single vapor-cooled radiation shield at a steady-state temperature of 150 K might have a heat leak to the helium, as measured by the evaporation rate, of 30 mW. Here the evaporation rate and the shield temperature are mutually interdependent. That is, a lower shield temperature would reduce the evaporation rate, but then the flow of cold vapor would not maintain the shield temperature at the lower value. On the other hand, if a cryocooler were used to cool the same one-liter volume and the same radiation shield, it could be designed to maintain the shield at 50 K instead of 150 K. If the heat leak to the one-liter volume were primarily thermal radiation, then it would be reduced by a factor of 81, from 30 mW to about 0.4 mW. If there were appreciable thermal conduction as well as radiation, the comparison would not be quite so dramatic, but still impressive.

We also described [1,2] an experimental cryocooler particularly suited for operating very low-power high-T_c superconducting devices. This cryocooler was a three-stage split Stirling-cycle [3] machine, which was operated more than 6000 hours at 1 stroke-per-second, and reliably maintained a temperature of 13 K or less for uninterrupted periods of up to 5 weeks. Its novel features were (1) non-magnetic, non-conducting plastics for the displacer and cold cylinder, (2) low operating power, and (3) mechanical simplicity. Solid nylon rod was used for the displacer and commercial spun-glass epoxy ("G-10") tubing for the cold cylinder. The input power of 50 W to an electric drive moter with about 15 W mechanical output power was a factor of 10 or more smaller than the power requirements of any previous machine for this temperature range, so far as we are aware. Regenerative heat exchange occurred in the narrow radial gap between the nylon displacer surface and the inner surface of the cold cylinder. Gap regeneration was used in Stirling's original engine in 1816, and, being mechanically trivial, is commonly used in miniature engines described in hobbyists magazines.

A machine similar to ours (plastic displacer, gap regeneration, and very low power) was built several years ago by du Pre and Daniels [4]. They achieved 130 K with a two-stage displacer and 98 K with a conical displacer. The latter may be regarded as the limiting case of a displacer with an infinite number of stages.

The temperature maintained by our three-stage machine is well within the range of high-T_c superconductors such as NbN and Nb_3Sn. Practical devices have been made to operate at 14 K and above [5].

A new four-stage displacer and cold cylinder (Figures 1, 2 and 3) were built to replace the three-stage unit. With this modification and some minor refinements, the machine has maintained around 8.5 K for a total of several hundred hours of operation. The four sections of the nylon displacer were, respectively, 4.7, 9.5, 19 and 28 mm diameter and 15, 10, 12 and 12 cm long. The cold cylinder was made from sections of commercial spun-glass epoxy tubing ("G-10") with 2.4 to 4 mm wall thicknesses. The displacer sections were carefully machined to fit the cylinder with almost no radial clearance, except for a few cm of the

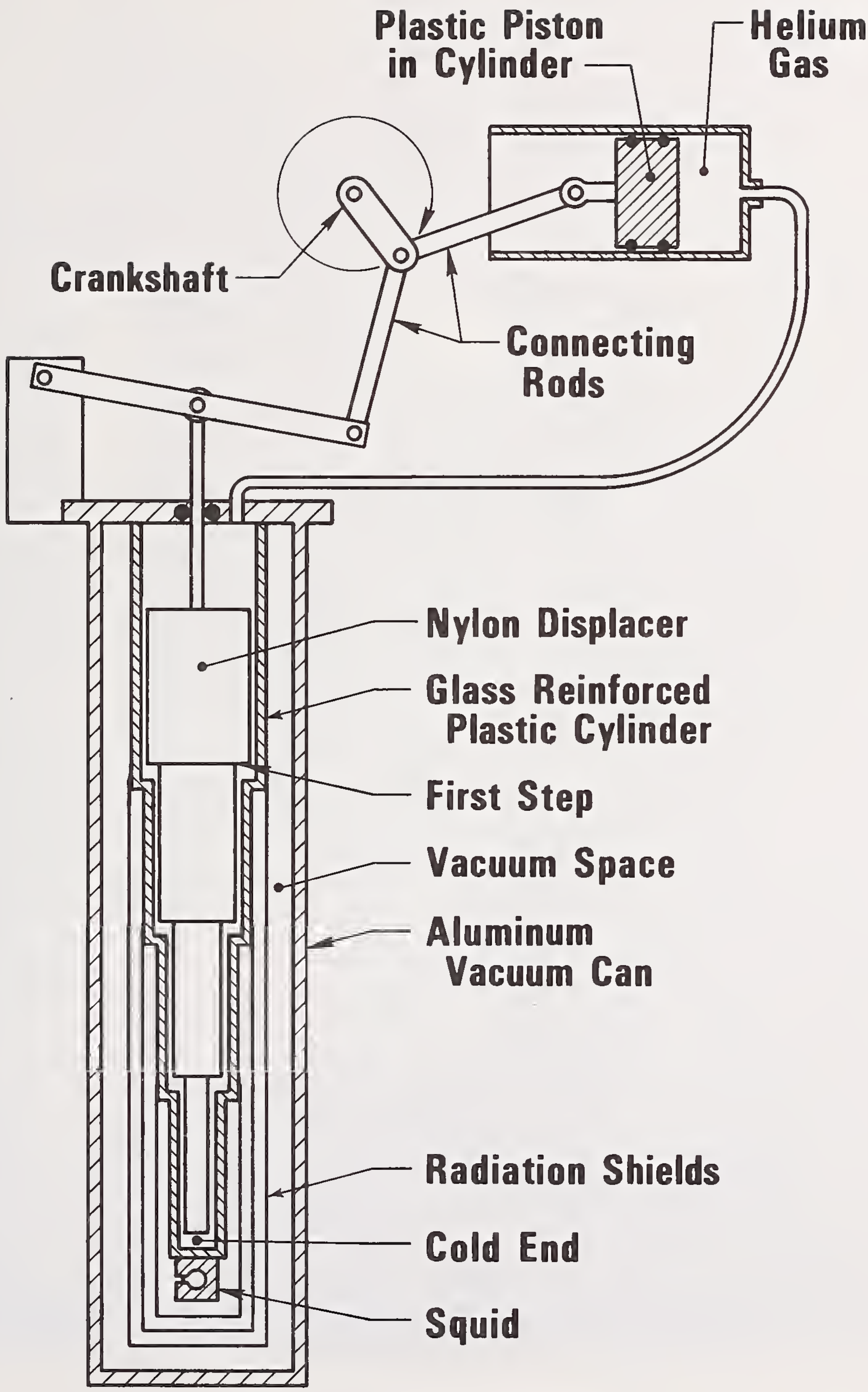

Figure 1. Schematic diagram of low-power SQUID cryocooler system, not to scale. Displacer dimensions and other data are given in text.

Figure 2. Cold cylinder and displacer of 8.5 K cryocooler. Left to right: 30 cm scale, nylon displacer, glass-reinforced epoxy cylinder with inner radiation shields in place, outer radiation shield, and vacuum jacket.

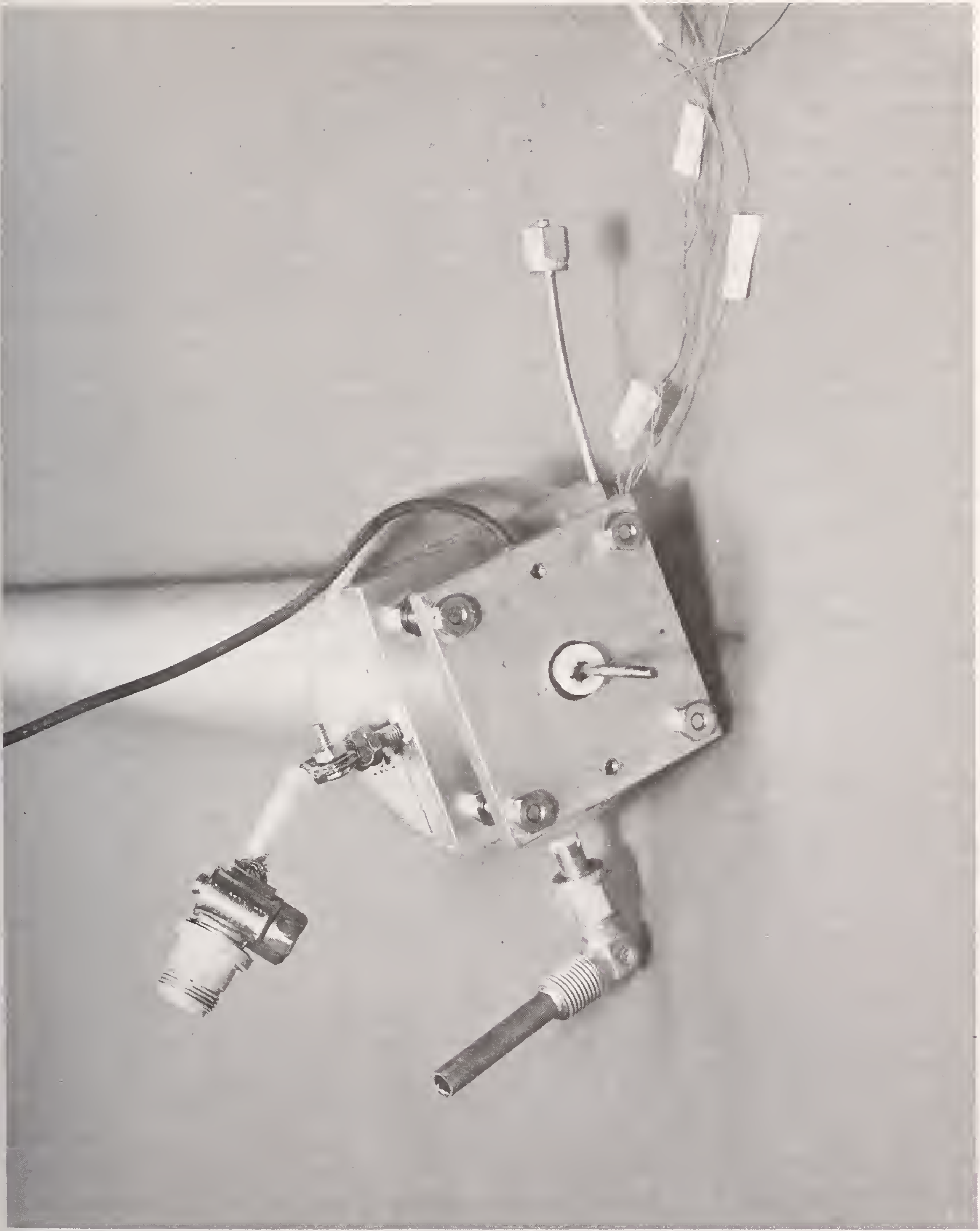

Figure 3. Room-temperature end of cold cylinder assembly. Clockwise from left: gas line to working cylinder, gas-thermometer line, thermocouple wires, vacuum connection, and rf SQUID connector.

large end where about 0.1 mm radial clearance was provided. During cooldown, differential contraction of the nylon rods and the glass-epoxy tubes provides about one percent radial clearance, except at the large (warm) end. This technique of fitting the displacer to the cylinder is quite simple, and it also gives the minimum possible regenerator gap volume, which is important for achieving minimum temperature. As in the earler model, the exact lengths of the sections were calculated to take account of differential contraction, so as to give precise longitudinal fit in each section after cooldown. Here the fitting technique is not so simple. The important thing is to avoid any appreciable dead volume at the small (cold) end. Slight misfitting at the larger steps seemed to have little effect on the cold-end temperature.

Our measurements of the various components of stray heat inputs, including "shuttle heat," reported separately [6], led us to conclude that lower temperature would be achieved by reducing the displacer stroke. Thus, the four-stage displacer has been operated with a 7 mm stroke, as compared to the 12 mm stroke of the three-stage model. Other operating parameters were essentially the same for both models, namely: operating speed 1 Hz, average pressure 0.5 MPa (5 atm), and piston displacement 38 cm^3. The average pressure, the speed, and the displacer stroke could be varied considerably around these values without changing the cold-end temperature very much. It was found that the values of these three parameters giving lowest ultimate temperature were generally lower than the values giving fastest cooldown -- a result not entirely unexpected.

The machine was mostly operated with the cold end down. However, it was also operated for a few hours with the cold cylinder horizontal, and also with the cold end up. In the latter case, the steady-state temperature was about 0.2 K greater than for the other two positions, e.g., 8.7 K instead of 8.5 K. We did not investigate the reason for this small gravitational effect.

Temperature of the first (large) step was measured with a thermocouple, and the cold-end temperature was measured by a helium gas bulb clamped directly to the small (1 cm diameter) end of the cold cylinder. A simple permanently-adjusted point-contact rf-biased Nb SQUID was clamped to the gas bulb. Low-conductivity parallel wires were used as rf coil leads, rather than the usual copper coaxial line, in order to reduce heat leak. Temperature of the first step stabilized at values of 180 K for average pressure 0.5 MPa to 150 K for average pressure 0.7 MPa. The lowest stable cold-end temperature was obtained at about 0.5 MPa, as noted above.

Our present data on magnetic and mechanical interference are meager. With the SQUID oriented North/South in the earth's magnetic field, there was a 0.5 nT ac component in the output at the 1 Hz operating frequency of the cryocooler. This was most likely due to pressure flexing of the cold cylinder, which would result from lateral inhomogeneities in wall thickness or elastic properties. Other lower-amplitude noise components at higher frequencies have not yet been measured or identified. The 0.5 nT interference at 1 Hz is only about 10^4 times greater than typical SQUID sensitivities. If the hypothesis of pressure flexing is correct, then this component could perhaps be reduced by a factor of 100 by correcting the inhomogenieties in the cylinder walls. Another factor of 100 could probably be achieved by accurately measuring the wave shape and amplitude and subtracting it from the output. In any case, this particular interference would not so seriously affect measurements at frequencies other than 1 Hz.

Measurements of the full self-generated interference spectrum for the system remain to be done. At this point we believe that a useful low-cost system can be built for magnetic measurements in the picotesla range. Similar systems could be built for other device applications [2]. The Josephson voltage standard [7] seems a particularly good candidate.

Just as the point contact made Josephson devices such as SQUID's available to everyone who took the time to understand a simple but unfamiliar principle, the work reported here demonstrates that superconducting temperatures are also available to everyone who takes the time to acquire modest skill with a lathe.

References

[1] J.E. Zimmerman, R. Radebaugh and J.D. Siegwarth, "Possible Cryocoolers for SQUID Magnetometers," Superconducting Quantum Interference Devices and Their Applications. H.D. Hahlbohm and H. Lübbig, eds., Walter de Gruyter, Berlin (1977) p 287.

[2] J.E. Zimmerman, R. Radebaugh and J.D. Siegwarth, "Refrigeration for Small Superconducting Devices," Conf. German Refrigeration Society, Munich (October 1976) (in press).

[3] G. Walker, Stirling-Cycle Machines, Oxford University Press (1973).

[4] F.K. du Pré, A. Daniels, "Gap-Regeneration Method for Stirling and Similar Cycles," Progress in Refrigeration Science and Technology, Vol. 1, Proc. XIII International Congress of Refrigeration, Wash. D.C., (1971) AVI Publishing Co., Inc. Westport, Connecticut, p 137 (1973).

[5] M. Beasley in this publication.

[6] R. Radebaugh and J.E. Zimmerman, in this publication.

[7] L. Holdeman, in this publication.

SHUTTLE HEAT TRANSFER IN PLASTIC DISPLACERS AT LOW SPEEDS *

Ray Radebaugh and J. E. Zimmerman
Cryogenics Division
National Bureau of Standards
Boulder, Colorado 80303

ABSTRACT

Previous analyses of shuttle heat transfer in refrigerators with displacers have neglected radial temperature gradients in the displacer or cylinder. Such analyses are valid when the gas gap is the dominant thermal resistance. We show that with plastic materials for the displacer and cylinder, shuttle heat transfer can be dominated by the thermal penetration depth of the plastic when operating at low speeds. An equation is derived for the shuttle heat transfer in such cases. Experimental data on shuttle heat transfer is obtained for temperatures down to 120 K for different strokes and speeds and the agreement with calculated values is good.

* Supported in part by the Naval Electronic Systems Command

SHUTTLE HEAT TRANSFER IN PLASTIC DISPLACERS AT LOW SPEEDS

Ray Radebaugh and J. E. Zimmerman
Cryogenics Division
National Bureau of Standards
Boulder, Colorado 80303

INTRODUCTION

The Stirling-cycle refrigerator described previously [1] requires no net refrigeration power to keep a SQUID cold. The lowest temperature reached is the point where the total refrigeration power is cancelled by various heat flows to the low temperature end. These heat flows come from several sources, including radiation, heat conduction down the displacer, regenerator inefficiency, and shuttle heat transfer. Radiation heat flow to the lowest temperature can be made negligible in most cases with good shielding. For temperatures somewhat above 10 K the regenerator inefficiency can be made fairly small. Thus the major heat flow in much of the refrigerator is from the conduction and shuttle processes. Shuttle heat transfer occurs when the displacer, with an axial temperature gradient, reciprocates inside a cylinder with a similar temperature gradient. Because shuttle heat transfer is a major source of heat leak, it must be well characterized in order to optimize the design of the refrigerator.

PREVIOUS WORK

Zimmerman and Longsworth [2] discussed shuttle heat transfer and derived an equation for it based on a simplified theory. Their theory contained four simplifying assumptions: (i) properties are only weak functions of temperature, (ii) heat capacity of the displacer and wall are infinite, (iii) negligible gas pressure cycling, and (iv) interaction of axial conduction effects in the displacer are neglected. For square-wave motion of the displacer they derive the equation

$$\dot{Q}_s = \frac{k_g \pi D S^2}{4t} \frac{\left(T_h - T_c\right)}{L} \tag{1}$$

for the shuttle heat transfer, where k_g is the thermal conductivity of the gas, D is the displacer diameter, S is the stroke length, t is the radial clearance, L is the length of the displacer, T_h is the hot temperature, and T_c is the cold temperature. For sinusoidal motion the average temperature drop across the gas gap is $2/\pi$ times that for square-wave motion. Hence for sinusoidal motion the average shuttle heat transfer becomes

$$\dot{Q}_s = \frac{k_g D S^2}{2t} \frac{\left(T_h - T_c\right)}{L} \tag{2}$$

More exact calculations may give different numerical doefficients, but the functional dependence of the shuttle heat loss on the various parameters will remain the same.

Harness and Neumann [3] calculated shuttle heat transfer when assumption (iv) was relaxed. The problem then becomes very complex and can be solved only by numerical integration of a second-order differential equation. Their results for the total heat flow differ from that of adding the static heat conduction down the displacer to the simple shuttle heat transfer equation given above. The difference ranges from 5 to 40%, depending on various parameters, and is not always of the same sign.

As far as we know, attempts to solve the shuttle heat transfer problem with any of the other three assumptions relaxed has never been done. However, we were concerned that assumption (ii) was not satisfied when the displacer and wall materials were of plastic and their operation was at the low speed of about 60 rpm. When the heat capacity of the displacer and wall are assumed to be infinite, radial temperature gradients are thus neglected. In high-speed operation little heat is transferred across the gas gap in each cycle. As a result, the surface temperature of the displacer and wall remain nearly constant in time and the assumption (ii) is satisfied. Temperature cycling of the surface does become important at low speeds. The use of plastic materials instead of metal increases the amount of temperature cycling because the lower thermal conductivity decreases the thermal penetration depth.

THEORY

In order to keep the problem from becoming too complex, we first make the following assumptions: (i) properties are nearly constant with temperature, (ii) thermal resistance of the gas gap is negligible, (iii) the effect of gas-pressure cycling is neglected, i.e., regenerative action is perfect and heat capacity of the gas in the gap is negligible, (iv) interaction of the axial conduction effects in the displacer and wall are neglected, and (v) motion of the displacer is sinusoidal.

The shuttle heat transfer is just the net enthalpy flow resulting from the motion of the displacer. Its temperature is higher during the hot-to-cold motion than during the reverse motion so enthalpy is transported toward the cold end. The net enthalpy flow is just equal to the heat transferred to the displacer during one-half the cycle over a length equal to the stroke. To evaluate this heat transfer we first let the wall have infinite heat capacity so that it has no temperature cycling. We relax this condition later. Because of assumptions (ii) and (iii) above, we can say that the surface of the displacer takes on the temperature of the wall adjacent to it at any moment in time. The sinusoidal motion of the displacer then causes a sinusoidal temperature fluctuation of the surface, provided the axial temperature gradient is constant over the distance of the stroke. The problem of sinusoidal temperature fluctuations on the surface of a semi-infinite solid is commonly treated in texts on heat conduction. Schneider [4] treats such a problem and the total heat transferred during one-half of the cycle is given as

$$Q = 2A\Delta T_o\sqrt{kC/\omega} \ , \qquad (3)$$

where A is the surface area, ΔT_o is the peak of the temperature fluctuation, k is the thermal conductivity of the displacer, C is its specific heat per unit volume, and ω is the frequency of oscillation. For $\dot{n}$ cycles per second $\omega = 2\pi\dot{n}$. Now $A = \pi DS$ and $\Delta T_o = (dT/dx)(S/2)$. Thus the heat transfer during one-half cycle and the net enthalpy flow per cycle become

$$Q = DS^2 \left(\frac{dT}{dx}\right)\sqrt{\frac{\pi kC}{2\dot{n}}} \tag{4}$$

If the wall material has the same specific heat and thermal conductivity as that of the displacer, then ΔT_0 will be just one-half of that considered above. The average shuttle heat transfer with $\dot{n}$ cycles per second then becomes

$$\dot{Q}_s = (1/2)\dot{n}DS^2\left(\frac{dT}{dx}\right)\sqrt{\frac{\pi kC}{2\dot{n}}} = \frac{DS^2}{2}\left(\frac{dT}{dx}\right)\sqrt{\frac{\dot{n}\pi kC}{2}} \tag{5}$$

As before, the functional dependence should be correct, but more exact calculations may give slightly different numerical coefficients.

For a thermal conductivity independent of T we can write $dT/dx = \left(T_h - T_c\right)/L$. The primary difference between this shuttle heat transfer and that derived by Zimmerman and Longsworth is the $\sqrt{\dot{n}}$ dependence in the present calculation. Thus at low speeds the thermal resistance of the solid material limits the shuttle heat transfer, whereas at higher speeds the thermal resistance of the gas gap limits the shuttle heat transfer and Eq. (2) must be used. For intermediate speeds we derive the total shuttle heat transfer by considering the two thermal resistances to be in series. Hence

$$1/\dot{Q}_s = 1/\dot{Q}^g{}_s + 1/\dot{Q}^s{}_s\ , \tag{6}$$

where $\dot{Q}^g{}_s$ and $\dot{Q}^s{}_s$ are the shuttle heat transfers limited by the gas gap and by the solid material, respectively.

Equation (5) will be valid as long as the radius of the displacer and the wall thickness is somewhat greater than the thermal penetration depth in the material. The thermal penetration depth λ is defined as that depth where the amplitude of temperature fluctuation is 1/e of that at the surface and is given approximately by [4]

$$\lambda = \sqrt{k/\dot{n}\pi C}\ , \tag{7}$$

where k/C is just the thermal diffusivity. Table 1 shows values of k, C, and λ for nylon at various temperatures with $\dot{n}$ = 1 Hz. Values for k are from Ashworth, et al. [5], and values for C are estimated from two different sources [6,7]. The specific heat and thermal conductivity of G-10 glass-reinforced epoxy is roughly the same as that of nylon [8]. From the penetration depths given in Table 1 we see that finite size effects can be neglected in most practical cases.

Table 1. Thermal conductivity, specific heat, and thermal penetration depth of nylon for $\dot{n}$ = 1 Hz

T (k)	k (mW/cm K)	C (mJ/cm^3 K)	λ (mm)
300	3.66	2000	0.24
200	3.40	1430	0.28
100	2.97	833	0.34
50	2.19	440	0.40
20	0.948	112	0.52
10	0.385	22	0.75
5	0.156	3.2	1.25

EXPERIMENTAL

To our knowledge previous measurements of shuttle heat transfer have not been made. It was felt that such measurements were necessary to check the accuracy of the calculations from a simple theory. Shuttle heat transfer can be measured by first observing the warm-up rate of a known thermal mass at the cold end of the displacer cylinder. During this measurement the displacer is operating but the compressor is not. Next, the displacer is shut off and the static warm-up rate is measured. The difference in the two measurements gives the shuttle heat transfer. Effects of gas pressure cycling are determined by varying the average pressure in the system. In this paper measurements down to 120 K are reported and for this temperature range the gas pressure had no effect.

Measurements were made using a Stirling-cycle refrigerator with a single stage displacer. The displacer was made of nylon and the cylinder wall was of G-10 epoxy, 2.3 mm thick The displacer was 0.95 cm in diameter and 30.3 cm long. The speed and stroke could be varied. The radial clearance between the displacer and wall was about 0.1 mm at 145 K and 0.06 mm at room temperature. Some measurements were made with nitrogen gas instead of helium gas in the system to increase the thermal resistance of the gas gap.

RESULTS

Figure 1 shows the shuttle heat transfer as a function of the cold-end temperature when the warm end was at 300 K. The calculated values consider both the gas gap and penetration depth limit using Eq. (6). Agreement between experimental and calculated values is excellent for a stroke of 1.19 cm. For a 2.45 cm stroke the agreement is excellent at higher temperatures but worsens at lower temperatures. The disagreement may be a result of the temperature gradient not being constant over the stroke length or it could be a result of interaction with static thermal conduction.

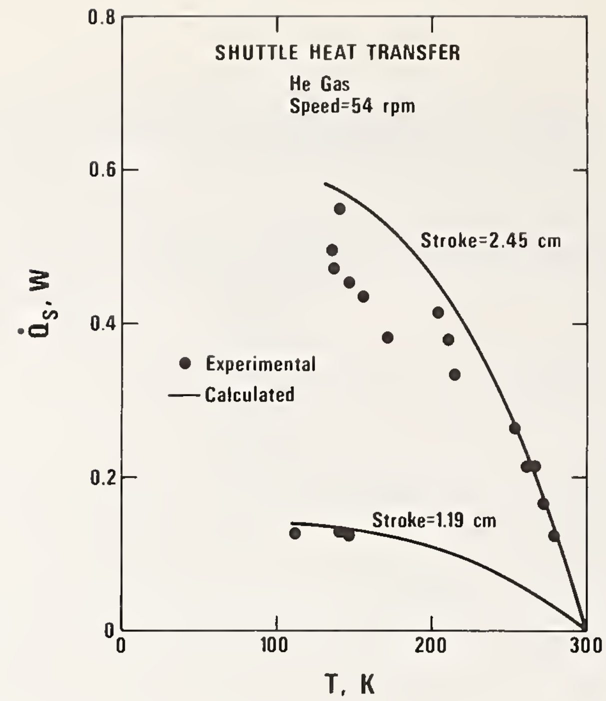

Figure 1. Measured and calculated shuttle heat transfer as a function of cold-end temperature with the hot end at 300 K.

Figure 2 shows the speed dependence of the shuttle heat transfer. This figure shows how the shuttle heat transfer gradually varies from a $\dot{n}^{1/2}$ dependence at low speeds to an independence of $\dot{n}$ at higher speeds. The experimental results agree fairly well with calculated values for both He and N_2 gas in the gap.

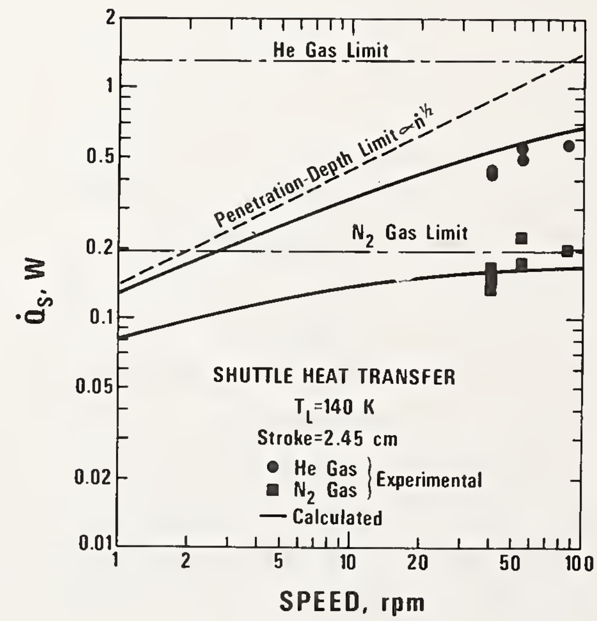

Figure 2. Measured and calculated shuttle heat transfer as a function of displacer speed for a cold-end temperature of 140 K.

We conclude that at least for the parameters used in this experiment, shuttle heat transfer can be estimated to within about 15% by combining the two expressions given by Eqs. (2) and (5) in the manner prescribed by Eq. (6). This imples the two thermal resistances are in series and that the necessary simplifying assumptions can be met in practice. Optimization of the parameters of the Stirling refrigerator can then be carried out analytically. In the tests done here the shuttle heat transfer was about five times the static conduction for a stroke of 1.19 cm. These results show that a more optimum design would have a shorter stroke and larger diameter to minimize the total heat transfer. Because k and C are proportional to T^3 at lower temperatures, the calculated values may not be in quite so good agreement with experiment at such temperatures unless Eq. (5) is integrated properly between T_h and T_c. Measurements down to about 5-10 K would be useful and are in progress.

REFERENCES

[1] J.E. Zimmerman and Ray Radebaugh, this publication.

[2] F.J. Zimmerman and R.C. Longsworth, Adv. Cryog. Eng. 16, 342 (1970).

[3] J.B. Harness and P.E.L. Neumann, Proc. Int'l Cryog. Eng. Conf., 5th (1972) p 97.

[4] P.J. Schneider, Conduction Heat Transfer, Addison-Wesley, Cambridge, MA (1955) p 276.

[5] T. Ashworth, J.E. Loomer and M.M. Kreitman, Adv. Cryog. Eng. 18, 271 (1973).

[6] W. Reese and J.E. Tucker, J. Chem. Phys. 43, 105 (1965).

[7] B. Wunderlich, Rensselaer Polytechnic Institute Report No. TR-17, Office of Naval Research Contract Nonr-591(19) (1968).

[8] J.A. Barclay, S.S. Rosenblum and W.A. Steyert, Cryogenics 16, 539 (1976).

Scaling of Miniature Cryocoolers to Microminiature Size

W. A. Little
RAI
15 Crescent Dr.
Palo Alto, Ca. 94301

The very small size and thermal dissipation of superconducting sensors imposes an extremely small load on the supporting refrigeration system. Present day refrigerators generally are grossly mismatched to such loads. For this reason we have considered the possibility of scaling down a miniature refrigerator to microminiature size. A set of scaling laws is derived. These have been applied to the design of a N_2 - H_2 refrigerator which might use a NbN sensor. Such microminiature refrigerators appear to offer a number of attractive design and manufacturing advantages.

Key words: refrigerator, cryocooler, Joule-Thomson cycle, heat exchanger design.

1. Introduction

During the past decade a host of new superconducting devices have been developed which are based on the Josephson effect. These include supersensitive magnetometer, gradiometers, voltage standards, current comparators, rf attenuators, bolometers and logic elements. In these devices the power dissipated in the cryogenic environment is typically of the order of microwatts. However, the refrigeration systems which are available to maintain the low temperature environment for the devices have a capacity of watts to tens of watts. Such refrigerators are thus poorly matched to the refrigeration requirements of the sensors. For this reason we have considered the problem of scaling down a small refrigerator to microminiature size. We have derived a set of scaling laws which allow one to estimate the size and performance of such a refrigerator. The proposed microminiature refrigerators appear to offer a number of attractive features both in manufacture and operation, viz., ease of mass production, compact construction, fast cooldown and long operating time. On this basis one can visualize the superconducting sensor and refrigerator as a single package, the size of a miniature vacuum tube which would be inexpensive, replaceable and disposable.

We have considered three refrigeration systems for miniaturization, the Kirk-Stirling, Gifford-McMahon and Joule-Thomson systems. The first two cycles are more efficient in general than the last but are somewhat more complex in view of their several moving parts. Because of the simplicity of the J-T system and its absence of moving parts we chose it for further study. Our analysis focusses primarily on the properties of the heat exchanges so has some relevance to other cooling cycles.

Miniature J-T refrigerators using N_2, H_2 and He circuits are commercially available [1] and have been described in the literature [2]. These refrigerators typically produce watts of refrigeration at 80K, 20K or 4K. Our purpose was to scale this down by a factor of the order of a hundred.

2. Heat Exchanger Design Considerations

The design of countercurrent heat exchangers is described in two excellent reviews:

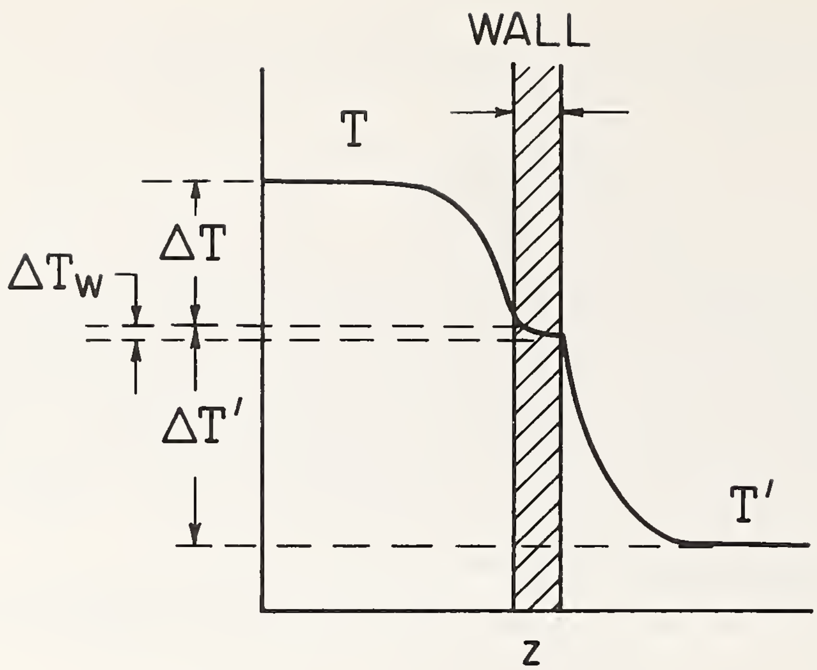

Figure 1. Schematic plot of the temperature profile from one gas to the other counter flowing gas across the wall of a heat exchanger.

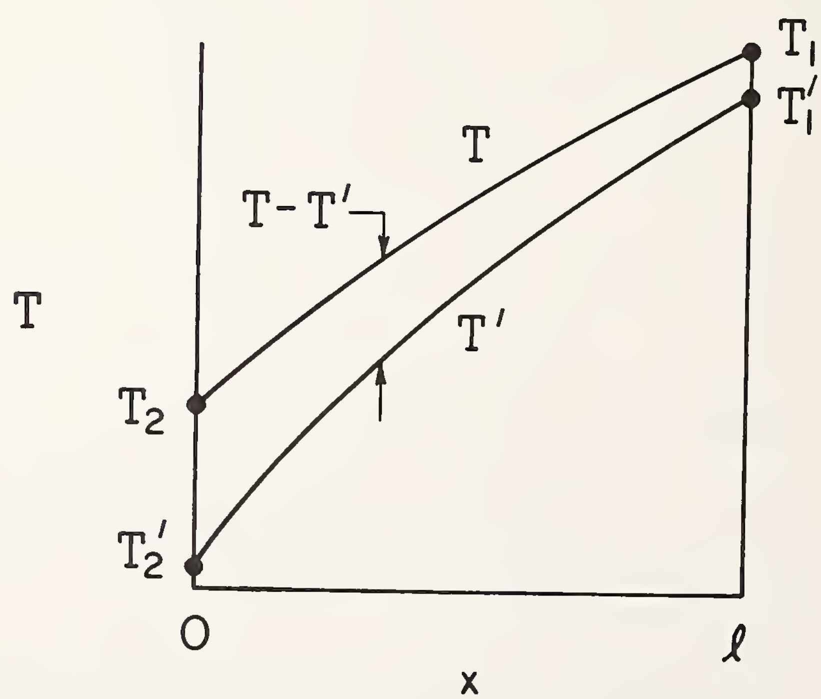

Figure 2. Temperature along the length of a countercurrent heat exchanger. T is the temperature at each point in the exchanger of the incoming gas and T' that of the outgoing gas.

"Experimental Cryophysics," Chapter 2 by Hoare, Jackson and Kurti, [3] and J. G. Daunt's article in the Encyclopedia of Physics, Springer Verlag [4]. The temperature profile from the one fluid at temperature T to the other at temperature T' across the wall of the exchanger is illustrated in Figure 1. Here ΔT is the drop in temperature in the gas on one side, ΔT_w the drop across the wall and $\Delta T'$ the drop in the gas on the other side. Daunt states that one can usually neglect ΔT_w, so if the heat transfer/sec/unit area of wall is $\dot{q}$ then $\dot{q} = \alpha\Delta T = \alpha'\Delta T'$, where α and α' are certain quantities to be derived later. Then $T - T' = \dot{q}/\kappa$, where $\frac{1}{\kappa} \approx \frac{1}{\alpha} + \frac{1}{\alpha'}$.

The heat transfer/sec/unit <u>length</u> of the exchanger, $d\dot{Q}$ will thus be given by

$$d\dot{Q} = \kappa(T - T')P d\ell = \dot{m}_1 \; Cp(\frac{\delta T}{\delta \ell}) d\ell \quad , \tag{1}$$

where P is the perimeter of the wall, Cp the heat capacity of the gas/unit mass and $\dot{m}_1$ is the mass flow of the input gas per unit time.

Likewise for the cold return

$$\dot{m}' \; C_p' (\frac{\delta T'}{\delta \ell}) d\ell = -d\dot{Q} \quad . \tag{2}$$

Integrating $d\dot{Q}$ from (1) we have

$$\int_0^\ell \frac{d\dot{Q}}{T-T'} = \kappa P \ell \quad , \tag{3}$$

assuming κ is constant, or where it is not, some mean value as discussed by Daunt.

Using the other part of (1) and equation (2) one obtains an expression for T and T' along the exchanger. This is illustrated in Figure (2). It is conventional to define the efficiency of the exchanger as $\varepsilon = 1 - \frac{T_1 - T_1'}{T_1 - T_2'}$ (See Figure 2). From the above integration for a "balanced" exchanger i.e. with no draw off of liquid it can be shown that $\varepsilon = \frac{\kappa P \ell}{\kappa P \ell + \dot{m} C_p}$.

It is convement to measure $\kappa P \ell$ in units of $\dot{m} C_p$. Then we have

$$\varepsilon = \frac{(\kappa P \ell / \dot{m} C_p)}{(\kappa P \ell / \dot{m} C_p) + 1} = \frac{N}{N+1} \tag{4}$$

and we call the ratio $(\kappa P \ell / \dot{m} C_p)$ the number of "thermal transfer units," N of the exchanger.

We can calculate α and α' and hence obtain κ as discussed in reference [1]. In general we want $\alpha \approx \alpha'$ so it is sufficient to calculate α. One finds

$$\ell P \alpha = 0 \cdot 10 \; C_p \eta^{0.2} \left(\frac{\dot{m}}{d}\right)^{0.8} \ell \quad , \tag{5}$$

η = viscoscity. Since $\frac{1}{\kappa} \approx \frac{1}{\alpha} + \frac{1}{\alpha'} \approx \frac{2}{\alpha}$, so

$$\kappa P \ell \approx 0.05 \; C_p \dot{m} \left(\frac{\eta d}{\dot{m}}\right)^{0.2} \left(\frac{\ell}{d}\right) \tag{6}$$

where d = diameter of the tube. Reynolds number Re is defined as Re = $(4\dot{m}/\pi\eta d)$. In terms of it

$$N = 0.05 \left(\frac{\pi}{4}\,\mathrm{Re}\right)^{-0.2} \left(\frac{\ell}{d}\right) \tag{7}$$

The pressure drop in the high pressure line can be related to N. Following reference [1] again

$$\Delta p = 0{\cdot}10\ \rho v^2 \left(\frac{\ell}{d}\right) (\mathrm{Re})^{-0.2} \tag{8}$$

But $v = (4\dot{m}/\rho\pi d^2)$ so

$$\Delta p = 2\rho v^2 * N * \left(\frac{\pi}{4}\right)^{0.2} \approx 2N\rho v^2 \tag{9}$$

So $(\Delta p/\rho v^2)$ = M = number of "pressure heads" and therefore M = 2N. Hence

$$\Delta p = 2N \left(\frac{16\dot{m}^2}{\pi^2 \rho d^4}\right) \tag{10}$$

3. Scaling Considerations

The amount of refrigeration for a given gas is proportional to $\dot{m}$. For a refrigerator of given exchanger efficiency working between fixed T_1, T_1', T_2 and T_2', N is fixed. For the same efficiency and with the same pressure drop we see from (10) that this requires

$d \approx (\dot{m})^{0.5}$	1st Scaling Law

We see from the definition of Reynolds number taking in to account the above constraint on d that Reynolds number Re is proportional to $(\dot{m})^{0.5}$ and hence from (7) for fixed N, that

$\ell \approx (\dot{m})^{0.6}$	2nd Scaling Law

The intrinsic cooldown time of the exchanger itself is determined by the ratio of mass of exchanger to the refrigeration capacity. If we assume a fixed aspect ratio of the heat exchanger tubing then its mass will be proportional to $d^2\ell$, which from the above is proportional to $(\dot{m})^{1.6}$. Hence the cooldown time is given by

Cooldown time $\approx (\dot{m})^{0.6}$	3rd Scaling Law

The length of time the exchanger can operate before fouling up with contaminants one would expect to be proportional to ratio of the volume of the exchanger to $\dot{m}$. The volume is proportional to ℓd^2 and hence from the above

$$\boxed{\text{Operating time} \approx (\dot{m})^{0.6} \qquad \text{4th Scaling Law}}$$

This indicates that the microminiature refrigerators would be somewhat more sensitive to contamination (eg. Ne in H_2) and hence would need high purity gas. However, as we shall show the very fast cooldown could allow one to warm up, flush clean and cool down again in less than a minute. This might be an acceptable mode of operation for several instrumentation applications.

As an example of the above scaling we consider a 110 milliwatt liquid nitrogen refrigerator scaled from an Air Products J-T refrigerator [5] which produces 7 watts of refrigeration at 80K using 1360 st. litres/hr of N_2. Typical exchanger efficiency is 95% hence N = 20 and we assume 100 atm inlet pressure and $\Delta p \approx 6$ atm. Using the above scaling and the dimensions of the larger refrigerator we find $d \approx 10^{-2}$ cm, $\ell \approx 24$ cm, Re ≈ 8000 and a cooldown time of 25 seconds. The greatly reduced gas consumption would allow operation of the order of 400 hours per standard cylinder of gas.

Scaling of a similar N_2 - H_2 refrigerator would allow operation at 20K and below with a refrigeration capacity of 60 milliwatts.

The very small size of the heat exchanger system suggests the possibility of constructing the heat exchanger, expansion valve and particulate filter using planar photoresist technology similar to that used in the semiconductor industry. The successful development of such a technique would greatly reduce the price of the refrigeration unit and make it feasible to design and construct as an integral package the refrigerator and superconducting circuit elements for use in ambient temperature circuitry. Mercereau has recently demonstrated [6] the operation of a Nb_3Sn quantum interference device at 17K. Similar results can be expected for NbGe at 21K. These temperatures are within range of those attainable with J-T refrigeration alone using the N_2 - H_2 cycle.

4. Acknowledgements

I am indebted to Dr. J. Mercereau for several useful discussions on the refrigeration needs of superconducting sensors.

5. References

[1] For example; Bendix Instrument and Life Support Division, Hickory Grove Road, Davenport, Iowa 52808; Air Products, Inc., Allentown, Pennyslvania; Santa Barbara Research Center, 75 Coromar Dr., Goleta, California.

[2] Geist, J. M. and Lashmet, P. K., Adv. Cryogenic Engineering 5, 73 Plenum Press, N.Y. (1961); Buller, J. S., Advances in Cryogenic Engineering 16, 205 (1970).

[3] Hoare, F. E., Experimental Cryophysics, pg. 14, edited by Hoare, F. E., Jackson, L. C., and Kurti, N., Butterworth and Co. (Publishers) Ltd 1961.

[4] Daunt, J. G., Encyclopedia of Physics, pg. 1, edited by Flügge, S., Vol. XIV, Low Temperature Physics I, Springer-Verlag, Berlin 1956.

[5] Geist, J. M. and Lashmet, P. K., Adv. Cryogenic Engineering 5, 73 Plenum Press, N.Y. (1961), and data on commercially available units from Air Products Inc.

[6] Palmer, D. W., Notarys, H. A., and Mercereau, J. E., Appl. Phys. Lett. 25, 9 (1974) 527-528.

Small Magnetic Refrigerators to Pump Heat from Helium Temperatures to above 10 K*

William A. Steyert
Los Alamos Scientific Laboratory, Los Alamos, NM 87545

A brief summary will be presented of measurements of the thermodynamic properties of several paramagnetic salts useful as magnetic refrigerants in the 1 to 4 K region. A low power "conventional" (two switch) magnetic refrigerator design, using these materials and the magneto-resistive switch elements studied at NBS, Boulder, will be discussed. Also discussed will be less conventional magnetic refrigerators where the paramagnetic refrigerant forms the rim of a wheel; each section of the material rotates into a field, where it expells heat and rotates out of the field where it absorbs heat.

Key words: magnetic refrigeration; paramagnetic materials.

1. Introduction

In 1926 Giauque [1] and Debye [2] independently suggested the use of magnetic refrigeration to produce temperatures below those previously attainable. Giauque and MacDougall [3], in 1933, used the proposed method of adiabatic demagnetization to cool from 3.5 K to 0.5 K. Since that time magnetic refrigeration has generally been used in a "one shot" mode. An applied magnetic field is used to force heat out of the paramagnetic material and into a thermal reservoir. After breaking contact with that reservoir, the subsequent removal of the field produces the desired cooling of the experiment, which is in contact with the paramagnetic material. The paramagnetic material and the experiment subsequently rise to the reservoir temperature at a rate determined by the heat capacity of the isolated system and the heat flow into it. These devices, which are still used to attain temperatures in the millikelvin range, are described by White [4].

The first device for continuously maintaining a fairly constant low temperature using adiabatic demagnetization was constructed by Heer, Barnes, and Daunt [5] in 1954. This device made use of superconducting thermal switches and a low temperature reservoir of high heat capacity to smooth out temperature variations during successive cycles of magnetization and demagnetization of the working salt. This refrigerator was able to maintain 0.26 K with a heat load of 7 μW. A further refinement of this design by Zimmerman, McNutt, and Bohm [6], using superconducting solenoids, was able to maintain 0.26 K with a heat load of 100 μW. More recently, Rosenblum, Sheinberg and Steyert [7] reported a similar device using the demagnetization of a pressed gold-cerous magnesium nitrate composite cylinder to pump heat from a thermal reservoir consisting of 0.6 g of cobalt metal at 10.5 mK. The nuclear specific heat of the cobalt acted as a thermal reservoir restricting the cyclical temperature swings to ± 0.5 mK. The device had a refrigeration capacity of 0.1 μW. A magnetic refrigerator to pump 0.2 W from a bath at 2 K into a bath at 4 K has been built and tested [8].

*Work performed under the auspices of the U.S. Energy Research & Development Administration.

The reasons for considering magnetic cooling as an alternative to gas expansion cooling above 1 K are:

1. The refrigeration power per unit volume is large; we are dealing with a solid instead of a gaseous working substance (the density of working atoms is much higher for the solid). Each liter of working material removes hundreds of joules of heat from the low temperature heat source during each cycle.

2. The magnetic cycle can operate at nearly 100% of Carnot efficiency. For magnetic refrigeration, losses which lead to less than Carnot efficiency are readily anticipated and can be minimized. Such losses are: irreversible losses associated with heat flows across a finite temperature gradient, frictional losses in moving parts or moving fluids, eddy current and hysteresis losses in magnet and refrigerator components, and losses from heat leaks. Losses associated with finite spin-lattice relaxation times are complex, being associated with relaxation in an applied field where the Zeeman splitting is comparable with the thermal energy, kT. Phonon bottlenecks may also play a role. However, a judicious choice of salt can make relaxation times short enough for our devices.

3. The materials for the refrigerants are inexpensive - about $30 per pound for rare earth ceramics, $200 per pound for rare earth metallic alloys.

Thus the small size and high efficiency of the system can result in substantial cost reductions in low temperature applications. In principle there is no upper temperature limit for magnetic refrigeration. In fact, magnetic refrigeration has already been achieved at ambient temperature [9,10].

2. Refrigerants

The requirements for the selection of a material for use below the 20 K range are as follows:

1. It should have a small electronic and lattice specific heat, otherwise some of the refrigeration capacity will be lost in cycling the refrigerant temperature.

2. It should have its magnetic ordering temperature below that of the lowest temperature sought as it is difficult to self cool an antiferromagnetic material below its Neel temperature or a ferromagnetic material below 80% of its Curie temperature.

3. It should have a large magnetic moment, so that the isothermal application of a modest magnetic field will force a large amount of heat out of the working material.

4. It should be chemically and physically rugged, inexpensive, and easy to fabricate.

As a first step we have measured the thermodynamic properties [8] of the following materials for use in the region below 20 K: $Dy_2Ti_2O_7$, $Gd(OH)_3$, $Gd(PO_3)_3$, $Gd_2(SO_4)_3 \cdot 8H_2O$, $Gd_3Al_5O_{12}$, Er_2O_3, Dy_2O_3, and $DyPO_4$. These measurements were carried out in a calorimeter located in the bore of a 10-T superconducting magnet. A commercially available glass capacitance thermometer (Lawless type) [11] was used to measure the temperature of a refrigerant under test. This type of thermometer is not sensitive to magnetic fields and can be calibrated by comparison with the vapor pressure of liquid helium, hydrogen, and neon, and also by a comparison with a calibrated germanium resistance thermometer.

The results for all the materials can be described semi-empirically in the following manner:

1. A main contribution to the entropy from the free spin value $S/R = \ell n(2J+1)$, where $2J+1$ is the number of degenerate energy levels for the ion of spin J and R is the gas constant. If the spin has a magnetic moment $\mu\beta$ (β is the Bohr magneton), we can define an effective magnetic moment $p_{eff} = \mu[(J+1)/J]^{1/2}$. (If we average over three different μ's along the three axes, we have $\mu = \sqrt{(\mu_x^2 + \mu_y^2 + \mu_z^2)/3}$ when we are not near saturation.) In an applied magnetic field H at temperature T the entropy will change by an amount $\Delta S/R = -p_{eff}^2\beta^2H^2/6k^2T^2$, for $\mu\beta H/kT$ small. This approximation is of interest to us, as it is most economical to work with as low a magnetic field as possible. Inserting numerical values for the Bohr magneton β and the Boltzmann constant k in this expression, we obtain $\Delta S/R = -0.075\ p_{eff}^2H^2/T^2$, where H is in tesla.

2. A field-independent lattice specific heat $C_L/R = \alpha\ T^3$ (a lattice entropy $S_L/R = \int \frac{C_L}{R}\frac{dT}{T} = \frac{\alpha}{3}T^3$).

3. Specific heat and entropy contributions associated with the thermal population of high lying energy levels. These levels are created by crystalline field splittings associated with the electric fields of nearby ions acting on the magnetic rare earth ion. If there is a high lying pair of levels at an energy Δ (expressed in kelvins), then the specific heat in zero applied field is readily calculated as $C/R = \left(\frac{\Delta}{T}\right)^2 e^{-\Delta/T}$ and the corresponding entropy as $S/R = (1 + \frac{\Delta}{T})(e^{-\Delta/T})$ for $T \ll \Delta$. In a non-zero field these values are slightly different.

4. In zero field, the contributions to the total specific heat and total entropy due to ferro- or antiferromagnetic transitions which are approximately $C_o/R = \frac{1}{4}\left(\frac{T_o}{T}\right)^2$, $S_o/R = \int \frac{C_o}{R}\frac{dT}{T} = -\frac{1}{8}\left(\frac{T_o}{T}\right)^2$ for $T > T_o$. Here T_o is roughly equal to the low temperature ordering temperature. (These equations are correct for the two-level Schottky anomaly [12], and we use the same specific heat coefficient, 1/4, for our definition of T_o as well.)

Reference [8] reports the results of measurements on a variety of compounds in more detail. In this report we will discuss only measurements on $Gd_2(SO_4)_3{\cdot}8H_2O$ for use down to 0.5 K and $Dy_2Ti_2O_7$ for use down to 4 K.

In Fig. 1 we show the complete entropy-temperature diagram for the material for $Gd_2(SO_4)_3{\cdot}8H_2O$. These curves are calculated using the known magnetic and lattice properties of this salt as measured by us and by others. From these curves, it is easy to calculate the heat removal capacity per liter for $Gd_2(SO_4)_3{\cdot}8H_2O$ ($Gd_2(SO_4)_3{\cdot}8H_2O$ occupies 120 cm^3/g-ion of Gd^{+++}). For $Gd_2(SO_4)_3{\cdot}8H_2O$, consider a field of 6.4 tesla applied isothermally at 10 K resulting in $S_{TOT}/R = 1.3$ (see Fig. 1, ignoring the thermodynamic cycle shown for later reference). After demagnetizing to 2 K, the amount of heat which can be absorbed by removing the field is $\Delta Q = T\Delta S = 2 \times 0.75 \times 8.3 = 12.5$ J/mol; for one liter we get $\Delta Q = 12.5 \times 1000$ $(cm^3/\ell)/120\ (cm^3/\text{g-ion}) = 104\ J/\ell$ for each cycle. For refrigeration at 2 K, $Gd_2(SO_4)_3$ and $GdPO_4$ appear even more promising [8] as they occupy only 73 cc/g-ion and 50 cc/g-ion, respectively, and have ordering temperatures which are thought to be below 1 K, and have lower lattice specific heats.

Figure 2 shows the S-T diagram for $Dy_2Ti_2O_7$, which occupies 37.6 cc/g-ion of Dy^{+++}.

This material is useful for refrigeration at 4 K and above. In addition to detailed calculations of 2 K refrigeration, we will quote expected performance for a $Dy_2Ti_2O_7$ refrigerator pumping heat from 5 K to 15 K.

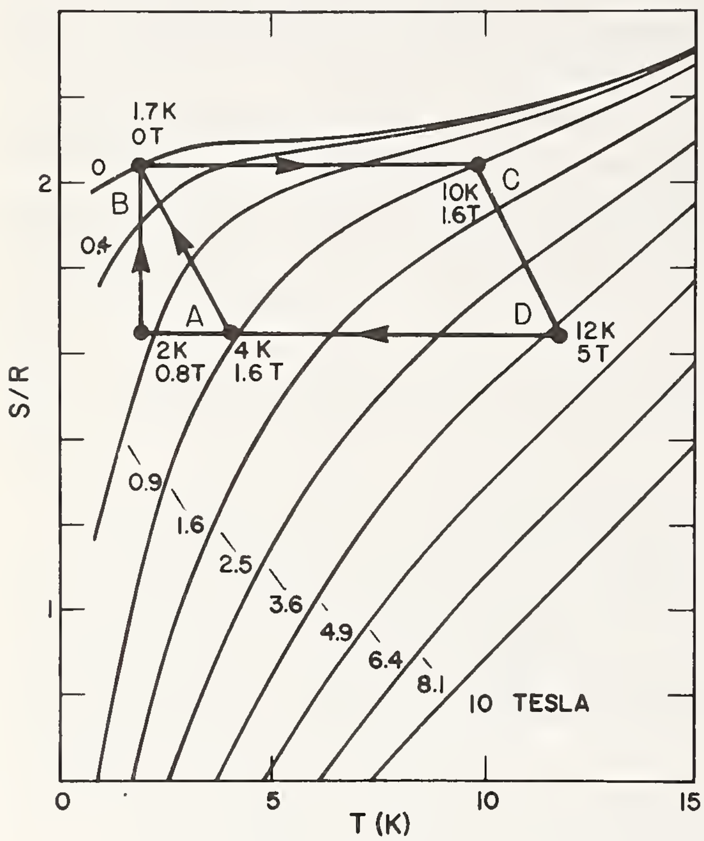

Figure 1

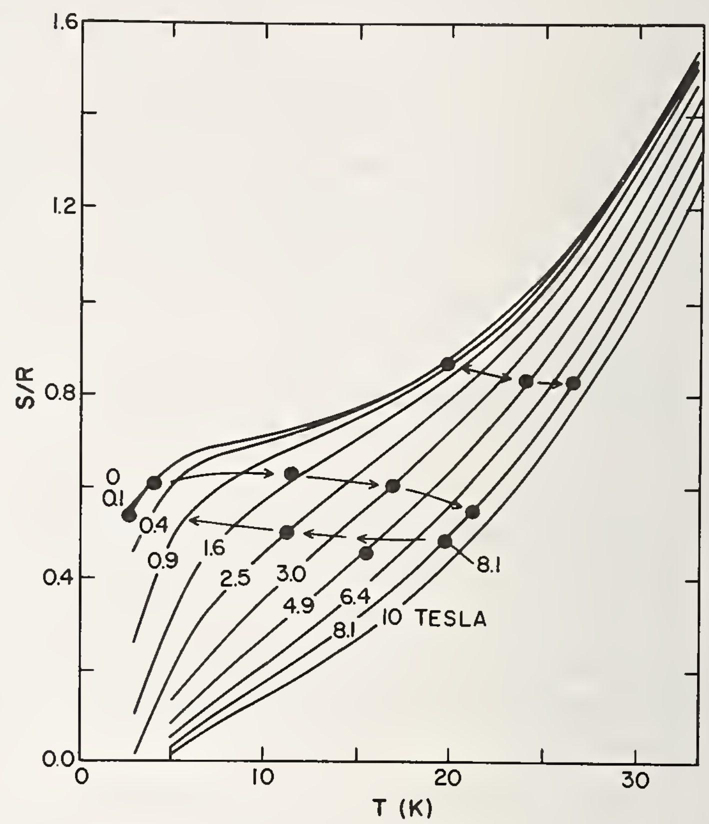

Figure 2

Figure 1 Temperature-entropy diagram for $Gd_2(SO_4)_3 \cdot 8H_2O$ as a function of applied magnetic field. R is the gas constant. The thermodynamic cycle shown is discussed in connection with the Carnot-wheel refrigerator, Sec. 4.

Figure 2 Entropy vs temperature for various applied magnetic fields for $Dy_2Ti_2O_7$. These results are derived from fitting specific heat data in various fields (to 8.1 T) with the parameters described in text. The parameters then determine S for all fields and temperatures in the range of measurement. Two adiabatic demagnetization and magnetization results are given as arrows in the figure. These results are not quite adiabatic because of the effect of cooling and heating the calorimeter, requiring a measured entropy 0.08 R for each gram-ion of Dy^{+++}. Similar magnetization and demagnetization tests were carried out on $Gd_2(SO_4)_3 \cdot 8H_2O$ but are not shown in Fig. 1.

3. Conventional Magnetic Refrigerators

The primary limitation on previous units [5,6] used to pump heat from ≈1/4 K into a helium bath at 1 K has been the poor on-off thermal conduction ratio of superconducting/normal switches with hot ends held at 1 K. The on-off ratio was 45. With the advent of magneto-resistive single-crystal beryllium [13] switches, ratios of ≈1000 even at 15 K are possible.

A myriad of conventional designs could be contemplated (by conventional we mean refrigerators using two switches of one kind or another). The design we will discuss here is shown in Fig. 3. The lower switch to the thermal load is an array of four single-crystal Be switches that is made nonconducting by the application of the magnetic field. Thermal contact to the refrigerator is made and broken by turning on and off the flow of refrigerated helium through the heat exchange area.

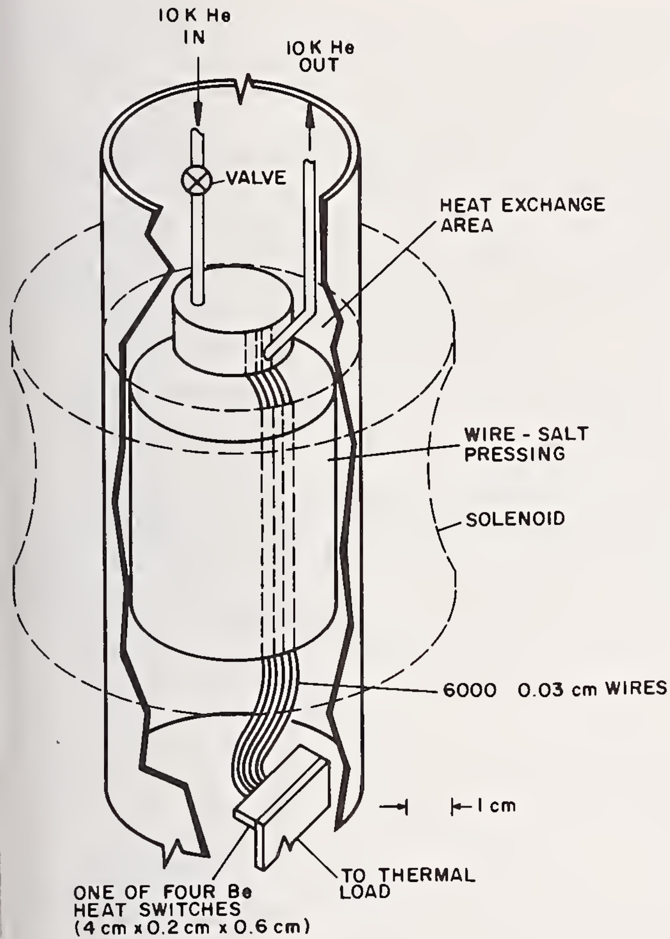

Figure 3

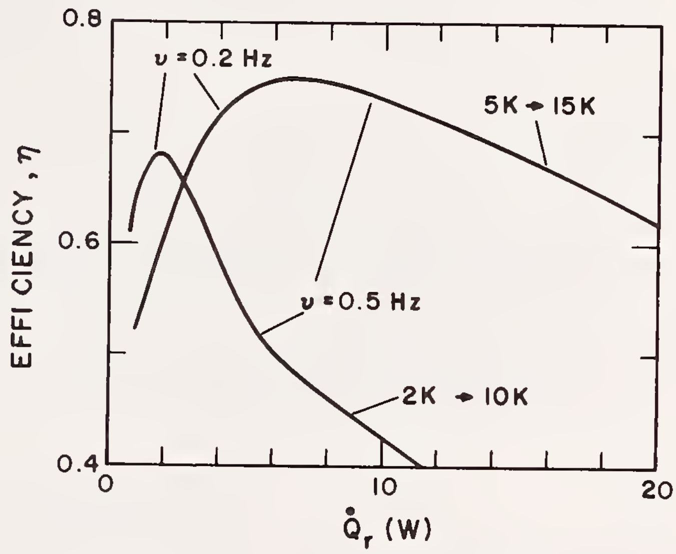

Figure 4

Figure 3 Conventional magnetic refrigerator. The wire-salt pressing absorbs heat from thermal load at 2 K through wires and Be switch. It then expells the heat into 10 K helium gas flow. Alternating field can be provided through pill or magnet motion, or at lower cycle frequencies, by changing the current to the magnet. This figure also applies to the $Dy_2Ti_2O_7$ unit except it pumps heat from 5 K to a 15 K gas stream.

Figure 4 Calculated efficiency, as a fraction of Carnot, as a function of refrigeration capacity for the two conventional refrigerators discussed in the text. The points on the curves corresponding to cycle frequencies ν of 0.2 and 0.5 Hz are indicated.

Let us first examine the performance of this unit when used to pump heat from 2 K into a refrigerated helium gas flow at 10 K. We can consider a refrigerant like $Gd_2(SO_4)_3$; if we use $GdPO_4$ or $Gd_2(SO_4)_3 \cdot 8H_2O$ we will get slightly more or slightly less g-ions of refrigerant in the refrigerator shown in Fig. 3. The construction of pressed pills is discussed in Ref. [7] and [8]. Taking 73 cc/mole and 80% filling factor gives 1.08 g-ions; with a magnetic field of 5 to 6 tesla we extract $\Delta S = 0.65$ R per g-ion each cycle. Therefore we extract in each cycle an energy ΔQ where

$$\Delta Q = T\ \Delta S \times 1.08 = 11.7\ \text{J/cycle} \quad . \tag{1}$$

The thermal load of the copper is small [14]. The helium gas entrained in the heat exchanger must be kept small; we neglect both of these [15].

To carry the heat we use high purity copper wires, oxygen treated to provide very high thermal conductivity [16]. We take a value of 3000 for the electrical residual resistivity ratio (room temperature to 4 K). This value may be a little pessimistic, as high purity polycrystalline copper typically gives 10,000 to 12,000 with oxygen treatment; however, we have allowed for some degradation associated with mechanical mistreatment of the wires during assembly. Using the Weidemann-Franz law and taking the appropriate Lorenz-number as 2×10^{-8} W-ohm/K^2 and the resistance of copper as 1.7×10^{-6} μ ohm-cm at room temperature, we find the thermal conductivity $\kappa = 2 \times 10^{-8} \times 3000 \times T/1.7 \times 10^{-6} = 70$ W/cm-K at 2 K. To calculate average temperature drop $\overline{\Delta T}$ in these wires, we use 6.2 cm as the effective length [17], and an area of 4.4 cm^2, or

$$\dot{Q}/\overline{\Delta T} = 70 \times \frac{4.4}{6.2} = 50\ \text{W/K} \quad . \tag{2}$$

For $\dot{Q}/\overline{\Delta T}$ in the salt [17]

$$\begin{aligned} \dot{Q}/\overline{\Delta T} &= 8\pi \times L' \times \kappa \times 0.15 \\ &= 111\ \text{W/K} \end{aligned} \tag{3}$$

taking $\kappa = 10^{-3}$ W/cm-K (we use the value for pressed $Gd_2(SO_4)_3 \cdot 8H_2O$ powder [8], pressed $Gd_2(SO_4)_3$ has not been measured) and the length, L', of wires as 5 × 6000 cm. The constant 0.15 is appropriate for small wires evenly distributed in a matrix in a roughly hexagonal array [18]. Kapitza resistance is negligible.

The thermal switches are placed in the fringing magnetic field; the wires are soldered to the Be with indium; the indium-wire composite will probably have $\kappa = 4$ W/cm-K but could be further improved by using higher purity In. Thus [19],

$$Q/\overline{\Delta T}\Big|_{\text{indium}} = 3\ \kappa\ \frac{A}{\ell} = \frac{4 \times 16 \times 0.2 \times 3}{0.4} = 90\ \text{W/K} \quad . \tag{4}$$

For the switch itself, with $A/\ell = 0.2 \times 4 \times 4/0.6 = 5.3$ and κ [13] at 2 K = 10 W/cm-K

$$\dot{Q}/\Delta T = \kappa \frac{A}{\ell} = 53 \text{ W/K} \quad . \tag{5}$$

The heat leak from 10 K to 2 K through the switch, when it is in an applied field where $\kappa = 3 \times 10^{-3}$ T, is

$$\dot{Q}_\ell = 3 \times 10^{-3} \times \frac{A}{\ell} \left(\frac{10^2 - 2^2}{2}\right) = 0.76 \text{ W} \quad . \tag{6}$$

The switches are designed to minimize eddy current heating effects. Without going into detail, eddy current heating is estimated as $\dot{Q} = 0.1\ \nu^2$ watts (where ν is the cycle frequency). Because we will be concerned with $\nu \leqslant 1$, eddy currents will be neglected.

For ease of calculation we take the helium heat exchange unit to be helium gas flowing parallel to the 6000 wires (in the space between the close-packed wires) over a 1-cm length. A sintered powder or copper screen device could be used instead. In the case we consider, we have for 13 g/s flow of helium at 5 atm pressure a calculated pressure drop of 2000 Pa ($\approx$ 0.02 atm). The heat transfer is

$$\dot{Q}/\Delta T = 86 \text{ W/K} \quad . \tag{7}$$

We use equations for turbulent flow heat transfer and pressure drops from White [4]. We neglect the ΔT in the wires; copper is a very good conductor at 10 K and the effective length is very short.

The refrigeration capacity, $\dot{Q}_r$ is, from Eqs. (1) and (6) taking the heat leak for a half-cycle

$$\dot{Q}_r = 11.7\ \nu - 0.38 \text{ W} \quad . \tag{8}$$

The fraction of Carnot efficiency η is taken as Carnot refrigerator work divided by the actual refrigerator work

$$\eta = \frac{\dfrac{\dot{Q}_r}{T_C}(T_H - T_C)}{\dfrac{\dot{Q}_r + \dot{Q}_\ell}{T_C - \Delta T_C}[T_H + \Delta T_H - (T_C - \Delta T_C)]} \quad , \tag{9}$$

where T_H and T_C are the temperatures of the hot reservoir and cold heat source, respectively, and ΔT_H and ΔT_C are the total previously calculated temperature drops. In the expression for η, $\dot{Q}_r/T_C$ and $(\dot{Q}_r + \dot{Q}_\ell)/(T_C - \Delta T_C)$ are the entropy flows $\Delta\dot{S}$ in refrigerators pumping heat from temperatures T_C and $(T_C - \Delta T_C)$, respectively. The remainder of the numerator and denominator uses the first law plus $\dot{Q} = T\ \Delta\dot{S}$ to calculate the work (energy) required to move the heat between the indicated temperatures.

By allowing a half cycle for the expulsion of ~ 10/2 times as much heat at 10 K than is absorbed at 2 K (accurate for high efficiencies), we have $\Delta T_H = 11.7\ \nu \times 2 \times \frac{10}{2}/86 = 1.36\ \nu$. Combining the ΔT's of Eqs. (2), (3), (4), and (5) we use $\Delta T_C = 2 \times 11.7\ \nu/17 = 1.38\ \nu$. Thus

$$\eta = \frac{(11.7\ \nu - 0.38)\ \frac{10 - 2}{2}}{11.7\ \nu\ \frac{10 + 1.36\ \nu - 2 + 1.38\ \nu}{2 - 1.38\ \nu}} \qquad (10)$$

The results, plotted in terms of η vs $\dot{Q}_r$ are shown in Fig. 4.

We have done a similar calculation for a $Dy_2Ti_2O_7$ refrigerator pumping heat from 5 K into helium at 15 K. The only modification of the unit shown in Fig. 3 was to decrease A/ℓ of the switches by a factor of 2. Eq. (1) becomes $\Delta Q = 21$ J/cycle, Eq. (2) becomes $\dot{Q}/\overline{\Delta T} = 122$, Eq. (3) becomes $\dot{Q}/\overline{\Delta T} = 565$, Eq. (4) becomes $\dot{Q}/\overline{\Delta T} = 225$, and Eq. (5) becomes $\dot{Q}/\Delta T = 196$ (all in W/K). The heat leak, Eq. (6) becomes $\dot{Q}_\ell = 1.85$ W and we keep Eq. (7) unchanged.

Now

$$Q_r = 21\ \nu - 0.925\ \mathrm{W} \qquad (11)$$

and

$$\eta = \frac{(21\ \nu - 0.925)\ \frac{15 - 5}{5}}{21\ \nu\ \frac{(15 - 5 + 1.465\ \nu + 0.82\ \nu)}{5 - 0.82\ \nu}} \qquad (12)$$

These results are also plotted in Fig. 4.

The efficiency in these devices is limited by the limited heat conduction of the path to the load and is affected even by the 1000-to-1 on-off ratio of the heat switch. The utilization of an even better switch to make contact between the load and the source could be a significant improvement (an arrangement using superfluid helium, for example).

4. Carnot Wheel Refrigerator

Figure 5 shows a schematic of a wheel-type Carnot cycle refrigerator discussed in Ref. [21]. Figure 1 illustrates the two thermodynamic cycles executed by the paramagnetic material. (Either cycle could be used, depending on the application.) On the upper left of Fig. 5 and Point A in Fig. 1, supercritical helium enters the porous wheel and is forced to flow in heat exchange through the moving wheel. (Figure 6 gives one example of how the heat exchange might be implemented.) The wheel absorbs heat from the helium as it is demagnetized to Point B in Fig. 5; the paramagnetic material cools the helium to 1.7 K. The helium then absorbs heat $\dot{Q}^C$ from the load and reenters the wheel heat exchanger area at 2 K (or 4 K). Similarly in the lower right of Fig. 5 supercritical helium (at essentially the same pressure as the helium in the left) enters the porous wheel at 10 K; this corresponds to Point C in Fig. 1. The wheel deposits heat in the helium as the material is magnetized to Point D, while the fluid leaves the wheel at 12 K. This heat $\dot{Q}^H$, is deposited externally, completing the cycle with the net result that work is used to rotate the wheel and heat is absorbed in a low temperature and expelled at a high temperature. Note in Fig. 5 that the wheel is adiabatically magnetized as it goes from the lower left to the lower right and adiabatically demagnetized as it goes from upper right to upper left.

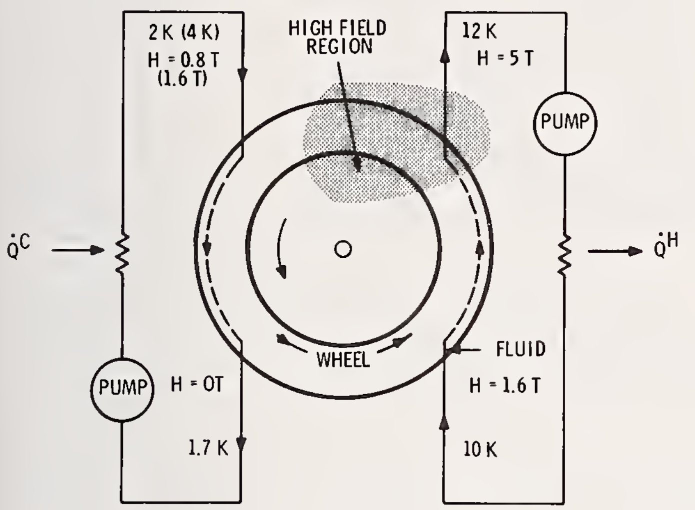

Figure 5

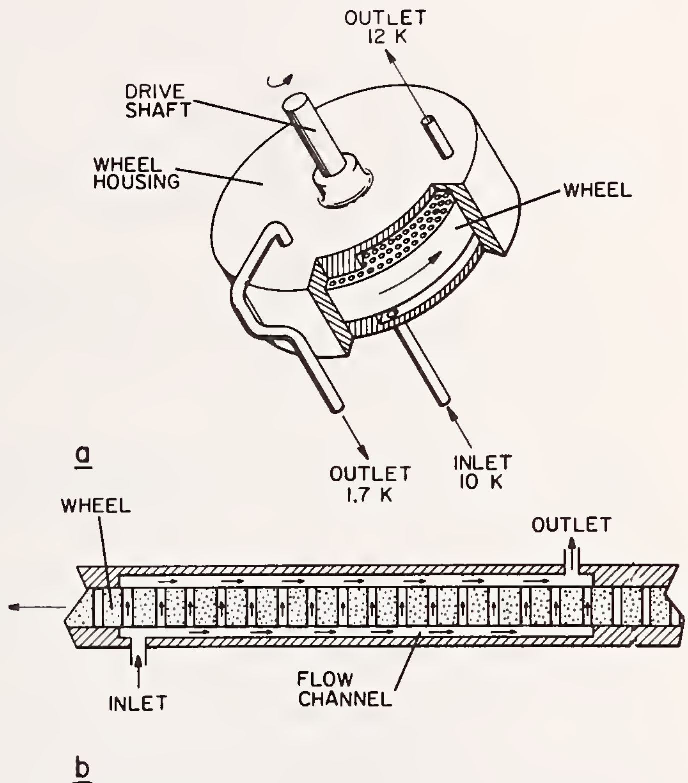

Figure 6

Figure 5 Schematic of Carnot wheel refrigerator. The paramagnetic material forming the rim of the wheel rotates in a counter clockwise direction. Supercritical helium is cooled by the demagnetizing material on the left and is warmed by the magnetizing material on the right. Power $\dot{Q}^C$ is absorbed from the load and $\dot{Q}^H$ is deposited in the upper stage refrigerator. Magnetic field (H) and temperatures are indicated. In an actual device the pumps would be located at the highest possible temperatures in contrast to this schematic.

Figure 6 a. Construction of wheel and housing. Fluid flow is axially through the wheel. The wheel porosity here is represented by cylindrical channels for ease of calculation. A racetrack shaped superconducting magnet supplies the desired field shape.

b. Radial view of the wheel and wheel housing.

It may be necessary to avoid superfluidity in the helium in order to prevent undesirable thermal conduction between the hot and cold sides of the refrigerator. Thus, it may be necessary to add a small amount of ^{3}He to the ^{4}He to suppress the superfluidity. For operation at 1.8 K and above, 20 atm of pressure on pure ^{4}He will also prevent superfluidity. Efficient heat exchange between the wheel and the helium fluids will require forced flow.

Reference [21] details the capacity and efficiency calculation of this refrigerator, and will not be reproduced here. However, the results of that calculation are shown in Fig. 7.

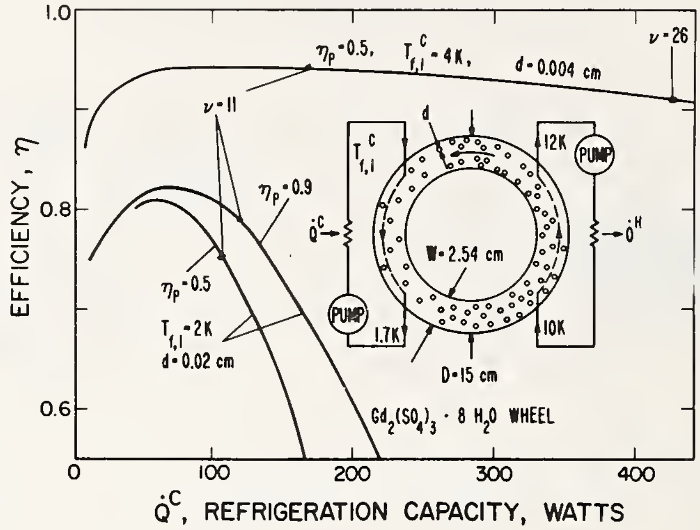

Figure 7

Figure 7 Expected performance of 15 cm $Gd_2(SO_4)_3 \cdot 8H_2O$ Carnot wheel refrigerator. The thickness in the axial direction is taken as 2.54 cm. Fraction of Carnot efficiency vs refrigeration capacity for various assumed values of the pump efficiency, η_p and temperature of cold fluid at inlet, $T^C_{f,i}$. Some values of rotation rate ν (in Hz) required are shown on the curves. A maximum field of 5 tesla is required for this refrigerator.

5. Conclusions

Two different approaches to the problem of pumping heat from the liquid helium temperature region to 10 K and above have been presented in this report.

The "conventional" unit discussed here has a much smaller capacity than the wheel refrigerator but has the advantage of straightforward design and fabrication. It is easy to instrument; thus weak spots in its design can be easily located and corrected. On the other hand, the more powerful wheel design is a marked departure from conventional magnetic refrigeration techniques and the concept needs to be proven. It requires a pump operating at low temperatures and is harder to instrument. While the magnetic susceptibility of the wheel is easily measured, its temperature is not.

The two approaches discussed here show promise in developing magnetic refrigeration above 1 K. Much better approaches and better materials will certainly be utilized in the future.

6. References

[1] Giauque, W. F., J. Am. Chem. Soc., 49, (1927) 1870.

[2] Debye, P., Ann. Physik, 81, (1926) 1154.

[3] Giauque, W. F. and MacDougall, D. P., Phys. Rev. 43, (1933) 768.

[4] White, G. K., Experimental Techniques in Low Temperature (Oxford University Press, London 1968) 2nd edition.

[5] Heer, C. V., Barnes, C. B., and Daunt, J. G., Rev. Sci. Inst. 25, (1954) 1088.

[6] Zimmerman, J. E., McNutt, J. D. and Bohm, H. V., Cryogenics 2, (1962) 153.

[7] Rosenblum, S. S., Sheinberg, H. and Steyert, W. A., Cryogenics 16, (1976) 245.

[8] Pratt, W. P., Jr., Rosenblum, S. S., Steyert, W. A. and Barclay, J. A., Cryogenics, in press.

[9] Brown, G. V., J. of Appl. Phys. 47, (1976) 3673.

[10] Rosenblum, S. S., Steyert, W. A., Pratt, W. P., Jr., Los Alamos Scientific Laboratory Report, LA-6581 (1977).

[11] Lake Shore Cryotronics, Eden, NY, USA.

[12] Morrish, A. H., "The Physical Principles of Magnetism," (John Wiley & Sons, NY, 1965) p. 86.

[13] Radebaugh, R., J. Low Temp. Phys. 27, (1977) 91.

[14] We have ≈380 g of copper representing a $\Delta S/R$ of 0.02 between 2 and 10 K.

[15] If we allow 1 cc of intrained helium gas or about 0.02 g of helium for a $\Delta S/R$ again of about 0.02.

[16] Rosenblum, S. S., Steyert, W. A. and Fickett, F. R., in press, Cryogenics.

[17] Reference [20] can be used to show that for heat $\dot{Q}$ deposited uniformly along a wire of area A and conductivity κ and of length L (the section inside the salt pill), that the average temperature drop $\overline{\Delta T}$ along L is given by $\dot{Q}L/3\ \kappa A$. Thus, the effective length of the wires is 1/3 the length inside the pill plus the full length external to the pill.

[18] Reference [20] calculates the average temperature drop $\overline{\Delta T}$ for heat $\dot{Q}$ deposited uniformly in a cylinder of length L', outside diameter D and inside diameter d and conductivity κ. If the heat is removed on the inside and if no heat escapes from the outside and if $D/d \approx 10$ then $\overline{\Delta T} = \dot{Q}/8\pi\ \kappa\ L' \times 0.15$ (for large D/d, $\overline{\Delta T}$ is only logarithmically dependent on D/d). We model the salt pill as many hexagonal shells (with wires of diameter d in the middle of each shell). By symmetry, the heat flow across the outside of the hexagon is zero. The hexagon is approximated by a circle to make the problem analytic.

[19] The wires deposit heat uniformly along a distance ℓ (measured perpendicular to the Be surface) in the indium-wire composite. As with Ref. [17] $\overline{\Delta T} = \dot{Q}\ell/3\ \kappa A$

[20] Steyert, W. A. and Stone, N. J., submitted to Cryogenics.

[21] Steyert, W. A., in press, J. App. Phys.

ELECTROCALORIC REFRIGERATION FOR THE 4-20 K TEMPERATURE RANGE

Ray Radebaugh
Cryogenics Division
National Bureau of Standards
Boulder, Colorado 80303

ABSTRACT

This paper reviews the principles and experimental results on electrocaloric refrigeration. The temperature range of 4-20 K is emphasized. Since work input comes from the electrical polarization of the dielectric material, no moving parts are required for such a refrigeration technique. The paper discusses the various types of materials which have been studied and the disappointingly low values of the electrocaloric effect. The results are shown to be consistent with theoretical models. The paper concludes that practical refrigeration with this method is not possible with present materials. Suggestions for further materials research are given.

INTRODUCTION

Electrocaloric refrigeration can be obtained from materials in which the entropy is changed by an applied electric field. It is the electrical analog of magnetocaloric refrigeration, better known as adiabatic demagnetization. With a material in the paraelectric state, an applied electric field decreases the entropy by aligning the electric dipoles. Electrocaloric refrigeration has the advantage that an electric field can be applied easily to materials in the form of thin plates with electrodes. High electric fields are easier to produce than high magnetic fields. The first measurements on the electrocaloric effect were done in 1930 on Rochelle salt [1], only four years after the first measurements of the magnetocaloric effect [2]. After the ferroelectric state was better understood, several more measurements of the electrocaloric effect were made on such materials [3]. These measurements were all done near room temperature. Granicher [4] first suggested the use of $SrTiO_3$ for electrocaloric cooling at low temperatures. Measurements by Hegenbarth [5] on $SrTiO_3$ ceramic showed a depolarization cooling of 60 mK at 17.5 K. Somewhat larger effects were seen in later measurements [6,7] on single crystal $SrTiO_3$, but these cooling effects disappeared below about 4-5 K. Electrocaloric cooling at still lower temperatures was first demonstrated in OH-doped KCl by three independent investigations [8-10]. Cooling to 0.36 K from a starting temperature of 1.3 K was reported [10]. Cooling to as low as 0.05 K was demonstrated for CN-doped RbCl [11]. The implications of these and other work in regard to refrigeration from 15 to 4 K are discussed in the following sections.

THEORY

Many dielectric materials undergo a transition to a ferroelectric or antiferroelectric state at sufficiently low temperatures. As discussed by Radebaugh [12] in a separate paper, the entropy change associated with such a transition may be significant ($S/R \simeq \ell n2$). Above the transition temperature an electric field can have a significant effect on the electric dipole entropy. The second TdS equation gives this entropy change as

$$Tds = c_E dT + T(\partial P/\partial T)_E dE \quad , \tag{1}$$

where s is the entropy per unit volume, c_E is the specific heat per unit volume at a constant field, and P is the polarization. The largest entropy change occurs when $(\partial P/\partial T)_E$ is largest and that usually occurs near the transition temperature. The polarization is related to the relative dielectric constant ε by the relationship

$$P(T,E) = \varepsilon_0 \int_0^E \varepsilon(T,E')dE' + P_r(T) \quad , \tag{2}$$

where ε_0 is the permittivity of free space and $P_r(T)$ is the remanent polarization in the material. For an ideal material above the transition temperature, P_r will be zero. In such cases measurements of the dielectric constant in various fields can give the expected depolarication-cooling effects via Eqs. (1) and (2). However, it has not been realized until recently that P_r can exist in many materials even though they are not in the ferroelectric state. Siegwarth [13] has suggested that this remanent polarization is a result of a thermal electret behavior. He suggests that small amounts of impurities can give rise to impurity-vacancy dipoles which can be frozen in position when the sample is cooled in an electric field. He shows that the resultant dielectric constant can have a peak at some temperature. In the past such peaks were taken as an indication of polar ordering (ferroelectric or anti-ferroelectric). When $P_r(T) \neq 0$, measurements of dc polarization instead of dielectric constant should be used in Eq. (1).

EXPERIMENTAL PROGRESS

Before the significance of the P_r term in Eq. (2) was known, it was thought that a material with a high $\partial\varepsilon/\partial T$ at 4 K would give rise to a large electrocaloric effect. A $SrTiO_3$ glass-ceramic material developed by Lawless [14] had a large $\partial\varepsilon/\partial T$ in the range 4 - 15 K. Because $\partial\varepsilon/\partial T$ was positive below about 30 K, cooling was expected to occur during polarization Evidence suggested the material was in the antiferroelectric state and not subject to hysteretic heating [16]. The feasibility of using these $SrTiO_3$ glass-ceramics for electrocaloric cooling was studied in a joint NBS/Corning Glass Works effort. Detailed results of that study are given elsewhere [17]. In that study the materials were to be used in a Carnot cycle between about 4 and 15 K. It would thus serve as a last stage below a 15 K mechanical refrigerator. Heat switches were to be utilized to carry out a Carnot cycle.

Extensive tests on these $SrTiO_3$ glass ceramics showed that only hysteretic heating occurred at 4 K. Small cooling effects of about 30 mK were seen during depolarization in the 10 - 40 K temperature range. Direct measurements of dc polarization showed a zero temperature derivative at 4 K and only a negative derivative above that [13]. The slope was consistent with the cooling observed, i.e., Eq. (1) was valid. At this point the inconsistent behavior of the dielectric constant with respect to polarization was explained by Siegwarth [13] to be due to electret effects.

Measurements on several other materials were made in the NBS/Corning study. These included $SrTiO_3$ ceramic, $KTaO_3$ single crystal and ceramics, lead zirconate titanate (PZT) ceramics and $Pb_2Nb_2O_7$-type ceramics. The largest electrocaloric effects were seen in $SrTiO_3$ ceramics [17,18] followed closely by a $KTaO_3$ single crystal [17,19]. In $SrTiO_3$ ceramics a temperature drop of about 0.1 K was observed at 10 K when depolarized from 26 kV/cm. It was estimated that the cooling would be about 0.5 K if the hysteretic effects could be eliminated. The cooling effects became insignificant at 4 K in this material and in $KTaO_3$ single crystal. The results were reasonably consistent with a theoretical model based on the lattice dynamics of these materials. It was shown [17] that since these materials were the displacive type, the electrically active entropy was associated with the transverse optic mode of the material. Since the calculated electrocaloric effect was slightly lower than observed values, it was suggested that there may be some interaction of the optic mode with the acoustic modes [17]. Through this interaction the electric field has some influence over the entropy of the acoustic phonons. From that analysis it was concluded that the maximum optic-mode entropy change in $SrTiO_3$ at 4 K is about $\Delta S/R \simeq 5 \times 10^{-6}$ at 4 K. Even if the total acoustic mode entropy could be removed by an electric field, it would still give only $\Delta S/R \simeq 10^{-4}$ at 4 K. These entropy changes are much too small [12] to be of any practical significance. Such behavior is typical of the displacive type materials. In these materials a transition to the ferroelectric state occurs when the transverse optic mode energy at the Brillouin center becomes zero at some finite temperature. No permanent electric-dipoles exist in these materials above the transition temperature. Thus, there is no analogy between these materials and paramagnetic materials. There is no reason to expect entropy changes for these materials on the order of $R\ell n2$ as is the case for magnetic systems [12].

SUGGESTIONS FOR FURTHER WORK

Order-disorder ferroelectrics do have permanent dipoles above the transition temperature and are analogous to magnetic systems. Potassium dihydrogen phosphate, KH_2PO_4, is a classical example of such a material and its entropy change [20] at the ferroelectric-paraelectric transition is $\Delta S/R = (1/2)\ell n2$. However, since the transition occurs at 122 K it has no controllable entropy available in the 4 - 20 K temperature range. At present there is no other known order-disorder ferroelectric or antiferroelectric with a lower transition temperature, except for doped materials. If such a material were found it would be useful for refrigeration at a lower temperature. The strength of the electric dipolar interaction may preclude [21] a transition temperature lower than about 15 K unless the dipoles are diluted.

As mentioned earlier, the doped alkali halides such as KCl:OH and RbCl:CN have been used for cooling at temperatures below 1 K. These are order-disorder materials and the entropy change from the ordered state to the disordered (paraelectric) state is $R\ell n6$. This change, however, is on a mole basis for the OH or CN dopant. Since these materials are doped to only about 5×10^{18} cm^{-3}, the refrigeration power per unit volume is rather small. At temperatures above 1 K the lattice heat capacity of the host material is so large that the electrocaloric cooling effects become too small to be of any use for refrigeration. If the concentration can be increased to at least 10^{20} cm^{-3}, refrigeration in the 4 - 15 K temperature range with these materials may be practical if high enough fields can be reached without breakdown. Some effort along this line is now in progress [22]. The problem to overcome in this approach is the clustering of the dopant dipoles when the concentration becomes high. Since clustering is an ordering mechanism, the dipolar entropy is partially or entirely removed even at room temperature. It is uncertain whether or not a dipole concentration of 10^{20} cm^{-3} can be achieved without clustering, but this line of research should be pursued further.

REFERENCES

1] P. Kobeko and J. Kurtschatov, Zeit. fur Physik 66, 192 (1930).
2] P. Weiss and R. Forrer, Ann. Phys. (Paris) 5, 153 (1926).
3] See, for example, P.D. Thacher, J. Appl. Phys. 39, 1996 (1968), and references cited therein.
4] H. Granicher, Helv. Phys. Acta 29, 210 (1956).
5] E. Hegenbarth, Cryogenics 1, 242 (1961).
6] A Kikuchi and E. Sawaguchi, J. Phys. Soc. Japan 19, 1497 (1964).
7] E. Hegenbarth, Phys. Stat. Sol. 8, 59 (1965).
8] W. Kanzig, H.R. Hart, Jr. and S. Roberts, Phys. Rev. Lett. 13, 543 (1964).
9] U. Kuhn and F. Lüty, Solid State Commun. 4, 31 (1965).
10] I. Shepherd and G. Feher, J. Phys. Chem. Solids 28, 2027 (1967).
11] R.O. Pohl, V.L. Taylor and W.M. Gouban, Phys. Rev. 178, 1431 (1969).
12] R. Radebaugh, this conference.
13] J.D. Siegwarth and A.J. Morrow, J. Appl. Phys. 47, 4784 (1976); J.D. Siegwarth, J. Appl. Phys. 48, 1 (1977).
14] W.N. Lawless, Rev. Sci. Instrum. 42, 561 (1971).
15] W.N. Lawless, U.S. Patent No. 3,638,440 (1972); Proc. Cry. Cooler Conf. (1973), Tech. Report AFFDL-TR-73-149, Vol. 1, p 417.
16] W.N. Lawless, Ferroelectrics 7, 379 (1974).
17] R. Radebaugh, J.D. Siegwarth, W.N. Lawless and A.J. Morrow, Tech. Report NBSIR 76-847 (1977).
18] W.N. Lawless and A.J. Morrow, Ferroelectrics 15, 159 (1977).
19] W.N. Lawless, Phys. Rev. B16, 433 (1977).
20] F. Jona and G. Shirane, Ferroelectric Crystals, Macmillan, New York (1962), p 251.
21] S.K. Kurtz, Trans. Amer. Crystallographic Assoc., Vol. II on Appl. Crystal Chem. (1975).
22] S. von Molnar, private communication (1977).

One Million Hours at 4.5 Kelvin*

W. H. Higa and E. Wiebe
Jet Propulsion Laboratory
California Institute of Technology
Pasadena, California 91103

A decade ago the authors published a paper [1] describing some novel approaches to simplify the construction of a 4.5 K closed cycle refrigerator (CCR). These CCR's are used to cool traveling wave masers (TWM) which are used on the large antennas of the Deep Space Communications Complex which JPL operates for the National Aeronautics and Space Administration.

Since that publication, some thirty of these CCR's have been installed, and a total of more than a million hours of operation have been logged. The purpose of this paper is to review the innovative features, the changes and the improvements which have been made, and to summarize the operational experiences of the past decade.

Key words: Cooling capacity monitor; cryogenic heat exchangers; fixed J-T valve; Gifford McMahon; masers.

1. Introduction

Figure 1 shows the flow diagram for the Joule-Thompson (J-T) circuit which has been added to a 15 K refrigerator in order to produce approximately 1 watt of refrigeration at 4.5 K. Although the CTI Model 350 refrigerator has been used by JPL, any comparable unit which can provide around 3 watts of cooling at 15 K and around 15 watts at 70-80 K may be used.

A compressor assembly supplies helium gas at 20 atmospheres pressure with return pressures of 7 atmospheres from the Gifford-McMahon cooler and 1 atmosphere from the J-T stream. The reciprocating displacer-regenerator assembly causes large pressure fluctuations, and it is necessary to use a pressure regulator (set at 18 atmospheres) to provide constant pressure to the J-T circuit in order to minimize temperature variations. Two charcoal traps are used at 70 K and 4.5 K respectively in order to remove contaminants before they reach the J-T valve.

In order to accelerate the cool-down procedure, especially when heavy superconducting magnets are used with the TWM, provision has been made to use liquid nitrogen precooling of the 4.5 K stage. The heat switch [2], which uses hydrogen gas to provide thermal conduction between copper plates, is used to further assist in the cool-down process. The fixed J-T valve has proven to be completely reliable and reproducible.

Further details are given in the next section. A subsequent section deals with instrumentation to facilitate the operation and maintenance of the CCR system. Special applications are discussed in the final section along with operational experiences to date. For the benefit of those not familiar with our original paper, we have tried to provide sufficient details so that there is no need to refer to that publication.

2. Joule-Thompson Components

The use of flexible metal hoses with helical convolutions for cryogenic heat exchanger applications has proven to be completely successful. The thin-walled phosphor bronze hoses (Anaconda Copper) have been found to have excellent transverse conductivity and very adequate longitudinal insulation. Figure 2 shows the principal elements of the heat exchanger prior to assembly. The inner surface of the flexible hose and the outer surface of the smaller stainless-steel tube form one passageway for the helium gas; while the outer surface of the flexible hose and the inner surface of the large stainless steel tube form the

*This paper presents the results of one phase of research carried out at the Jet Propulsion Laboratory, California Institute of Technology, under Contract No. NAS 7-100, sponsored by the National Aeronautics and Space Administration.

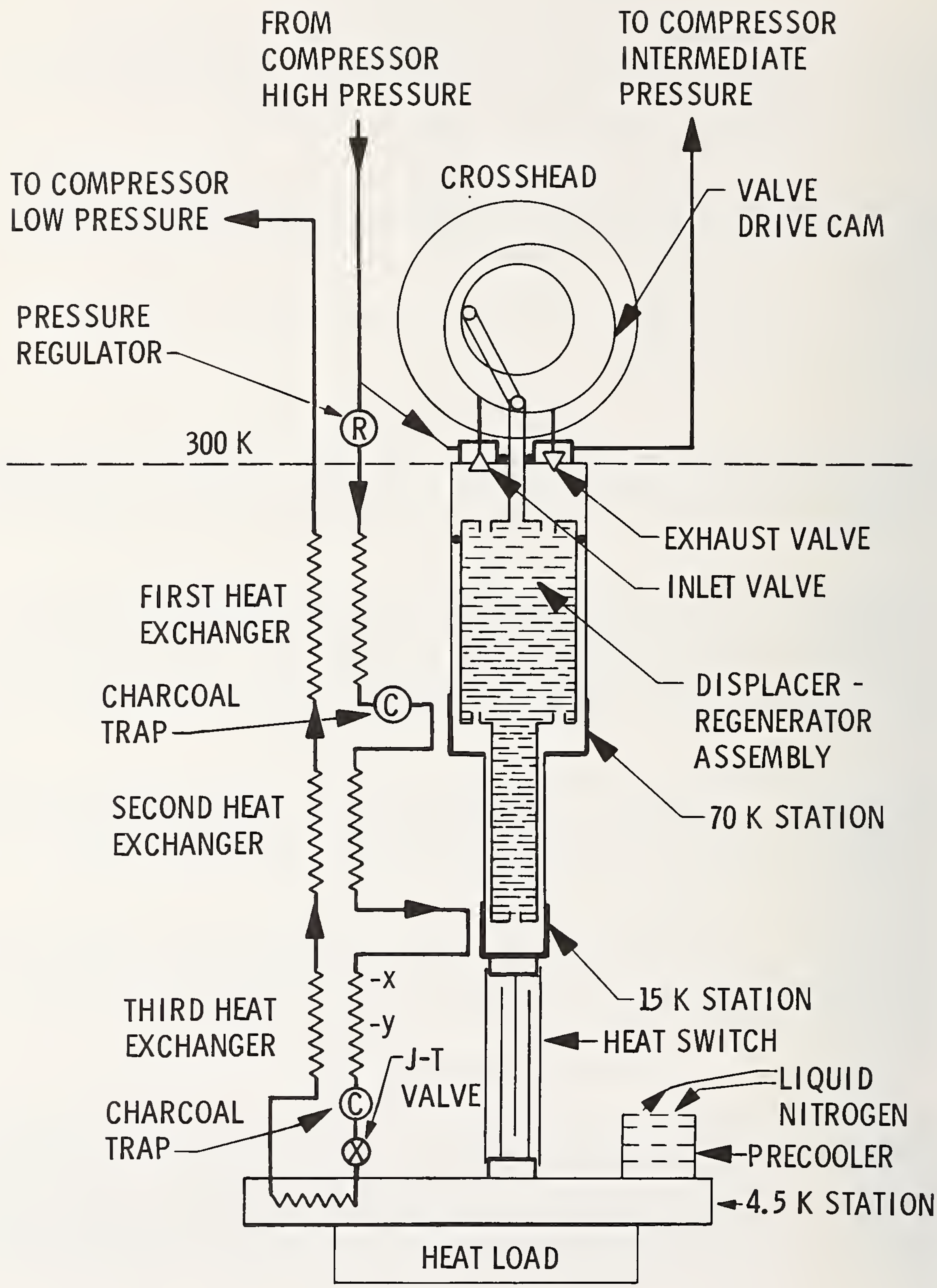

Figure 1. Schematic diagram for CCR.

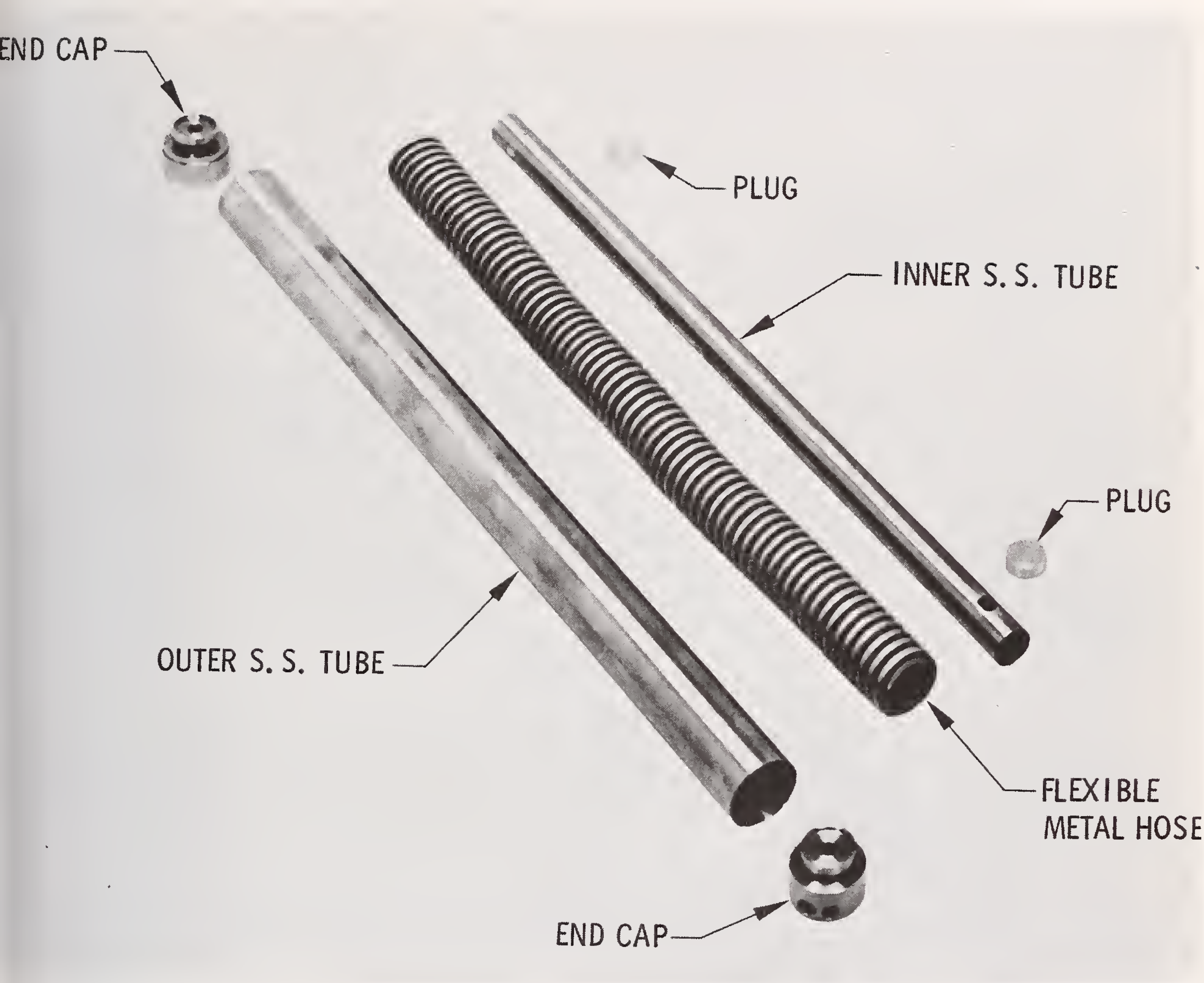

Figure 2. Elements of a cryogenic heat exchanger prior to assembly (see text).

counter flow passage. Careful welding and brazing techniques are essential for a good exchanger. The design of the end flanges is a matter of choice on the part of the designer; Figure 2 shows an early configuration.

For applications requiring less flow restrictions than the exchanger of Figure 2, we have also used the alternative shown in Figure 3, again using thin-walled flexible metal hose in a self-explanatory configuration. The exchanger in Figure 2 may be referred to as a parallel flow type, while that in Figure 3 is an orthogonal flow type. Figure 3 also shows a more recent end flange design which we now use in our exchangers. Table 1 gives the dimensions of the heat exchangers and charcoal filters.

Figure 4 shows a cutaway view of the fixed J-T valve which has been used in all of our CCR's. The hypodermic needle is pressed into the body of the valve, and the flow rate is adjusted by sizing a stainless-steel wire to the proper diameter and inserting into the needle. The 6-mil wire (not shown in Figure 4) fits into a 7-mil hole, and the end cap is soldered after flow adjustment has been made. The adjustment is made at ambient temperature; a flow meter is connected to the low pressure side of the J-T valve, and a flow of 0.14 SCFM with 18 atmospheres on the high pressure side assures a flow of around 1.4 SCFM under operating conditions.

The thermal switch [2] consists of concentric copper tubes with one set attached to the 15 K flange and the other set attached to the 4.5 K flange. The entire assembly is then enclosed in a stainless-steel tube and filled with hydrogen gas to a pressure of around 4 atmospheres. The hydrogen gas provides thermal conduction from flange to flange until it freezes out at around 20 K. Thereafter, the only conduction is due to the thin-walled stainless-steel tube. It is to be noted that this thermal switch is operable in any orientation relative to the local vertical, a feature which was important in a special application to be described later. The liquid nitrogen precooler consists of an arrangement for providing a large surface-to-volume container for a liquid nitrogen stream which is supplied through thin-walled stainless-steel tubes. After precooling of the maser and superconducting magnet assembly, the liquid nitrogen inlet and outlet tubes are shunted to each other via a flexible rubber hose and need no further attention.

3. Instrumentation

The successful performance of the cryogenic system described, in a worldwide network of tracking stations, has been due largely to the monitoring instrumentation employed. These instruments provide information on the operating condition of the overall system during the cool-down and while operating. Operating personnel are quickly trained to anticipate problems in the system.

Thermocouples are used on all three stages (70 K, 15 K, 4.5 K) shown in Figure 1. Accurate monitoring of the 4.5 K stage is provided by a helium vapor pressure gauge. An electric heating element is also attached to the 4.5 K station so that a variable heat load may be applied to test the cooling capacity of the cryocooler. During cool-down the operator may record on a strip chart the output from any of the sensors as a diagnostic procedure when necessary.

Table 1. Dimensions of heat exchangers and charcoal filters

Component	Outer diameter, cm	Length, cm	Comments
Heat exchanger No. 1	3.1	28	
Heat exchanger No. 2	2.3	20	
Heat exchanger No. 3	1.7	19	2 in series
Charcoal trap No. 1	2.3	20	
Charcoal trap No. 2	1.3	8.8	

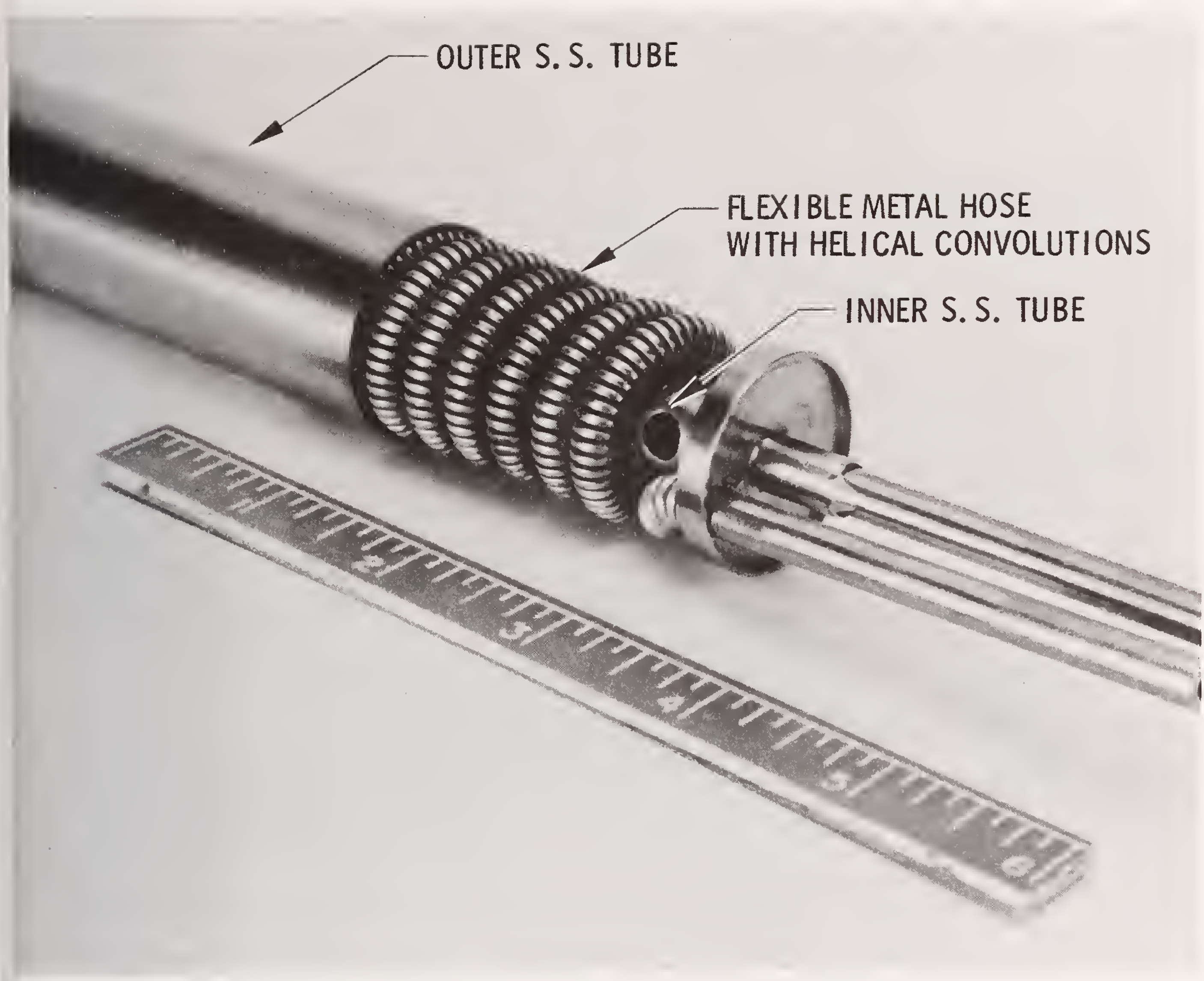

Figure 3. Orthogonal flow heat exchanger partially assembled (see text).

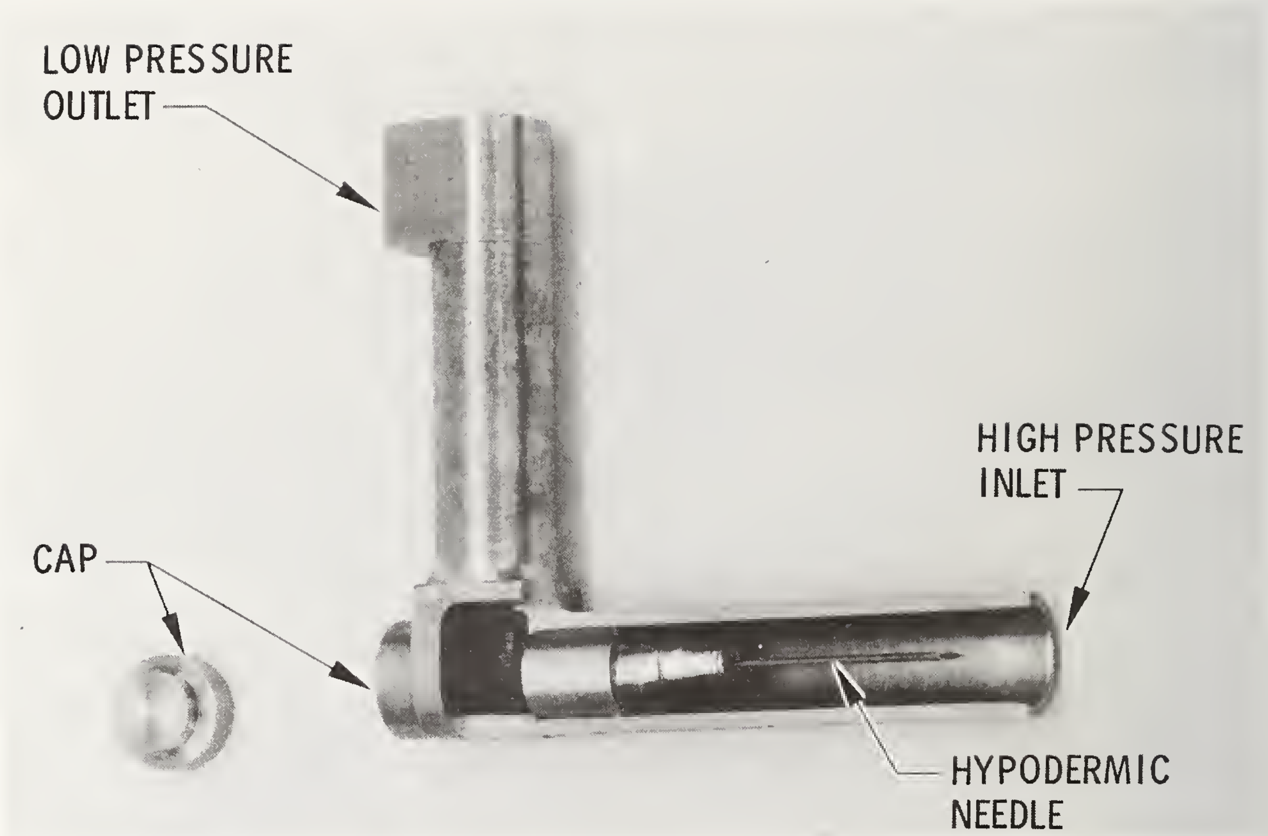

Figure 4. Cutaway view of J-T valve employing a hypodermic needle.

A challenging problem has been that of determining the cooler capacity while the system is in use, and particularly during critical missions. The use of the electrical heater on the 4.5 K stage provides a positive means of measuring the capacity, but it can also overload the cooler and require many minutes to recover. A solution [3] to this perplexing problem has been found and may be used in the future on all systems.

It was found that by monitoring the temperatures at two judiciously selected positions (x and y in Figure 1) on the final heat-exchanger, one could easily monitor the cooling capacity of the CCR. Resistors at x and y form two sides of a bridge circuit; the unbalanced condition may then be directly calibrated against the heater power input at the 4.5 K station. Once calibrated, the monitor provides a continuous indication of cooling capacity. A flow meter in the J-T return line is used concurrently with the capacitor monitor to remove any possibilities for ambiguous readings.

4. Applications

Figure 5 shows the cryocooler just prior to the installation of the TWM assembly at the 4.5 K station. A radiation shield (not shown) is attached to the 70 K station and surrounds all areas cooled by the 15 K and 4.5 K stations. The noise temperature at the coaxial line input terminal for an S-band TWM was around 5 K. The coaxial signal input line contributed approximately 3 K of the above noise temperature.

During the Mariner to Venus and Mercury (MVM) mission a request was received to reduce the 5 K noise temperature by at least 2 K. This was achieved [4] by replacing the 0.5-meter-long input transmission line with a shortened coaxial line as shown in Figure 6. The center conductor was made of copper and attached directly to the 4.5 K station. The fused quartz dome provided the vacuum seal required. The noise temperature at the waveguide input was 2.1 K and is believed to be a record low for an S-band maser operating at 4.5 K.

In concluding this brief discussion on applications to masers, we would like to point out that the last application required that the cryocooler be operated upside-down relative to the usual configuration. Very little difference in the operating characteristics was noted.

5. Conclusions

The tracking stations in which masers are used are located in Goldstone, California, Woomera, Australia and Madrid, Spain. Some training of station personnel was provided when equipment was originally installed; however, repairs and maintenance procedures are now carried out on a routine basis by station personnel. Only major repair operations are performed at a repair depot in California. Routine mechanical maintenance is scheduled once annually, and the only other operator procedure required is to purge the J-T circuit with a vacuum pump once or twice per year. The latter operation requires but one or two hours to execute. An operational 4.5 K cryocooler has, indeed, been realized.

Other organizations, with and without cryogenics experience, have successfully duplicated the CCR described here.

6. References

[1] Higa, W. H., and Wiebe, E., A simplified approach to heat exchanger construction for cryogenic refrigerators, Cryogenic Technol. (March/April 1967).

[2] U. S. Patent No. 3,260,055 issued to E. Wiebe on Thermal Switch.

[3] U. S. Patent No. 3,914,950 issued to E. Wiebe on Capacity Monitor.

[4] U. S. Patent No. 3,902,143 issued to R. Clauss and E. Wiebe on Ultra Low-Noise Input Transmission Line for Masers.

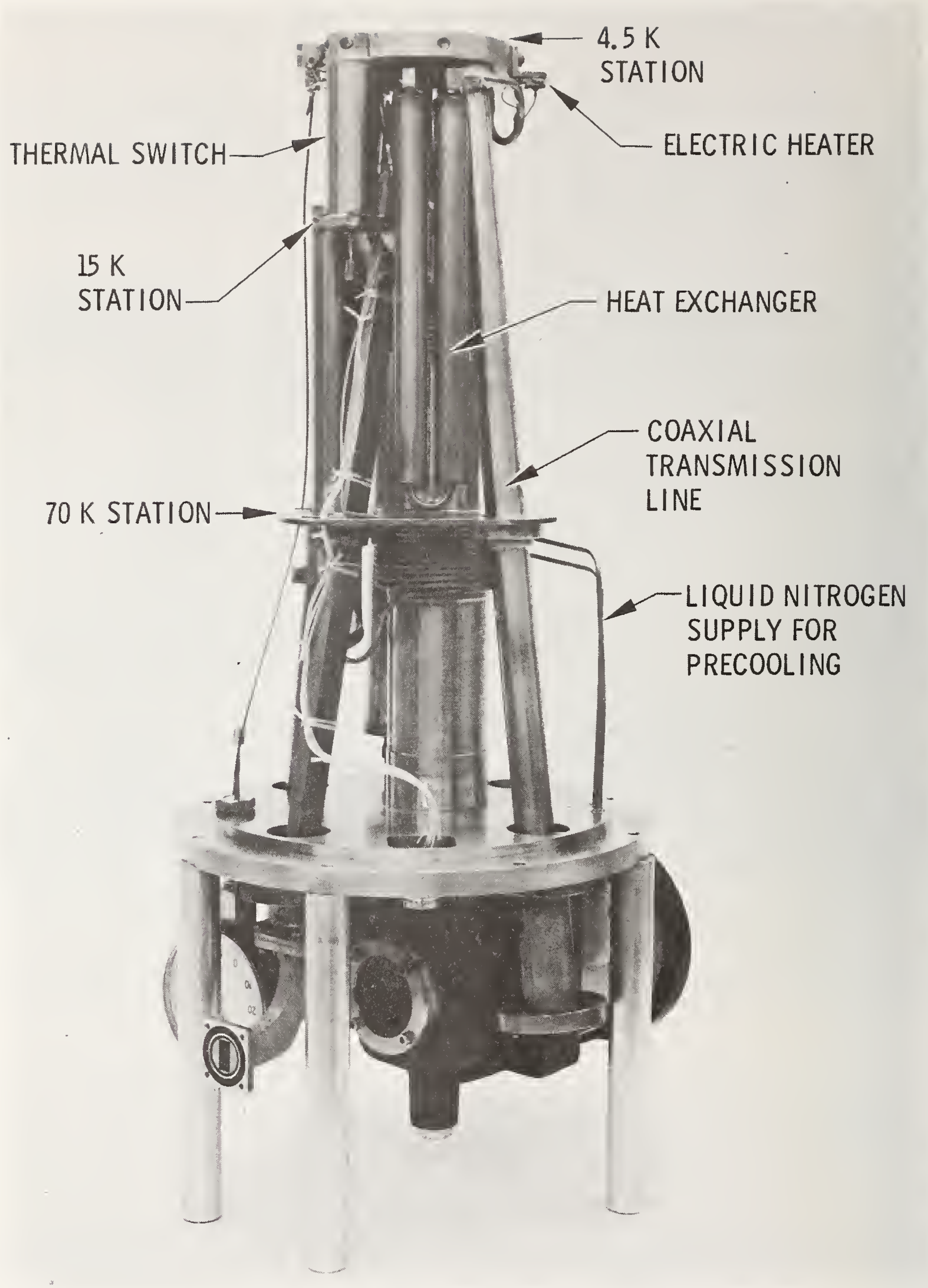

Figure 5. Partially assembled CCR with some components identified. A radiation shield is attached to the 70 K station and surrounds all the lower temperature parts.

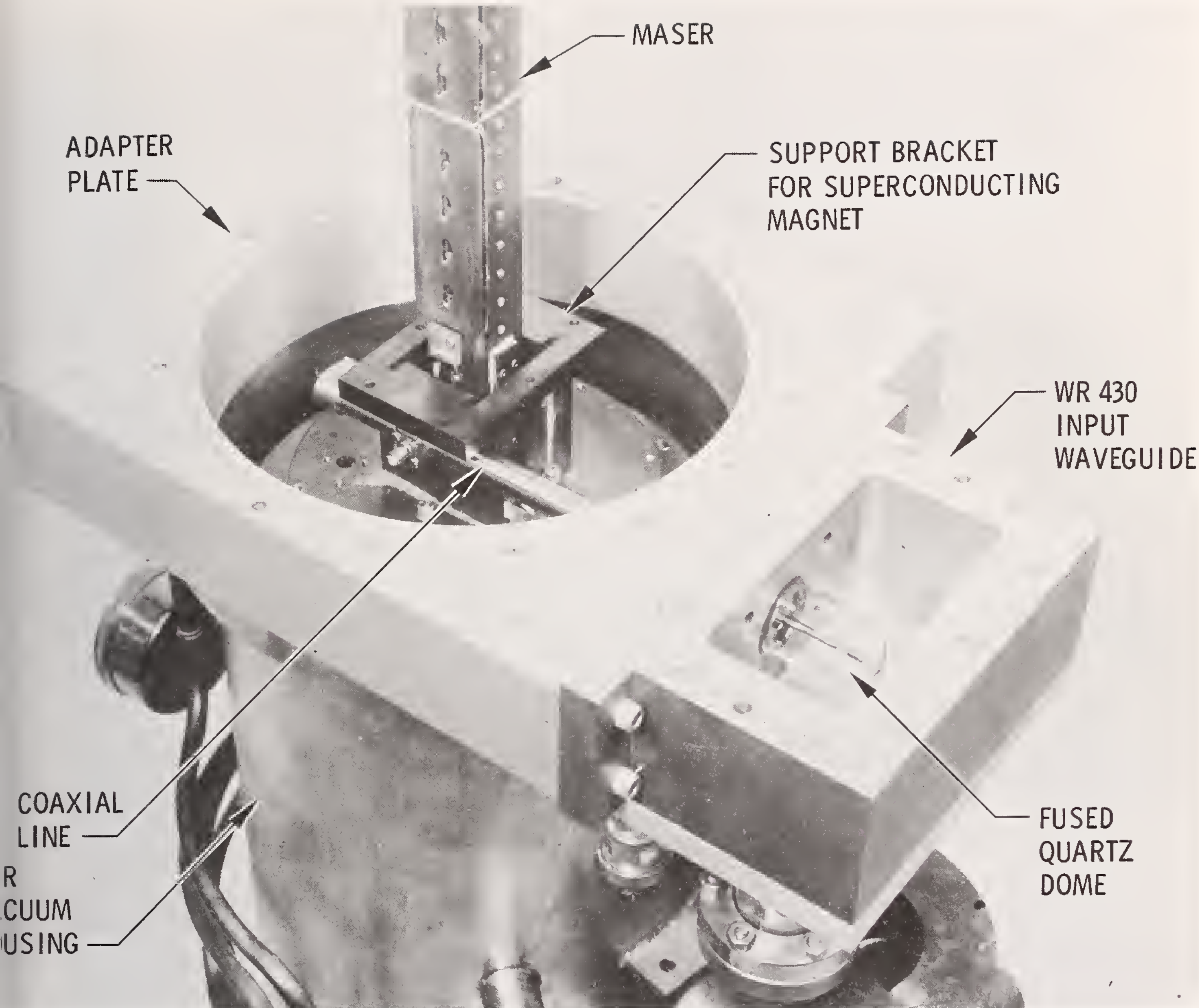

Figure 6. Signal input transmission line for 2.1 K S-band maser.

Acknowledgments

The authors are grateful to their many colleagues who have helped in this effort. Special thanks are due R. Clauss and R. Quinn.

Design Compromises in the Selection of Closed-Cycle Cryocoolers

Fred F. Chellis
Development Engineer - CTI-CRYOGENICS, Military Products Group

The systems designer is often faced with a dilemma when choosing a closed-cycle cryocooler for a specific application. He must choose between his need for extremely long operating life, and his desire for small size and minimum weight. The perfect all-purpose closed-cycle cryocooler does not exist. Each application has its own special requirements which affect the cryocooler configuration: A paramp cooler in a satellite communications antenna is not limited as to size and weight but must operate 24 hours a day continuously for over two years with hands-off operation; whereas, a cooler in an airborne infrared set must be designed primarily for minimum size and weight.

This paper describes some of the problems in designing a cryocooler for a specific application and stresses early cooperation between the user and the designer of the cryocooler. Actual case histories will be discussed.

Key words: Cryocooler, infrared, SQUID, Josephson junction, satellite communications.

1. Introduction

One of the earliest closed-cycle cryocoolers was developed in 1958 for cooling a 3 channel ruby laser in a target tracking radar set. This system included 3 stages of expansion, plus a Joule-Thomson stage to provide cooling at 3.8K. Soon thereafter similar systems were installed in the Telstar antenna in Andover, Maine for intercontinental telecommunications via satellite, and in the giant antenna at Goldstone, California for deep space tracking. The Goldstone installation provided the principal communications link with our astronauts and is still in service today providing communication with the Mariner deep space probes, as they travel the outer reaches of our solar system.

With the development of the parametric amplifier (paramp), which operates at 20K, a simplified and somewhat smaller two-stage cryocooler was developed with an emphasis on high reliability and long unattended operating life. These machines typically operate continuously for over 2 years without repair or overhaul. To accomplish this, they are conservatively designed with an oil-lubricated compressor and low operating speeds.

In the early 1960's the closed-cycle cryocooler was adapted to the cooling of small infrared devices for military airborne applications, including reconnaissance and target acquisition. Here the emphasis was upon miniaturization to reduce size and weight of the cryocooler and to minimize cool-down time. In order to get the most cryocooler in the smallest package, it was necessary to reduce the size of mechanical components and to increase operating speed and charge pressure levels. Many of these coolers were built and are presently in service. However, the cost of maintenance and the training of specialists in field repair of these systems has prompted the search for a low life cycle cost system for future applications. Here the emphasis is not really on miniaturization and infinite operating life, but upon an acceptable system size with an operating life of about 3000 hours with no maintenance. Today with the rapid improvement in electronics design, and ever smaller electronic packages, the cryocooler stands out as the largest, most expensive single component in an infrared system. Therefore, there is a continuing effort to develop more reliable cryocoolers in smaller sizes, at lower cost of ownership.

2. Types of Closed-Cycle Cryocoolers

All closed-cycle cryocoolers in general usage today operate on a cyclic thermodynamic process and employ the following components: A compressor with an aftercooler heat exchanger that removes the heat of compression from the working gas, and an expander with a reciprocating displacer element and a regenerative heat exchanger that alternately removes and restores heat to the working gas flowing through it. Closed-cycle cryocoolers may be subdivided into the following classes in accordance with their operating principles (also see Figure 1):

2.1. Gifford-McMahon (G-M)

In Gifford-McMahon cryocoolers the compressor assembly and the expander assembly are typically widely separated from one another, and two interconnecting gas lines join them. The expander requires a small motor to move the displacer up and down and to operate the valves in the expander head. The presence of valves in both the compressor and the expander isolates them from one another and allows the compressor to operate at a different speed from the expander. This arrangement allows the interconnecting lines to be of almost any desired length since their volumes are effectively isolated from the thermodynamically active volumes in the system. The long lines allow separation of the compressor package from the expander, thereby removing the principal mass and source of heat and vibration from the critical region of the device being cooled. These advantages are somewhat offset by the larger size and higher power requirements of this type of system.

2.2. Integral Stirling

The basic integral Stirling cryocooler consists of a compressor section and an expander section combined in one integrated package. The reciprocating elements of the expander and compressor are mechanically driven from a common crankshaft with the proper phase relationship so that no valves are required in the system. The integral Stirling cycle cryocooler is inherently the most efficient of all cryocoolers and has a particular appeal because of its basic design simplicity, compactness, and lower power input. The integral Stirling does have the disadvantage that the compressor, with its heat and vibration output, must be located in close proximity to the cooled device, since the compressor and expander are combined in one assembly.

2.3. Split Stirling

In the split Stirling system the compressor, with its motor and heat exchanger, comprise one package while the expander comprises a second package and the two are interconnected by a single gas line. This overcomes the principal objection to the integral Stirling design, since it allows the compressor to be separated from the expander thus removing the bulk, heat and vibration of the compressor from the sensitive region of the detector, amplifier or other cooled device. This also considerably simplifies the packaging problem.

Reciprocal motion for the displacer is provided by a compact pneumatic drive wherein the sinusoidal pressure fluctuations, generated by the compressor, provide the necessary forces to drive the displacer up and down in proper timed relationship with the compressor. Since the system uses no valves, the gas line constitutes an important void volume which must be minimized by limiting the line length and, therefore, the distance between the compressor and expander. Gas lines up to five feet in length have been evaluated but 12 to 18 inch line lengths are more practical. Because of the added void volumes associated with the interconnecting line and the lack of a direct mechanical linkage between the displacer and compressor, the split Stirling cooler is inherently less efficient than the corresponding one-piece Stirling.

2.4. Integral Vuilleumier (VM)

The VM cryocooler is best described as a Stirling cycle cooler wherein the mechanical compressor component has been replaced by a thermal compressor. The only mechanical input which is required in this type of system is that needed to shuttle the displacers back and forth and this can be accomplished with a very small electric motor, (compared with the larger motor in the Stirling cycle machine). Since the mechanical forces required to drive the VM are substantially lower than those in other types of cryocoolers, it follows that mechanical wear would be significantly reduced with a consequent increase in operating life and reliability. However, because the compression is provided by transfer of electrical heat to the working gas, this cycle is inherently less efficient than the one-piece Stirling counterpart, and an added electronic package is required to control the heater at the hot end. Because of high operating temperatures in the compressor, wear of the hot displacer sealing and riding surfaces is a significant design consideration.

2.5. Split VM

The split VM configuration bears the same relationship to the VM as the split Stirling does to the Stirling configuration. Here we have a thermal compressor (instead of a mechanical compressor) communicating with a remotely-located pneumatically-actuated expander through a single gas line. This system incorporates the advantages of the split Stirling configuration with those of the VM and shares the disadvantages of both.

3. Design Considerations and System Trade-offs

Very small closed-cycle cryocoolers (in the capacity range of about 0.5 watt at 77K or smaller) have a sufficiently low input power requirement (100 watts or less) that they may be conductively cooled by bolting them to a large metal mass or convectively cooled by ambient air. However, cryocoolers with a higher input power require forced air cooling to move air over external fins on the compressor section of the cryocooler for proper heat rejection.

With very large systems, where the input power is more than 400 watts, heat rejection may require special liquid cooling techniques involving oil or a special coolant, a circulating pump and a liquid-to-air heat exchanger with a fan or other source of forced air cooling. These additional elements add considerably to the size and weight of the closed-cycle cryocooler system.

Because of mechanical wear and other considerations, it is unreasonable to expect that a cryocooler will maintain the same level of cooling capacity throughout its operating life. The wear of compressor piston seals and displacer seals degrades performance in two ways. Firstly, the seals begin to leak, which allows gas blow-by, and secondly, the wear products accumulate in gas passages and the regenerator matrix to restrict gas flow. Additionally, outgassed organic materials from bearing lubricants, motor windings, etc. migrates to, and freezes out in, the regenerator matrix and in the clearance spaces at the cold end of the expander. It is therefore necessary to provide excess cooler capacity in the basic cooler design, in order to have sufficient capacity at the end of the required operating period. The problem is that added cooling capacity requires a larger system, and a larger system requires more power input. Since a cryocooler is a 100% loss device, all the electrical power which goes in to drive the system must be rejected as heat. So, the larger the system, the larger the fan, fins, heat exchanger, etc. needed to get rid of the heat.

Therefore, there is an important trade-off between cooling capacity (system size) and operating life requirements. If the physical size of the closed-cycle cryocooler is of great importance, then the systems designer should concentrate upon minimizing his cooling requirements. This can be done through careful design of the actual cooled device to minimize thermal loads caused by heat conduction and radiation and by the elimination of unnecessary factors of safety in his design. A realistic overall factor of safety is best arrived at through close and early cooperation between the cryocooler design engineer and the designer of the cooled system.

Some of the most difficult conditions are created in military airborne applications where a cryocooler must operate in a 55°C environment and often in a totally enclosed chamber close packed with other heat rejecting apparatus. A cryocooler's main purpose in life is to reject heat and it is happy only when it receives proper cooling.

Closed-cycle cryocoolers have a reciprocating displacer/regenerator element in the expander which is driven by either mechanical or pneumatic means. The motion of the displacer is, typically, not balanced and so creates a vibration which is transmitted to the cooled device which is mounted on the cold tip. This is not generally a problem so long as the expander, with its cantilevered cold tip, is rigidly mounted. However, some of the newer devices including Josephson junctions and SQUID's are so sensitive to microphonics that integrating them with a closed-cycle cryocooler presents a serious problem which has not yet been solved.

Another problem that is often encountered is that of thermophonics. The problem is inherent in the cyclic operation of the cryocooler wherein the actual temperature at the cold tip fluctuates a few millidegrees with each expansion event of the cooler. This problem is especially noticeable with some of the new supersensitive devices such as SQUID magnetometers and Josephson junctions. The thermal "ripple" can often be smoothed out by the interposition of a thermal mass (lead block, for example) between the cold tip and the load (cooled device). However, the cooldown time of the system is increased, and the system's designer must choose between signal interference due to thermophonics and minimum system cooldown time.

4. Examples of Actual Cryocooler Applications

When selecting a closed-cycle cryocooler for a particular application, it is helpful to know how others have faced this problem and what concessions they had to make in order to fulfill their needs. Past experience has shown that nearly every application has its own particular requirements which can best be met by tailoring the design of the cryocooler to the specific application. The following examples demonstrate the variety of available systems and briefly describe the life history of each. (See Table 1.)

4.1. Ground Based Closed-Cycle Cryocooler for Satellite Communications Application

At the present time there are over 800 satellite communications ground stations in continuous around-the-clock operation scattered around the entire globe. Some of these are in military communications networks; others are in civilian telecommunications duty. Some are in the U.S., but most of them are located in foreign countries, (including Russia and the Peoples Republic of China). These systems use a parametric amplifier cooled to 20K and operate continuously for 16,000 to 18,000 hours without repair or maintenance. The total useful life of a system is well in excess of 100,000 hours. A closed-cycle cryocooler working on the Gifford-McMahon principle was chosen for this application since it permitted installation of the expander assembly at the focal point of the parabolic antenna, with the parametric amplifier components mounted on the cold tip of the expander for cooling to 20K. (See Figure 2.) The 175 pound compressor package was located at ground level in the base of the antenna with 100 feet of gas lines communicating with the expander. The overriding design requirement for this system was extremely long, maintenance-free, operating life. The size of the total system was unimportant and the total input power requirements were of secondary importance. These cryocoolers have accumulated an impressive reliability record. After millions of hours of total accumulated running time, the demonstrated MTBF of these systems is in excess of 20,000 hours. Since shutdown of these coolers would incur a severe penalty in terms of loss of TV programming or telephone and data links, the servicing and maintenance schedule calls for replacement of an adsorber trap at 3,000 hour intervals (without system shutdown) and scheduled overhaul of the expander head every 16,000 hours (2 years) of operation. This impressive reliability experience was achieved by using a medium speed (1,800 rpm) oil-lubricated compressor combined with a slow speed, semi-dry lubricated expander employing a 72 rpm drive motor (hence, eliminating the requirement for extra gears and bearings which would have impacted the life expectancy of the system).

4.2. Airborne Infrared Cryocooler for Use in B-52 Bomber

This cryocooler (Figure 3) was tailored to meet the requirement for cooling a Forward Looking InfraRed (FLIR) detector array to 20K for use in the B-52 bomber. Here again, the overriding consideration was for a cryocooler to operate reliably and continuously for extremely long periods, and it was decided to incorporate the design philosophy which was used in the satellite communications coolers but to scale down the size to meet the airborne requirements. The compressor package for this system utilizes a high speed, oil-lubricated compressor pump in conjunction with a medium speed gear motor driving a semi-dry lubricated expander operating on the Gifford-McMahon principle. Three foot gas lines allow the compressor to be located away from the expander. The service schedule for this system calls for adsorber replacement at 600 hours. There is no scheduled maintenance. Over 400 units of this system have been installed and are in current use. The demonstrated MTBF for this system is in excess of 1000 hours. It will be noted that we have sacrificed some operating life in order to gain a more compact package for airborne use. Since the useful operating life of the system is only required to be 3000 hours, and since aircraft are overhauled at regular intervals, such a sacrifice is reasonable.

4.3. Airborne Infrared Coolers for High Performance Aircraft

Because of space limitations on small aircraft the overriding consideration in closed-cycle cryocooler selection is minimum size, weight and power input. A G-M system is generally not applicable. The Stirling (or, more recently, the split Stirling configuration) is the type of cryocooler most often selected for this application. The integral Stirling cryocooler is available in both 20K and 77K configurations for airborne infrared systems. A typical 20K system is the one used for cooling the AN/AAS-18 infrared system on the RF-4C reconnaissance aircraft (Figure 4). Over 1,200 of these systems are in service. This system uses liquid cooling in the cooler heat exchanger to remove the heat of compression and has a coolant circulating pump and an auxiliary heat exchanger and associated liquid coolant piping. In this capacity and temperature range it will be noted that the integral Stirling system has essentially the same size and weight requirements as a comparable G-M system. However, the power input requirement for the integral Stirling is about half that for the G-M system.

4.4. Miniature Stirling Cryocoolers for Infrared Applications

Recent innovations in electronics design have made it possible to build a truly compact infrared set with minimum cooling requirements. For this application integral Stirling cryocoolers have been developed to provide up to 1 watt of cooling at 77K with less than 100 watts of input power and a total system weight of about 3 pounds (Figure 5). To accomplish this, it was necessary to employ high operating speeds and elevated charge pressure levels which adversely affect the operating life of the machine and increases vibration level at the cold tip where the infrared detector is located. Even though the cryocooler may be well balanced mechanically, vibration transmitted from the compressor creates microphonics which are picked up by the infrared detector on the more sensitive applications. This problem has been solved in some applications by use of the split Stirling system (Figure 6) wherein the expander is separated from the compressor package by a distance of one or two feet thus minimizing transmitted vibration and importantly easing packaging problems. These systems are in the advanced development stage and are beginning to appear in a limited number of airborne applications. Extensive life testing is underway to prove reliability and demonstrate a reasonable maintenance schedule.

4.5. VM Cryocooler for Airborne Uses

The U.S. Air Force has been the principal sponsor in the development of VM and split VM cryocoolers for airborne uses, with the emphasis on reduced life cycle cost. The reasoning is that the total cost of a really reliable cryocooler, over its operating lifetime, will be lower (in spite of higher initial purchase cost) because of lower maintenance and repair costs. Wright Patterson Air Force Base is currently funding a program for the procurement of a split VM cooler (Figure 7) which will be known as the Air Force Standard Cooler. The goal is to have one standardized cooler in the Air Force inventory which would be specified for a wide range of future airborne cryocooler needs. Although these systems are not yet in common useage, they will be incorporated into a variety of airborne applications in the near future.

5. Summary

In summary, there is no single cryocooler design that is optimized for all applications. Each type of cryocooler has inherent advantages and disadvantages. The factors of size, weight, power, operating life and reliability must be carefully evaluated and suitable trade-offs made in order to select the optimum cryocooler configuration for a specific application.

The presently accepted procedure is to modify an existing cryocooler design or to develop a new one to fit the interface requirements of each specific application. This approach is both time consuming and expensive.

The recent trend in military cryocooler design is toward standardization. The U.S. Army has developed a modular approach to infrared set design which includes a standard cryocooler configuration of the integral Stirling type. The U.S. Air Force is concentrating on a standardized cooler employing the split VM configuration. These are both small systems operating in the capacity range of 1 watt @ 77K, and they will find their place in a variety of applications where the cooling and interface requirements are similar. However, a new generation of cryocooled devices is in the planning stage, which will have greater sensitivity and will require cooling at 20K or lower. These include such exotic devices as MFPA's (Monolithic Focal Plane Arrays), SQUID's (Superconducting QUantum Interference Devices) and Josephson junctions. These systems will require a new generation of cryocoolers with greater emphasis upon reduced vibration and thermal stability in order to minimize problems of microphonics and thermophonics in the cooled device.

The perfect all-purpose, closed-cycle cryocooler has yet to be discovered.

Table 1 A Comparison of Closed-Cycle Cryocoolers

CRYOCOOLER TYPE	COOLING CAPACITY		INPUT POWER	COMPRESSOR		EXPANDER		MTBF	APPLICATION
				SIZE	WT.*	SIZE	WT.		
	WATTS	°K	WATTS	INCHES	LBS.	INCHES	LBS.	HOURS	
G-M	3	20	2,100	28 x 16 x 16	175	18 x 10 x 6	22	20,000	Ground Based Paramp
G-M	1	26	790	10 x 10 x 10	20	11 x 6 x 2.5	5	1,000	Airborne IR
Integral Stirling	1	26	475	14 x 10 x 6	26	- - - - - - - -	---	250	Airborne IR
Integral Stirling	1	77	100	11 x 4.5 x 3	3.5	- - - - - - - -	---	250	Airborne IR
Split Stirling	1	77	135	10 x 5.5 x 2.5	5	3 x 2.5 x 2	.3	1,000	Airborne IR
Split VM	1	77	350	10 x 4 x 3	10.5**	3 x 2.5 x 2	.3	2,200	Airborne IR

* Includes Fan

** Includes Motor Inverter and Electronic Temperature Controller for Hot End

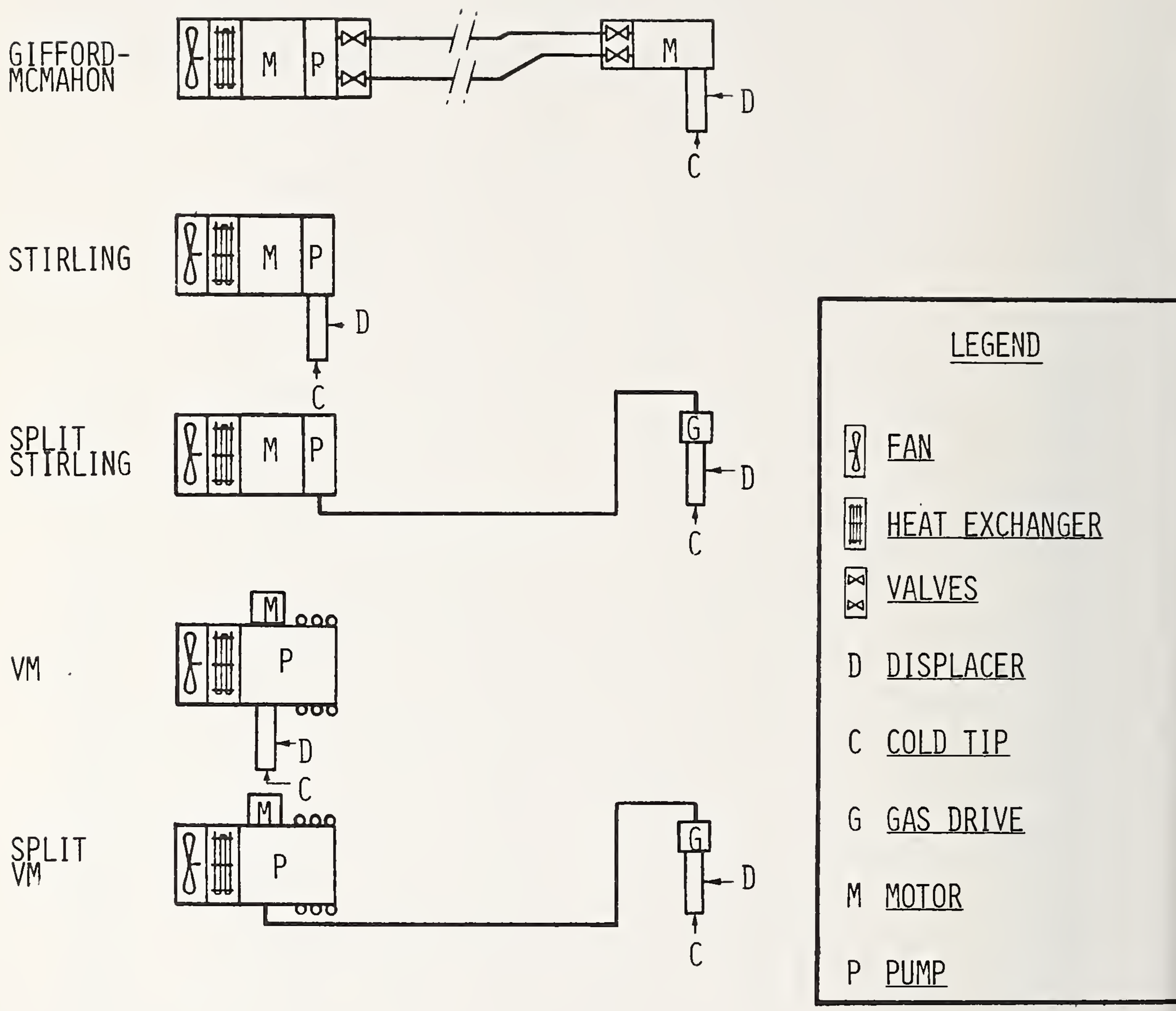

FIGURE 1. TYPES OF CLOSED-CYCLE CRYOCOOLERS

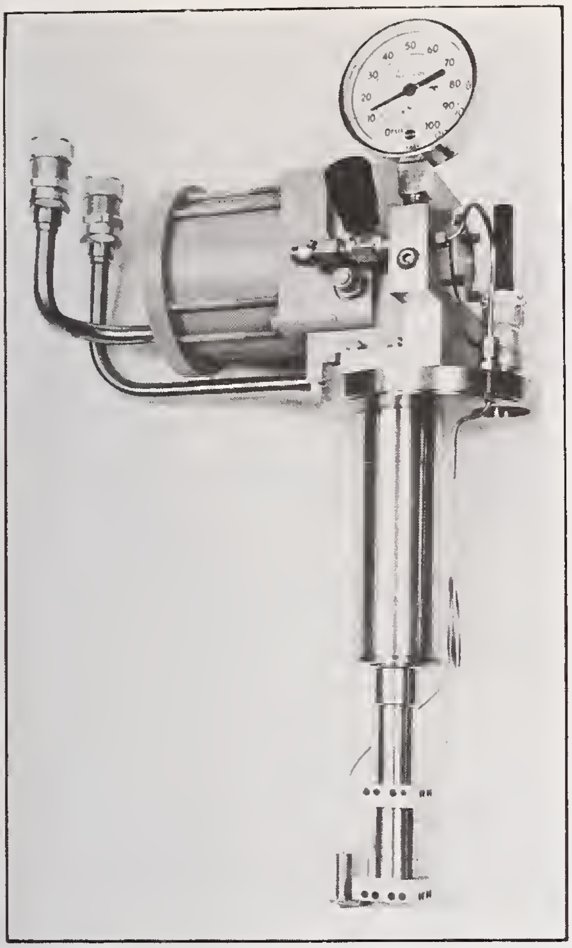

REFRIGERATOR ASSEMBLY

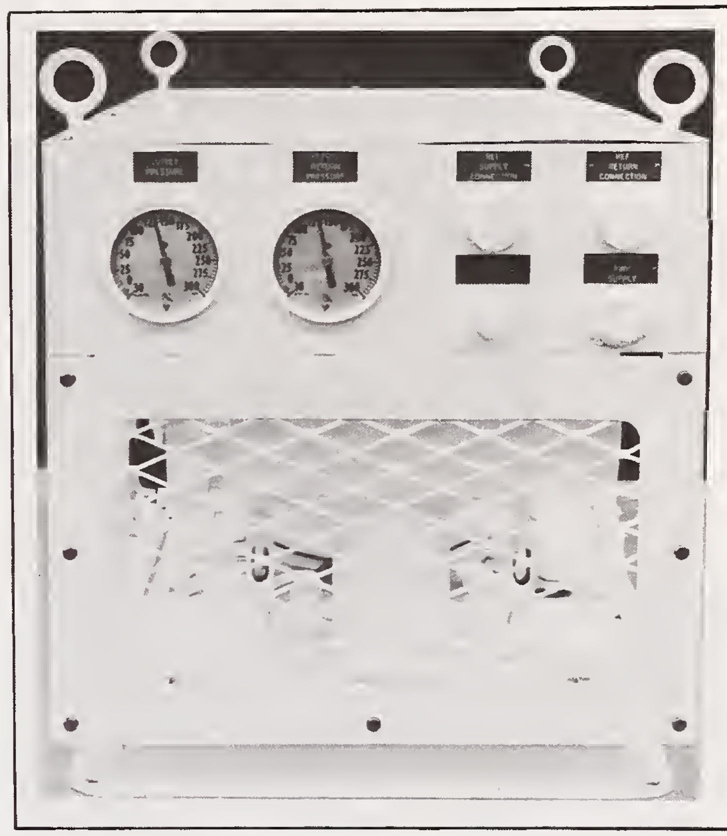

COMPRESSOR ASSEMBLY

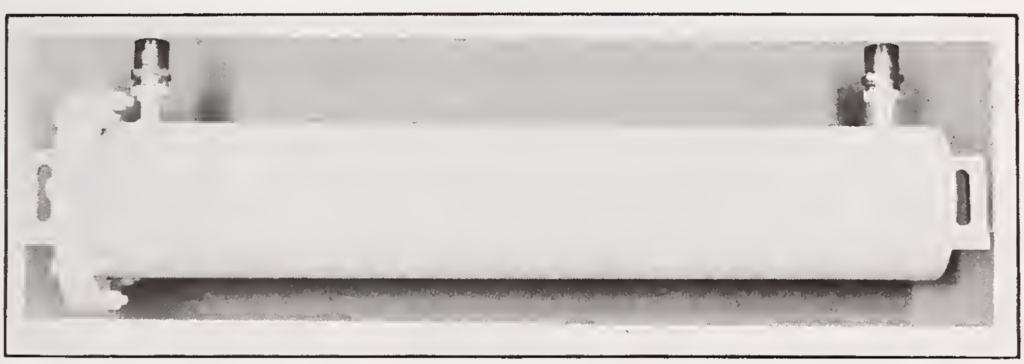

ADSORBER TRAP

Figure 2. Ground-Based Paramp Cryocooler
3 Watts @ 20 K; G-M Cycle

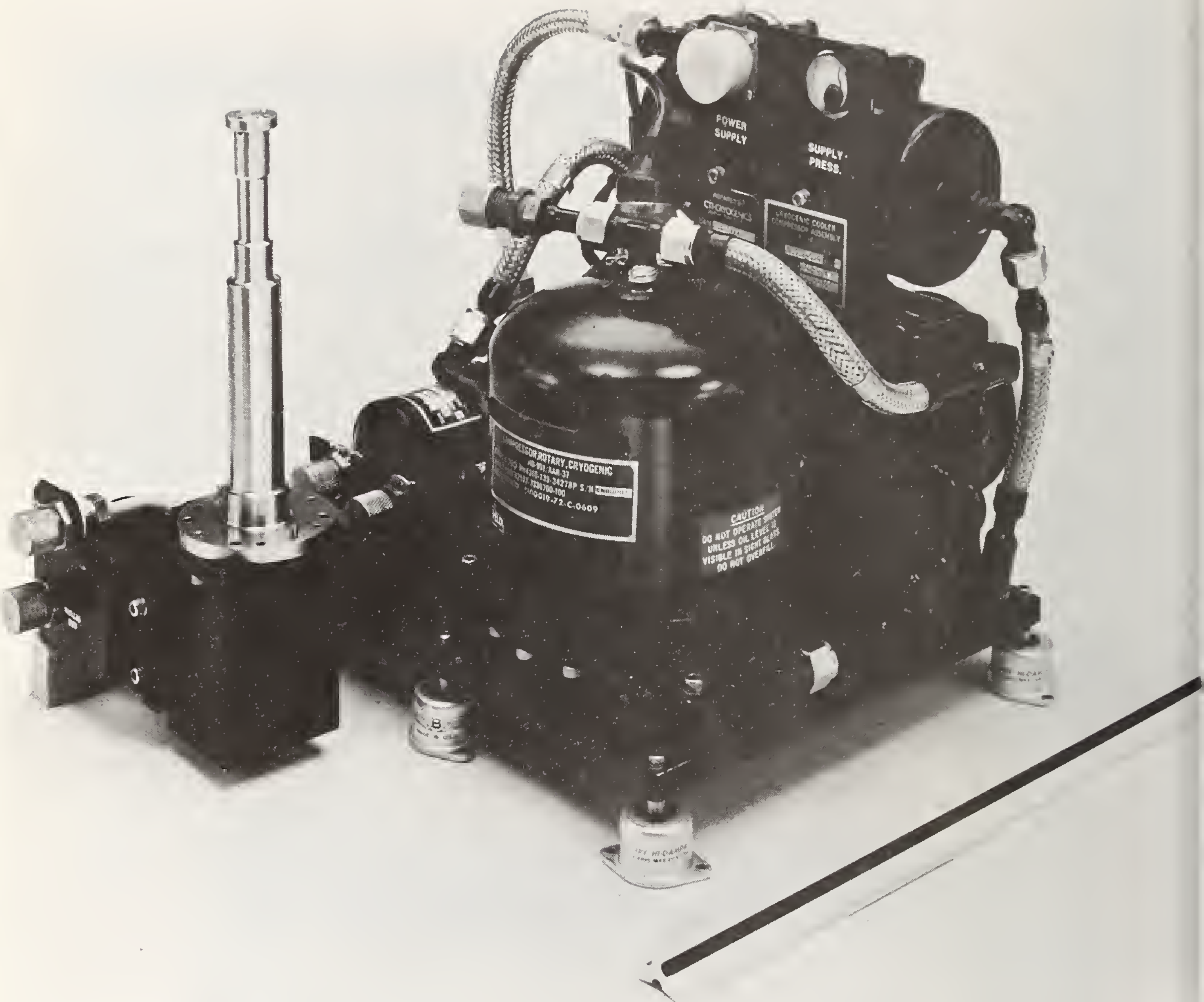

Figure 3. Airborne Infrared Cryocooler
1 Watt @ 20 K; G-M Cycle

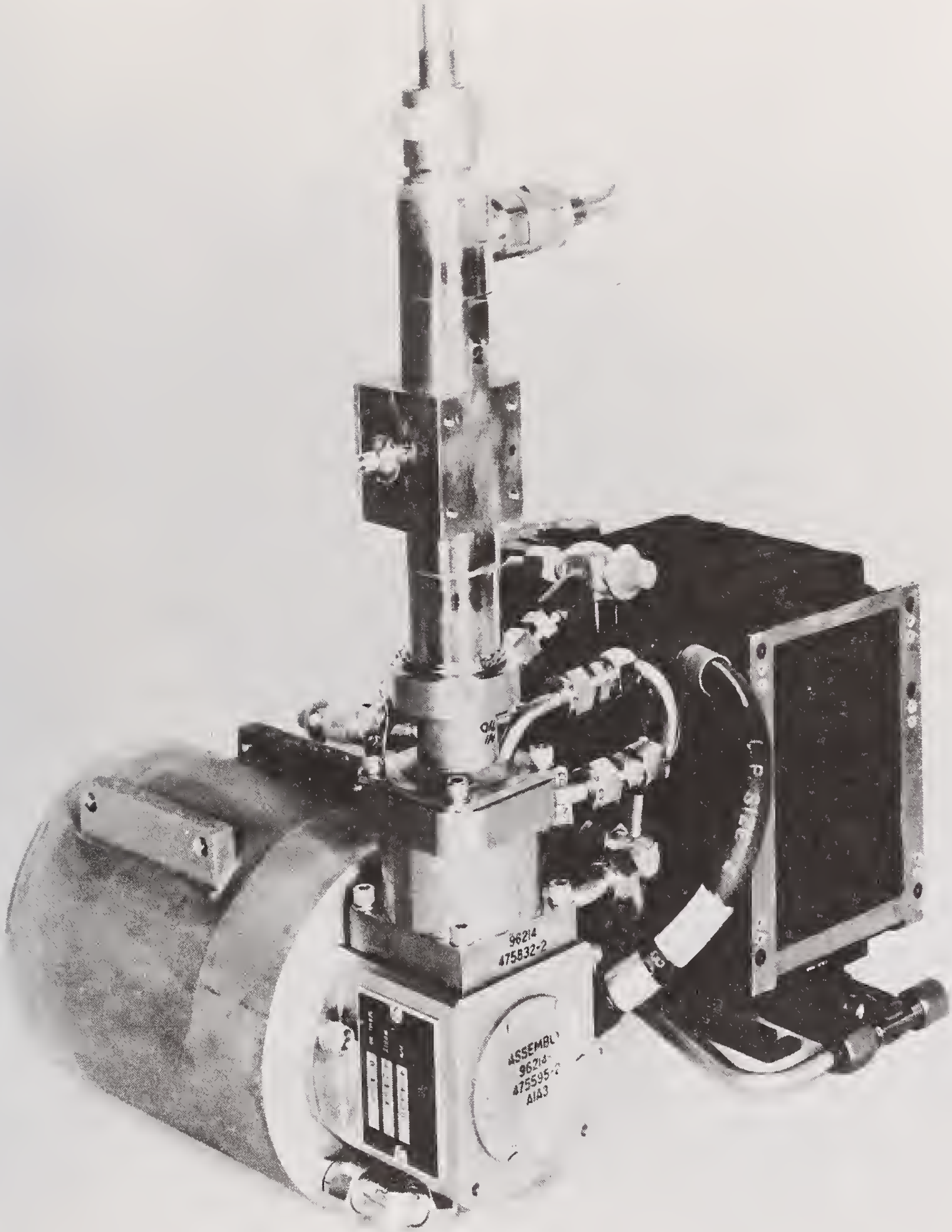

Figure 4. Airborne Infrared Cryocooler
1 Watt @ 20 K; Integral Stirling

Figure 5. Airborne Infrared Cryocooler
1 Watt @ 77 K; Integral Stirling

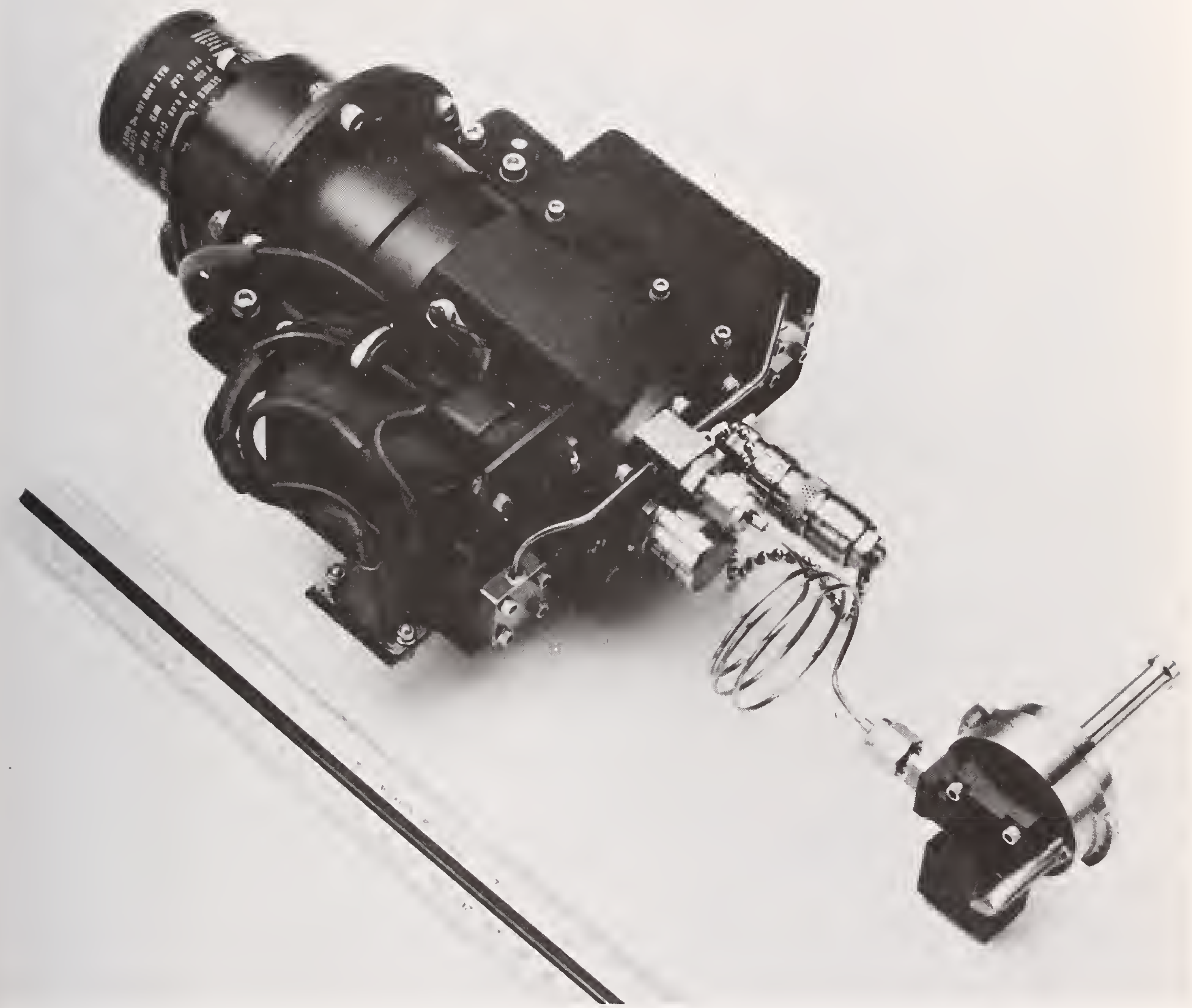

Figure 6. Airborne Infrared Cryocooler
1 Watt @ 77 K; Split Stirling

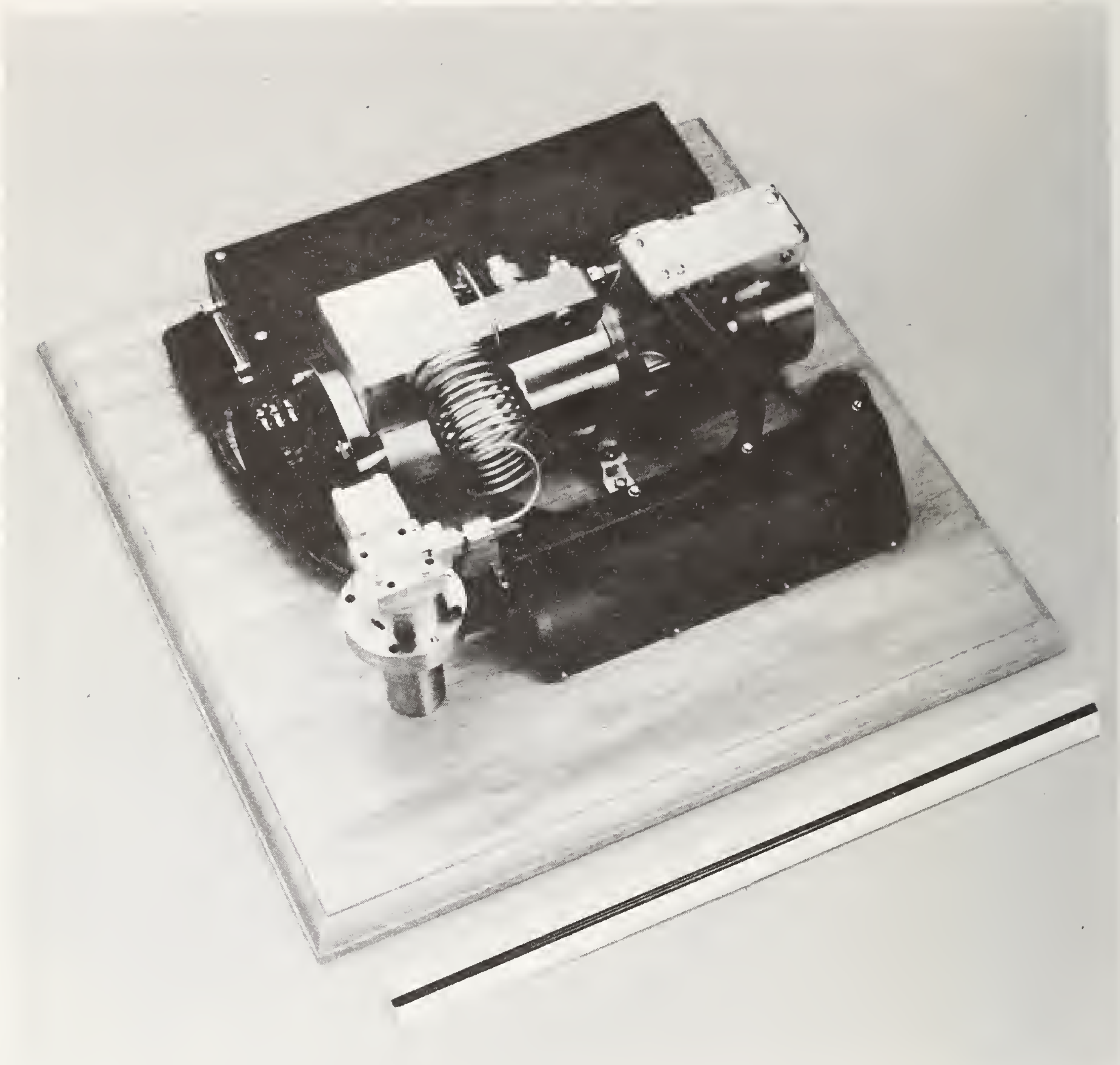

Figure 7. Airborne Infrared Cryocooler
1 Watt @ 77 K; Split VM

MAGNETIC AND VIBRATIONAL CHARACTERISTICS OF A CLOSED CYCLE REFRIGERATOR

John E. Cox and Stuart A. Wolf
Naval Research Laboratory
Washington, D. C. 20375

ABSTRACT

A hybrid 4.5K refrigerator consisting of a CTI 1020 cryodyne with a Joule-Thomson expansion valve, has been evaluated with regard to its magnetic and vibrational signatures for frequencies up to 500 Hz in both cases. Data suggest that an off-the-shelf system of this type is not compatible with the use of Josephson devices as sensitive detectors of magnetic field changes.

Key Words: cryogenic refrigerator, closed cycle refrigerator, vibration spectrum, magnetic signature.

1. Introduction

The coming of age of superconducting circuit elements such as coils, cavities and Josephson devices served as the genesis of renewed interest in closed cycle cryogenic refrigerators. If compact, l ight-weight refrigerators could be utilized to maintain an ambient temperature of 4 to 12 kelvin without excessive mechanical vibration, magnetic noise or maintenance routines, then machines of this nature could be interfaced with the superconducting devices for remote or unattended deployment. ONR funded the purchase of several such refrigerators, and NRL obtained one of them. At that time, there was interest in commencing superconducting cavity research, and it was deemed desirable to obtain a 4.5K machine that could potentially be married to the cavity and auxillary components. This report describes some of the characteristics of a 4.5K two watt Cryogenic Technology Inc. (CTI) hybrid refrigerator.

2. Description of the CTI Refrigerator

A CTI model 1020 cryodyne refrigerator is the nucleus of the 4.5K machine, shown in Figures 1, 2 and 3. The 1020 is a two-stage Gifford-McMahon cycle refrigerator operated at 1.2 Hz by a 60 Hz permanent magnet motor. In steady state operation, the first stage is capable of achieving 50K and the second stage can achieve 10K operation. Appended to this machine is a Joule-Thomson (JT) loop, consisting of counterflow heat exchangers, a parallel plate heat exchanger, the JT valve, 4.5K cold station, and a back pressure regulator to increase the temperature of the 4.5K station without electrical heaters.

Fig. 4 shows the underside of the base plate, consisting of two vapor pressure gauges, gauges for helium pressures at three points of the JT loop, vacuum gauge, motor housing, and various valves for charging the vapor pressure bulbs and directing the helium flow.

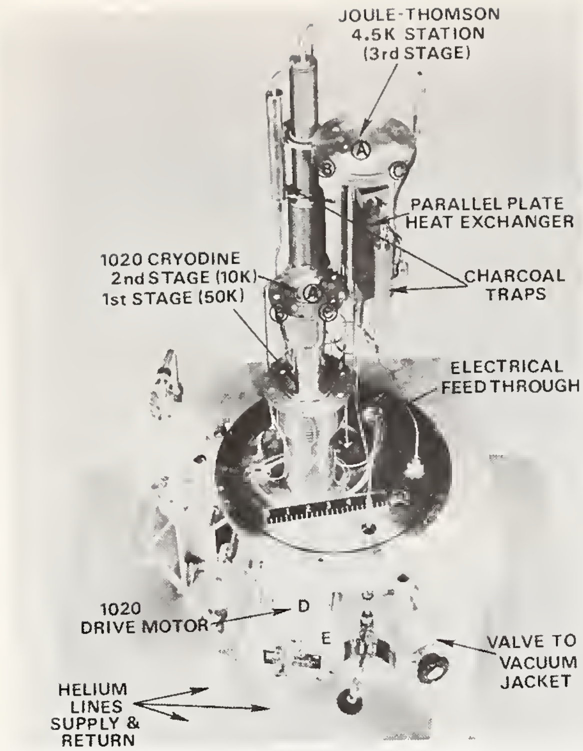

Fig. 1 — Top view of the NRL-CTi 4.5-K refrigerator

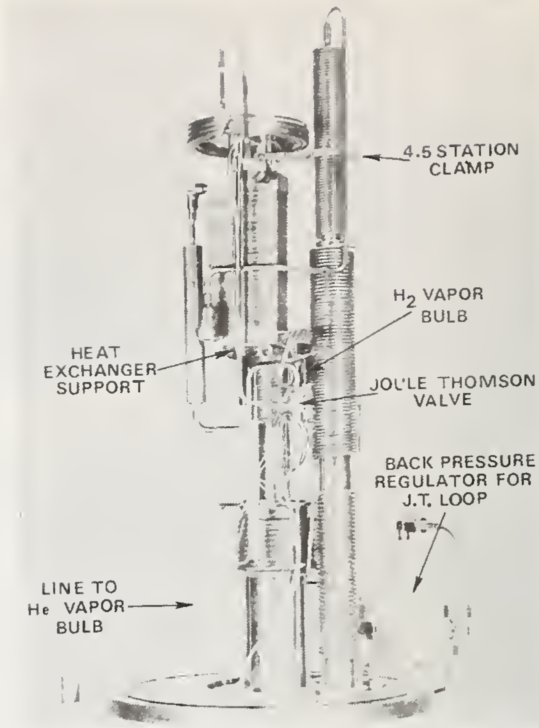

Fig. 3 — Front sideview of the NRL-CTi 4.5-K refrigerator

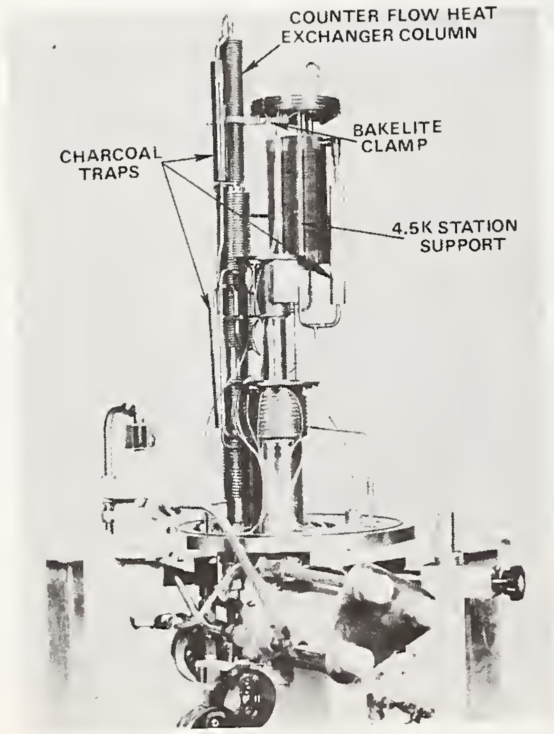

Fig. 2 — Back sideview of the NRL-CTi 4.5-K refrigerator

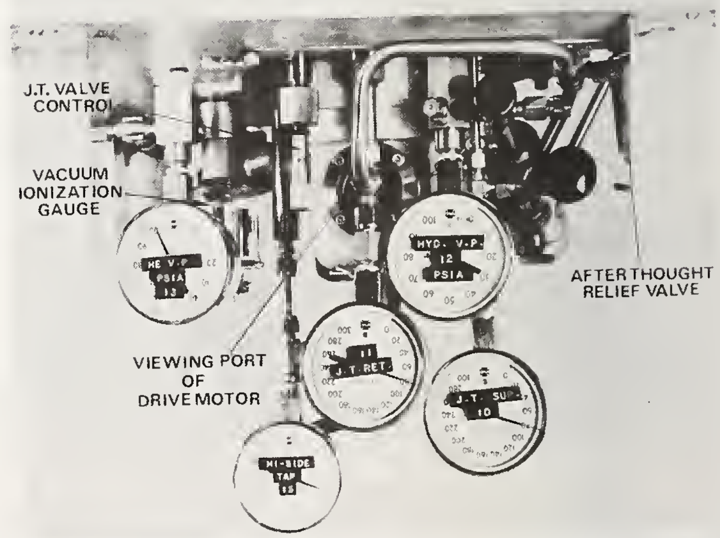

Fig. 4 — Bottom sideview of the NRL-CTi 4.5-K refrigerator

The components above the base plate are wrapped in 4 to 6 layers of aluminized mylar "super insulation" which serves to restrict radiant thermal energy from impinging on the cold parts. The entire assembly is then enveloped in another 8 to 10 layers of aluminized mylar, and a stainless steel vacuum bell jar is placed over the ensemble. A 10^{-5} Torr or better vacuum is necessary to eliminate convective air currents and ensure the attainment of 4.5K.

There are two electrical feed throughs in the base plate (Fig. 1) that carry leads to a carbon resistance thermometer located on the underside of the 4.5K heat station, and a thermocouple and a heater for each of the three heat stations (4.5, 10 and 50K). The plates of the heat stations, and the heat exchangers are of copper, while all other parts visible in Figures 1, 2 & 3 are of 304 stainless steel.

One can impose heat loads on the various stations, and monitor the temperature variation via the thermocouples. For the 4.5K station, one can also raise the temperature by increasing the back pressure seen by the expanding gas. On the other hand, one can bleed off some of the helium charge, lower the compressor input to less than one atmosphere and reach temperatures of 3.8K. Ostensibly, one can vary the temperature from 3.8K to essentially 300K, depending on the heat station used and the thermal load imposed.

The NRL-CTI machine is a hybrid model. The 1020 by itself utilizes a 3-hp compressor supplying 275 psig and returning the expanded helium at 75 psig for a compression ratio of 3.6. A JT loop requires supply pressures on the average of 250 psig with a return near atmospheric pressure, a compression ratio of 16 or so. Thus, one had the option of using two compressors, each with compression ratios of approximately 4, or a two-stage compressor capable of doing the job by itself. It was decided to use the 25-hp Dunn & Bush compressor incorporated in the CTI model 1400 liquefier, the successor of the famed Collins liquefiers. This compressor has nearly three times the capacity necessary for the refrigerator, but its ready availability and known characteristics were the deciding factors. There are bypass regulators on the compressor to shunt the extraneous helium around the refrigerator and back into the input side of the compressor.

The compressor package is approximately 44 inches square, 32 inches high and weighs 1800 lbs. It is a water cooled device, requiring six gallons per minute at 90F max and 30 psig min. Power requirements are 23 kW, 208/220/440 V, 30, 60 Hz.

The refrigerator is 12" in diameter and 44" high overall. Inside the bell jar is approximately 9" vertical clearance above the 4.5K station. The refrigerator weighs approximately 100 lbs. Electrical requirements are 100 watts, 120V, 60 Hz for the displacer motor. The compression and refrigerator are connected by three 20-ft. flexible lines with Aeroquip 5400 series self sealing couplings.

3. Vibrational and Magnetic Characteristics

The vibrational and magnetic characteristics of closed cylce machines are of particular interest to people working with Josephson detectors, for these instruments are sensitive to fields as small as 10^{-14} tesla. Magnetic interference can come about from time varying magnetic fields either directly or by moving the detector in the presence of a static field.

The vibrational modes of the 4.5K and 10K stations were measured by a piezoelectric type Endevco accelerometer. The signal was fed through charge amplifiers to a Sangamo Sabre III tape recorder. The taped output was subsequently passed through a Ubiguitous spectrum analyzer which presented a plot of acceleration in gravity units vs frequency in Hz. Displacements were determined numerically by the equation

$$D = \frac{G}{0.0511\nu^2}$$

where D is the double amplitude excursion in inches, G is the acceleration in g's and ν is the frequency in hertz. A plot of excursions (peak to peak) vs frequency is shown in Figure 5 for both the 4.5K and the 10K station locations.

Because the accelerometer is an oil filled device, it was impossible to cool the refrigerator to its working temperature. Rather, the vacuum bell jar was removed, the super insulation covering the 4.5K and the 10K station was removed and the accelerometer was placed on the respective stations. Operating for any length of time in air in this manner, the 10K station would ice up and the accelerometer response become sluggish. Therefore, data had to be taken before any significant change from room temperature could occur.

As is expected, there is a large impulsive vibration at 1.2 Hz, as well as vibrations at 60 Hz and many of its harmonics, due to the 1020 displacer. The 4.5K station is mounted on what is essentially a cantilevered beam. In Figure 3, one can see the parallel plate heat exchanger attached to the 10K station via a stainless steel bracket. The 4.5K station is mounted above this heat exchanger by two stainless steel rods attached to the same bracket. In addition to picking up vibrations from the 1020 engine, the 4.5K station is susceptible to vibrations due to the helium flow through the JT valve, parallel plate heat exchangers and the charcoal traps. The spike at 180 Hz for the 10K station seems to be shifted slightly to 190 Hz for the 4.5 station. It is believed that this shift is real and can be attributed to the factors just mentioned, as can the relatively broad band of vibrations below 30 Hz.

Signals with frequencies that are harmonics of 60 Hz are always subject to suspicion, especially when one is making ac electrical measurements. However, the profile of Figure 5 is such that the indicated displacements are real. The profile of the displacements of the two stations is different, with the magnitude of the displacement of the 4.5K station larger and at times shifted slightly in frequency from 10K station data. Again, this is to be expected from the cantilevered nature of the 4.5K station.

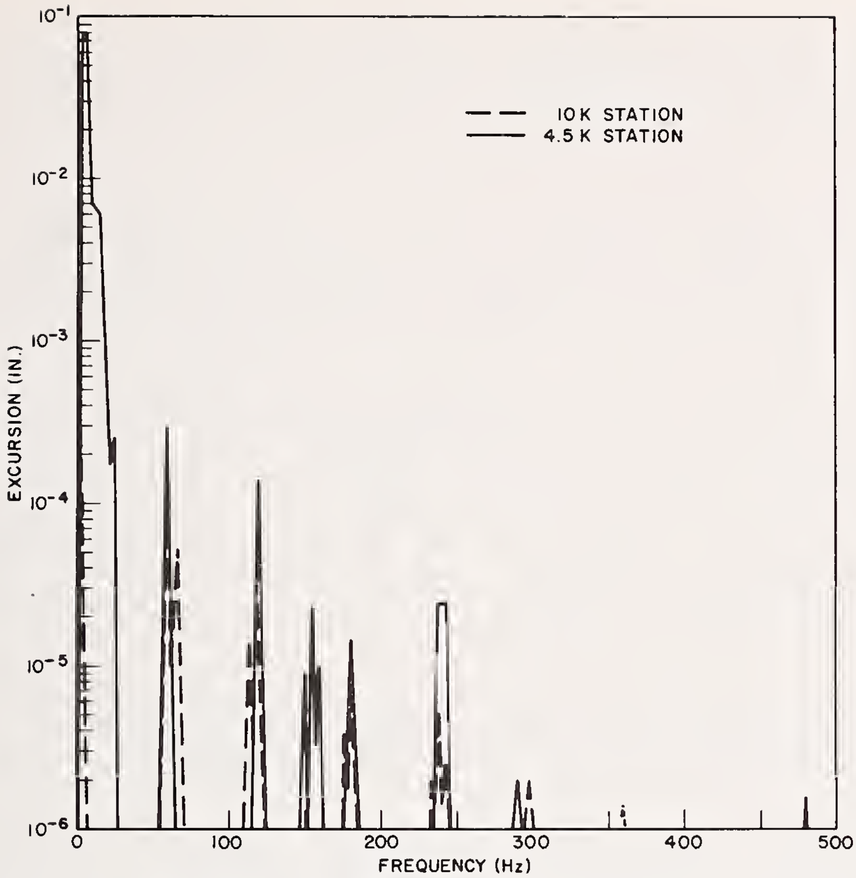

Fig. 5. Double Amplitude Vibrational Spectra as a Function of Frequency.

TABLE I
AC MAGNETIC FIELDS (10^{-7} TESLA)

Location	Motor on	Compressor on	Frequency (Hz) 1.2	60	190	480
A			2.5*		6.8	
	X		4			
	X	X	4.5		8.8	
B					4	3
	X				4	4
	X	X			8	8
C				7	3	
	X			8	3	
	X	X		9	7	
A′			2.8	2.7		
	X		10.5	2.8		
	X	X	13.5	4.8		
B′			<1			5
	X		2.5			5
	X	X	4			8
C′			0			3
	X		3			3
	X	X	4			5

TABLE II
DISPLACER MOTOR FIELDS (10^{-7} TESLA)

Location	Motor on	Compressor on	1.2	2.4	60
D	X		300	100	2,000
	X	X	300	150	2,500
E	X		300	200	5,000
	X	X	600	200	2,500

A pair of Siemens hall probes model RHY18 were calibrated for dc fields at liquid helium temperatures and installed in the CTi refrigerator. However, ac measurements using a dc biasing voltage resulted in inadequate sensitivity. Instead, a Bell model 240 incremental gaussmeter was fed into a PAR 210 selective amplifier and PAR 220 lock-in detector used as a tuned amplifier and the subsequent signal was monitored on an oscilloscope. Because we did not want to damage the factory packaged calibrated probe, we decided against severing the leads to install the probe so as to make measurements with the refrigerator operating. Instead, these measurements were made in a manner analogous to the accelerometer data. Sensitivities of 10^{-3} gauss were realized with these instruments.

Magnetic data were taken at eight locations, as listed in Table 1 and Figure 1. At each of the refrigerator locations, three sets of measurements were made; background field, field with motor on and compressor off, and field with both motor and compressor on. Positions A and A' measure the vertical fields on the two stations, while the others determine the horizontal fields. Position B is approximately 90^{o} from the bakelite clamp holding the 4.5K station to the counterflow heat exchanger column. Position C is essentially opposite this clamp. Postions B' and C' are located on the 10K station with the same relative orientation as positions B and C.

All harmonics of 60 Hz were checked, but in most cases the background was a strong as the signal detected with the refrigerator on; the exceptions being those indicated in Table I. The frequency range checked was from 1 to 500 Hz.

The asterisk at location A for 1.2 Hz fields means that there is a measurable field at this frequency with the displacer off, but the cause of the field is a natural structural resonance at 6.75 Hz. The Q of the measuring circuit was approximately 20 which allowed a signal at 1.2 Hz to be detected. When the motor was turned on a real 1.2 Hz vibration was established, and this motion in the earth's field caused additional pickup. Since only the vertical field is present, we reason that the motion is due to building vibration. There were no frequencies present in the magnetic measurements that were not also present in the vibration measurements.

In Fig. 1 positions D and E indicate the location of the Hall probe for determining the radial and axial fields due to the displacer motor. These values are shown in Table II. The 2.4 Hz vibration detected here could not be seen on the 10K or 4.5K stations. The reason for the amplification of field values with the compressor on is not understood.

4. Operating Experiences

During shipment, the check value in the suction line of the compressor worked loose, thereby bleeding down the helium charge in the compressor module. Before the refrigerator could be connected, the compressor had to be evaucated and purged to remove contaminants. When the refrigerator had approximately 1000 hours running time, that same check valve leaked at least three additional times. Another source of difficulty is one of the shunt regulators for diverting that portion of the supply gas not needed by the refrigerator. The orifice seat became deformed, thereby causing continuous bypassing of compressed helium and reducing the supply pressure from 245 psi to 175 psi. A new seat was installed, but the regulator continued to leak helium to the atmosphere despite three retightenings of the valve housing, two of them with uniform tension supplied via torque wrench.

As an afterthought CTI engineers decided that a pressure relief valve ahead of the back pressure regulator was a desired safety feature. The elbow was removed and returned to CTI for insertion of the regulator, but re-installation of the elbow resulted in a leak around the Swagelok stainless steel fittings. The leak was finally isolated, but it is not certain that it is ful sealed. A non-detectable leak may still be present. Another after-thought was a pressure relief valve on the bell jar. In the event of a helium leak developed in the cold end, the bell jar could become a bomb. The recommended valve was purchased and installed, but it would never seal vacuum tight. A second type of valve was installed, but at present one cannot maintain a good vacuum. The cause of the leak is unknown. Because of possible helium leaks in the closed cycle system, one cannot be certain that it is not helium leaking out to the vacuum volume. On the other hand, the many layers of aluminized mylar present large virtual leaks to a leak detector, thereby making it impossible to conclusively identify real leaks from these virtual leaks. In retrospect, it is unfortunate that the advice of CTI regarding the relief value in the bell jar was taken. Instead, one should merely have removed the bolts attaching the bell jar to the base plate, thereby permitting easy exit for any catastrophic helium buildup.

The CTI design engineers and their field service engineers seem to be at odds regarding the configuration of the bypass regulation system and the associated surge tanks. One needs a ballast tank to store helium that is excess when the refrigerator is warm but is necessary when the refrigerator is at operating temperature, due to the volume reduction of the cold gas. It would seem that improvements in this system could be made.

5. Conclusions

While a detailed evaluation of this machine has not been carried out, it is clear that the machine in this configuration is not suitable for interfacing with current SQUID devices. SQUID operating range is typically 10^{-6} to 10^{-14}T. Therefore, the noise produced at the cold stations is greater than the operating range of the least sensitive SQUID. Non-cryogenic magnetometers would be more suitable in this field range.

6. Acknowledgements

We are indebted to J. Kennedy for his assistance with the Hall probe measurements, and to H. Forkois for the accelerometer measurements.

Closed-Cycle Refrigerator for a Superconducting Susceptometer

Daniel A. Vincent
College of Engineering
University of South Florida
Tampa, Florida

A closed-cycle 4.5 K refrigerator has been used to cool a chamber for condensing helium. The liquid helium is transferred to a SQUID superconducting susceptometer dewar by gravity flow with the boil-off gas recirculating to the condensing column. Vibration and electromagnetic noise isolation is maintained between the refrigerator and the susceptometer.

Key words: Cryocooler; helium refrigerator; refrigeration, helium; SQUID refrigeration.

1. Introduction

The continued advances in commercially available superconducting instruments has stimulated the need for reliable low capacity helium liquefaction systems. The refrigerator described here incorporates a commercially available cold head utilizing the Gifford-McMahon (G-M) cycle capable of reducing the temperature to about 15 K. This refrigerator precools and sustains a separate closed-cycle helium flow at sufficiently low temperature to permit liquefaction through a Joule-Thompson (J-T) throttling valve. The J-T loop incorporates countercurrent heat exchangers to transfer a portion of the incoming heat load to the exhaust gas. A two stage compressor and filter unit is used to compress the helium gas from the two expansion exhaust pressures to the required supply pressure. To maintain a high level of reliability and long operating periods between overhauls, the helium circulating in the refrigerator circuits must be ultra pure. A 30 liter storage tank included in the compressor unit provides a source of pure gas and maintains constant operating pressure as the gas volume changes during cooldown and heat load variations. Pressure regulating valves admit the gas in and out of the tank as the demand requires. The gas contained in this tank and the compressor unit and piping is purified by circulation through a cryogenic adsorption device prior to initial cooldown.

Refrigerators of this design have proven to be very reliable after many years of continuous operation [1,2]. Unfortunately mechanical vibration and electromagnetic interference make them incompatible with direct connection to superconducting (SQUID) instrumentation [3]. The secondary liquefaction system shown in Figure 1 has been added to allow sufficient separation of the refrigerator and the instrument dewar to permit vibration damping and electromagnetic shielding between the two units.

2. System Description

Referring to Figure 1, commercial purity helium gas is admitted into the condensing chamber through a precooling column thermally connected to the 60 K and 15 K G-M refrigeration stations. The condensing chamber is a copper container thermally linked to the 4.5 K refrigeration station of the J-T loop. Refrigeration capacity of the two G-M stations is on the order of 10 watts in excess of the cooling required for the J-T loop. The liquefaction station has a capacity of 2.5 watts at 4.5 K. The J-T exhaust is maintained at a pressure slightly above atmospheric (about 980 mm Hg) to overcome line losses and insure a positive pressure at the compressor inlet.

The condensing chamber is maintained at a sufficient pressure to provide a temperature drop to the 4.5 K station capable of condensing approximately one liter of helium per hour. The condensed liquid is transferred into the superinsulated instrument dewar by gravity with the room temperature

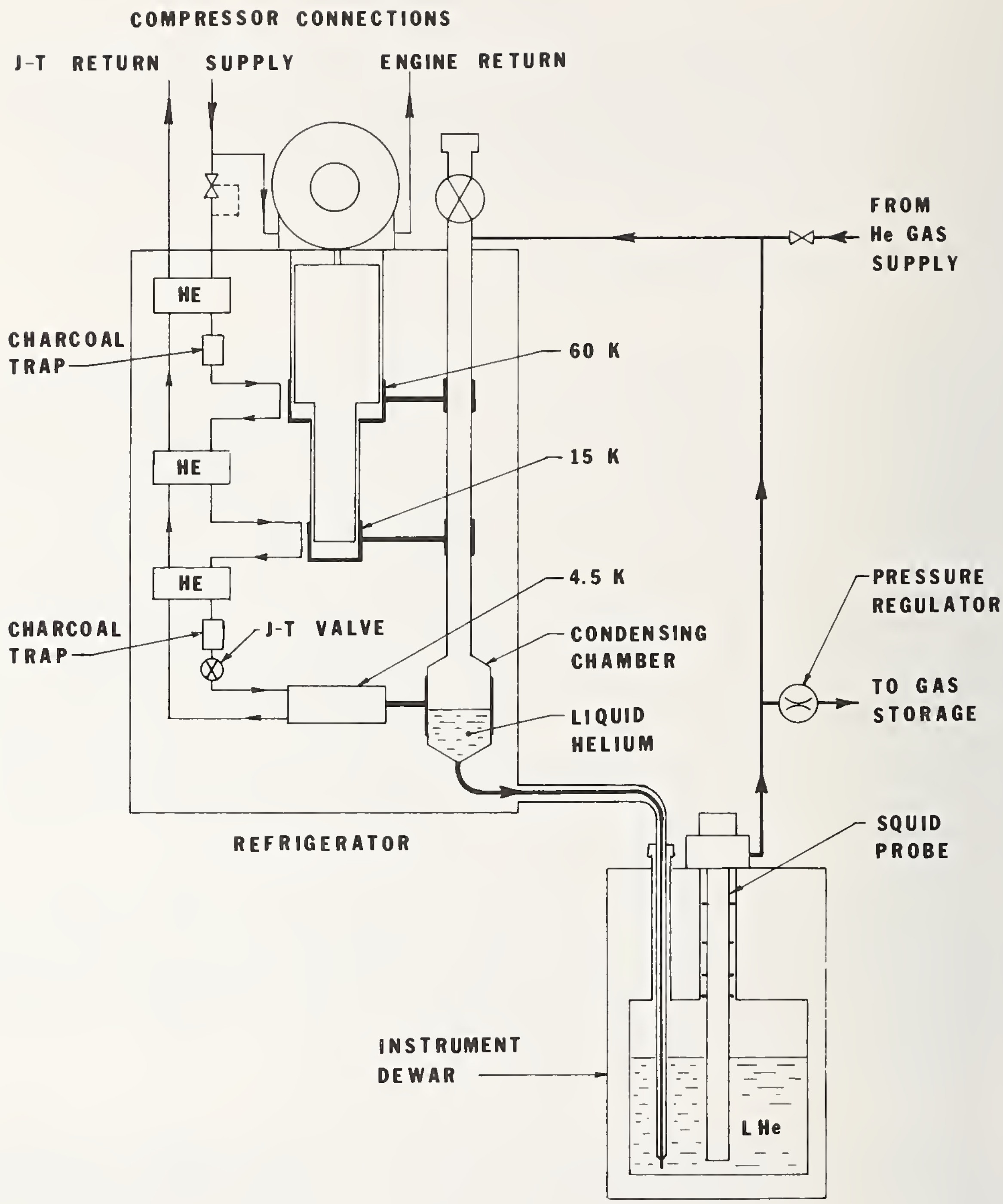

Figure 1. Schematic Diagram of the System

boil-off gas returning to the top of the condensing column. Since there are no small passages in this circuit, the purity requirement of this fluid is much less stringent than in the refrigerator circuit.

The flow rate is low (one liter or less per hour) and the only transfer mechanism between dewars is a small differential pressure created by the helium liquid level drop. An efficient transfer tube is essential to effect liquid transfer under these conditions. The liquid passage is a 6 mm thin wall tube wrapped with aluminized Mylar superinsulation inside a copper heat shield connected to the 60 K station of the refrigerator. This copper shield is also wrapped with superinsulation and encased in a stainless steel vacuum jacket. The transfer tube vacuum communicates with the refrigerator vacuum space which is continuously cryopumped by getter material mounted on the 15 K and 4.5 K stations.

In addition to the liquid helium transfer method described here, the condensing chamber is provided with a gas-locked room temperature access for "dip stick" experiments compatible with the refrigerator noise. For this application the liquid helium can be retained in the condensing chamber by temporarily raising the pressure in the instrument dewar.

3. Acknowledgments

The author would like to thank Professor Bascom Deaver and his associates at the University of Virginia for their assistance in acquiring and modifying much of the equipment used in this project.

4. References

[1] Higa, W. H., and Wiebe, E., A Simplified Approach to Heat Exchanger Construction for Cryogenic Refrigeration, Cryogenic Technology (March/April 1967).

[2] Higa, W. H., One Million Hours at 4.5 K, in this publication.

[3] Cox, J. E., Evaluation of a 4.5 K Closed-Cycle Refrigerator, NRL Memorandum Report 3088 (July 1977). See also J. E. Cox and S. A. Wolf in this publication.

Cryogenic Applications of Closed-Cycle Mechanical and Adsorption Refrigeration

William H. Hartwig
The University of Texas at Austin
Austin, Texas 78712

Experiments were conducted to observe the effects of the superconducting transition of a lead X-Band cavity cooled to 6.7°K by a closed-cycle Cryodyne refrigerator[1]. The Q changes rapidly below 7.2°K, and both drift and short-term stability undergo large changes near the transition. The refrigerator did not liquify the Helium gas. The overall objective was to develop an experiment chamber to measure photodielectric changes in semiconductors[2,3,4]. Cooling time, vibration effects and temperature gradients were among the problems to be overcome. Results of the experiments are analyzed and related to the characteristics of the mechanical refrigerator.

Subsequent research, on a non-mechanical gas compressor [5], with potential applications to pre-coolers, radiation shields, and the prospects for achieving low temperatures, is also discussed.

Key words: Adsorption refrigeration; closed-cycle refrigeration; infrared detector cooling; non-mechanical gas compression; superconducting cavities.

1. Introduction

Applications of cryogenic devices such as superconducting resonant circuits (SCR's) and infrared detectors would be greatly enhanced by advancing the technology of cooling. Work done in past years in the author's laboratory demonstrated two aspects of studies on SCR's pertinent to this subject. Closed-cycle mechanical refrigerators could be used as convenient and reliable systems for some purposes, but the vibration and periodic energy removal of reciprocating expansion engines introduced large temperature excursions as the specific heat dropped with temperature.

An experimental X-band oscillator using a superconducting lead cavity was built to study the stability and spectral purity as a function of temperature. The cavity was cooled to 6.7°K by a closed-cycle CRYODYNE refrigerator. Near the transition temperature, 7.2°K, the Q changed rapidly and both the drift and short-term stability were undergoing large changes. Unloaded Q's of 10^4-10^6 were achieved in the operating range above 6.7°. Q's in excess of 10^{10} have been observed at lower temperatures by numerous investigators. The anticipated outcome was an oscillator which can provide superior short-term stability and utilize a Cesium beam tube to provide long-term stability.

Another advantage of a superconducting cavity is its clean spectrum. The quartz crystal, while a highly refined component, cannot match the cavity at X-band frequencies. Means are readily available to tune the cavity over a wider range than available to the quartz crystal. Frequency multiplication, which degrades the spectrum of a quartz oscillator, is not needed. The advantages of closed-cycle refrigeration is the freedom from liquid transfer problems and absence of the logistics associated with maintaining a reliable supply of liquid. Closed-cycle systems can be manufactured to operate over a wide temperature range, particularly above 4.2°K, which is awkward for liquid helium. The CRYODYNE refrigerator used in this experiment could be redesigned with a Joule-Thompson expansion valve to operate well below 4.2°K.

Later experience by NASA using mechanical refrigerators to cool crystals used for IR detection, showed the piezoelectric noise introduced was objectionable. This paper describes briefly the results of those experiments, and goes on to discuss new concepts in non-mechanical gas compression that may offer some alternatives, particularly for temperatures of 20K and above.

2. Advantages of Superconducting Resonant Circuits

Superconducting resonant circuits (SRC's) have been fabricated which span the frequency range from 10 MHz to 12 GHz at the fundamental frequency. Higher frequency operation is possible, but increases in the RF losses suggest that harmonic, rather than fundamental, operation must be used above 30 GHz. Typical Q's range from 10^6 to 10^{11}, depending on the frequency, geometry, surface condition of the SRC, coupling, magnetic shielding, and the operating temperature.

The geometry of the SRC establishes the frequency and will limit the lower usable frequency. Bulk circuits, consisting of helical inductors in parallel with concentric capacitors, resemble conventional L-C elements and can be conveniently fabricated in the 10 MHz-100 MHz range. Above 100 MHz and continuing to about 700 MHz, helical resonators represent the most favorable configuration. At approximately 700 MHz the helical resonator degenerates to a quarter-wave transmission line cavity, which can be used to approximately 1000 MHz. Above this frequency, microwave cavities are utilized.

The high Q's obtainable from SRC's are unparalleled by those of any other available circuit element. The exceptional frequency and phase stability characteristics of the SRC make it particularly attractive as a frequency control element[5]. The SRC can be used at the fundamental frequency to approximately 30 GHz, which ordinarily are approached only by normal conducting, medium Q microwave cavities. No quartz crystal can attain these frequencies without the added complexities of frequency multipliers.

The SRC is particularly suited to both slow and fast tuning arrangements. Mechanical tuning can be used to slowly adjust any long-term drift of the SRC. Optical tuning can be used to slowly adjust any long-term drift of the SRC. Optical tuning can be used for high-rate correction of short-term instabilities, with some depreciation in Q. This tuning capability represents another advantage not directly possessed by the quartz crystal.

Excellent spectral purity is assured, with the high Q providing greater than 80 db reduction of spurious modes. Closely spaced cavity modes are readily filtered or suppressed via coupling or mode traps.

3. Limitations on Stability of Superconducting Resonant Circuits

Although SRC's unquestionably hold great promise for frequency control applications, there are certain limiting factors of their stability which must be recognized. Some of these limitations may be substantially overcome through compensation techniques, but can never be completely eliminated. The primary mechanisms involved are temperature control and mechanical vibrations. Other limitations are less effective, but must be considered.

a. Temperature Effects

The surface reactance of the superconductor is only a slow function of the temperature, T, when operation is well below the transition temperature, T_c. However, for extremely stable circuits, even minute changes are important. The surface reactance is given by

$$X(t) = \omega\mu\lambda(t) \tag{1}$$

or

$$L(t) = \mu\lambda(t), \ \mu = 4\pi(10^{-7}) \text{ hy/m}, \ t = T/Tc \tag{2}$$

The empirical equation for the penetration depth, λ, is given in the literature[6] as

$$\lambda(t) = \lambda_o(1 - t^4)^{-1/2} \tag{3}$$

$$\lambda_o = \text{penetration depth at } 0°\text{K}.$$

The total circuit inductance is the sum of L(t) and the geometrical inductance. Assuming a temperature control swing of $\pm$ 50μ°K at 4.2°K, straightforward calculations give a frequency stability of

$$\frac{\Delta f}{f_o} = \pm 2(10^{-12}) \tag{4}$$

This assumes a cylindrical cavity operated in the TE_{011} mode at a frequency of 10 GHz.

The temperature control range of 50μ°K may be exceeded if enough thermal inertia exists in the system. It has been observed by the authors that considerable thermal inertia exists in a helium bath when operation is below 4.2°K, but above the superfluid state of helium. The specific heat of the cavity is diminishing as temperature drops, and this becomes a critical factor when mechanical refrigerators are used.

Cavities constructed of metal are subject to dimensional changes upon variation in the ambient temperature. Both the length and diameter of the TE_{011} cavity are effective in controlling the center frequency. However, at liquid helium temperatures, many materials no longer suffer appreciable dimensional change. For example, the thermal coefficient of linear expansion of copper is so small as to be undetectable below 20°K[6,7]. An upper limit is taken as the value near 20°K of 10^{-7} per °K. Thus, for the X-band cavity mentioned above, a ± 50μ°K deviation produces a frequency shift:

$$\frac{\Delta f}{f_o} = \pm 5(10^{-12}) \tag{5}$$

This is a conservative figures, since $\alpha = 10^{-7}$ per degree is an upper limit.

Another problem involving dimensions and temperature is repeatability. Because of the simple geometry of the cavity, this difficulty can be minimized. The cavity can be made of a single cylinder, having no solder joints, and annealed. This should eliminate thermal deformation due to hysteresis in regions of strain. Also, a cavity of this type could be constructed easily with a quartz substrate. Mechanical or dimensional changes due to pressure differentials between the interior and exterior of the cavity can be eliminated by providing a vacuum sealed isolating can or jacket. This also adds some thermal inertia to the system.

b. Effects of Mechanical Vibration

The structural deformation of the cavity due to mechanical vibrations is a negligible effect for rigidly designed microwave cavities. However, the vibration of the coupling system may not be negligible, since the cavity frequency can be, to a lesser or greater degree, influenced by the coupling.

For an inductively coupled cavity, the inductance of the loop which is coupled in series with the cavity inductance is given by[7]:

$$L_c = \frac{\beta L_o X_1}{Q_o Z_o} \tag{6}$$

where β = the coupling factor; L_o = equivalent cavity inductance; X_1 = isolated reactance of the loop; Q_o = unloaded Q of the cavity; and Z_o = characteristic impedance of the transmission line. Thus, the resonant frequency, given by $\omega_o^2 = [(L_o + L_c)C]^{-1}$, will be controlled by β, which in turn can cause a frequency error due to vibrations in the probe. The power coupling factor, γ, is given approximately as 4β for $\beta \ll 1$. Using $L_o = 3.2 \times 10^{-8}$ hy, Z_o = 50 ohms, $Q_o = 10^8$, and X_1 = 15 ohms, a frequency instability of 2×10^{-13} is caused by a 3 db increase in (assuming 20 db initial decoupling per probe), and a frequency instability of 2×10^{-12} is caused by a 12.8 db probe increase in γ. These increases in γ correspond to rather strong vibrations. Mechanical snubbing of the probes and proper choice of β will render the vibrational effects negligible. Fixed iris coupling will also circumvent this problem.

c. Other Effects

Measurements on a 30 MHz SRC oscillator indicated that a frequency instability of 5×10^{-12} can result due to magnetic field variations on the order of the earth's field[5]. This can be eliminated by shielding the SRC in the r and ϕ direction and cancelling the z component of the earth's field with a Helmholtz coil. Such an arrangement leads to less than a milligauss environmental magnetic field. Also, this low field environment improves the upper limit on Q by minimizing losses due to trapped flux[2].

The center frequency of a resonant circuit can be approximated by

$$\omega_o \simeq \omega_i \; (1 + 1/2Q^2)] \tag{7}$$

$$\text{where:} \quad \omega_i = (LC)^{-1/2}$$

A change of a factor of 2 in the quality factor of a cavity having an initial Q of 10^8 causes a frequency change of 1 part in 10^{16}. Thus, this effect is negligible for cavities having Q's in excess of about 10^6.

Thus, even though basic limiting factors exist for the frequency stability of SRC's, they are generally so small as to limit the total instability to 1 part in 10^{11} for either a 50μ°K temperature change or large mechanical vibrations. Considerably better stability figures can be achieved if thermal inertia exists and proper design and operating procedures, including compensation, are followed. No estimate of the ultimate stability is possible due to lack of experience data.

4. Design of an X-Band Oscillator Using a Closed-Cycle Refrigerator

a. Cavity and Electronic Systems Design

The cavity chosen for the X-band oscillator is a cylindrical microwave structure operated in the TE_{011} mode. The degenerate TM_{111} mode is partially suppressed by coupling and the degeneracy is further removed by the use of a mode trap.

Since all currents are circular, the cavity can be made in three parts for ease of fabrication with little effect on the losses. The circuit is shown in Figure 1. The mode trap for the TM wave consists of the extra length, ℓ, in a region of maximum TM_{111} fields, but minimum TE_{011} field.

Two coupling methods were tried. First a small loop placed at a maximum H field position in the cavity and the waveguide were tried. This method proved to be unsatisfactory because of apparent probe resonances as the loop was moved into and out of the cavity. Finally, fixed iris coupling was successfully used. A 0.125" diameter iris, 0.030" thick, was placed midway on the cavity's radius. This coupling provided adequate signal and loaded Q which which was not coupling-limited when the circuit was operated at 6.7°. For lower temperatures, the size of the iris would have to be reduced to prevent an overcoupled condition.

The cavity was fabricated from brass and finely sand-blasted to obtain a homogeneous surface. The lead surface was electroplated to a thickness of approximately 5 microns by standard processes.

The electronics used to phase lock a 2K25 klystron to the high Q cavity are shown in Figure 2. A standard Pound's stabilized microwave bridge was employed. The phase lock amplifier was provided with variable gain so as to be able to vary the tightness of the lock as the temperature was changed. The frequency monitor was a HP 2590B microwave frequency converter used in conjunction with a standard UHF counter. One second gate times were used for all frequency measurements. The phase error voltage returned to the klystron repeller was monitored with a high frequency oscilliscope. All RF coupling out of the cryogenic environment was through thin wall, stainless steel waveguides.

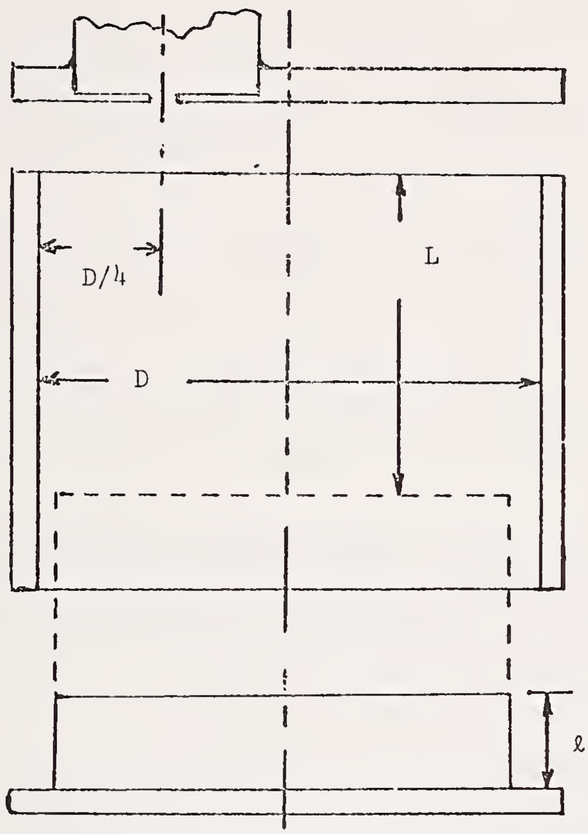

X-Band Cavity
FIGURE 1.

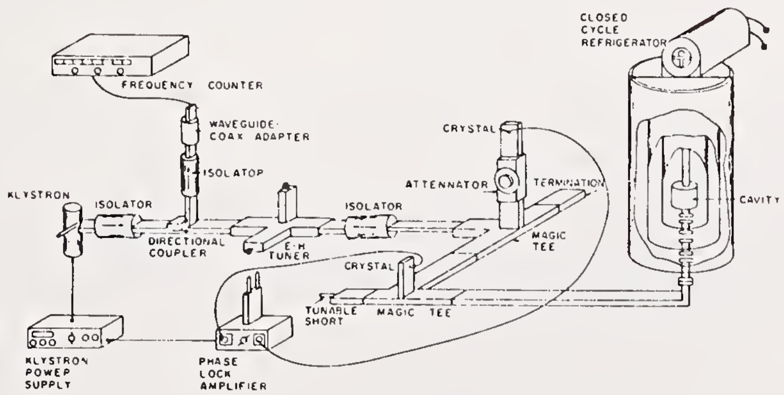

X-Band Oscillator System

FIGURE 2.

b. Closed Cycle Refrigeration

The heat load of the SRC was very small and as a result was ideally suited for use with certain closed cycle refrigerators. The refrigerator used in these experiments was a three-stage version of the CRYODYNE. The unit was capable of approximately 6.7°K with zero heat load, using only standard expansion-compression techniques with gaseous helium as the coolant. (Lower temperatures would have been available with the addition of a Joule-Thompson expansion valve.) This unit is particularly well suited for studying the effects of a rapidly changing Q on frequency stability for lead circuits, since lead's transition is 7.2°. Use of higher temperature materials would give much improved Q's at the same temperature.

A careful thermo-mechanical design was undertaken to minimize heat loads due to radiation. The following design resulted. Two radiation shields, individually connected to the two upper temperature stations (T_1 = 77°, T_2 = 12°), were conductively connected to the waveguide connecting the cavity to the outside environment. Microwave choke flanges were used with a 0.030" separation at each of the connections to eliminate thermal conduction between stages. The radiation shields were made of polished aluminum, and an additional two layers of aluminized mylar were used inside each of the shields. Finally, a vacuum shield can was used as the outer container, and the vacuum integrity was obtained with a plexiglass vacuum window.

The temperature of the cavity was monitored by calibrated carbon resistors and an additional lead resistor was provided to indicate when transition to the superconducting state occured. The second stage temperature was read from a hydrogen vapor pressure gauge and the first stage was monitored by an Au/Co-Cu thermocouple. An initial vacuum of 100 microns was obtained before starting the refrigerator. The system was then cryopumped below the scale of the vacuum gauge, i.e., less than 1 micron.

The cavity was conductively connected to the third stage with a 0.25" disc of lead between it and the temperature station. The relatively high specific heat of lead at low temperatures, and its relatively good thermal conductivity, provide sufficient thermal inertia to damp out the temperature variations that may occur in the third stage. Indium gaskets were used in all conduction joints to provide quicker and more uniform cooling, and the waveguides were painted flat black on the insides.

5. Performance

At room temperature, with a Q of approximately 20,000, the frequency stability is 1 part in 10^7. At 6.7° the stability improved to 1 part in 10^8, in agreement with the predicted increase in Q to approximately 200,000.

The cooling time for 6.7° operation was approximately seven hours with continuous operation available after this. No large short term fluctuations were noticed indicating that the lead disc was effective in providing thermal inertia of the quality required for these experiments. Frequency modulation was observed due to temperature variations at the refrigerator expansion engine frequency. Q measurements did not depend on precise frequency control, however. The cooling was very slow and uniform as indicated by an hour lag time between the time that the upper part of the cavity became superconducting and the time the bottom of the cavity reached equilibrium.

6. Cryogenic Refrigeration Concepts Utilizing Adsorption Pumping in Zeolites

Refrigeration without lubrication, vibration and noise has heretofore been accomplished in at least three distinct forms; thermoelectric junctions that pump heat across a semiconductor PN junction [9], ammonia-water systems that remove heat in an adsorption-percolation-condensation-evaporation cycle [10], and chemisorption systems that exchange hydrogen from lanthanum nickel or other metal hydrides to develop a pressure difference for circulation of H_2 gas in a 20K refrigerator [11,12]. While technically sound, these systems have a mix of advantages and disadvantages that render them unsuitable as the basis for complete cryogenic refrigeration cycles.

The author and his associates at The University of Texas at Austin have explored the properties of zeolites as potential adsorption compressors which might lead to a complete range of cryogenic refrigerators operating against ambient conditions [13,14]. Zeolites are in a class of aluminum silicate clay minerals that have crystal structures composed of interconnected voids which enable them to adsorb a variety of gas molecules, depending upon their diameter, dipole and quadrupole moments, and other physical properties. The adsorption of gas molecules on the interior surfaces of the voids is an ionic interaction with a characteistic potential energy called the heat of adsorption. The molecular adsorption process results in an exothermic attachment of the gas molecules to the surface of the voids, resulting in gas storage at near-liquid densities. This is the basis for using zeolites in a variety of gas separation processes, such as removal of highly polarized H_2O molecules from industrial gases. D ue to their high electrochemical activity, zeolites are also widely used as catalysts. This section of the paper describes the use of zeolites as non-mechanical gas compressors, since adding the activation energy to a zeolite charged with gas molecules drives them out under pressure.

7. Adsorption of Gas in Zeolites

The zeolite crystalline structure takes a variety of forms, with the unit cell containing hundreds of atoms [15]. Zeolite X, for example, has a typical unit cell content: $Na_{86}[(A\ell O_2)_{86}(SiO_2)_{106}] \cdot 264\ H_2O$ and a cubic unit cell volume of about 15,500Å^3. The unit cell contains about 8 voids, or cages, about 13Å in diameter, so the crystal volume is about fifty percent void volume. Normally the voids are filled with H_2O molecules, but these can be removed by heat and high vacuum activation. The voids are interconnected with each other by apertures of various diameters which makes the void inaccessible to molecules which cannot enter because of their own "kinetic" diameters.

Figure 3 is a two-dimensional representation of a zeolite crystal consisting of a matrix of interconnected voids. The internal surface of the voids is typically made up of the ions of oxygen, aluminum, silicon and sodium or some other metal. The zeolite can be used as a selective adsorber of gas molecules with natural of induced dipole moments. As a crude picture, one can visualize a layer of polarized gas molecules attaching themselves to the surface. This creates a smaller void volume in the process, but still one with an attractive surface that can adsorb another layer, and so on until the void is full. In the process of filling the voids the weight increases, giving an experimental method to measure the mass of gas adsorbed.

8. Zeolite Adsorbers as Gas Compressors

The standard instrument for measuring the adsorbed massof gas is the differential gravimetric analyzer that records the apparent weight of a known mass of zeolite plus its adsorbent as a function of temperature and pressure. The true ratio of mass of gas per unit mass of zeolite is found by subtracting the error due to bouyancy as the pressure changes. Figure 4 is a plot of gas-zeolite mass ratio, x/m, as a function of pressure for various constant temperatures for N_2O in the zeolite NaY for pressure up to 7 Atm.

Gas molecules adsorbed in the zeolite cages are packed into a much smaller volume of space than normal at any temperature, T, above their boiling points. The actual density is close to that of the liquid, after they lose their heat of adsorption. All physical adsorption processes are exothermic, and for the Gibbs Free Energy to be a minimum, the heat of adsorption, H_a, is negative since entropy change, ΔS, is negative, and

$$\Delta G = \Delta H_a - T\Delta S \qquad (8)$$

The integral heat of adsorption is the total heat evolved from a condition of zero adsorbate loading to some final value. Differential heat of adsorption is the slope of the integral heat with a change in adsorbed gas. Heat of adsorption must be removed and then re-supplied as an adsorption cycle takes up and discharges gas at constant pressure.

The state of theoretical knowledge is not yet satisfactory for pressures above one atmosphere. The epic works of the past on the mathematical modeling of low pressure adsorption phenomena have been contributed by a number of workers including Freundlick [16], Lee

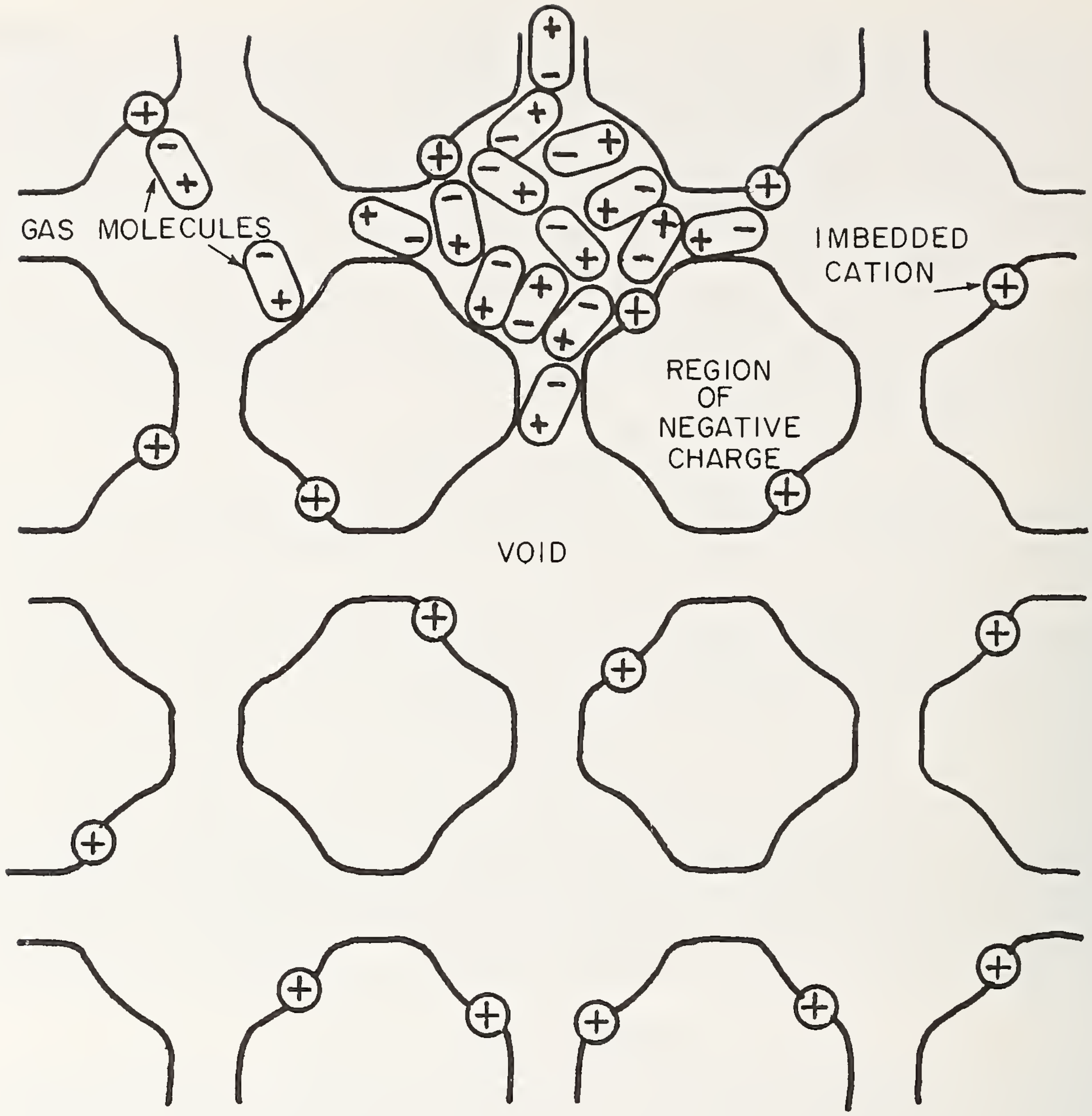

Fig. 3 Two dimensional representation of a zeolite with sodium cations imbedded in the surface of internal voids. Gas molecules are adsorbed on the surface due to their polarization in the ion fields. Other molecules are adsorbed due to dipole-dipole interactions, or other more complex potentials.

and Basmadjian [17], Riekert [18], Dubinin and Polanyi [19], Ruthven [20], Lippens and DeBoer [21], Langmuir [22], and Brunauer, Emmett and Teller [23].... to cite only a few.

Work at The University of Texas at Austin is directed at extending the theory to non-dilute situations using solution theory. The methodology of treating concentrated solution theory. The methodology of treating concentrated solutions have been given by I. Prigogine [24] and other [25, 26]. There are several reasons for this choice: (1) forming a solid solution by two substances is analogous to forming an adsorbed phase in the zeolite, (2) the theory of solutions is well understood and its mathematical techniques are powerful, and (3) the state-of-the-art in modeling adsorption phenomena in zeolites is basically em--pirical; solution theory could provide constants that are pleasing because they are physically related to the actual phenomena.

The adsorption isotherm, derived from lattice solution, theory, has the form,

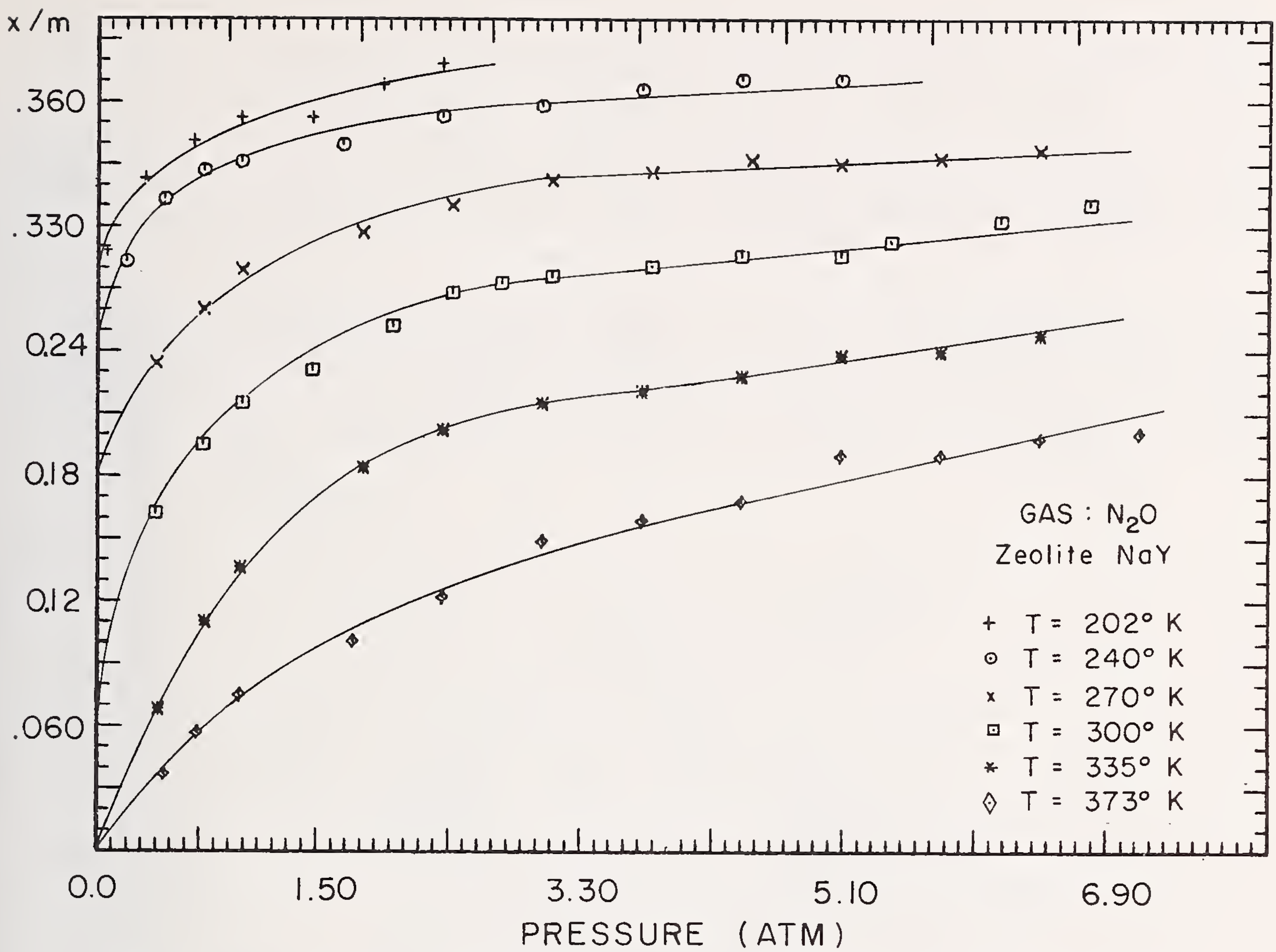

Fig. 4 Weight ratio of gas to zeolite, x/m for N_2O adsorbed in zeolite 13X.

$$p = P_o \left[\frac{x/m}{1/a + x/m}\right] \exp\left[-\frac{c}{(1 + ax/m)^2} \cdot \frac{\omega}{2kT}\right] \tag{9}$$

The term ω is the sum of all the potential energies which the gas molecules experience within the zeolite void or on the void surface. The potential may also be modified by any effects of the zeolite surface itself, as for example shifts in the position of metal (Na, K, Ca) cations across the distributed anion surface. All the components of ω are basically electrostatic, traceable to the interaction of a polarizable molecule in the electric fields of the zeolite ions and other gas molecules. The interactions are quantum-mechanical in nature, and include dispersion, repulsion, polarization, dipole and qudrupole contributions. The constants P_o, a, and c are calculated from both physical and experimental data.

The state of theortical knowledge is not yet adequate to calculate accurate adsorption isotherms from equations derived from first principles. It is adequate, however, for such problems as selecting promising gas/zeolite combinations for specific applications.

9. Performance of Experimental Compressor

Experimental adsorption and desorption data for pressures above 1 Atm are taken with an experimental compressor, and shown in Figure 5. An adsorption compressor unit consists of two or more pressure vessels containing zeolite, plus means to selectively admit return gas from the expansion and to discharge gas under pressure. To achieve this, means must exist to lower the temperature, or extract the heat of adsorption, and also to supply the heat of adsorption for raising the pressure. This is done by a finned helicoidal tube inside the compressor body which contains an electric heating element and also provision for circulation of a cooling fluid. The apparatus is used to study the adsorption and desorption processes separately. The heater is also used to activate the zeolite. This is the initial process of driving off adsorbed water. The compressor is held under a vacuum for several hours while the heater maintains a zeolite temperature of 350°C or greater. Valves are the only moving parts, and are located to open and close the low pressure intake line, the high pressure discharge line, and the vacuum line. The mass of any refrigerant gas that can be put in circulation is limited by the adsorption of that gas in the particular zeolite under ambient temperature and pressure. Figure 6 is the x/m vs. T isobars for three gases of interest - N_2O, CO_2 and N_2.

The desired shape and location of an isobar is that it drop steeply but be at a high value at ambient temperature. In this way, a large fraction of the adsorbed gas will be desorbed as the temperature increases without excessive addition of heat. At 300°K adsorbed N_2O adds 21% to the mass of the zeolite 13X, while N_2 adds only 2%. This parameters sets one limit on the size of the compressor since it is a multiplier, along with mass desorption rate, on the capacity of a refrigerator operating at a given high side pressure, and re-

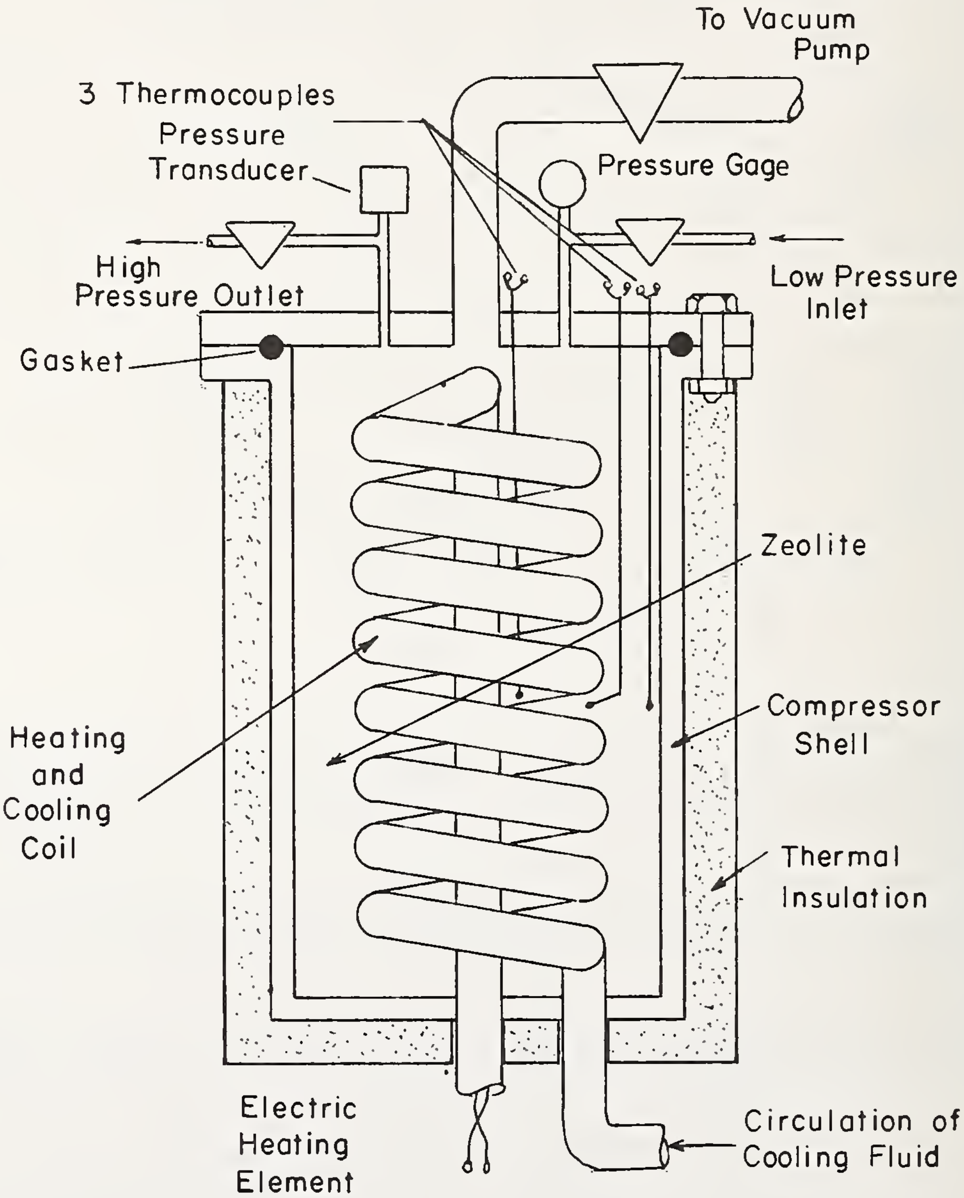

Fig. 5 Schematic diagram of experimental zeolite adsorption compressor.

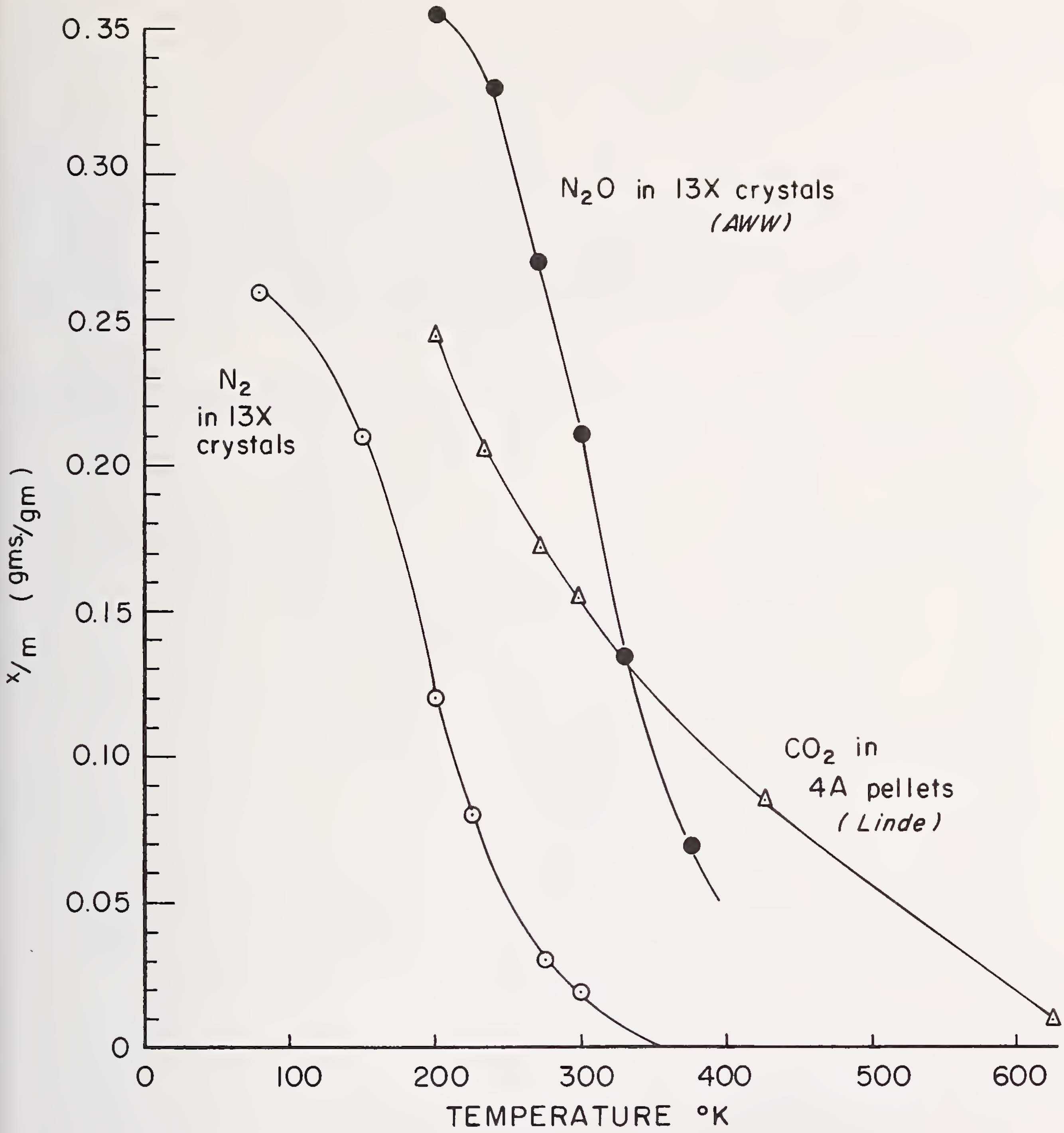

Fig. 6 Adsorption isobars for N_2, CO_2, and N_2O for one atmosphere pressure. Pellets contain about 80% zeolite crystals by weight.

adsorbing at 1 Atm low side pressure.

Figure 7 shows a refrigeration cycle in terms of the mass of adsorbed gas remaining in the zeolite as a function of pressure. The particular set of data is for N_2O in 13X with a delivery pressure of 21 Atm. T2 is the highest temperature reached by the zeolite during the desorption phase. Point a is the starting point for the pressurization phase which ends at point b. Between a and b $\bar{x}/m$ drops from 0.150 to 0.133 grams N_2O/gram of zeolite, and represents the gas in the free volume of the compressor outside of the zeolite voids. From b to c gas is discharged under 21 Atm pressure, with a total transfer of gas measured by the corresponding change $(x/m)_b - (x/m)_c$. From c to d the discharge and inlet valves are both closed and the zeolite is cooled. This causes the pressure to drop rapidly and the zeolite re-adsorbs gas from the free volume, $(x/m)_d - (x/m)_c$. When pressure reaches 1 Atm the inlet valve is open and gas is adsorbed to complete the cycle.

10. Molecular Adsorption Refrigeration System

The complete single stage MARS is shown schematically in Figure 8. With the exception of the compressors and their associated heating, cooling and solenoid valve control subsystems, the system uses existing heat exchange and Joule-Thomson expansion technology. An experimental system now in operation delivers 3 watts at 185°K using N_2O with about 3 KW input. The limiting factor in the coefficient ofperformance is heat exchange within the zeolite bed, since this sets the rate of change of pressure with heating. The present cycle time is about 30 minutes, with each of three compressors desorbing at 21 Atm for 10 minutes, circulating about 0.20 gm/sec through the expansion valve.

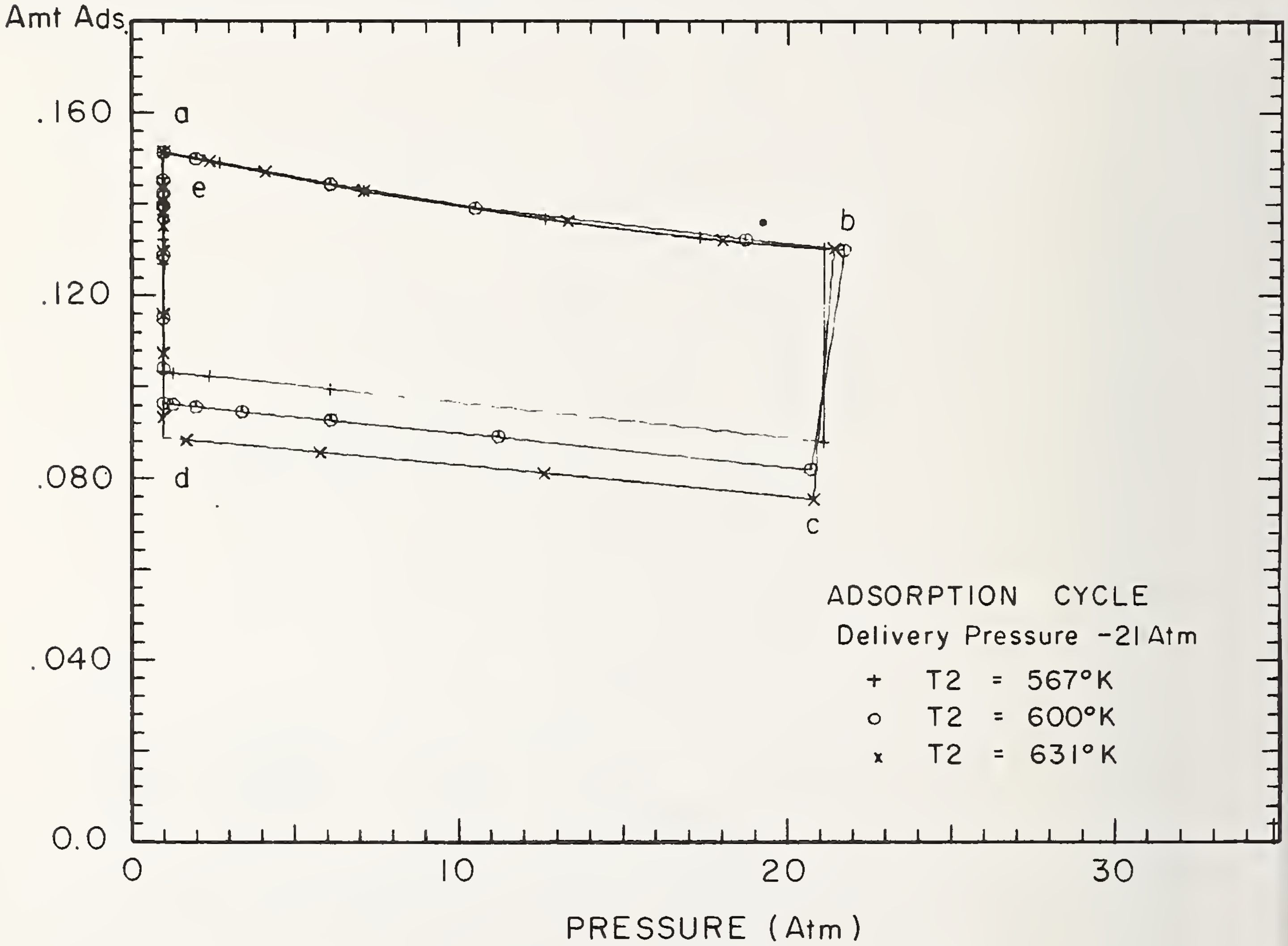

Fig. 7 Adsorption cycle of N_2O in 13X with delivery pressure of 21 Atm. Temperatures are peak value for zeolite at the end of the desorption phase, point "c". Adsorption is at 1 Atm. pressure.

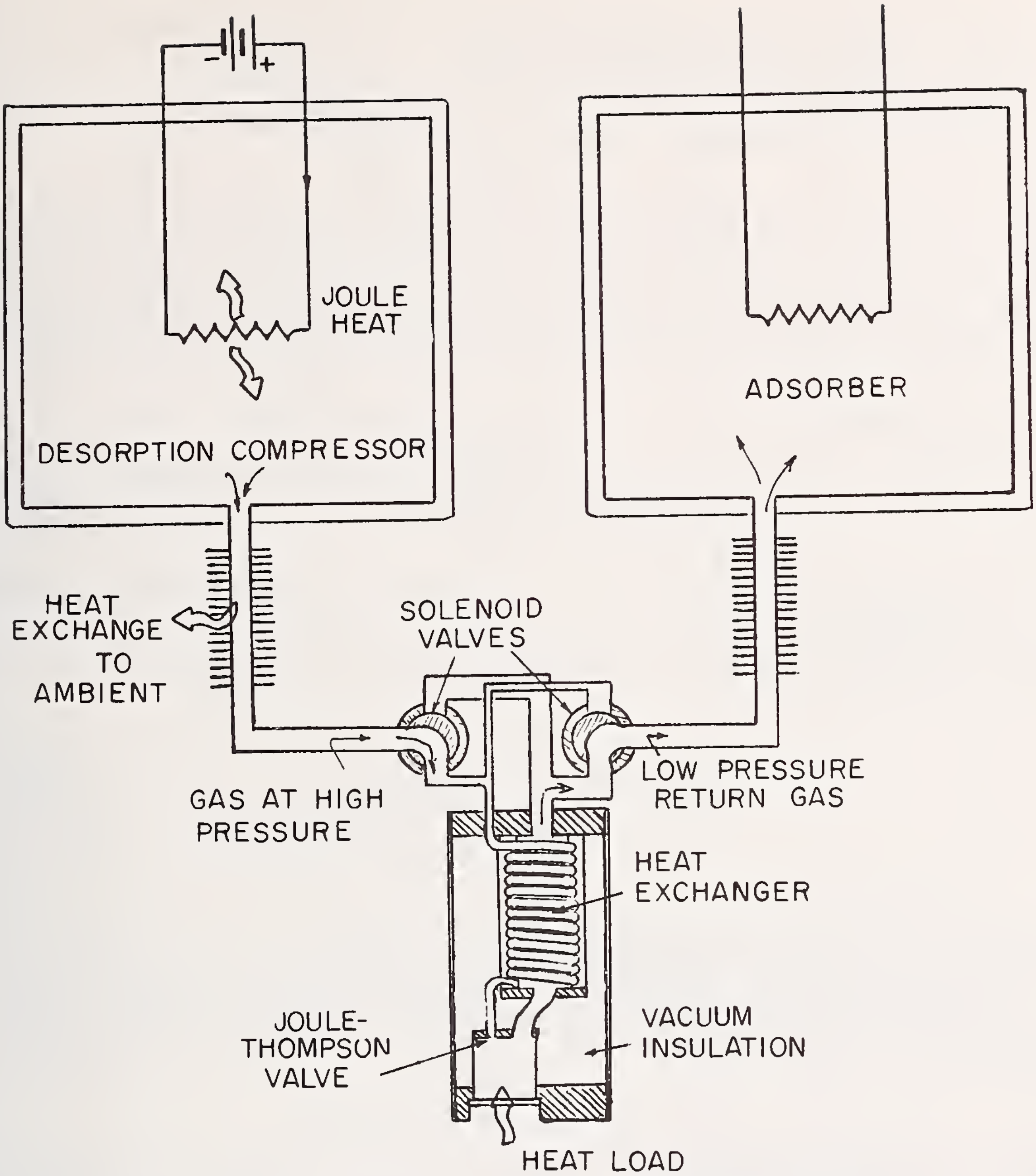

Fig. 8 Schematic of a single-stage refrigerator utilizing adsorption pumping. A third compressor, not shown, is in pressurizing or cool-down.

11. Coefficient of Performance

The refrigeration cycle is divided into four distinct time periods, adsorption, (t_a), pressurization, (t_p), desorption (t_d), and cool-down, (t_c). Each compressor can be in only one of the four states, so there exists a set of time relations between the four periods. Flow continuity requires the adsorption time be equal to the desorption time for two compressors working together. With three compressors in a set, the sum of cooling and pressurizing times must also equal the other two, and this yields an expression in terms of cycle time, to;

$$t_a = t_d = t_c + t_p = 1/3\ t_o \tag{10}$$

During the adsorption period a compressor must take in a mass of gas equal to $\Delta\frac{x}{m}$ times the zeolite mass. In terms of the refrigeration load,

$$W = \Delta H\ \dot{m}_g = \Delta H\ M_z(\Delta\frac{x}{m})/t_a = \frac{3\ \Delta H\ M_z\ (\Delta\frac{x}{m}}{t_o} \tag{11}$$

where; ΔH = enthalpy change by expanding gas, $\dot{m}_g$ = mass flow rate of gas, and M_z = mass of zeolite.

The Coefficient of Performance is the ratio of Wt_o to the total energy added in the cycle, or

$$\text{C.O.P.} = \frac{M_z\ (\Delta\frac{x}{m})\ \Delta H}{C_{pz}M_z\Delta Tz + C_{px}M_x\Delta T_x + C_{ps}M_s\Delta T_s + \int_0^{t_a} H_a(\frac{x}{m})\cdot M_z\cdot(\dot{\frac{x}{m}})\cdot dt} \tag{12}$$

where the $C_pM\Delta T$ terms refer to sensible heat in the zeolite, heat exchanger and compressor shell.

Over the range $\Delta\frac{x}{m}$ the value of H_a is nearly constant, so we can write

$$\text{C.O.P} = \frac{\Delta H}{H_a}\left[\frac{(\Delta\frac{x}{m})\ \Delta H}{(\Delta\frac{x}{m}) + \Sigma C_{pi}\ M_i\ \Delta T_i/M_z\ H_a}\right] \tag{13}$$

For N_2O at 21 Atm pressure expanding to 1 Atm and 185°K, $\Delta H \simeq 10$ Btu/lb and $H_a \simeq 200$ Btu/lb, so the maximum value of COP is approximately 0.05 neglecting the specific heat terms. For CO_2 the value is potentially much greater as desorbed gas pressure is about 750 psi for condensation at ambient temperature prior to expansion. At present the COP's are much lower than theoretical maxima due to large heat storage in the zeolite, heat exchanger, and compressor shell.

12. Advanced MARS Concepts

Figure 6 illustrates a fundamental aspect of adsorption pumping, namely the temperature dependence of the adsorption isobar. To extend the MARS concept to lower temperatures, means must exist to pressurize such gases as nitrogen, hydrogen and helium, and other cryogenic gases. Work has continued along three lines, each analogous to mechanical gas compressors: multiple stage - single gas systems, single stage - multiple gas systems, and multiple stage - multiple gas systems. Significantly enhanced adsorption x/m is observed as pressure is increased, with respect to the perfect gas density change. While it is inevitable this approach will penalize the performance, as it does in two-state mechanical compressors, the sensible heat from the first stage desorption would be available to desorb gas from the pressure-sorbed second stage.

Multiple stage - multiple gas systems could utilize the first stage for two purposes; precooling the second stage adsorber to enhance the x/m of the second stage gas, and precooling the gas in the high pressure leg of the second stage. Figure 9 is a schematic diagram of such a system.

13. Conclusions

It has been established that zeolites can be used for adsorption pumping with the distinct advantages of light weight, low cost, very large compression ratios per stage, and absence of noise, vibration, lubrication and wear. In addition, the danger of high pressure gases, such as N_2O, in the presence of lubricating oils and greases is eliminated.

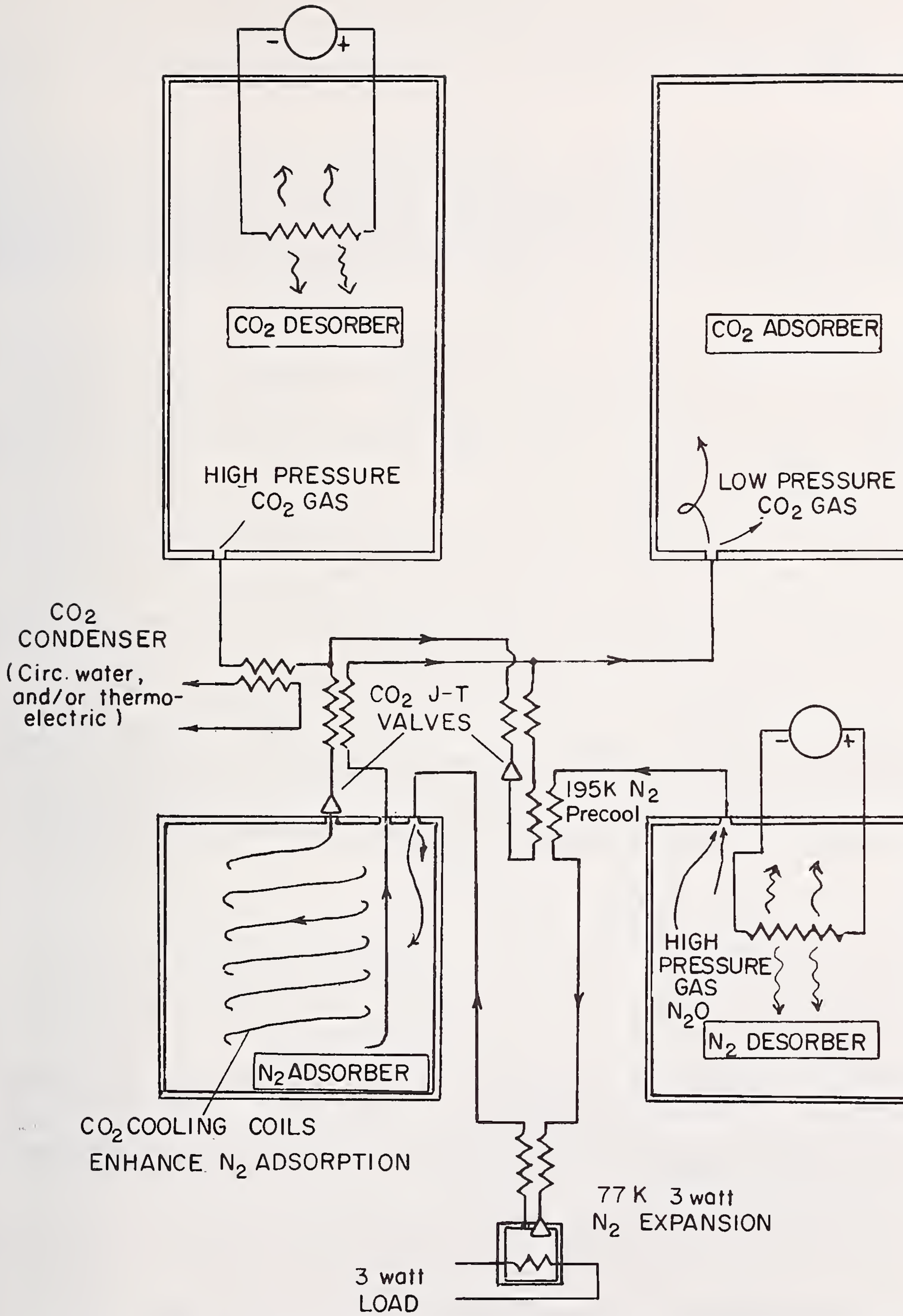

Fig. 9 Schematic diagram of a Two-Fluid, Two-Stage cryogenic refrigerator using CO_2 stage to cool zeolite in N_2 adsorber and to precool high-pressure N_2.

Danger of explosion or rupture of high pressure vessels is greatly reduced because adsorbed gases cannot escape at excessive rates. The way appears to be open for a complete range of temperatures down to 20 K utilizing various cryogenic gases in different compressor configurations. Preliminary computations suggest ultimate overall performance may approach mechanically pumped cryogenic refrigerators using Joule-Thomson expansion, when all factors are weighed.

14. Acknowledgements

The author is grateful for the expert consultation of the late Walter H. Hogan on various technical aspects of this project, to Richard R. Richard of the Johnson Space Center, NASA, for technical monitoring and confidence in the concepts, to H. Steinfink for his deep knowledge of the structure and properties of ze9lites, and to J. P. Masson and A. W. Woltman for their steady production of solutions and ideas in the course of the work.

15. References

[1] C. R. Haden, W. H. Hartwig, and J. M. Victor, "Magnetic Losses in Superconductors at High Frequencies," IEEE Trans. Magnetics, Vol. May-2, September, 1966, p. 331-333.

[2] J. M. Victor and W. H. hartwig, "Radio-Frequency Losses in the Superconducting Penetration Depth," J. Appl. Phys., Vol. 39, May, 1968, p. 2539-2546.

[3] A. F. Hildebrandt, Private Communication.

[4] J. P. Turneasure and Ira Weissman, "Microwave Surface Resistance of Superconducting Niobium," J. Appl. Phys., Vol. 39, August, 1969, p. 4417-4427.

[5] J. L. Stone and W. H. hartwig, "Performance of Superconducting Oscillators and Filters," J. Appl. Phys., Vol. 39, May, 1968, p. 2665-2671.

[6] D. Shoenberg, Superconductivity (Cambridge University Press, New York, 1965).

[7] B. L. Rhodes, C. E. Moeller, V. Hopkins, and T. I. Marx, "Thermal Expansion of Several Technical Metals from -255° to 300°C," Advances in Cryogenic Engineering, Vol. 8, p. 278-286, (Plenum Press, New York, 1963).

[8] C. G. Montogomery, Technique of Microwave Measurements, Radiation Laboratory Series, Vol. 11, (McGraw Hill Book Co., New York, 1948).

[9] Chang, S. S. L., Energy Conversion, (1963).

[10] Lee and Sears, Thermodynamics, Addison-Wesley, Reading, Mass. (1955).

[11] H. H. van Mal and A. Mijnheer, Fourth Cryog. Eng. Conf., Eindhoven, (1972).

[12] J. J. Reilly, and R. H. Wiswall, Jr., Inorg, Chem. 13: (1974).

[13] W. H. Hartwig, H. Steinfink, J. P. Masson and A. W. Woltman, Proc. 1976 Region V IEEE Conf., IEEE Cat. 76Ch1068-6 Reg 5, (1976).

[14] W. H. Hartwig, paper presented at 1977 Cryogenic Engineering Conf., to be published in Adv. in Cryogenic Engineering, K. D. Timmerhaus, ed., Plenum Press, New York.

[15] D. W. Breck, Zeolite Molecular Sieves, John Wiley, New York, (1974).

[16] Harper, et al., Canadian Journal of Chemistry, 47: 4661 (.969).

[17] Lee, A. K., and Basmadjian, D., Canadian Journal of Chem. Eng., 48: 682 (1970).

[18] Riekert, L., Advan. Catal., 21: 281 (1970).

[19] Dubinin, M. M., J. Colloid Interface Sci., 23: 487 (1967).

[20] Ruthven, D. M., Nature, Phys. Sci., 232: 29, 70 (1971).

[21] Lippens, B. C., and DeBoer, J. H., J. Catal. 4: 319 (1965).

[22] See Reference 15, p. 628.

[23] See Reference 15, p. 629.

[24] Prigogine, I., Molecular Theory of Solutions, Amsterdam: North Holland, (1957).

[25] Hill, T. L., Intro. to Statistical Thermodynamics, Addison-Wesley, (1960).

[26] Guggenheim, E.A., Mixtures, Oxford. (1952).

Cryogenic Cooling Requirements of Photoconductive Infrared Detectors for Orbiting Astronomical Telescopes

John W. Vorreiter and Craig R. McCreight
NASA-Ames Research Center
Moffett Field, California 94035

Abstract

Astronomical telescopes designed for high sensitivity require cryogenic cooling for the photon detectors. Recently developed photoconducting detectors show high sensitivity to infrared radiation but, unfortunately, this sensitivity also depends upon the detector temperature. This sensitivity to temperature is discussed for several common infrared photoconducting materials, and temperature levels and temperature stability requirements are suggested. The power dissipated in typical detector circuits is also discussed to define the heat loads that the cryogenic cooling systems must absorb.

Key words: Cryogenic cooling, IR detectors, orbiting telescopes.

Introduction

The sensitivity of photoconductors used as infrared detectors is a function of many variables. These variables include: the wavelength of radiation, detector field of view, temperature of the radiation background, temperature of the detector, charged particle environment, electrical contact type, bias voltage, and others. The basic measure of detector sensitivity is the radiant power on the detector which produces a signal to noise ratio of one. This quantity, called the Noise Equivalent Power (NEP) is defined by Equation 1.

$$\mathrm{NEP} = \frac{H A_d V_N}{V_S} \ (\mathrm{W/Hz^{1/2}}) \tag{1}$$

where:

H = Irradiance ($\mathrm{W/cm^2}$)

A_d = Detector Area ($\mathrm{cm^2}$)

V_N = Noise Voltage normalized to unit bandwidth ($\mathrm{V/Hz^{1/2}}$)

V_S = Signal Voltage (V) .

A more common parameter is D* (pronounced dee-star), which is related to NEP by Equation (2).

$$D^* = \frac{(A_d)^{1/2}}{\mathrm{NEP}} \ (\mathrm{cm\ Hz^{1/2}/W}) \tag{2}$$

More precise definitions of these and other detector parameters were developed by R. C. Jones [1].

Temperature Requirements

The detector sensitivity data reported below include substantial uncertainties, typically in the amount of 30% or more. These uncertainties arise, for example, through the difficulty in accurately determining the signal and background fluxes falling on the detector, electronic measurement errors, and geometrical effects within the test chamber influencing detector illumination angles. Despite those shortcomings, the best available D* vs temperature data are presented and approximate best-fit curves through the data are included. The authors recognize that the temperatures and temperature ranges here derived from uncertain data necessarily contain a significant inherent uncertainty. Nevertheless, they present them to define preliminary cryogenic cooling requirements.

When deducing the intensity of an observed astronomical object, any change in detector calibration caused by temperature effects must be considered. Knowing the D* (and noise voltage) vs temperature characteristics allows one to quantify the calibration change, which is referred to here as a source intensity error, and which is directly proportional to the relative D* decrease. Source intensity errors of 10 and 50% are used to determine suitable temperature control ranges for the various detectors.

Three photoconductor materials were selected for discussion from the literally dozens of combinations of host and dopant materials developed. Gallium-doped germanium (Ge:Ga), bismuth-doped silicon (Si:Bi), and beryllium-doped germanium (Ge:Be) will be discussed, in that order, due to their peculiar cooling requirements.

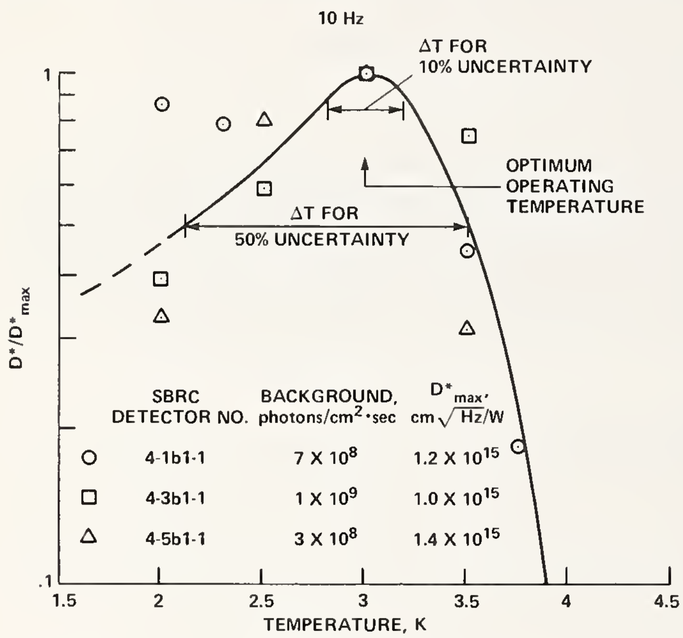

Figure 1. Relative response vs temperature for gallium-doped germanium detectors.

Germanium doped with about 2.4×10^{14} Ga atoms/cm^3 is a useful detector material for wavelengths from about 30 μm to 120 μm [2]. The sensitivity of several detectors made from a common crystal have been measured by P. R. Bratt [3]. The normalized D* vs temperature curve for this material is shown in Figure 1. These data can be translated into requirements for optimum temperature and temperature control ranges for various values of source intensity uncertainty. Within the accuracy of the experimental data, Figure 1 shows the optimum temperature for Ge:Ga to be 3.0 K. Also, if a source intensity uncertainty of 10% was allowable, the corresponding allowable temperature range would be approximately 2.8-3.18 K. For 50% source intensity uncertainty the control range would be broadened, and the minimum and maximum temperatures would extend from 2.1-3.5 K.

Bismuth-doped silicon (Si:Bi) [4] is a useful photon detector between the wavelengths of 4-20 μm. Its relative sensitivity is shown in Figure 2, which indicates the optimum operating temperature to be 31 K and the required control range to be 25-32 K for 10% source uncertainty. For 50% allowable uncertainty the minimum temperature in the control range is below 5 K and the maximum temperature is 33.5 K. If necessary, silicon-based detectors can be operated significantly below their optimum temperatures with some loss of performance. However, in this situation, a phenomenon called spiking becomes much more frequent. This spiking has been measured by the Infrared Devices Group at the Naval Ocean Systems Center [5,6] and it is not clearly understood at this time. All other conditions being equal, the spiking frequency for arsenic-doped silicon (Si:As) reaches a minimum at about 10 K and increases at lower temperatures [6]. Spiking is typically filtered out of the signal stream by pulse circumvention circuitry with some loss in signal/noise ratio. The discrimination of spikes vs real signals is based on the much faster rise time for spikes.

The third detector material, beryllium-doped germanium (Ge:Be), has a sensitivity curve which is different in shape from those mentioned above. Its useful wavelength range is approximately 30-50 μm [7]. Germanium doped with approximately 1×10^{15} Be atoms/cm^3 has been evaluated [2], and the normalized D* vs temperature curve for these detectors is shown in Figure 3. For the temperature range shown, and within the experimental error, these detectors appear to have a higher D* for successively lower temperatures. This atypical behavior may be due to several factors. The reported photon background under which the tests were conducted may have been incorrectly high, so that the detectors may not have

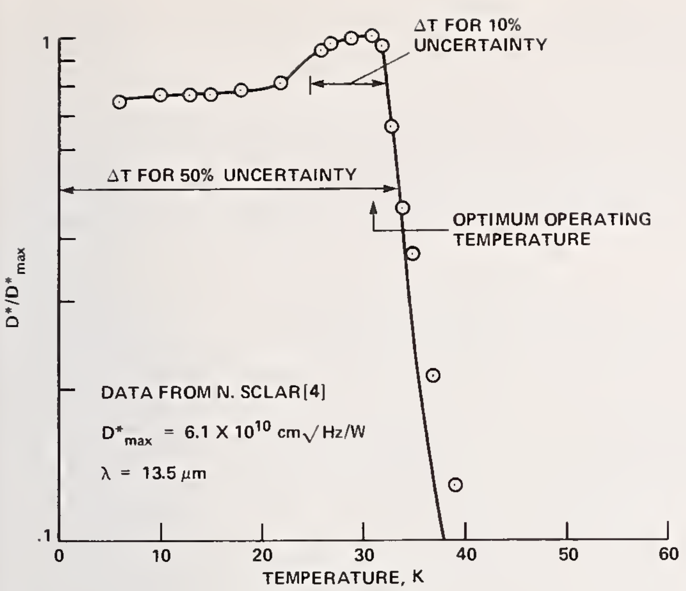

Figure 2. Relative response vs temperature for bismuth-doped silicon detectors.

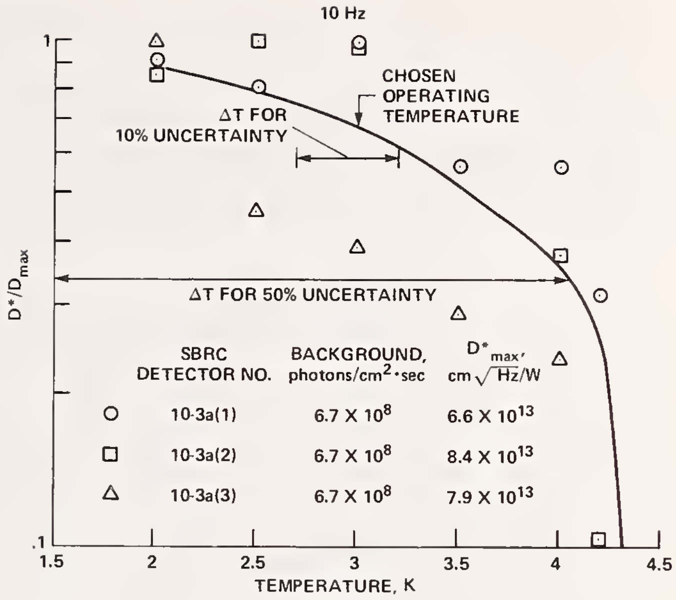

Figure 3. Relative response vs temperature for beryllium-doped germanium detectors.

been background-limited, a condition for which astronomical detector systems are normally designed. Also, impurities other than beryllium, which remain photon-active at these temperatures, may have been present in the germanium crystal structure. After additional detector development, one could expect these impurities to be eliminated, and a response similar to Ge:Ga to apply to Ge:Be.

In circumstances like this, detector operating temperature can be chosen for factors other than just ultimate detector performance. Two of these factors could be the minimum temperature capability of the cooling system or optimum operating temperature of some adjacent detector. For example, the Ge:Be detector may be operated with a Ge:Ga detector which is optimized for 3.0 K. In the case where the Ge:Be is operated at 3.0 K the temperature control range for 10% source intensity uncertainty is 2.7 and 3.2 K. For the 50% relative uncertainty, the range would be between approximately zero and 4.05 K.

Heat Dissipation

Heat dissipation for all the previously mentioned detectors is determined by the associated preamplifier electronics that is typically located within 1 or 2 mm of the detectors. The circuitry commonly employed is shown in Figure 4. Virtually all of the heat dissipation for this circuitry takes place in the MOSFET preamplifier, and the amount depends strongly upon MOSFET design. Specifically designed MOSFETs have been developed and tested at power dissipations as low as 25 μW per detector [8]. Other MOSFETs dissipate as much as 1 mW apiece. With arrays of several hundred detectors which are being contemplated, this power dissipation can approach substantial heat loads of almost 1 W. These power levels then, in conjunction with the chosen detector temperatures, define the requirements which the cryogenic system must satisfy.

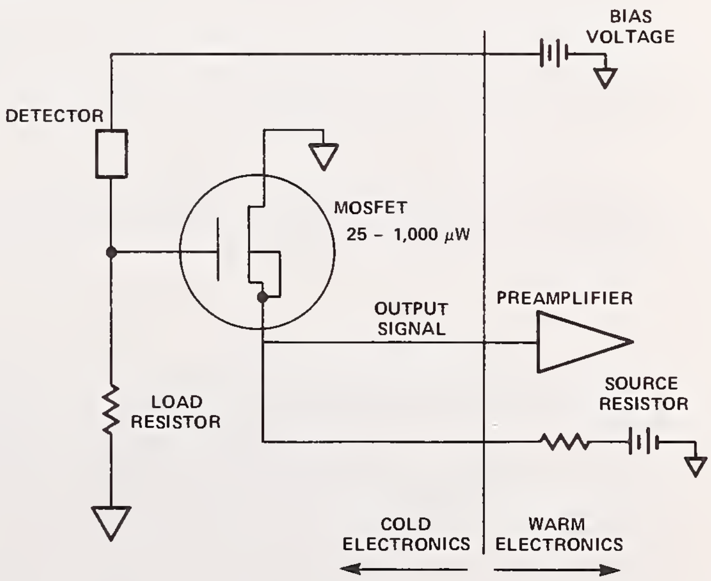

Figure 4. Photoconductive detector circuitry.

Cooling Methods

Table 1 summarizes the operating temperature requirements for the Ge:Ga, Si:Bi, and Ge:Be detectors considered. Si:Bi detectors should be cooled to about 31 K, and they can tolerate temperature excursions on the order of 7 K within the 10% effective source uncertainty limits. The doped-germanium detectors, however, require cooling to below the ^4He normal boiling point and very good temperature stability.

Table 1. Operating temperatures and temperature stability requirements for Ge:Ga, Si:Bi, and Ge:Be detector materials.

Detector Material	Optimum Temperature, K	10% Source Intensity Uncertainty		50% Source Intensity Uncertainty	
		T_{min}, K	T_{max}, K	T_{min}, K	T_{max}, K
Ge:Ga	3.0	2.8	3.18	2.1	3.5
Si:Bi	31	25	32	≈0	33.5
Ge:Be	3.0*	2.7	3.2	≈0	4.05

*Arbitrary temperature chosen for compatibility with Ge:Ga.

An important factor in choice of the detector cooling system is mission lifetime. Planned infrared astronomical experiments aboard non-refurbishable freeflying spacecraft require one year or more of cooling, which is provided by maximized-lifetime open-cycle, or by high-reliability closed-cycle systems. Shuttle sortie missions, on the other hand, can include non-optimized open-cycle cooling systems because of their short durations.

It appears that the ability to cool the doped-germanium detectors to 3 K with a fraction of a kelvin tolerance for periods of up to a year with closed-cycle machines is many years away, since minimum temperatures of about 10 K and unattended lifetimes of just a few thousand hours are the current performance capabilities of the best closed-cycle systems. This will either limit exploration of the infrared sky to wavelengths below 30 μm where doped-silicon detectors can be used, or spur technology development in superfluid helium open-cycle cooling systems and supercritical helium Joule-Thomson systems of the open or closed type. At least one major program, the Infrared Astronomical Satellite (IRAS), a joint U.S.-Dutch-British venture which includes Ge:Be and Ge:Ga detectors, has chosen to proceed with an open-cycle superfluid helium cooling system.

Extended lifetime or increased reliability of the cryogenic cooling system is quite important, for many missions. Extreme efforts must be made to extend cooling system lifetimes to a minimum of several years if the cost per useful orbital observation is to remain realistic.

Summary

The change in relative detector sensitivity (D^*/D^*_{max}) vs temperature was presented for Ge:Ga, Si:Bi, and Ge:Be photoconductors. Although the data were somewhat scattered, preliminary conclusions as to optimum detector temperature and temperature control ranges for 10 and 50% source intensity uncertainties were drawn. The doped-germanium detectors require cooling to the 3 K region, with small allowable temperature excursions. The doped-silicon detector discussed, Si:Bi, has a much less severe cooling requirement in terms of both absolute temperature and temperature range. Dissipation levels can range from 25-1000 or more μW per channel, and total power levels vary directly with the number of channels in the detector array. In the near-term, the temperatures for the doped-germanium detectors can be provided only by open-cycle helium cooling systems. Closed-cycle machines can satisfy

doped-silicon cooling requirements for limited periods, and decreased temperatures and extended lifetimes for both cooling approaches appear to be highly desirable.

Acknowledgment

The authors wish to express their sincere appreciation to Dr. W. L. Eisenman of the Naval Ocean Systems Center, San Diego, California for his assistance in locating suitable detector performance references.

References

[1] Jones, R. C., Phenomenological description of the response and detecting ability of radiation detectors, Proc. Institute of Radio Engineers 47, 1495 (1959).

[2] Moore, W. J., and Shenker, H., A high-detectivity gallium-doped germanium detector for the 40-120 μ region, Infrared Physics 5, 99 (1965).

[3] Bratt, P. R., Development of doped germanium photoconductors for astronomical observations at wavelengths from 30 to 120 micrometers, Santa Barbara Research Center (Oct. 1977). Final Report for Contract NAS2-9385, NASA CR-152,046.

[4] Sclar, N., Extrinsic silicon detectors for 3-5 and 8-14 μm, Infrared Physics 16, 435 (1976).

[5] Anon, Characterization of IRAS doped silicon detectors, Naval Ocean Systems Center, NASA CR-151-941, (Dec. 1976).

[6] Anon, Further characterization of IRAS doped silicon detectors, Naval Ocean Systems Center, NASA CR-152,014 (June 1977).

[7] Shenker, H., Swiggard, E. M., and Moore, W. J., Photoconductive and electrical properties of uncompensated beryllium-doped germanium, Trans. Metallurgical Society of AIME 239, 347 (1967).

[8] Nielsen, R. L., Private communication, Santa Barbara Research Center, Goleta, Calif., (Sept. 1977).

Cooling of Josephson MM-And SubMM-Wave Systems: Requirements, Results And Applications

J. Edrich
Denver Research Institute
University of Denver
Denver, Colorado 80208

Performance and potentials of Josephson receivers for mm and submm wavelengths are discussed. It is shown that these systems can achieve up to ten times lower noise and several times wider bandwidths than other known systems and will most likely dominate the submm wave range because of low noise and local oscillator power, wide bandwidth and tuning range. In order to find more field applications in certain broadband communications, radiometry and medical thermography small and simple closed cycle refrigerators for $T \leq 9K$ with more than 100 mW cooling capacity, small vibration and plastic displacers are needed; they could possibly be scaled-up versions of a recently reported miniature Stirling refrigerator for 8K. The influence of High-T_c superconductors and hybrid cooling systems using 20K refrigerators for reduction of liquid helium boiloff rates are discussed. As a practical example, the development and preliminary results on the first closed cycle cooled mm/submm wave system are given which uses permanent point contacts for a mixer in the 220 to 325 GHz range.

Key words: Amplifiers; closed cycle refrigerators; detectors; Josephson effect; low-noise and broadband communications; millimeter and submillimeter receivers; mixers; radiometry; thermography.

1. Introduction

Josephson devices utilizing superconducting junctions [1,2] are highly nonlinear and exhibit relatively small parasitic reactances. Laboratory results and one field test have shown very promising performance of these devices as detectors [3], mixers [4,5,6] and parametric amplifiers [7] for applications in low-noise receivers for millimeter and submillimeter waves.

However, before these devices can be moved from the laboratory into the field several obstacles have to be removed which presently prevent long term and reliable field operation. One major problem is presented by the cooling mode of present day systems using liquid helium. Closed cycle refrigerators are needed for most practical field uses of such systems. However, existing refrigerators for temperatures below 9K are not suitable for most applications because of their large weight and size, their complexity and high cost. Recent results achieved with relatively small cryocoolers for SQUID systems [8] indicate that small cryocoolers could also be developed for the somewhat larger mm wave systems.

This report will therefore start out by discussing potentials and applications of such systems. Secondly, an attempt is made to outline the cooling requirements based on our recent successful cooling tests of Josephson junctions using a closed cycle refrigerator.

2. Potentials of Josephson Receivers

Figure 1 illustrates in solid curves the noise of existing receivers as a function of frequency between 1 and 1000 GHz. There are only a few short, solid-line sections and measurement points shown for Josephson mixers and paramps representing early laboratory results. Only one system, a 1 mm Josephson video detector, has so far been used in the field (on a telescope) and shown a r.m.s. noise temperature fluctuation

$$\Delta T_{r.m.s.} = \frac{AT}{B\tau} = 0.25K \qquad (1)$$

where A, T, B and τ are the detection constant, equivalent noise temperature, bandwidth and time constant, respectively. This $\Delta T_{r.m.s.}$ value was significantly lower than previously achieved with helium cooled germanium bolometers. However, the Josephson detector used in this system was not too well matched, filtered and shielded, and substantial improvements can be expected in future systems. The same statement can be made for the first laboratory results on Josephson paramps and mixers for 30 GHz [5,7] and 320 GHz [6]; these systems, nevertheless, exhibited a fairly attractive noise performance as compared to other known receivers. The dashed curves in Figure 1 indicate the projected performance for superconducting receivers expected within the next 5 to 10 years; these curves, and even the ones of the already existing systems indicate the rather large noise improvements that can be expected from these relatively new devices.

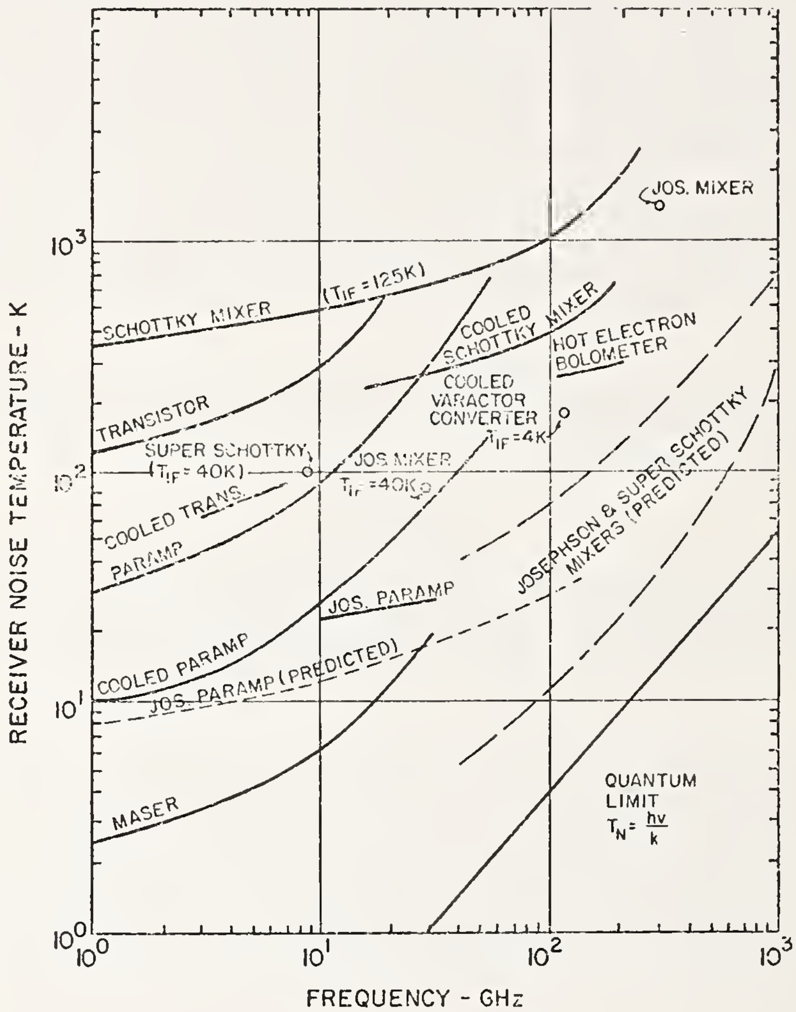

Figure 1. Comparison of receiver noise temperatures for the 1 to 1000 GHz frequency range. Projected performance for superconducting receivers is indicated by dashed curves.

Equation (1) for the broadband receiver noise fluctuation shows that the noise temperature T is not the only determining factor; another important parameter in reducing the noise fluctuation $\Delta T_{r.m.s.}$ is the bandwidth B. Values for bandwidth, noise, operational temperature, cost and upper frequency limit of Josephson systems and other types of receivers are summarized in Table 1. Line 2 of this Table shows that all of the Josephson devices exhibit a relatively wide bandwidth which makes them particularly useful for certain broadband communications and radiometry systems. Another attractive feature of Josephson systems for high mm and low submm frequencies is their low local oscillator power requirement of typically less than 10 μW [5,6]. Most other devices require two to three orders of magnitude more power in the frequency range above 100 GHz. Unfortunately, power available in this range is up to now extremely scarce and ocstly, and requires inefficient and short-lived tubes with high voltages (reflex klystrons or carcinotrons). It is there-

Table 1

COMPARISON OF IMPORTANT CHARACTERISTICS OF LOW NOISE RECEIVERS FOR THE 1 TO 1000 GHz FREQUENCY RANGE

PARAMETER	FET	MASER	CRYO-PARAMP	CRYO-SB MXR	HOT ELECTRON BOLOM.	CRYO-VARACTOR CONV.	JOS. MIXER	JOS. PARAMP
BANDWIDTH (%)	WIDE 10-200	NARROW .1-3	MEDIUM 5-14	MEDIUM .5-3	VARY NARROW <.002	NARROW** <1	MEDIUM .1-4	WIDE* 3-15
				IF LIMIT	IF LIMIT	IF LIMIT	IF LIMIT	IF LIMIT
NOISE (K)	MEDIUM 70-600	LOW 5-80	LOW 10-160	MEDIUM 200-500	MEDIUM 200-300	LOW 120-200	LOW 30-150	LOW 20-100
OP. TEMP. (K)	77-300	4	20	20	4	4	4-9	4-9
COST	LOW	HIGH	MEDIUM	MEDIUM	LOW	MED-HIGH	MEDIUM	MEDIUM
FREQ. LIMIT (GHz)	35	100	100	300***	7230	200***	300	>300*

* CIRC. LIMIT
** MASER IF LIMIT
*** LO POWER LIMIT

fore likely that Josephson systems will dominate the upper mm and the submm frequency range in applications requiring low noise and wide bandwidth.

A major disadvantage of superconducting devices is their need for a relatively low operating temperature of less than 9K and their cumbersome cooling with liquid helium.

3. Existing Cooling Techniques and Requirements for Future Small Closed-Cycle Cryocoolers

Josephson junctions can take four basic forms: a) Sandwich-type superconducting thin films b) proximity bridges c) microbridges d) point contacts. Up to now only microbridge arrays and point contacts have successfully been used in the mm and submm wavelength range [4-7] because of their small geometry and low parasitic capacitance. Microbridges with good performance characteristics for frequencies above 20 GHz, like the Sn junction arrays used in a 33 GHz SUPARAMP [7], have to be cooled below their relatively low transition temperature ($T_c \simeq 3.7$K for Sn). Most point contact junctions successfully used in the frequency range above 20 GHz were of niobium material which exhibits a more attractive, higher transition temperature of 9.4K [3-7]. Alloys with even higher transition temperatures, T_c, such as NbN and Nb_3Sn or others, would be very desirable for high frequency applications; however, successful tests have not been reported yet. Use of high T_c materials would not only ease the requirements on cryocooler temperature, power, size and cost, but it would also significantly improve the performance of mm and submm devices. The reason for this lies in the fact that the large energy gap Δ of these high-T_c materials gives rise to an increase of the product of the supercurrent I_c and the normal state resistance R_{NS}. [10]

$$I_c R_{NS} = \frac{\pi\Delta}{2e} \qquad (2)$$

where e is the electron charge. For good high frequency performance the largest possible product of I_c and R_{NS} is desired. High T_c materials may, however, not be suitable for sufficiently narrow microbridges or sharp point contacts with good stability and temperature cyclability as required for practical applications in cryocoolers. In this case, microbridge arrays or permanent point contact junctions look most promising for near term applications in closed cycle systems. Microbridges would offer the advantage of a higher resistance [11], permanent point contacts, on the other hand, would most likely allow higher operating temperatures and not suffer from the problem of low saturation power [12].

Besides the conventional cooling technique of using liquid helium "hybrid systems" have been reported for low frequencies [13] and are under development for the mm wavelength range [14]. These systems reduce the boiloff rates of helium by a factor 3 to 5 by using small, conventional 20K closed cycle refrigerators.

Up to now only two experiments have been reported where the Josephson devices were successfully conduction cooled by closed cycle refrigerators. One experiment involved cooling a small niobium SQUID using a miniaturized, all-plastic, Stirling cryocooler with a cooling capacity of a few milliwatt below 9K [8]. The other experiment involved permanent niobium point contact junctions for a 300 GHz mixer receiver using a 4K helium refrigerator* [15].

The mm/submm system, which will be described below in more detail, utilizes a fairly large compressor and a refrigerator with a Gifford-McMahon cycle and a Joule Thomson circuit. Its cooling capacity is in excess of 2 Watt at 4.3K. Such relatively large machines with low operating temperatures were required for cooling of masers, but are not needed and desirable for future Josephson receivers.

Table 2

DESIRABLE CRYOCOOLER CHARACTERISTICS
FOR JOSEPHSON MM AND SUB MM SYSTEMS

REFRIGERATOR	3 STAGES,*
VIBRATION	≤ 0.01 mm
DISPLACERS & CYLINDERS	PLASTIC PREFERRED
COMPRESSOR	< 50 kg, < 200 W
MAINTENANCE FREE FOR	3000 h
ΔT_{refr}	± 0.5 K, longterm,**
REFR. POWER FOR ≤ 9 K	100 - 300 mW

*NO JOULE THOMSON, IF POSSIBLE.
**PERMANENT POINT CONTACT

Table 2 outlines some of the important "desired" characteristics of small cryocoolers for future Josephson systems. Since permanent niobium point contacts appear to be most promising for near term applications at high mm and low submm frequencies this kind of device is used as basis for the Table. In the mixing mode it is followed by a Josephson or varactor paramp (T_{op} = 9 or 15 K!). As listed in this table a 3-stage refrigerator without a Joule Thomson circuit would be very attractive for most of these high frequency applications. Other desired characteristics include small vibration, i.e. low displacer speed, plastic displacers and cylinders, a small and efficient compressor, and 3000 hours of uninterrupted operation. Temperature stability is not very critical, at least for point contacts and the cooling capacity could be in the 100 to 300 mW range for $T \leq 9K$ depending on the frequency, application etc. A system using microbridge junctions would require significantly better temperature stability, lower operating temperature and increased cooling capacity approaching that of presently existing, relatively large, 4K closed cycle refrigerators.

*Cryodyne Mod. 400B of CTI, Inc.

4. A Josephson Millimeter/Submillimeter Wave System With Cryocooler Under Development

The first mm/submm wave Josephson system using a closed cycle refrigerator is presently under development *[15]; it incorporates permanent niobium point contacts which were successfully rf-tested at lower frequencies [12]. Recently, they have undergone a series of cooling tests attached to the fourth stage of the above mentioned 4K helium refrigerator. These experiments showed good mechanical stability, temperature cycling and dc characteristics [15]. The block diagram in Figure 2 presents more system details: The rf signal in the 220 to 325 GHz frequency range is first focussed via a lens into a scalar horn; subsequently, the local oscillator signal is added in a crosscoupler, and mixing down to an intermediate frequency (IF) of 4 GHz takes place in the Josephson mixer. A 4 GHz maser with a noise temperature T_{MA} = 3K and a bandwidth of 140 MHz amplifies the IF by 30 db. Further amplifications are provided by an uncooled paramp and a transistor amplifier.

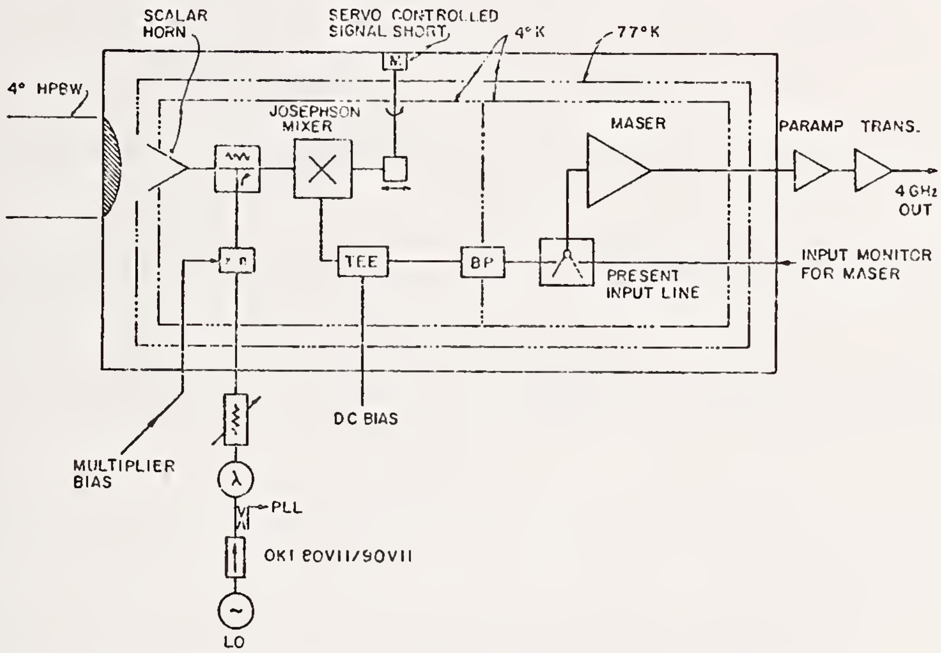

Figure 2. Permanent Josephson mixer receiver, tunable from 225 to 325 GHz and using the NRAO 4 GHz maser with closed cycle refrigerator

Both the maser and the Josephson mixer are conduction-cooled to 4.2K by the fourth stage (Joule-Thomson circuit) by the refrigerator. Separate rf and magnetic shielding and thermal radiation shielding are provided for the mixer. Based on laboratory results with a similar 300 GHz system, which, however, used an adjustable Josephson point contacts, a narrow-band X-band maser and liquid helium cooling, double- and single-sideband noise temperatures T_{DSB} = 510K and T_{SSB} = 1320K are expected for this system [6,15]. It should be noted that this figure is very conservative because no future improvement of essential system components (Josephson mixer, IF match etc.) as compared to the earlier laboratory system [6] was assumed.

5. Outlook

Low-noise and wideband receivers are needed for a variety of applications in the frequency range encompassing millimeter and submillimeter wavelengths. Table 3 lists a number of these areas and specific system tasks. Josephson devices are particularly attractive for applications requiring wide bandwidths and low noise temperatures like radiometry, continuum and spectral line measurements in radio astronomy [3,6,7,11,12], and millimeter wave thermography [16] where these devices could improve sensitivity and scanning speed by

*This system is planned to be used on the NRAO 36 ft. telescope for spectral line observation tunable over the entire 220 to 325 GHz range.

Table 3

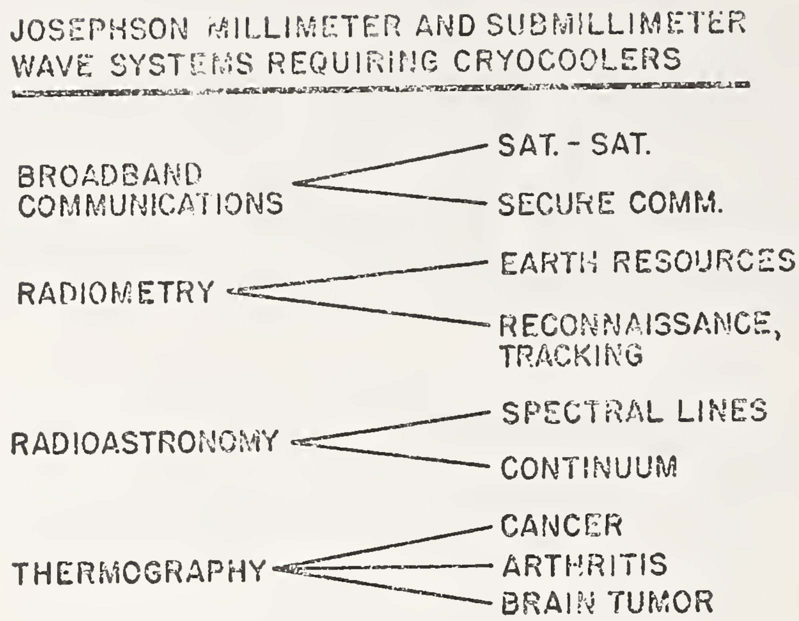

more than order of magnitude. Josephson receivers also represent up to now the only approach to low-noise reception for frequencies above about 300 GHz because of their low intrinsic noise and local oscillator power requirements.

6. References

[1] Josephson, B.D., Possible new effects in superconductive tunneling, Phys. Letters 1, 251-253 (July 1962).

[2] Solymar, L., Superconductivity Tunneling and Applications, Wiley, New York (1972).

[3] Ulrich, B.T., Josephson junction detector for astronomical applications, Rev. de Phys. Appl. 9, 111-118 (Jan. 1974).

[4] Kanter, H., Josephson junction mixer using an external local oscillator, Rev. de Phys. Appl. 9, 255-262 (Jan. 1974).

[5] Taur, Y., Claassen, J.H. and Richards, P.L., Josephson junctions as heterodyne detectors, IEEE Trans. MTT 22, No. 12, 1005-1008 (Dec. 1974).

[6] Edrich, J., Sullivan, D.B., and McDonald, D.G., Results, potentials, and limitations of Josephson-mixer receivers at millimeter and long submillimeter wavelengths, IEEE Trans. MTT 25, No. 6, 476-479 (June 1977).

[7] Chiao, R.Y., and Parrish, P.T., Operation of the SUPARAMP at 33 GHz, J. Appl. Phys. 47, No. 6, 2639-2644 (June 1976).

[8] Zimmerman, J.E., Operation of a SQUID in a low-power cryocooler, Proc. Conf. on Appl. of Closed Cycle Cryocoolers to Small Supercond. Dev., Boulder, in this report (Oct. 1977).

[9] Beasley, M., Progress report on high-T_c Superconducting, Proc. Conf. on Appl. of Closed Cycle Cryocoolers to Small Supercond. Dev., Boulder, in this report, (Oct. 1977).

[10] Zimmerman, J.E., Proc. of 1972 Appl. Supercond. Conf., Boulder, IEEE Conf. Rec. 72 CHO 682-5-TABSC, p. 544.

[11] Feldman, M.J., The thermally saturated SUPARAMP, J. Appl. Phys. 48, No. 3, pp. 1301-1310, March 1977.

[12] Edrich, J., A low-noise 47 GHz mixer using a permanent Josephson junction, IEEE Trans. MTT-24, No. 11, pp. 706-709, Nov. 1976.

[13] Goree, W., Use of cryocoolers to reduce liquid helium boiloff rates, Proc. Conf. on Appl. of Closed Cycle Cryocoolers to Small Supercond. Dev., Boulder, in this report, (Oct. 1977).

[14] Edrich, J., Shuter, W.L., McCutcheon, W.H., and Gregory, P.C., Spectral line search and observation around 110 GHz using a compact cryogenic mixer receiver without LO filter, Dig. URSI Meeting, Boulder, Pap. J-3b, Jan. 1978.

[15] Edrich, J., Development of a field-usable 300 GHz Josephson mixer system, Dig. URSI Meet., Boulder, Pap. J-3c, Jan. 1978.

[16] Edrich, J. and Smyth, C.J., Arthritis inflammation monitored by subcutaneous millimeter wave thermography, J. of Rheumatology, in press (Febr. 1978).

This work was supported by NSF Grants 76-23094 and 76-24241 with instrumentation support from the National Bureau of Standards and Associated Universities, Inc. (National Radio Astronomy Observatory).

Progress Report on High-T_c Superconducting Devices*

M. R. Beasley
Departments of Applied Physics and Electrical Engineering
Stanford University
Stanford, California 94305

Recent progress in the utilization of high transition temperature superconductors in superconducting electronic devices is reviewed.

Key words: Superconducting devices, high transition temperature superconductors.

Introduction

Throughout the recent history of superconductivity we have been told by a variety of proselytizers that, if we only had higher temperature superconductors, all our problems in the application of superconductivity would go away. Little [1], who has been known to proselytize a bit himself, has suggested at this conference that, even with today's high-T_c (i.e. high transition temperature) superconductors, if we only had integrated-circuit-technology-fabricated micro-refrigerators we might have SQUID's on refrigerated silicon chips contained inside an old-fashioned vacuum tube - a fascinating proposition, even if it is a bit of a mixed metaphor. In this paper I would like to review what the actual facts are about the use of high-T_c materials in superconducting electronic devices. Specifically: what the problems are, what has been accomplished, what seems likely, and what it may be good for. The present status is not all we might like, but some progress has been achieved recently. This is particularly significant considering that only three years ago there had been essentially no successful use of high-T_c materials in superconducting electronic devices. Happily this has now changed and there is a beginning.

1. WHY HIGH-T_c SUPERCONDUCTORS?

Let us begin by noting the potential advantages one might expect to gain from the use of high-T_c superconducting materials in superconducting devices. There are three basic advantages: (1) Successful use of high-T_c materials would greatly simplify the use of small, closed-cycle cryogenic refrigerators in cooling superconducting devices and circuits. (2) Even if operated at low temperatures, devices fabricated from high-T_c materials should in principle have better device characteristics because of the inherently superior superconducting properties of these materials. (3) Circuits fabricated from the presently known high-T_c materials would be chemically and physically robust, and therefore presumably more immune to damage, particularly due to thermal cycling.

The first advantage is probably the most obvious and exciting, but it must be borne in mind that high operating temperatures will bring some disadvantages as well, for example increased thermal noise. To illustrate the second advantage we recall that the superconducting energy gap Δ increases as T_c goes up $[\Delta(T = 0) = 1.76\ k_BT_c$ according to the BCS theory] and that the energy gap determines many of the superconducting properties and figures of merit important in real devices. For example, Josephson junctions and SQUID's fabricated from high-T_c materials should in principle have higher I_cR-products (in ideal Josephson junctions $I_cR \sim \Delta$) which are important in high-frequency applications of Josephson junctions and in SQUIDS's. Here I_c is the critical current of the junction and R the junction resistance. They also will have higher gap frequencies $\omega_g = 2\Delta/\hbar$ and therefore maintain their superconducting properties to higher frequencies. Finally the ideal RF surface resistance of a superconductor also depends on its energy gap, $R_s \propto (\omega^2/T)\exp(-\Delta/kT)$, and at a given temperature, decreases exponentially as the gap increases. The third advantage is not unique to high-T_c superconductors, as several of the low-T_c superconductors are physically and chemically hard, but is a desirable characteristic nonetheless.

2. AVAILABLE HIGH-T_c MATERIALS AND SOME OF THEIR PROPERTIES

Ultimately of course the properties of any high-T_c superconducting devices or circuits will be limited by the available materials and the ease with which they can be successfully fabricated into useful forms. In Table 1 we give a representative list of the superconducting materials generally considered of device interest. We arbitrarily place the dividing line between low and high T_c at $\sim$ 10K.

Table 1

Potential Materials for Superconducting Devices

	Material	T_c (K)	$\Delta(0)^*$ (meV)	$\xi(0)$ (Å)	Mechanical Properties		Thin Film Deposition Technique
Low-T_c	In	3.4	0.51	$\lesssim$ 3600	Soft		Therm. Evap.
	Sn	3.7	0.56	$\lesssim$ 2300	Soft		Therm. Evap.
	Ta	4.5	0.68	450	Hard		e-beam
	Pb/Pb alloys	7.2	1.35	$\lesssim$ 800	Soft		Therm. Evap.
	Nb	9.3	1.5	$\lesssim$ 400	Hard		sput; e-beam
	Nb-Ti	7-10	(1.5)	$\sim$ 30-50	Hard		e-beam
High-T_c	Mo-Re	15	(2.3)	$\sim$ 50	Hard	Heated Substrate T_s > 500 C	sput.
	NbN	16	(2.4)	$\sim$ 40	Hard		reactive sput. reactive e-beam
	V_3Si	16.9	2.5	$\sim$ 30	Hard		e-beam
	Nb_3Sn	18.3	3.3	$\sim$ 30	Hard		e-beam; sput.
	Nb_3Ge	23.3	3.9	$\sim$ 30	Hard		sput; e-beam

*Values given in parentheses are calculated from BCS theory. Other values have been experimentally measured.

There are several very important facts that are immediately apparent from this table. First, the high-T_c materials have larger energy gaps as expected. Second, in contrast to the low-T_c materials, the high-T_c materials are chemically and metallurgically more complicated, typically being interstial or intermetallic compounds as opposed to simple elements or alloys. As a result they are more difficult to fabricate, particularly in a useful form such as a thin film, requiring not only some sort of precise composition control but also a heated substrate. Fortunately, high quality films of these materials have recently become available thanks to efforts on the part of the superconducting materials community. Indeed, the recent successes in high-T_c devices probably would not have been possible without these improved materials. It is evident that continuing progress will require considerable attention to materials problems. Finally, also listed in Table 1 is the so-called Ginzburg-Landau (GL) zero-temperature coherence length $\xi(0)$ which is related to the temperature-dependent GL coherence length $\xi(T)$ by $\xi(T) = \xi(0)(T_c/(T_c-T))^{1/2}$. As we shall see below $\xi(T)$ is an important characteristic length in the operation of weak-link-type Josephson junctions.

3. WHAT KINDS OF DEVICES DO WE WANT?

Given high-T_c materials what do we want in the way of devices made from them? Obviously we want Josephson junctions, SQUID's, and high-Q RF cavities and resonators. These devices provide the unique properties that make superconducting electronics interesting and useful. They are not sufficient for a practical superconducting electronic technology, however. In complete superconducting electronic systems we need many other superconducting components such as transmission lines, impedance matching circuits, magnetic and electric ground planes, dc flux transformers, magnetic shields, gradiometer balancing elements, connectors, etc. We are still a long way from such a complete complement of components, but there has been progress recently in the primary components - Josephson junctions, SQUIDS's and RF cavities - and it is these results that we shall focus on in the remainder of this paper.

Josephson Junctions and SQUID's: There are several types of superconducting structures which yield Josephson junction behavior, but not all of them are equally well suited for high-T_c materials. The three principal types of junctions which are of practical interest are shown schematically in Fig. 1. Tunneling Josephson junctions (Fig. 1a) are probably the most familiar. They require two superconducting layers separated by a thin ($t \approx 10$ Å) oxide barrier though which the superconducting electrons tunnel to give the Josephson effect. In some cases artificial tunneling barriers (e.g. a semiconductor with $t \approx 50 - 100$ Å) can be used. Tunnel junctions incorporating the high-T_c A-15 compounds (i.e. the A_3B-type compounds in Table 1) and exhibiting the Josephson effect have been successfully produced recently by Moore, Rowell and Beasley [2] and Moore, Zubeck, and Beasley. [3] A crucial factor in the success of these authors has been the excellent thin films of these materials produced using the dual electron beam codeposition method developed by Hammond. [4] Two examples of these junctions are shown in Fig. 2. The I-V characteristics are nearly ideal. While not high-T_c junctions because of the Pb(T_c = 7.2K) counter electrodes, these junctions are still of potential practical interest because of the large energy gaps of the materials. They appear suitable and probably superior in applications where Pb/Nb tunnel junctions are used or may be desirable. A firm conclusion in this regard must await thorough exploration of their Josephson properties, however.

One intriguing aspect of these A-15 tunnel junctions is that artifical Si barriers appear to work quite well. In fact, in the case of V_3Si good tunneling was obtained only when a Si barrier was used, the natural oxide yielding rather poor junctions. [3] This is illustrated in Fig. 3. Because comparatively thick barriers of Si can be used, the possibility exists that A-15 tunnel junctions with hard superconducting counter electrodes (e.g. Nb or NbTi alloys) or even another high-T_c superconductor can be made.

Josephson behavior in devices operating at temperatures above 10K has apparently been obtained by several groups using proximity effect (Fig. 1c) weak-link-type Josephson junctions. High-T_c microbridge Josephson junctions (Fig. 1b) are probably impossible to construct because of the very small bridge dimensions required. In this type of junction ideal Josephson behavior (i.e. a sinusoidal current phase relation) is obtained only for bridge lengths $L \lesssim \xi(T)$. [5] Such short lengths are impossible to obtain with presently available thin film lithography. Bridges with lengths as small as 0.2 to 0.5 µm can be made, but even with such short lengths, microbridge Josephson junctions of the high-T_c materials would have to be operated within a few mK of T_c. This is clearly impractical. Microbridge Josephson junctions can be successfully made using the low-T_c superconductors (e.g. In, Sn and even Pb), however, because of their relatively large coherence lengths.

In proximity effect bridges [6] this size requirement can be circumvented by making the bridge itself out of a nonsuperconducting material, for example another superconductor with a lower transition temperature $T_c' < T_c$ (SS'S bridge), or a normal metal (SNS bridge), or a degenerate semiconductor (SSemiS bridge). According to the available theory [7] Josephson behavior exists for $T_c' < T < T_c$ in the SS'S case and for $0 < T < T_c$ in the SNS and SSemiS cases. However, even in these proximity bridges, in order to obtain good device characteristics it is desirable to make the devices small as well. Current thinking suggests that SNS bridges with $L \leq 0.5$ µm and SSemiS bridges with $L \leq 0.2$ µm should have good device characteristics, the actual lengths being determined in each case by the proximity decay length of the actual bridge material. These dimensions are small but not prohibitively so as in the high-T_c microbridge case. In practice proximity bridges of the SS'S type must be operated at temperatures just above T_c'. Note also that in these proximity-type weak links a short GL coherence in the banks (i.e. the S-regions) may be an advantage since it helps localize the weakened region totally within the bridge.

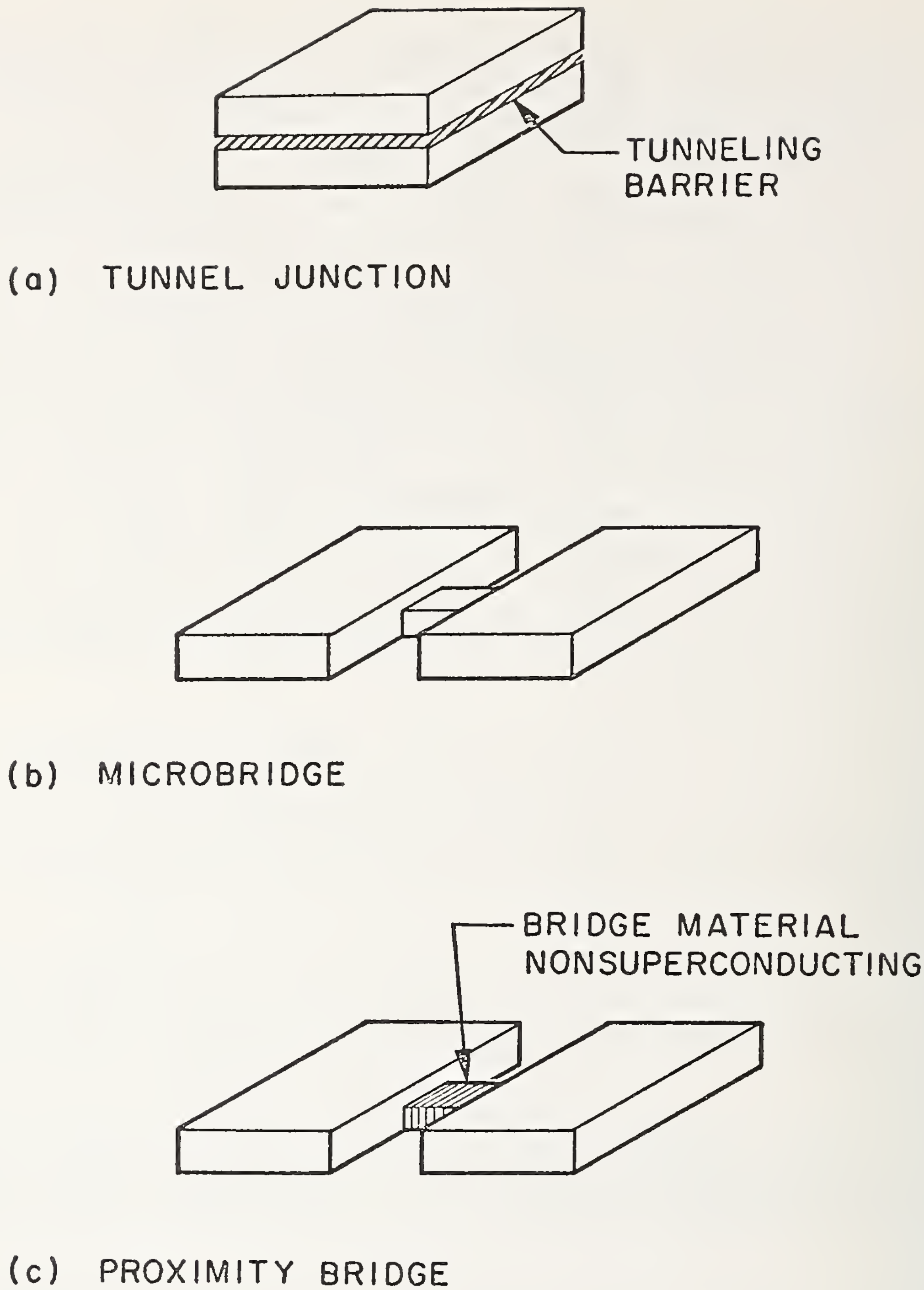

FIG. 1--Various types of Josephson junctions of potential practical device interest.

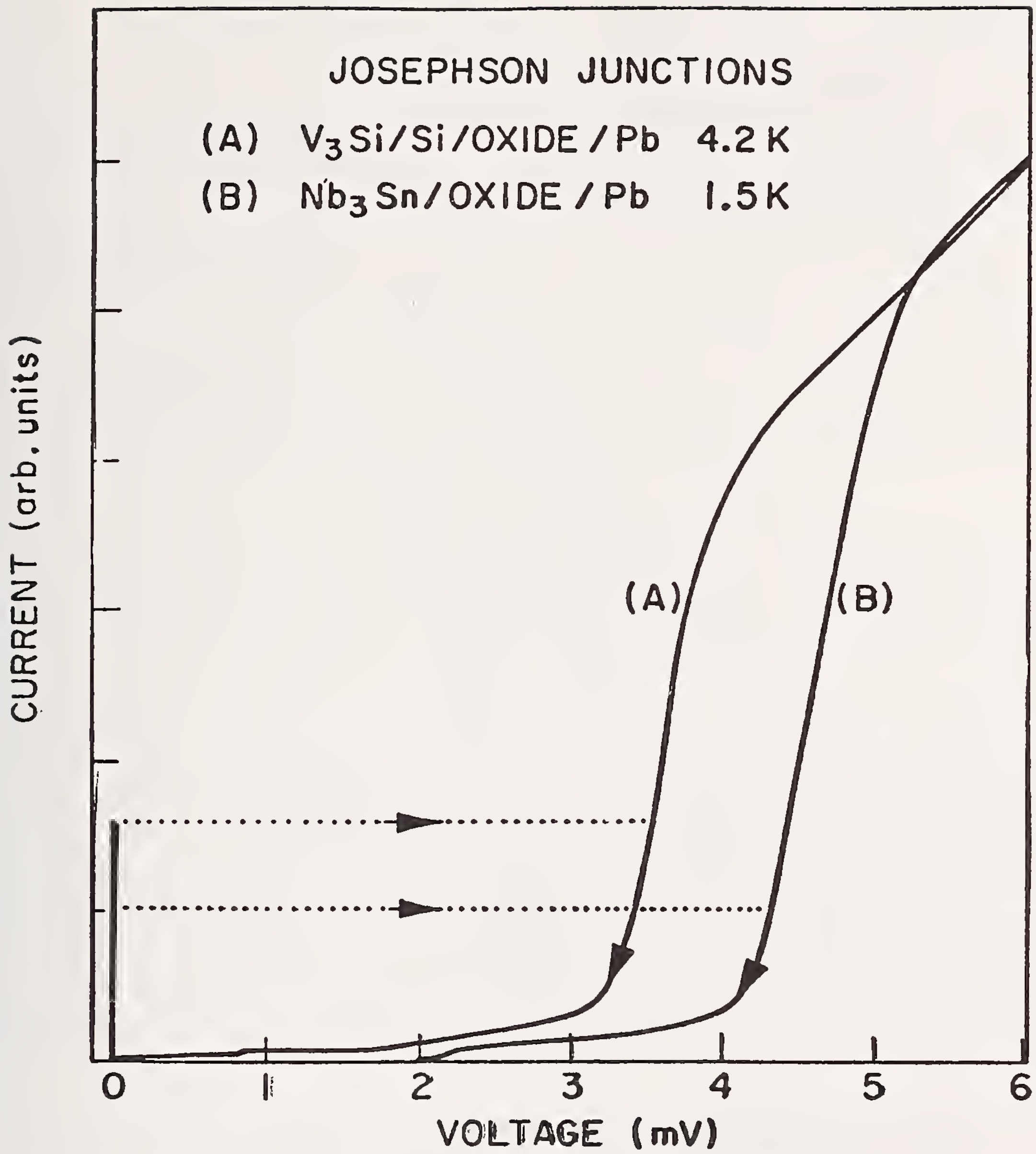

FIG. 2--Josephson tunnel junctions on Nb_3Sn and V_3Si. The counter-electrode for these junctions is Pb.

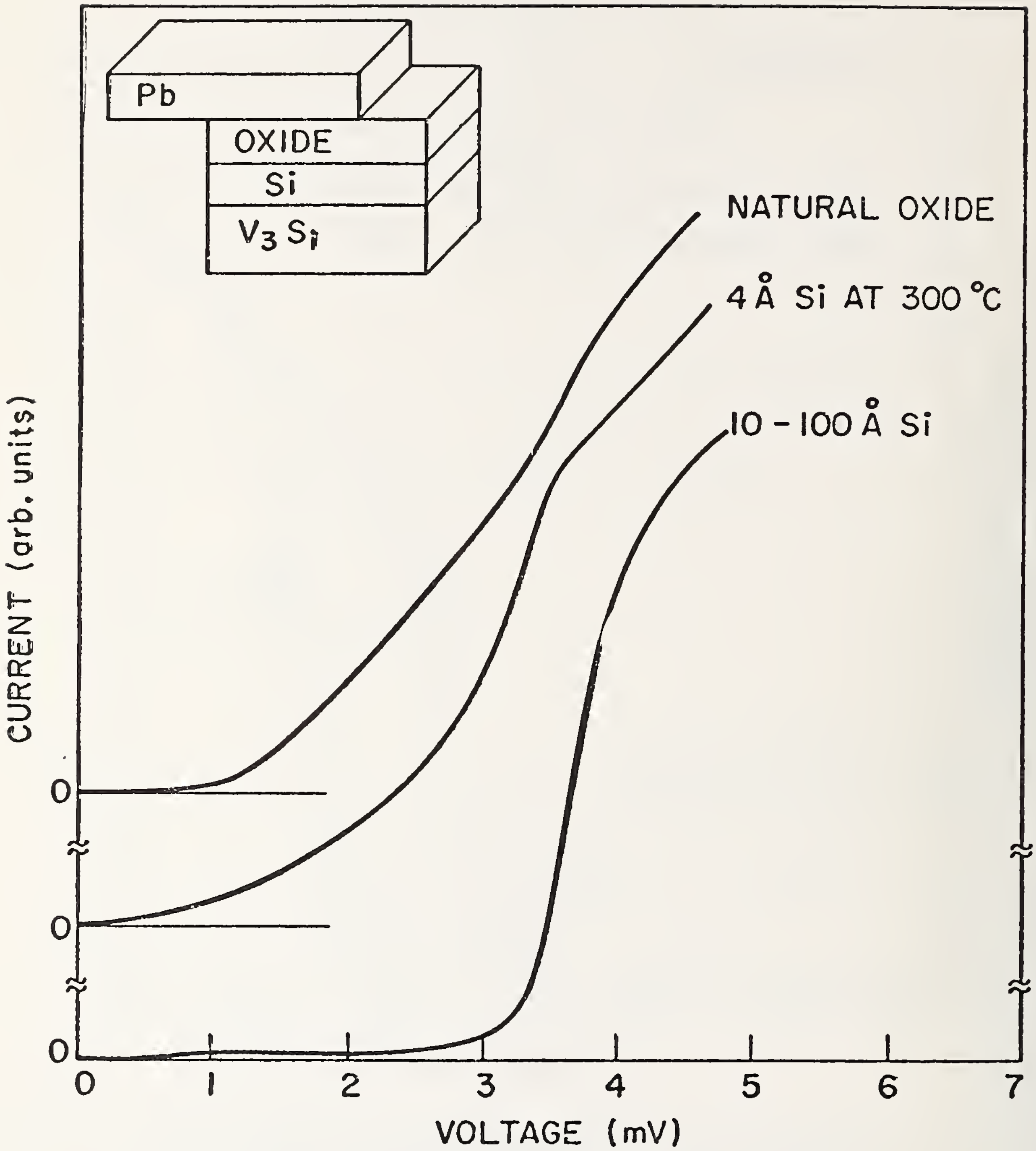

FIG. 3--A series of V_3Si tunnel junctions showing the effectiveness of the artificial Si barrier. Good tunneling is only obtained with the Si barrier.

The first reported case of anything like Josephson behavior in a high T_c superconducting bridge structure was the work of Janocko et al. [8] who observed weak ac Josephson steps in 3 μm Mo-Re microbridges at ∿ 12 K. However, it appears that these steps reflect synchronized flux flow and not classical Josephson behavior. Fujita, Kosaka, Ohtsuka and Onodera [9] have made weak link Josephson junctions in NbN films expitaxially grown on MgO substrates by reactive sputtering. While it is not entirely clear, these bridges appear to be of the SS'S proximity type where the T_c of the bridge region was lowered (due to thinning or radiation damage) during the sputter-etching process used to form the bridge. These bridges have been successfully used in RF SQUIDS's operating up to ∿ 15 K and with a field sensitivity of 7×10^{-9} G. Palmer, Notarys and Mercereau [10] have made SS'S proximity bridges out of polycrystalline NbN and dual electron beam codeposited Nb_3Sn in which the T_c of the bridge region was lowered by reducing its thickness. (Although, because sputter-etching was used, radiation damage may also have been involved.) Using these Nb_3Sn bridges Palmer, et al., also fabricated dc SQUID's that operated at ∿ 17 K. Their SQUID's had very small sensing areas, however, (typically 20 μm × 50 μm,) and the field periodicities were only ∿ 20 mOe. Falco [11] has also successfully fabricated a Nb_3Sn SQUID. He used sputtered Nb_3Sn and reduced the T_c of the bridge by means of radiation damage. He reports RF SQUID operation at $T \simeq 14.5$ K. His device has a field periodicity of 5×10^{-6} Oe, but no noise performance figures have been given. Finally we note that weak RF induced Josephson steps have been observed in Nb_3Ge bridges [12,13]. However, these bridges are as yet poorly characterized and the observed steps are most likely due to synchronized vortex flow.

From the above it is clear that both high-T_c weak link Josephson junctions and SQUID's capable of operating up to 15-17 K can be made. The quality of these devices is unclear, however, as no careful investigation of device performance or physics has been reported. In short, the empirical evidence is encouraging but it is still premature to conclude that high-T_c superconducting devices with good operating characteristics are now a reality.

RF Cavities: As with the Josephson junction devices, progress has been made recently in fabricating high-T_c RF cavities. In particular the Siemans group in Germany has successfully made Nb_3Sn cavities by first forming a Nb cavity and then reacting it in a saturated Sn vapor at ∿ 1000°C. This procedure results in a Nb_3Sn coating on an otherwise Nb cavity. These workers have reviewed their results recently [14] and we summarize their main conclusions here. These are given in Table II where we compare the calculated and experimentally measured behavior. The calculated behavior is that expected from the BCS theory and is obtained by fitting the measured data to a surface resistance of the form $R_S = R_{BCS} + R_{res}$, where R_{BCS} is the BCS surface resistance and R_{res} is a non-intrinsic residual resistance. The data are for X-band cavities and at the temperatures indicated. Also, to put these results in physical perspective we show in parentheses the actually measured Q's of the cavities. The critical fields shown will be discussed below.

Table 2

Properties of High-T_c Nb_3Sn RF Cavities

	Calculated			
	$R_s(1.5K)$ (Ω)	$R_s(4.2K)$ (Ω)	$H_{c1}(0)$ (mT)	$H_c(0)$ (mT)
Nb	2.5×10^{-8}	2.0×10^{-5}	170	190
Nb_3Sn	1.5×10^{-12}	2.5×10^{-7}	50	540
	Experiment			
	$R_s(1.5K)$ (Ω)	$R_s(4.2K)$ (Ω)	(RF) $H_{cR}(1.5K)$ (mT)	(RF) $H_{cR}(4.2K)$ (mT)
Nb	2.6×10^{-8} ($Q = 3 \times 10^{10}$)	2.1×10^{-5} ($Q=3.9 \times 10^{7}$)	159	--
Nb_3Sn	3.5×10^{-7} ($Q = 2.2 \times 10^{9}$)	5.6×10^{-7} ($Q=1.4 \times 10^{9}$)	100	> 84

The figures quoted in Table 2 have a number of interesting features. First of all, as expected, at a given temperature the calculated R_s is much lower for Nb_3Sn than Nb, reflecting the larger energy gap in Nb_3Sn. Note, however, that the $R_s(1.5^\circ K)$ actually acheived in Nb_3Sn is far higher than the intrinsic calculated value, indicating that residual losses dominate at this temperature. Because of this residual loss the ultimate Q's of the Nb_3Sn cavities do not yet exceed those of Nb. However, at 4.2K Nb_3Sn is only a factor of 20 poorer than Nb at 1.5K and nearly two orders of magnitude better than Nb at 4.2K. This advantage increases as the temperature increases. Thus, already with these very early cavities we see that unless the ultimate Q's are required there is advantage in using Nb_3Sn since higher temperature operation is possible.

In the case of high-power cavities an additional superconducting property is of interest, namely the maximum surface RF field the cavity can successfully sustain. For type-II superconducting materials such as Nb and Nb_3Sn it was generally believed that this RF critical field $H_{cr}^{(RF)}$ would be H_{c1}, the field at which in equilibrium vortices enter the superconductor and produce loss. Indeed this was an important factor in the choice of Nb for the early high-power cavity work since Nb has the largest H_{c1} of any known superconductor. As seen in the table it is at least a factor of three better than Nb_3Sn. However, as also seen in the table, for Nb_3Sn the observed $H_{RF}^{(cr)} \simeq 100$ mT $> H_{c1}$. A similar delay in the flux entry into Nb_3Sn to applied fields in excess of H_{c1} is evident in recent experiments on superconducting power transmission lines. [15] It is now believed that a surface barrier to flux entry (i.e. a kind of magnetic superheating) is operative in these materials which makes them practical in both high-power cavities and AC power lines. In theory this surface barrier can be on the order of H_c, the bulk thermodynamic critical field of the superconductor. [16] As seen in the table $H_c \approx 540$ mT for Nb_3Sn. Using the same Nb_3Sn tunnel junctions described above, Moore and Beasley [17] have found that experimentally flux entry into Nb_3Sn can be delayed to fields at least as high as 170 mT. Superheating effects have also been observed in low-T_c superconductors. [18] The practical implications of these results could be dramatic in the ultimate performance possible in high-power superconducting RF cavities.

In summary, the last few years have seen a spurt of success in the application of the high-T_c superconductors in superconducting devices. While the full implications are not yet clear, the results are certainly encouraging. Since the results are so new, we expect further rapid progress. Indeed we are even optomistic that these early results will ultimately lead to high-quality, practical superconducting systems with superior performance and/or capable of high temperature operation.

*Work supported by the Joint Services Electronics Program at Stanford University and by the Office of Naval Research.

REFERENCES

1. W. A. Little, Cryocooler Conference, Boulder, Colorado, (1977).

2. D. F. Moore, J. M. Rowell, and M. R. Beasley, Solid State Commun. 20, 305 (1976).

3. D. F. Moore, R. B. Zubeck, and M. R. Beasley, Bull. Am. Phys. Soc. 22, 289 (1977).

4. R. H. Hammond, IEEE Trans. Mag-11, 201 (1975).

5. See for example, K. K. Likharev and L. A. Yakobson, Sov. Phys.-Tech. Phys. 20, 950 (1976) and references therein.

6. H. A. Notarys and J. E. Mercereau, J. Appl. Phys. 44, 1821 (1973).

7. See for example K. K. Lakharev, Sov. Tech. Phys. Letters 2, 12 (1976).

8. M. A. Janocko, J. R. Gavaler, and C. K. Jones, Proceedings of the 1972 Applied Superconductivity Conference, Annapolis, Maryland, IEEE Pub. No. 72CM0682-5-TABSC.

9. T. Fujita, S. Kosaka, T. Ohtsuka, and V. Onodera, IEEE Trans. Mag-11, 739 (1975).

10. D. W. Palmer, H. A. Notarys, and J. E. Mercereau, Appl. Phys. Letters 25, 527 (1974).

11. C. T. Wu and C. M. Falco, Appl. Phys. Letters 30, 609 (1977).

12. M. A. Janocko, J. R. Gavaler, and C. K. Jones, IEEE Trans. Mag-11, 880 (1975).

13. R. B. Laibowitz, C. C. Tsuei, J. C. Cuomo, J. F. Ziegler, and M. Hatzakis, IEEE Trans. Mag-11, 883 (1975).

14. B. Hillenbrand, H. Martens, H. Pfister, K. Schnitzke, and Y. Uzel, IEEE Trans. Mag-13, 491 (1977).

15. J. F. Bussiere, IEEE Trans. Mag-13, 131 (1977).

16. L. Kramer, Z Phys. 259, 333 (1973).

17. D. F. Moore and M. R. Beasley, Appl. Phys. Letters 30, 494 (1977).

18. T. Yogi, G. J. Dick, and J. E. Mercereau, Phys. Rev. Letters 39, 826 (1977).

Application of SQUID Detectors in Biomagnetism

Samuel J. Williamson and Lloyd Kaufman
Departments of Physics and Psychology
New York University, New York, New York 10003

Magnetic fields produced by biological activity in the human body have been studied in a number of laboratories during the past decade using both conventional and superconducting detectors. This paper summarizes the essential features of the techniques and some of the more important results. Sufficient detail is included so that the advantages of refrigerating superconducting detectors by cryocoolers instead of a liquid helium bath can be assessed.

Key Words: biomagnetism; cardiomagnetism; evoked fields; flux transporter; gradiometer; magnetocardiogram; magnetoencephalogram; magnetomyogram; magneto-oculogram; medical applications; neuromagnetism; pneumomagnetism; studies in perceptual psychology, superconducting quantum interference device.

1. Introduction

The past seven years have brought a steady growth of interest in the application of sensitive magnetic field detectors (called superconducting quantum interference devices or SQUID's) to an area of research known as "biomagnetism." This is the study of magnetic fields which are associated with biological activity. More than half a dozen organs in the human body are now known to produce magnetic fields, and the list continues to grow. One impediment to the widespread use of SQUID's is the need to deal with liquid helium which at present is used to cool them to a sufficiently low temperature that they become superconducting. Once the system is cooled by immersion in a bath of liquid helium the experimenter need have no cryogenic experience in order to carry out most of the experiments in biomagnetism now being conducted. An occasional improvement in the vacuum of the dewar containing the bath through use of a pumping station may be all that is required. But cryogenic experience is essential for safe and economical operation in the initial cooling of the dewar, transfer of liquid helium and response to any subsequent malfunction. And this demands the presence of either a low temperature physicist or technician trained in a cryogenics laboratory.

There is every indication that self-contained mechanical or circulating fluid cryogenic cooling devices would stimulate further interest in biomagnetic research. The reasons for this and the advantages of such cryocoolers will become apparent in this brief review. Our purpose is to summarize the techniques involved in biomagnetic research to make apparent the special problems for cryocooler applications. In addition we shall describe a few of the more significant areas of study to show how they are developing, with a view toward revealing future lines of growth. More complete discussions of the various areas of biomagnetism can be found in the review article by Williamson, Kaufman and Brenner [1].

2. Noise Considerations

The phenomena of biomagnetism derive from the movement of electrical charge which accompanies activity in muscle, nerve or other tissue. A magnetic field in the surrounding region is established by this electrical current, as follows from the law of Biot and Savart. Biomagnetic fields produced by the various organs of the body range in strength over four orders of magnitude, with 10 picotesla representing the approximate midpoint on a logarithmic scale, as depicted in Figure 1.

The principal difficulty in obtaining clean biomagnetic records is the extreme weakness of these fields in comparison with the fluctuations of background magnetic fields in the experimental area. The earth's steady field of about 50 μT is generally not a problem, because only time-dependent effects are often sought. Rather, concern centers on the ac fields from local sources in a laboratory such as elevators, ventilation fans and mechanical pumps which contribute background fluctuations of 0.1 - 1 μT. The geomagnetic fluctuations of the earth's field may also be a problem, because they amount to about 1 pT $Hz^{-\frac{1}{2}}$ at 10 Hz and have a frequency dependence which is approximately f^{-1} in the domain of

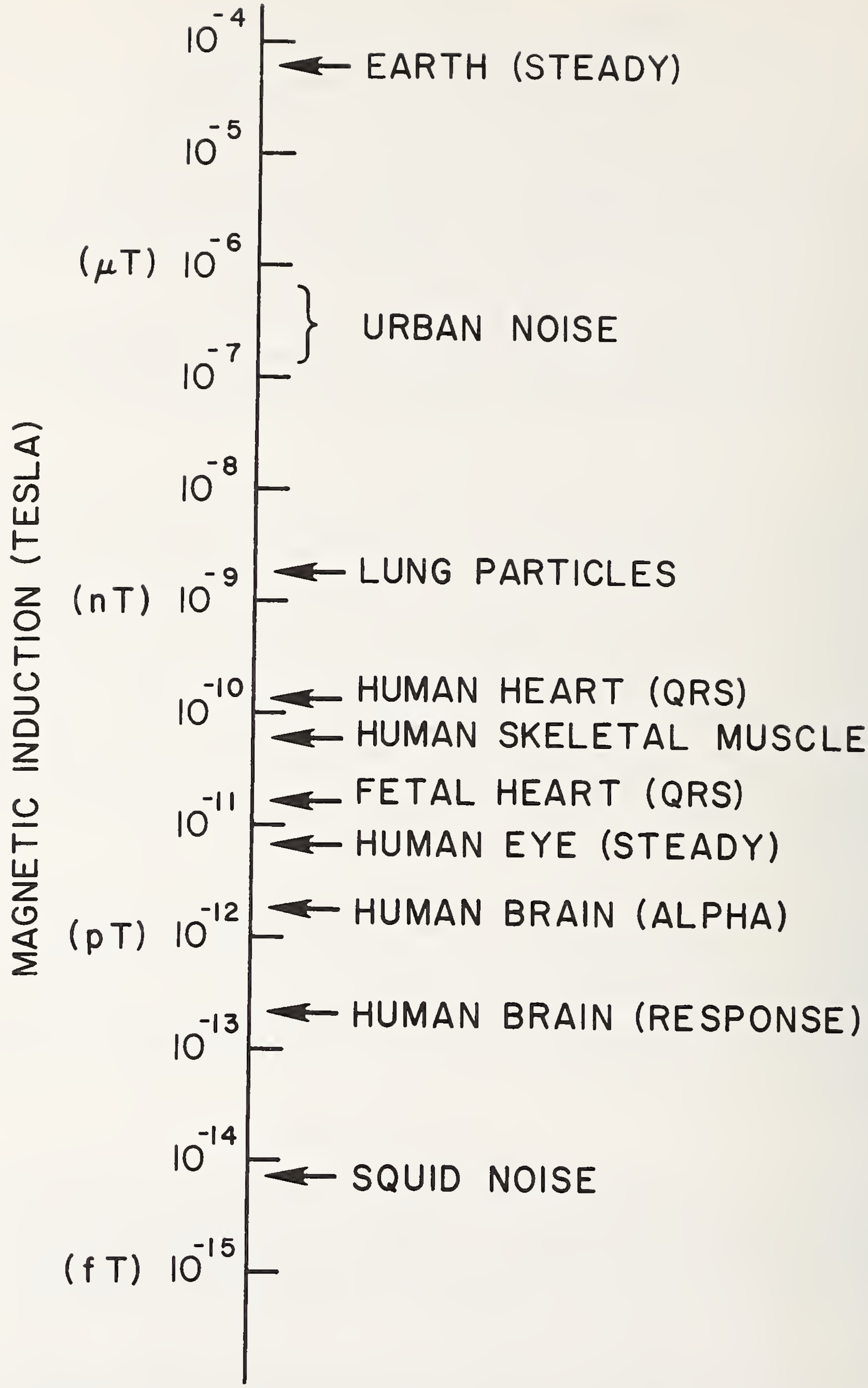

Figure 1. Typical biomagnetic field strengths compared with background (urban) noise and the intrinsic noise level within a 1 Hz bandwidth for present SQUID magnetic field detectors.

interest [2]. The steel structure of a building distorts the pattern of fields from laboratory and geomagnetic sources, so that it is not uncommon to find low frequency variations in field having an amplitude at 1 Hz as large as $\sim 1\ \mu T$ and variations in field gradient of $\sim 10\ \mu T/m$. In practice the greatest problem with background fields is found at low frequencies, say below 10 Hz, as the spectrum of this unwanted activity displays an amplitude that increases rapidly with decreasing frequency. Power lines also contribute to the background noise, but this can usually be eliminated by standard cancellation or filtering techniques. The intrinsic noise level of the SQUID sensor is negligible except in the most demanding applications.

2.1. Shielded Enclosures

The traditional method for reducing dc and ac background fields is to enclose the SQUID and subject in a chamber of high permeability material. Considerable care must be devoted to minimize mechanical vibrations in the shielding, or the moving walls will introduce unwanted field variations. The best performance to date has been achieved by D. Cohen at the Francis Bitter National Magnet Laboratory at the Massachusetts Institute of Technology [3]. When supplemented with ambient field-sensing magnetometers and feedback circuits which set up fields to oppose those of the earth, the dc field in the interior can be made as low as 5 nT, with typical gradients of 1 nT/m. The ac variations inside are less than the 8 fT $Hz^{-\frac{1}{2}}$ noise of the SQUID field sensor in the bandwidth 1 Hz - 5 kHz.

A simpler yet effective ac shield has been built by J.E. Zimmerman at the National Bureau of Standards in Boulder, Colorado [4]. His is an electrically conducting enclosure built from ~ 4 cm thick aluminum plate. The interior is shielded by eddy currents induced in the walls by changing external fields. The noise level for frequencies as low as 0.5 Hz is less than the 30 fT $Hz^{-\frac{1}{2}}$ limit set by the noise of the SQUID system used in the measurements.

2.2. Spatial Discrimination

Shielded rooms provide an important advantage when dealing with weak, low-frequency effects where background fields in a laboratory also tend to fluctuate strongly. However the relatively small space provided inside may be too confining for many types of experiments, and the cost of an elaborately shielded enclosure is high. One technique which is gaining in popularity eliminates the need for magnetic shielding for studies of a broad class of biomagnetic phenomena. This is called "spatial discrimination", whereby the detection system is designed to be insensitive to uniform fields and perhaps field gradients but retains sensitivity to higher spatial derivatives of the field. This proves advantageous, because background fields are produced by sources that are relatively distant from the detector and therefore are more uniform in space than the biomagnetic field produced by a source close by. Spatial discrimination favors the biomagnetic signal over the unwanted background. This advantage has been appreciated for more than a decade and was exploited when copper induction coils were first used in measurements of the heart's magnetic field [5].

The SQUID itself can be designed with appropriate geometry to provide discrimination [6]. But greater versatility is available if instead a superconducting flux transporter is chosen to couple the magnetic signal into a SQUID. Then the flux transporter can be designed with the appropriate geometrical configuration [7]. The flux transporter is a closed loop of superconducting wire with a primary coil (or "detection coil") connected in series with a secondary coil (or "input coil") which is inductively coupled to the SQUID as illustrated in Figure 2. Owing to magnetic flux conservation in the loop, when a field is applied in the region of the detection coil a current I_t flows around the transporter with appropriate direction and magnitude so as to counter this change and maintain the total magnetic flux within the loop invarient. As I_t flows through the input coil it imposes a magnetic field on the SQUID as a result of the mutual inductance M_i; and the response of the SQUID is sensed by the electronic systems which monitor its state. Thus the electronic output signal is proportional to the input coil current I_t, which in turn is proportional to the original net flux applied to the detection coil.

Figure 3 shows several possible configurations for the detection coil. They include the magnetometer (A) which provides no spatial discrimination, the gradiometers (B and C)

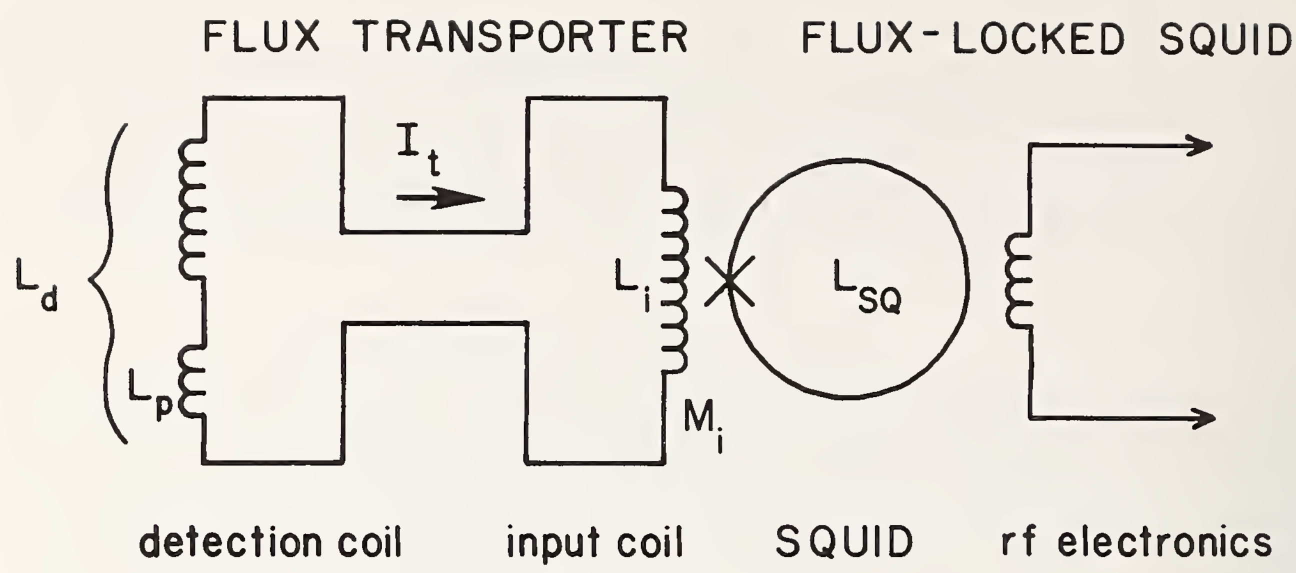

Figure 2. Elements of a flux transporter which couples field energy from a detection coil to a SQUID.

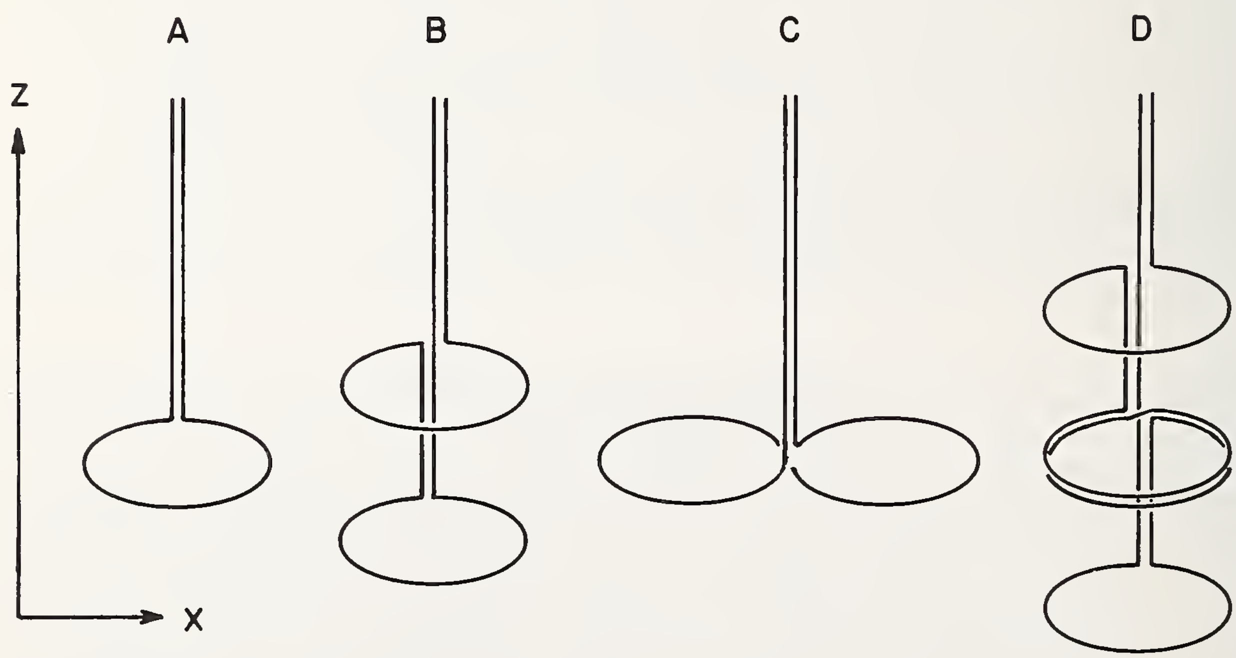

Figure 3. Possible configurations for a detection coil include: (A) magnetometer; (B) gradiometer; (C) off-diagonal gradiometer; (D) second derivative gradiometer. The plane of each loop is perpendicular to the Z-axis.

which are insensitive to uniform field, and the second derivative gradiometer (D) which is insensitive to uniform field and uniform field gradient [8]. The names of these derive from the lowest order spatial variation in field that produces a non-zero net flux. Their sensitivity to a biomagnetic field is not reduced if the baseline, or distance between coils, is sufficiently long that the field is appreciable only in the region of the lowest coil, called the "pickup coil". In this case the detection coil functions as a differential magnetometer for the biomagnetic field, with the signal from the pickup coil reduced only by the amount of flux coupled to the other coils wound in opposition.

An example of an early gradiometer arrangement is shown in Figure 4. Here the SQUID is mounted for convenience in the center of the detection coil. Now more commonly the SQUID will be mounted some distance above the gradiometer so that the perturbations of its shield have negligible effect on the gradiometer balance. An alternative approach is to fabricate both SQUID and flux transporter using thin film technology [9].

a. Sensitivity

Although a gradiometer or second derivative gradiometer provides a major advantage in reducing background noise, it also exacts a penalty in overall reduced sensitivity if the intrinsic noise of the SQUID detector remains the dominant noise source. The reason is that the magnetic field energy coupled into the pickup coil is shared by all of the other coils in the flux transporter; and the more compensating coils that are included, the less energy is available for the input coil and SQUID. This can be seen by considering the response of the flux transporter when an externally applied field couples a flux ϕ_p into the pickup coil. Flux quantization requires that $I_t(L_d+L_i) = \phi_p$, where the symbols are defined in Figure 2. The flux coupled into the SQUID is $\phi_{SQ} = M_i I_t = k(L_{SQ}L_i)^{\frac{1}{2}} I_t$, where k is the mutual inductance coupling constant between input coil and SQUID. From these we can express what fraction of the pickup coil flux is transferred to the SQUID:

$$\phi_{SQ} = \frac{k(L_{SQ}L_i)^{\frac{1}{2}}}{L_d+L_i}\,\phi_p \ . \tag{1}$$

To assess how the transfer is affected by the geometry of the detection coil, we introduce a parameter η that indicates the factor by which the coil's inductance exceeds that of the pickup coil: $L_d=\eta L_p$. For a gradiometer $\eta=2$, and for a second derivative gradiometer $\eta=6$, neglecting the mutual inductance between different sets of turns. Also in this assessment we are primarily interested in the system's sensitivity to field B (not flux) averaged over the area A_p of the pickup coil, and so we write: $\phi_p=KL_p^{\frac{1}{2}}A_p^{\frac{3}{4}}B$, where K is a constant relating the number of turns of wire N_p of a coil to its inductance: $N_p=KL_p^{\frac{1}{2}}A_p^{-\frac{1}{4}}$. As logarithmic terms have been neglected in this expression, it is accurate to only 10-20%, but this is adequate for practical purposes. Then eq. 1 can be re-written as:

$$\phi_{SQ} = \frac{kK(L_{SQ}L_pL_i)^{\frac{1}{2}}A_p^{\frac{3}{4}}B}{\eta L_p+L_i} \ . \tag{2}$$

For a given value of L_i, this expression indicates that ϕ_{SQ} will be maximum if the gradiometer is designed with $\eta L_p = L_i$. With this condition satisfied we have:

$$\phi_{SQ} = \frac{kK}{2}\left(\frac{L_{SQ}}{\eta}\right)^{\frac{1}{2}} A_p^{\frac{3}{4}}B \ . \tag{3}$$

Therefore the flux coupled into the SQUID is proportional to $\eta^{-\frac{1}{2}}$, which in this sense can be viewed as a figure of merit for the detection coil. A gradiometer as depicted in Figure 2B therefore has only 0.7 of the sensitivity of the magnetometer of equal pickup

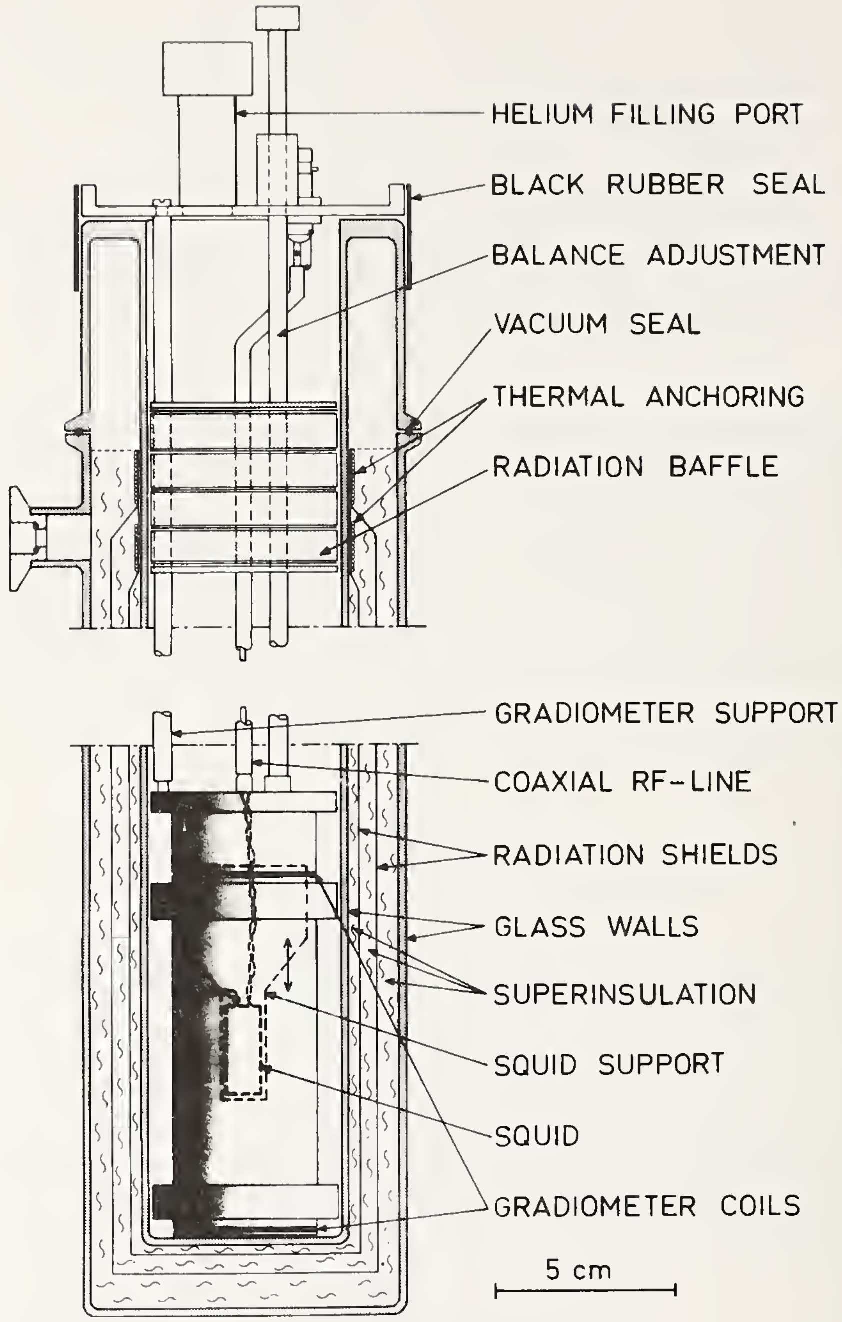

Figure 4. SQUID with a gradiometer detection coil mounted in a dewar containing liquid helium. The balance adjustment rod is used to position a superconducting object at the precise distance from one coil to render the gradiometer insensitive to uniform field. From Reference 28.

coil area; and a second derivative gradiometer, only 0.4. Eq. 3 shows that if spatial resolution is not an important consideration, greater sensitivity is always achieved by increasing the coil area A_p, provided of course that L_i can also be correspondingly increased to maintain optimization condition $L_i = \eta L_p$. The ultimate sensitivity of a flux transporter is modified somewhat by its slight loading of the SQUID [10].

At one time it was believed that a gradiometer type detection coil would always suffer from reduced sensitivity compared with a magnetometer having identical area for the pickup coil, when intrinsic SQUID noise is the limiting factor. This belief is no longer warranted. One technique that virtually eliminates this loss of sensitivity from flux division was suggested by J.E. Zimmerman [4]. The idea is to place the SQUID so that it directly senses the field of interest, and obtain the advantage of spatial discrimination of a second derivative gradiometer with two coils of low inductance mounted some distance above it and coupled to the SQUID as part of a flux transporter. The two coils and SQUID are designed to be balanced so that the combination is insensitive to uniform field and uniform field gradient.

A variation of this technique for minimizing loss in sensitivity is to arrange the detection coil of a conventional flux transporter so that it has an asymmetrical shape [4]. One possibility illustrated in Figure 5 has compensating coils which are larger than the pickup coil but with fewer turns of wire in order to maintain balance. Because the inductance of a closely wound coil is proportional to the square of the number of turns of wire, the pickup coil then comprises a much larger proportion of the total inductance L_d, and consequently η appearing in eq. 3 is made closer to unity. For example if a second derivative gradiometer has a 1 cm diameter pickup coil and 2.5 cm compensating coils, the pickup coil has n=6 times more turns than the coil at the other end, and we find $\eta^{-\frac{1}{2}} = 0.86$. This represents a factor of 2 improvement over the symmetrical configuration in Figure 2D having the same pickup coil area and is only 14% lower than the figure of merit for a magnetometer. Numerical calculations have been carried out by J.P. Wikswo, Jr., at Stanford, for the special case of ellipsoidal coils which are tilted with respect to the detection coil axis.

Unshielded second derivative gradiometers have succeeded in detecting the weakest of all biomagnetic fields--that produced by evoked neural activity in the brain [11]. Figure 6 shows such a system in operation at New York University. In this case the pickup coil is positioned in the bottom of the tail section of the dewar, placed immediately over the back of the subject's head to minotor the magnetic field produced by the visual cortex as it responds to a visual stimulus provided on an oscilloscope screen.

b. Noise Spectrum

Figure 7 illustrates the noise spectrum which can be obtained with an unshielded SQUID system in an urban environment. The upper spectrum represents a previous system operating at N.Y.U. [12] which exhibited a pronounced increase in background noise below 10 Hz. An improved SQUID with lower intrinsic noise is characterized by the lower curve. Both systems have about the same balance with respect to field (about 2 ppm), but the new system has an order of magnitude improvement in gradient balance, amounting to a few parts in a thousand. The rise in low frequency noise now appears below 6 Hz and increases less steeply with decrease in frequency. When operated outdoors away from buildings the noise does not appear until below 1 Hz. The structure at high frequencies comes from fields fluctuating at odd harmonics of the power line frequency. Buckout techniques could easily eliminate this, as has been done for 60 Hz and 180 Hz components. For many types of biomagnetic investigations listed in Figure 1 the noise level displayed in Figure 7 is more than sufficient.

A cryocooler used in place of the liquid helium bath may very well elevate the noise level. If the noise is periodic, this may not prove disadvantageous if a small computer is available to carry out adaptive filtering [13].

3. Cryogenic Aspects

When using a type of gradiometer detection coil, electrically conducting materials should be kept away to minimize perturbations from eddy currents caused by variations in background field. This also will minimize field fluctuations produced by Johnson noise

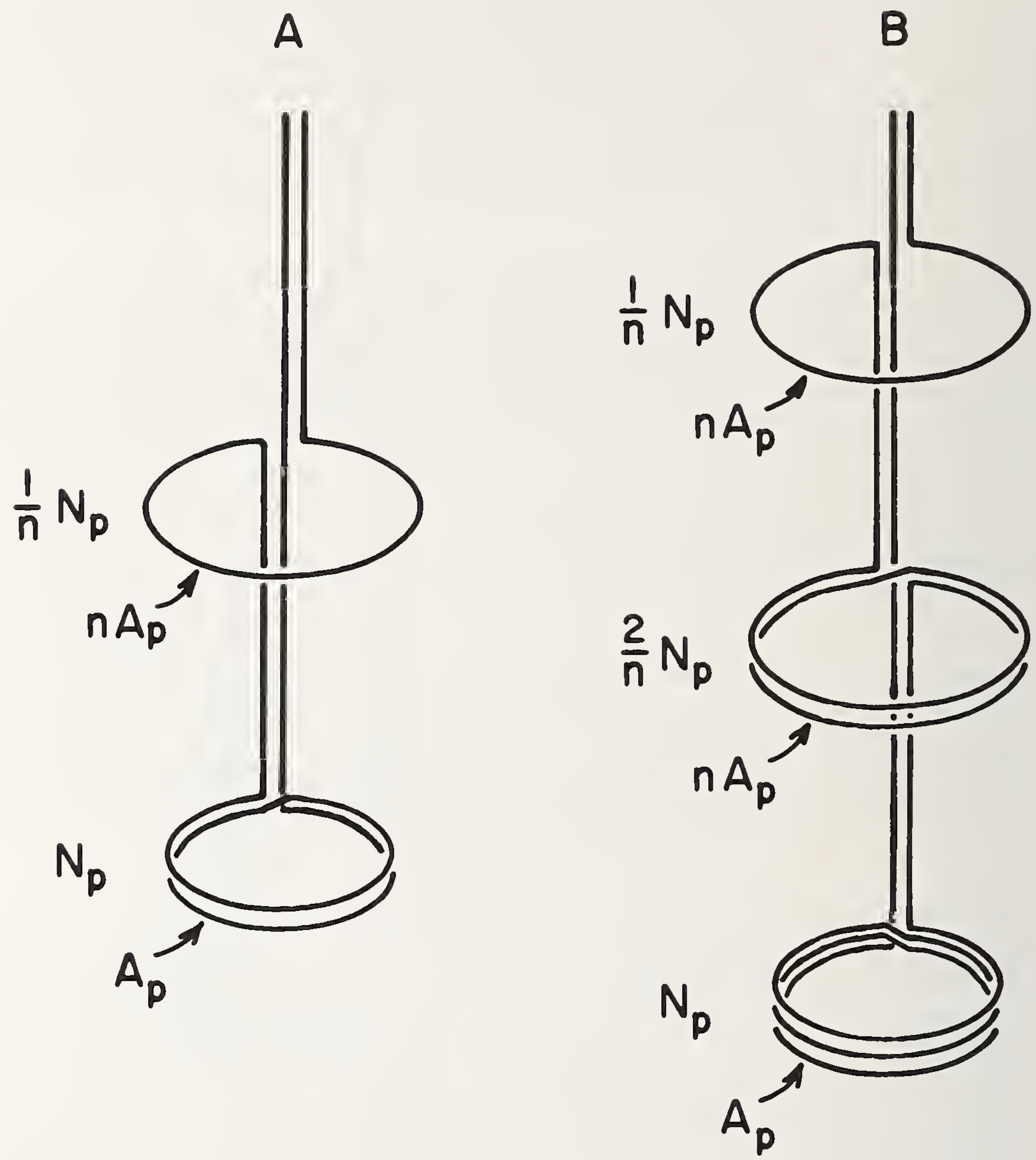

Figure 5. Asymmetrical gradiometer (A) and second derivative gradiometer (B), both of which have n times more turns in the pick-up coil than the uppermost compensating coil.

Figure 6. Arrangement at New York University for recording the magnetic field of the brain in an unshielded laboratory.

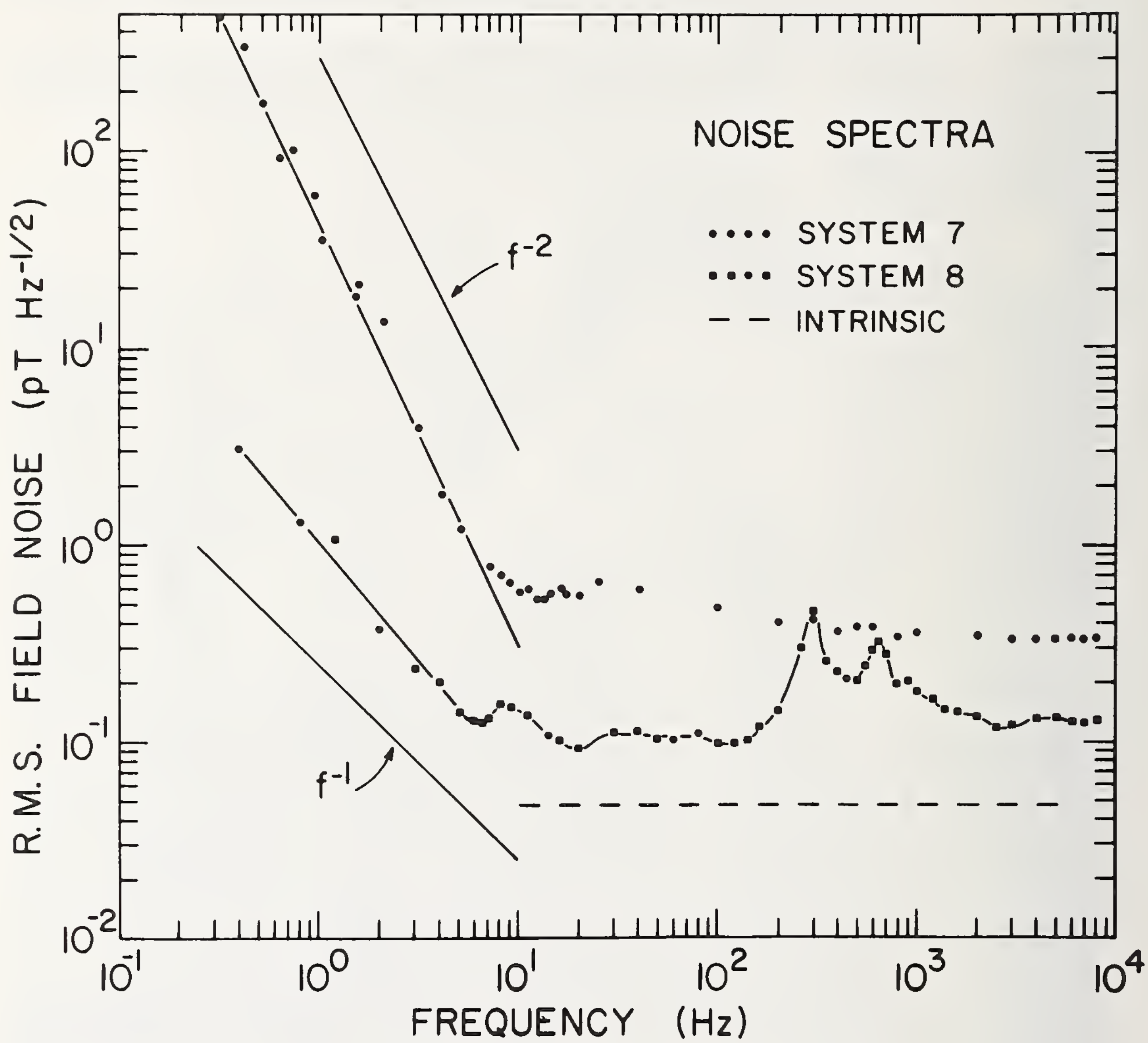

Figure 7. Noise spectra of two SQUID systems with second derivative gradiometers. The rms noise is expressed as the equivalent field noise at the pick-up coil. Below 6 Hz the noise may be a factor of 2 lower at night than the values shown.

currents which flow in all conductors. For this reason, dewars for cooling the SQUID and flux transporter are conventionally fabricated from glass, fiberglass or plastic. The SQUID is therefore exposed to the deleterious effects of rf pickup fed to it by the flux transporter, unless the dewar is protected by an rf shielded room. Alternatively, rf shielding may be introduced between the input coil and SQUID, but this tends to contribute Johnson noise and reduce the mutual inductance M_i. A simpler solution is to place a shield around the dewar itself, with a minimal amount of conducting material to avoid eddy currents being set up by fluctuations at low frequency.

As the system is usually kept cold for long periods it is economical to use a helium vapor cooled dewar and avoid the complications associated with a liquid nitrogen outer chamber. Especially with unshielded systems, where fine-balancing of the gradiometer involves several hours for adjusting the position of superconducting tabs near the coils, the desired mode of operation is to keep the system immersed in helium for several weeks or months at a time. Another peculiar cryogenic feature in studies of the weakest biomagnetic fields is the need to place the pickup coil as close as possible to the subject for maximum sensitivity. The insulating vacuum space between the helium container and outer shell of the dewar must be kept as thin as possible. Here is where the compromise between operational performance and heat input is most keenly felt.

Our experience at N.Y.U. has been with glass and fiberglass dewars having a narrow vacuum space at the bottom of the 2 cm ID tail section, so the pickup coil is placed only 7 mm from the outside. Liquid helium boils off at a rate which indicates a heat input of ~ 0.1 W. This increases by $\sim 30\%$ when the dewar is moved frequently during experiments. The cooling requirements in the low temperature region are therefore not severe. The boiloff rate could provide about 8 W of refrigeration from the cool vapor at higher temperature as it rises, assuming perfect heat exchange with the support structure, radiation shields and the neck of the dewar. This reasonably efficient system requires about 25 liters of liquid helium a week for continuous operation. The annual cost of helium would be approximately $4,000 at this rate.

The helium cost is sufficiently high in comparison with other expendables in research budgets that it is a consideration when planning a schedule of experiments. Nevertheless, more important factors encourage a search for an alternative refrigeration method. They include the nuisance of handling the delivery and transfer of helium, with attendant need for trained personnel; the desire to maintain a closed system that should exclude the accumulation of paramagnetic oxygen which could increase background magnetic noise; the possible advantage of more convenient operation "in the field" away from the laboratory; and--not the least in importance--the ability to orient the detection coil in any desired direction for scans around the human body. The present need to maintain the dewar axis within approximately 45° of the vertical is a significant restriction when carrying out studies of the brain and certain other organs.

With a view toward cryocooler schemes, there is a peculiar aspect of the conventional design for SQUID detectors that should be borne in mind. This is the fact that the SQUID and detection coils are separated by a distance that may amount to 20 cm or so. Thus a relatively extensive supporting structure and surrounding wall must be maintained at low temperature to keep both SQUID and flux transporter superconducting. The problem is solvable in principle if a material such as crystalline germanium or quartz serves as support for the detection coil and heat conduit to the SQUID, where the cryocooler may provide direct refrigeration. For example a 20 cm rod of 1 cm^2 cross sectional area with its upper end maintained at 10 K when receiving 0.1 W at its lower end would find that rise in temperature by only ~ 1 K. The surrounding walls could be allowed to remain at a somewhat higher temperature, so long as thermal radiation is not excessive.

4. Cardiomagnetism

The earliest efforts to detect biomagnetic fields were directed to studies of the heart. Since the electrocardiogram (ECG) was known as one of the strongest bioelectric signals, by analogy the corresponding magnetocardiogram (MCG) measured near the chest was expected to be comparatively strong. The first observation of the magnetocardiogram was reported by G. Baule and R. McFee in 1963, and it was achieved with a pair of induction coils arranged in gradiometer configuration placed over the chest [5]. Each coil was wound with 2×10^6 turns of wire which were wrapped around a ferrite core for enhancement. Signal averaging was used to improve the signal compared with the noise, using the ECG as a reference. The introduction of magnetic shielding and a SQUID magnetometer by D. Cohen, E.A. Edelsack and J.E. Zimmerman in 1970 made possible the MCG without signal averaging and with a quality which was comparable to that of the ECG [14]. Since then aspects of cardiomagnetism have been studied in a number of laboratories, including M.I.T. [15,16]; Helsinki University of Technology [17]; Stanford University [18]; TRW Systems at Redondo Beach, California [19]; and the Universite' Scientifique et Médicale at Grenoble, France. The last-mentioned group employs an induction coil gradiometer in a hospital setting without shielding the patient [20]. Signal-to-noise ratios of 10-30 are achieved by averaging 100 beats [21,22]. The other groups all utilize SQUID systems.

4.1. AC Magnetocardiogram

The minimal bandwidth normally employed for a MCG is 0.2 - 50 Hz, and signal amplitudes lie in the range 20 - 300 pT. Low frequency background noise poses a problem in an unshielded situation, but acceptable records can be obtained by systems employing spatial discrimination, perhaps supplemented by signal averaging.

Interest in cardiomagnetism centers on the possible application of the MCG as a diagnostic tool. Several formats have been devised to present data, including individual traces of the cardiac cycle for a particular component of the field measured at various locations over the chest [23] and indications of the direction and strength of the local field gradient at a particular time in the cycle, as measured at various locations [24]. One economical way of summarizing data is by determining the variation in the magnetic heart vector (MHV) throughout the cycle [25,26]. The MHV is the magnetic dipole which positioned at the center of the heart would give rise to the observed field. Measurements show that the field distribution around the chest is not dipolar [25], partially owing to the extended geometry of the heart and to currents which flow in the surrounding conducting medium. The effect of the latter can be minimized by choosing an appropriate detection coil geometry and position [27]. A system devised at Stanford and designated the "unipositional" lead system employs a SQUID gradiometer which is positioned above a supine patient with the axis normal to the chest wall and directly over the heart. Both pickup coils are oriented at $54^{\circ}44'$ to the instrument axis so that three components of the magnetic field can be recorded with successive 120° rotations of the magnetometer. From these the variations through the cardiac cycle of the three components of the MHV can be deduced. Figure 8 displays an example of the components (M_x, M_y, M_z) of a normal subject. For comparison the analogous electric heart vector (EHV) with components (P_x, P_y, P_z) obtained from the Frank ECG electrode arrangement is also shown.

Published results show a close similarity in MCG and ECG records for normal subjects, although the relative angles of the MHV and EHV vary throughout the cycle [26]. Abnormalities have been studied by several groups [16,17,26,28,29] and there is some evidence that the preferential sensitivity of the MCG to near-lying sources plays an important role in emphasizing certain abnormal features [17]. In addition the MCG compared with the ECG is more sensitive to tangential current components than ones that are directed radially from the heart [18,30-33]. As yet no remarkable abnormalities have been revealed by the MCG that are not at least suggested by the ECG. The relative advantages of the two records have not yet been firmly established, and we should not expect a definitive assessment of the MCG's clinical usefulness for several years. On the other hand, one advantage of the MCG is clear: this contactless technique is considerably more convenient for mass screening of a large population. During measurements, the background dc magnetic field should be reduced to avoid complications from changes in the diamagnetic moment of the volume of blood within the heart [25,34].

4.2. DC Magnetocardiogram

One very interesting application of the advantage afforded by SQUID systems for dc measurements has been reported by D. Cohen and L.A. Kaufman [35]. They sought to establish whether a dc current may be produced by the heart when it suffers injury. For example a shift of the ST segment of the ECG toward the R peak of the QRS complex is a clinical indication of an abnormality such as infarction or ischemia. The nomenclature for a normal ECG is given at the top of Figure 9. The ST shift illustrated in the center trace was commonly

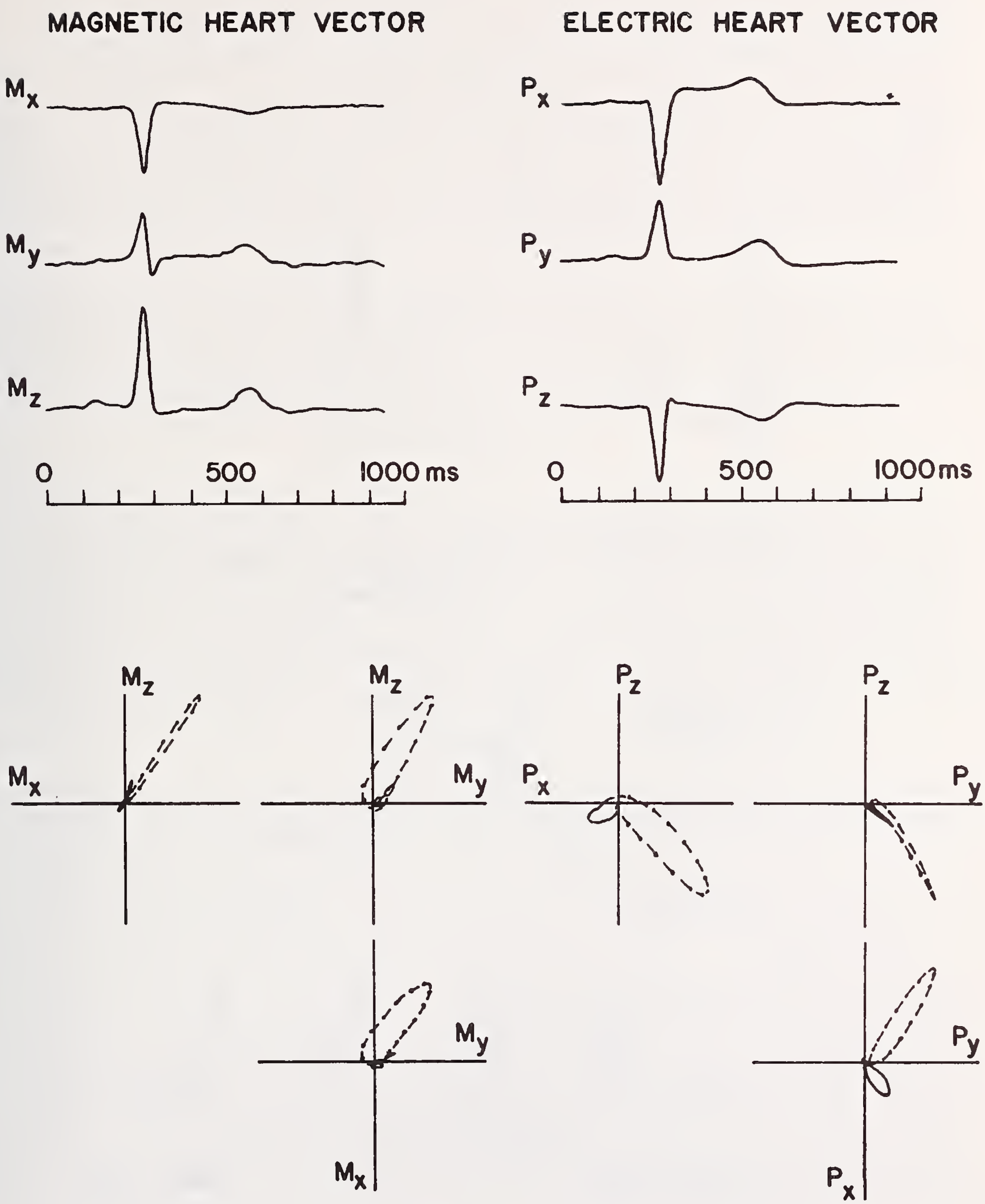

Figure 8. Variation in the components of the magnetic and electric heart vectors throughout a cardiac cycle. The X-axis is directed straight outward from the patient's chest, Y is toward his left and Z is toward the head. Adopted from Reference 25.

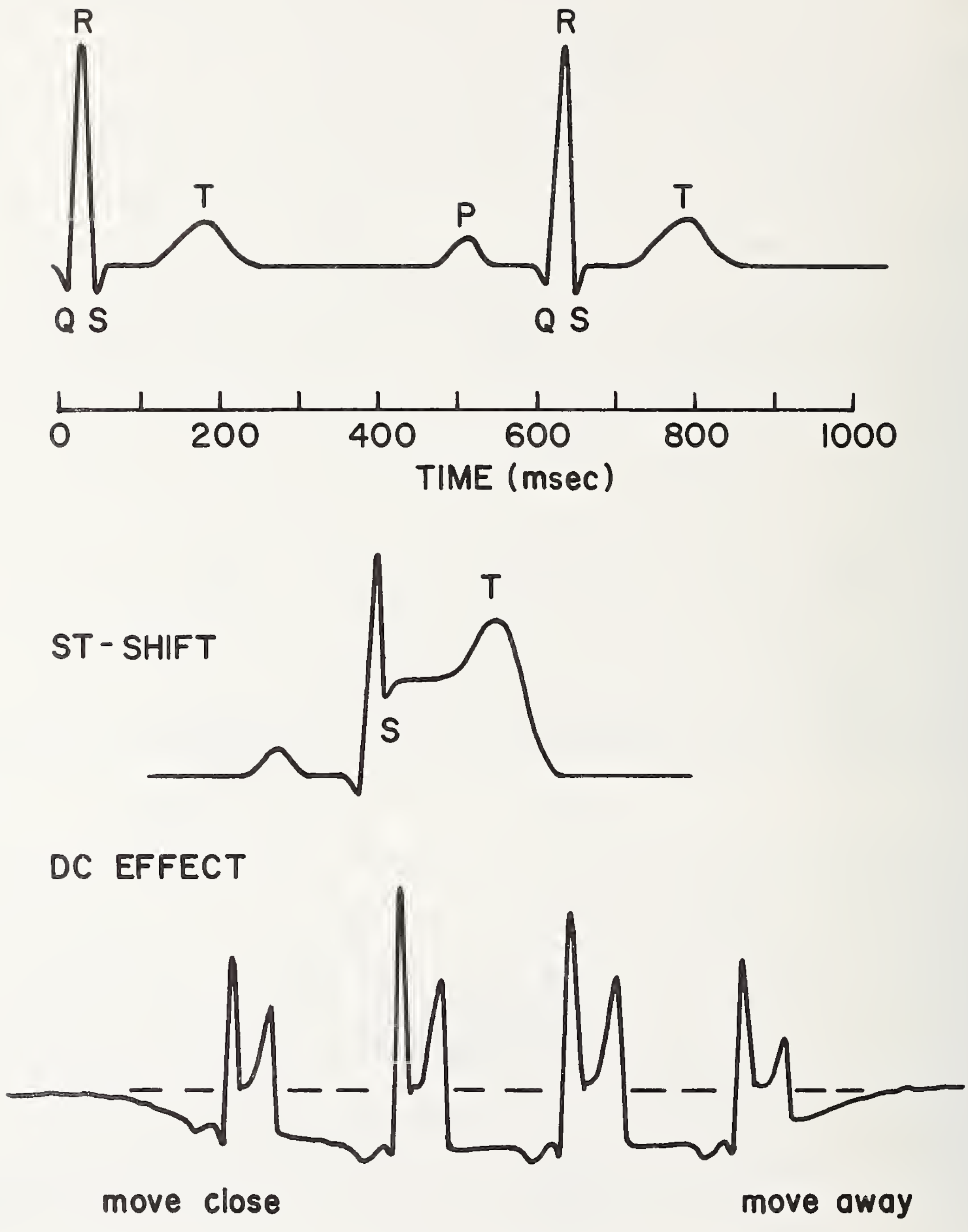

Figure 9. (a) Normal ECG waveform and notation; (b) upward shift of the ST segment; (c) observed MCG from a dog with constricted coronary artery being wheeled toward and away from the SQUID detector. Adopted from illustrations in Reference 35.

attributed to a current of injury that appears only during the ST portion of the cardiac cycle. Cohen and Kaufman's experiments on dogs indicated that quite the opposite is true during an occlusion of the coronary artery and that in fact a dc current of injury is set up which is arrested during the ST portion of the cycle. The occlusion was produced by inflating a tube that had been installed previously around the artery. The MCG results illustrated at the bottom of Figure 9 show the SQUID magnetometer output as a sedated dog is wheeled up to the detection coil, held in place for several cardiac cycles, and wheeled away. During conditions of occlusion the MCG reference line shifts downwards, indicating the presence of a dc current of injury. There is also an upward shift of the ST segment which nearly exactly compensates for the dc effect and thus indicates an interruption of the dc injury current. The ST shift is thus a secondary effect, and the primary effect is actually the dc current of injury, which is not detectable by conventional ECG measurements.

For measurements of the DC magnetocardiogram a bandwidth of 0.1 - 50 Hz may be sufficient. The patient is moved close to the detector, then away. The technique has not yet been applied clinically, partly because magnetic particles contaminating the body may provide a remanent signal which is sufficient to obscure the effect. To avoid an additional artifact, the patient as he is brought to the detector should be in a low field region to avoid the effect of diamagnetic moment of the human body when in the earth's field.

5. Pneumomagnetism

During Cohen's pioneering experiments on animals when looking for dc currents of injury to the heart, he observed a dc field from the stomach and tracked its origin to magnetic contaminants ingested with food. He subsequently found that humans exhibit similar remanent fields from contaminants which are either ingested or respired [36]. Considerable interest has arisen recently in applying magnetic monitoring techniques to lung investigations. The study of these fields whether produced by contaminants or by the lung itself is an area that we call "pneumomagnetism". Presently several groups are engaged in this type of research: at M.I.T., Helsinki University of Technology, Hannemann Medical College in Philadelphia, and the Institute for Environmental Medicine of New York University. Interest centers on two principal aspects: clinical applications and research.

5.1. Clinical Applications

Use of magnetic tracers has a potential application in epidemiological and clinical studies aimed at correlating magnetic dust retention with exposure, pathological condition and disfunction. This is possible because magnetic contaminants may be found in association with injurious particles, even though the magnetic component itself is harmless. For example, particles of ferrimagnetic magnetite (Fe_3O_4) are found attached to chrysotile asbestos fibers when mined, and therefore if the relative proportions at the source are established, a magnetic scan across the lung may reveal the amount and disposition of asbestos at low levels which X-ray techniques miss. In practice, a dc magnetic field ($\sim$ 50 mT) is first applied to the region of the chest to magnetize the contaminants and then is removed. The component of the remanent field which is normal to the chest in the case of asbestos miners and arc welders may be as strong as 1 nT and is easily measured with conventional fluxgate magnetometers. The sensors should be arranged in a gradiometer configuration to discriminate against background fields [36,37]. The rms instrument noise level in a 1 Hz bandwidth is $\sim$ 30 pT. Mapping across the chest is conventionally performed by momentarily moving the subject near the sensor, then away to check for background drift. Strong remanent fields may arise from other magnetic objects, such as belt buckles, steel bone pins, prosthetic devices, tooth fillings and bridgework. Where these cannot be removed and are not near the lung, the remanent artifact may be eliminated by a degaussing procedure. A hand-held magnetic recording tape eraser is passed slowly over the region and then is withdrawn slowly.

An example of the type of results obtained with a SQUID system is shown in Figure 10. Studies in Helsinki of arc welders of iron and steel display a strong correlation between the average field strength across the chest and the results of radiograms which reveal pathological conditions, despite the fact that measurements of respiratory function appear to be nearly normal [37].

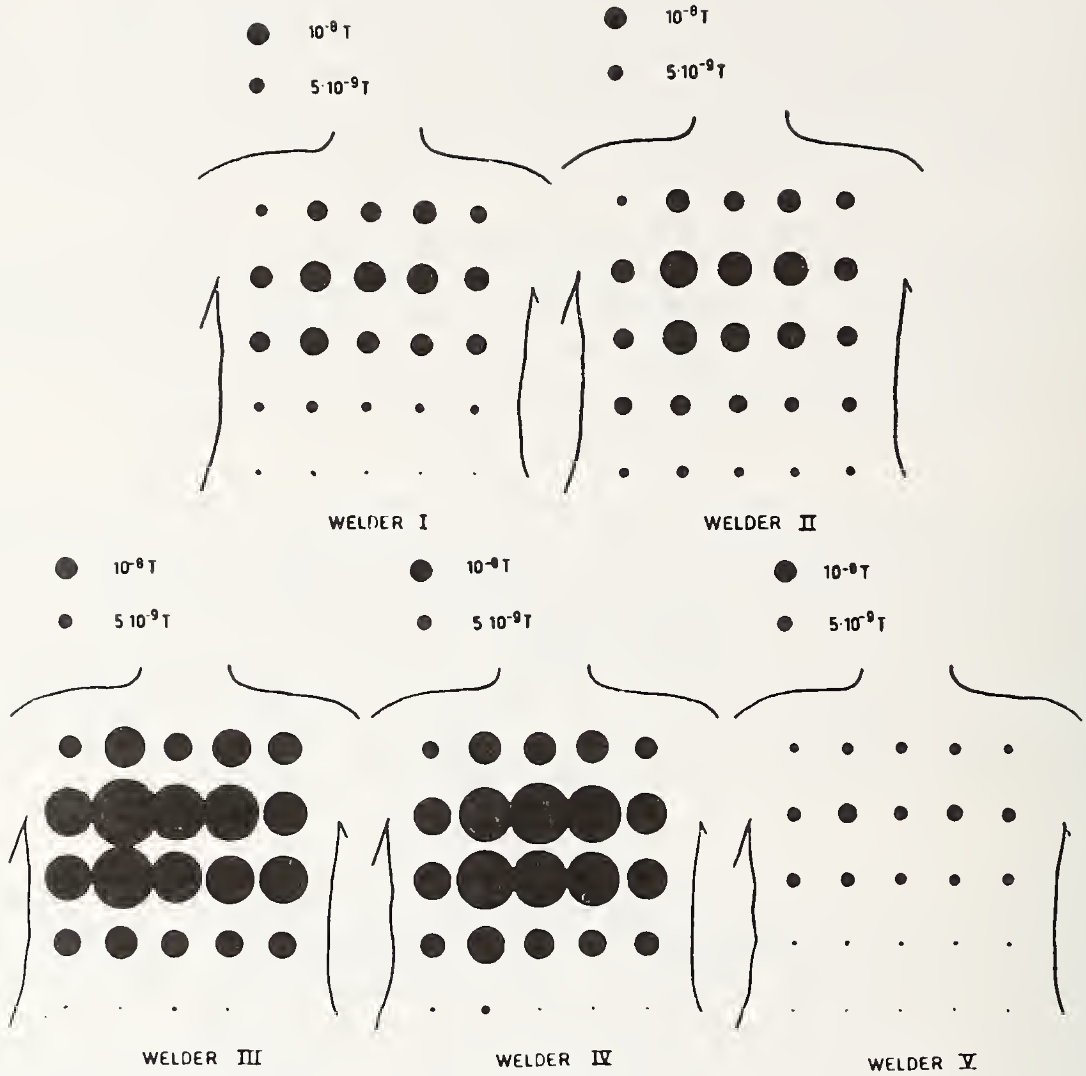

Figure 10. Remanent field from ferromagnetic contaminants at various locations over the chest for five arc welders. The area of each dot is proportional to the measured field at at that location. By comparison, the average signal measured over the pulmonary area of a non-exposed control group was ∿ 5 pT. All measurements shown here were carried out with a SQUID system. From Reference 37.

Work at M.I.T. is underway to solve what is called the "inverse problem". This is the challenge of deducing the distribution of magnetic dust within the lung, given measurements of the field components at various positions outside the chest. One of the important questions to be answered is how many measurements are needed for a given resolution of the source distribution, taking into account existing noise levels.

5.2. Lung Research

Pure magnetite is a benign dust, and milligram amounts are believed harmless when inhaled. A fluxgate gradiometer is adequate for detecting the subsequent remanent field (~ 0.5 nT) after the particles in the lung have been magnetized [36]. Therefore magnetic tracers can be used in experiments on humans and animals, where the more conventional radioactive tracers necessarily have more limited application [38].

D. Cohen has found a remarkable "relaxation" of the remanent field during the few hours after magnetization [39]. This appears to be caused by the randomizing of particle orientations induced by the motion of the alveolar walls in the lung. Although much remains to be learned, this promises to be an exciting area for study of alveolar activity and the nature of the fluid lining. In addition Cohen has found that the maximum remanent field decreases monotonically during the succeeding months following exposure. This may prove to be a measure of either the rate of lung clearance or the rate at which phagocytes immobilize particles in the lung. Relaxation and remanent moment studies may well provide direct information about pathological condition of the lung.

5.3. SQUID Applications

The future of pneumomagnetism has abundant possibilities, but one certainly is the extension of studies to other dusts such as coal, of prime interest in occupational medicine. Here SQUID systems may prove essential, because the percentage of magnetic contaminant is much lower than for asbestos and may turn out to be comparable to that for the unexposed population. Measurements should be conducted in a region of low field to eliminate the diamagnetic contribution of body tissue; or the diamagnetic effect can be estimated by taking the difference between the measured remanent fields when the lung is magnetized with the field applied first in one direction and then in the opposite.

The major problem is the need to establish reliable data for the remanent fields expected for members of the unexposed population. Even brief exposure to a foundry or welding shop can provide such heavy magnetic loading that it would mask the more subtle buildup from chronic exposure elsewhere. Extended research or epidemiological studies in the field are difficult to perform with the present requirement for liquid helium. Here the cryocooler may play a pivotal role.

6. Neuromagnetism

The weakest of all biomagnetic fields detected so far are those due to electrical currents associated with neural activity. The magnetic field generated by spontaneous activity of the brain was discovered in 1968 by D. Cohen using an induction coil in a shielded room together with signal averaging techniques [40]. He was able to detect variations in the magnetic field near the scalp that oscillated with a frequency in the range 10-12 Hz (the alpha rhythm). The strongest signals are typically ~ 2 pT in amplitude. With modern SQUID detectors this "magnetoencephalogram" (MEG) can be obtained with a quality that is comparable with that of the standard electroencephalogram (EEG) [41]. Studies of neuromagnetic activity have subsequently been pursued at M.I.T., Helsinki University of Technology [42], National Bureau of Standards at Boulder [43] and New York University. Both spontaneous activity and that evoked by sensory stimuli have been investigated.

6.1. Magnetoencephalogram

Electrical measurements of variations in skin potential show widespread activity over the scalp. In correspondance, when the alpha rhythm is well developed the field pattern is found to embrace the head as illustrated in Figure 11. The amplitude is suppressed when the subject has his eyes open, as shown in Figure 12. From a series of measurements in the N.B.S. shielded room M. Reite, J.E. Zimmerman, J. Edrich and J. Zimmerman report a strong

B

Figure 11. General features of the magnetic field patterns at the alpha frequency as reported in Reference 40.

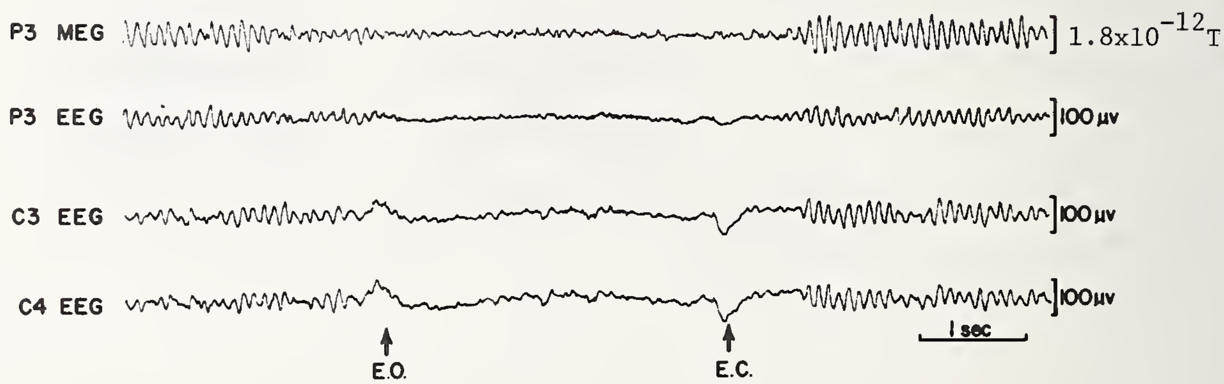

Figure 12. Simultaneous magnetoencephalogram (MEG) and electroencephalogram (EEG) recorded near the back of the head, with a bandwidth of 5-30 Hz. From Reference 43.

positive correlation between the amplitudes of the MEG and EEG from one subject to another [43]. Extensive comparisons between the MEG and EEG from seven normal subjects have been reported on the basis of measurements with a bandwidth of 2-45 Hz in the M.I.T. room by J.R. Hughes, D.E. Hendrix, J. Cohen, F.H. Duffy, C.I. Mayman, M.L. Scholl and B.N. Cuffin [44]. Numerous features of the magnetic and electrical records have been compared. There is some correlation in the alpha rhythms when the subject is awake, but this correlation is lost during sleep. But no correlation was ever observed for some components (below 5 Hz).

It is clear from these important results that a close, but not complete association exists between the generating sources for the alpha rhythm observed in the EEG and MEG. The sources for signals at other frequencies appear either to be disassociated, or the currents are preferentially oriented so that their magnetic fields are largely parallel to the scalp and hence remain undetected in these experiments. So little information is available about magnetic field patterns that it is premature to speculate about the nature of the sources. These spontaneous signals from the brain remain intriguing and unexplained. Even the physiological source and function--if any--of alpha rhythm activity has not been firmly established.

6.2. Evoked Fields

Enlightening studies of brain function have been carried out by evoking a response through application of a sensory stimulus such as a visual or tactual stimulus, a technique that is well-known in experimental psychology. One then knows where the initial brain activity takes place, i.e., the primary projection area of the cortex. In such studies, signal averaging techniques must be used for both potential and field measurements to bring the relatively weak evoked response (~ 0.1 pT) above the level of the spontaneous activity and background noise. Either transient or steady state responses can be measured. The former is the response to an isolated stimulus, separated in time from other stimuli so that the response to one ends before the next stimulus is presented. The steady state response is obtained when stimuli are presented in rapid succession at a constant rate.

a. Visually Evoked Field

Groups at M.I.T. [39,45] and the National Bureau of Standards [43] have reported observations of the transient neuromagnetic field which is evoked by a brief light flash. An example of the visually evoked field (VEF) is shown in Figure 13. The pattern is qualitatively similar to that of the visually evoked potential (VEP). As the flash is made brighter the response amplitude of the VEF continues to increase, but the amplitude of the VEP tends to level off [45]. The reason for this difference is not understood.

The work at N.Y.U. has dealt exclusively with the steady state response and has revealed new features of the nature of brain function. One stimulus consists of an array of vertical parallel bars on a dark field provided on an oscilloscope screen. When this so-called "grating" is appropriately shifted back and forth horizontally, synchronous variations in the neuromagnetic field near the scalp can be detected. With narrow band detection and a one-minute duration for signal averaging, responses as weak as 40 fT with a signal to noise ratio of 2 can be recorded without use of magnetic shielding. The grating pattern is inspired by the contemporary notion in psychology that at least for simple patterns the visual system responds to the pattern's spatial frequency content (in this sense, the visual system takes the Fourier transform of the scene).

D. Brenner, S.J. Williamson and L. Kaufman found that the VEF is sharply localized near the back of the head over the visual cortex--the vision center of the brain [11]. The VEP by comparison is considerably more widespread, being strong even at the vertex at the top of the head. The second remarkable finding is that the peak magnetic field is observed at a fixed time after the stimulus grating is shifted, regardless of the temporal frequency at which it is shifted [46]. This time delay is called the "latency" of the response, and it appears to be a characteristic feature of the human visual system.

A particularly interesting finding from the VEF studies was that the latency of the subject's response increases with the spatial frequency of the grating, i.e., with the number of bars that are included in 1 degree of visual angle. The effect illustrated in Figure 14 is quite dramatic. The relative insensitivity of latency to spatial frequency at

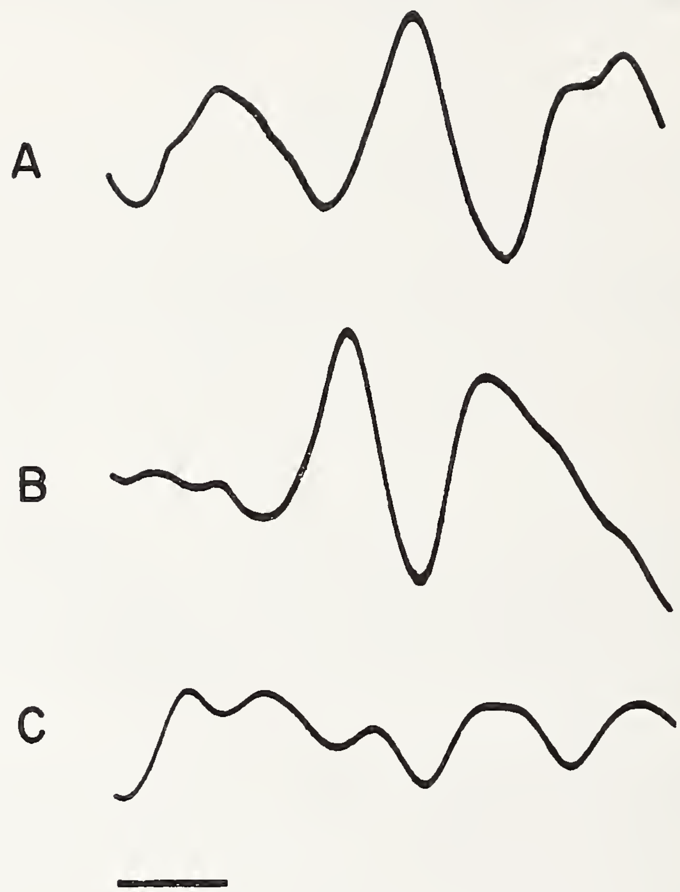

Figure 13. Visually evoked responses for a brief flash produced by a strobe lamp. The signals were averaged for 100 flashes. A: Magnetic response with upward deflection indicating a field directed into the scalp. B: Voltage response with upward deflection indicating positive potential at the field location. C: Magnetic noise level with the subject absent. The time calibration at the lower left is 50 msec. From reference 43.

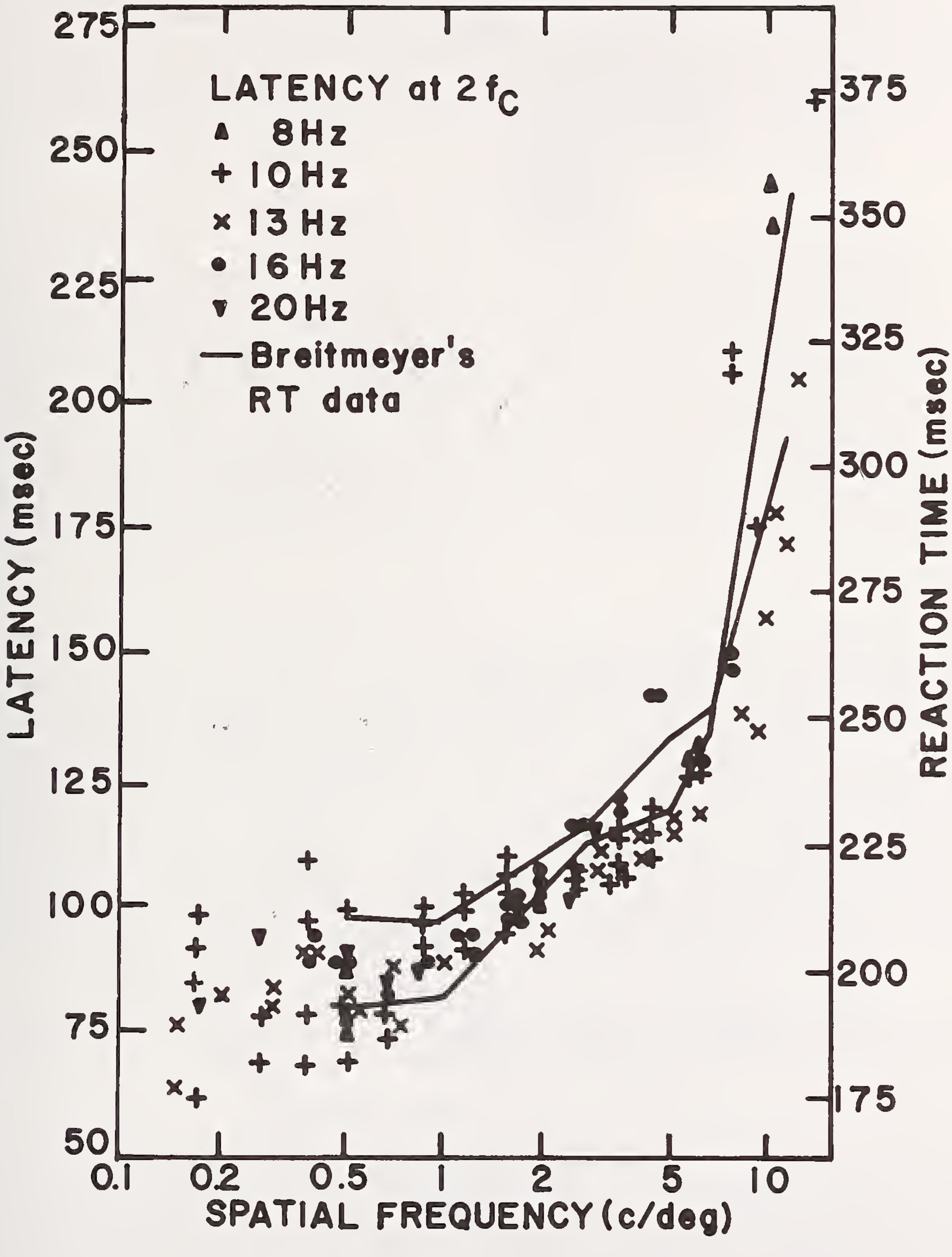

Figure 14. Latency of the magnetic response at the second harmonic of the frequency at which a grating is shifted a full cycle back and forth. Data for a number of different frequencies are included. The lines join points which indicate measured reaction times reported by B. Breitmeyer. From reference 46.

the low end of the curve and sharp rise at the high end correlate with characteristics of hypothesized specialized channels in the visual system, but it would not be appropriate to go into these details here. Of more relevance is the fact that there is a direct correlation between latency (a measure of neural activity) and a subject's reaction time (a measure of human performance). Also shown in Figure 14 are reaction times reported by B. Breitmeyer for two observers who were instructed to respond as quickly as possible to a briefly presented grating having various spatial frequencies [47]. The constant difference of approximately 115 ms between reaction time and latency is interpreted as the motor response time. Thus the neuromagnetic studies suggest that there is a serial arrangement of visual and motor responses. This result had not previously been obtained from conventional studies of the VEP.

b. Somatically Evoked Field

Electrical stimulation of various areas of the body provides a good test of the accuracy with which neuromagnetic techniques can locate active sets of neurons within the somatic cortex. Direct stimulation of the cortex during brain surgery, with portions of the skull removed, has previously revealed the locations of primary activity related to somatic sensation [48]. Areas of the body map onto corresponding regions of the cortex on the contralateral side of the head just behind a nearly vertical indentation of the cortex known as the Rolandic fissure. This ordering of projection areas is called the "sensory homunculus". D. Brenner, J. Lipton, L. Kaufman and S.J. Williamson have observed a somatically evoked field by applying a mild, repetitive, electrical stimulus to the little finger of the right hand and monitoring changes in the emerging magnetic field of positions over the left hemisphere [49]. Figure 15 illustrates the pattern of evoked field at an instant when the field has its maximum strength. One half cycle later the field pattern has reversed direction.

The center of the pattern can be located with an accuracy of about 1 cm and lies close to the appropriate position on the homunculus. When the thumb is stimulated instead, the pattern shifts downward along the Rolandic fissure by about 2 cm, again as expected from the homunculus. Such localization has not heretofore been achieved by conventional measurements of the VEP. Neuromagnetic responses with stimulus repetition rates ranging from 0.8 Hz to more than 30 Hz have been studied. For intermediate frequencies a latency of 70 ms has also been obtained for the neuromagnetic response. When compared with reaction times measured in separate experiments a motor response time of 102 ms is obtained, in good agreement with the value obtained from the visually evoked response. These results indicate that the VEF is caused by electrical currents flowing within the primary projection area of the cortex, not the skin where the VEP is measured. Neuromagnetic measurements hold out the promise of a method for revealing the functioning of the brain at a level that is intermediate between recordings from gross scalp electrodes and microelectrode studies of individual neurons.

7. Other Applications

Several other biomagnetic fields have been discovered which we shall not describe in detail but will just mention the more salient features.

7.1. Fetal Magnetocardiogram

The fetal magnetocardiogram (FMCG) was first observed by V. Kariniemi, J. Ahopelto, P.J. Karp and T.E. Katila [50] of the Helsinki group. It is of interest because the electrical analog (the FECG) often cannot be observed because it is masked by the much larger signal from the mother. By contrast the FMCG shows little effect from the mother's heart and can be observed after about the 20th week of gestation. This again illustrates the greater localization exhibited by biomagnetic fields near the strongest electrical currents when compared with the more diffuse variations of voltage on the skin. The amplitude of the FMCG of ~ 5 pT measured over the abdomen is about one-tenth of the mother's MCG measured over the chest. It was studied by the group at the Helsinki University of Technology with a gradiometer detection coil and SQUID, operating in a wooden cabin some distance from the nearest steel structure [51,52].

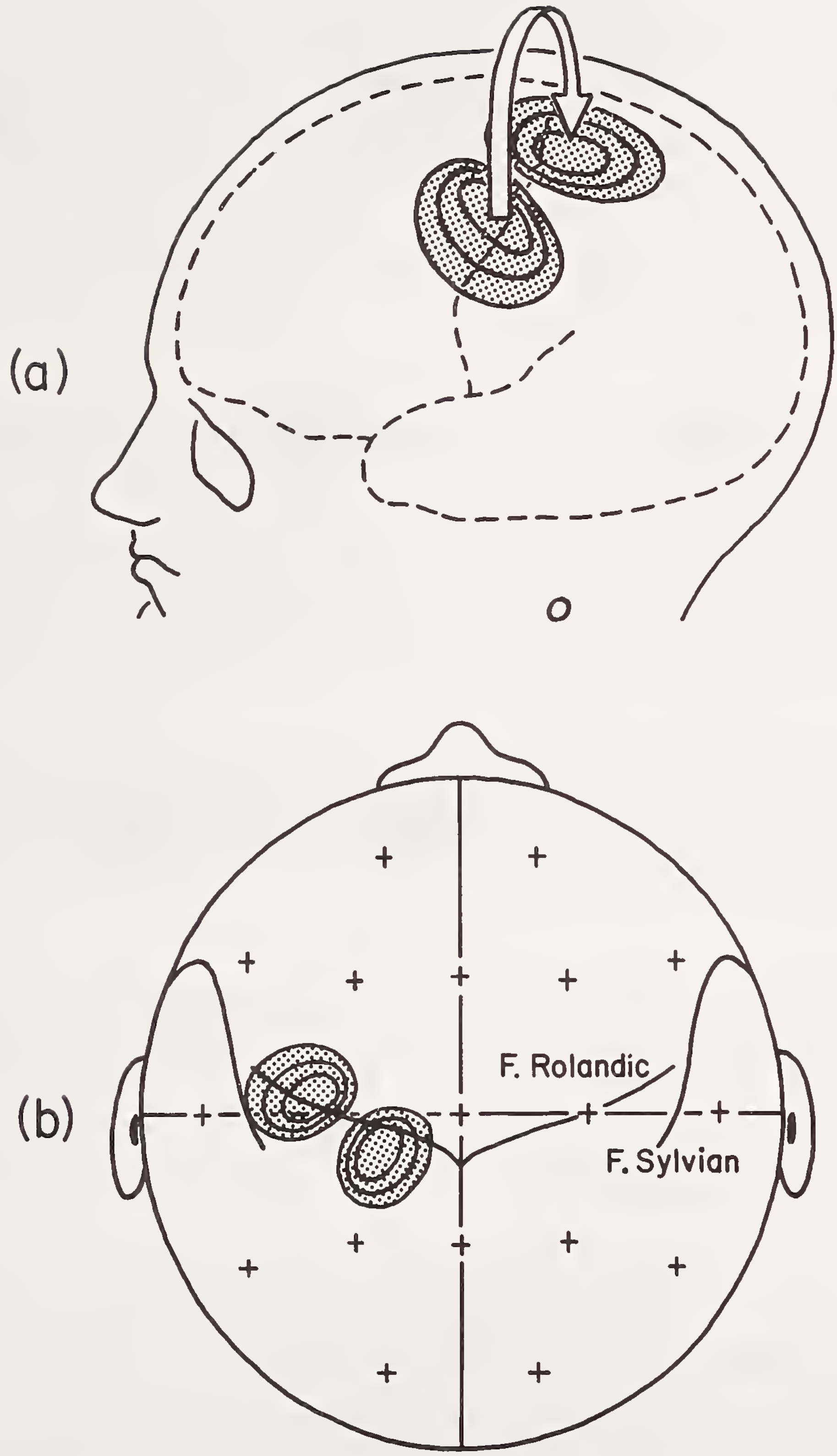

Figure 15. Pattern of the somatically evoked field when a mild electrical stimulus is applied to the little finger of the right hand. The stimulus consists of 1 ms dc pulses of voltage producing approximately 1 mA pulses of current transcutaneously, at a rate of 13 pulses/second. Contours of equal magnetic flux in the figure indicate the relative amplitude of response for 0.9, 0.7 and 0.5 of the maximum response at the stimulus frequency. The lower figure shows the same pattern drawn on the conventional 10-20 electrode map. From reference 49.

7.2. Magneto-oculogram

The normal human eyeball maintains a relatively high voltage of ~ 100 mV between the retina and cornea. Electric dipole models have been proposed to describe the current distribution in the surrounding medium in order to explain the changes in skin potential when the eyeball (with dipole) is moved. The observed effect is called the electro-oculogram (EOG). The change in dc field associated with the change in current distribution or magneto-oculogram (MOG) has been detected by P.J. Karp, T.E. Katila, P. Mäkipää, and P. Saar of the Helsinki group [53]. When the subject deflects his eye by about 75°, a shift in the field near the eye amounting to ~ 10 pT can be observed. The magnitude of this shift varies in much the same way as changes in skin potential when a decrease in illumination causes the eye to go from the light adapted to dark adapted state. It is not clear whether this technique offers an advantage over the EOG, which is commonly used in clinical diagnosis of retinal diseases, because as yet no new feature has been found in the MOG that is not known in the EOG.

7.3. Magnetomyogram

A particularly interesting area for future research is in measuring the magnetic field which results when skeletal muscle is flexed. This was first observed by D. Cohen and E. Givler using a SQUID magnetometer in the M.I.T. shielded room [54] and an example is shown in Figure 16. Wideband recording (up to ~ 2 kHz) is essential to recover the high frequency activity associated with asynchronous twitches from various motor units, though the signal amplitudes can be moderately strong (~ 10 pT). The electrical counterpart known as the electromyogram (EMG) is well known and has been used for a variety of applications, including the study of muscle movement, tension, and human relaxation. High frequency activity, is found to exhibit a maximum amplitude at about 40 Hz in the case of muscle just above the elbow and at 80 Hz for the palm.

A feature worthy of special note is a dc component which also appears when a muscle is flexed. The field slowly diminishes during a period of several seconds once the muscle is relaxed. It may be difficult to monotor this effect reliably with skin electrodes owing to the variation in contact potentials, so magnetic techniques offer a real advantage. There is considerable interest in the relaxation mechanisms in muscle, some of which are known to occur over a period of several seconds.

8. Summary

We have touched on a number of applications of superconducting magnetic field detectors in areas of interest to clinical medicine, epidemiology and psychology. Biomagnetic studies offer unique advantages in some cases over conventional bioelectric investigations: These include dc through high frequency sensitivity, the localization of magnetic fields near their generating currents, insensitivity to fields from relatively weak currents flowing in the dermis, and the contactless nature of the measurement. Fundamental questions of interest in biomedical research are being addressed now in several areas, and there is every evidence to indicate that biomagnetism will enjoy sustained growth during the next few years.

Present liquid helium cooled SQUID systems are adequate for most ongoing studies. Motivation for the introduction of cryocoolers will not be economic, at the present cost for liquid helium. Rather it would be greater convenience, simplification of carrying out studies in the field, the ability to orient detectors in any direction, and avoidance of the need for personnel highly trained in cryogenic techniques.

We express our appreciation to D. Brenner and J.P. Wikswo, Jr., for stimulating and informative discussions. The preparation of this manuscript was supported by the Office of Naval Research (00014-76-C-0568) and the New York State Health Research Council (C106219).

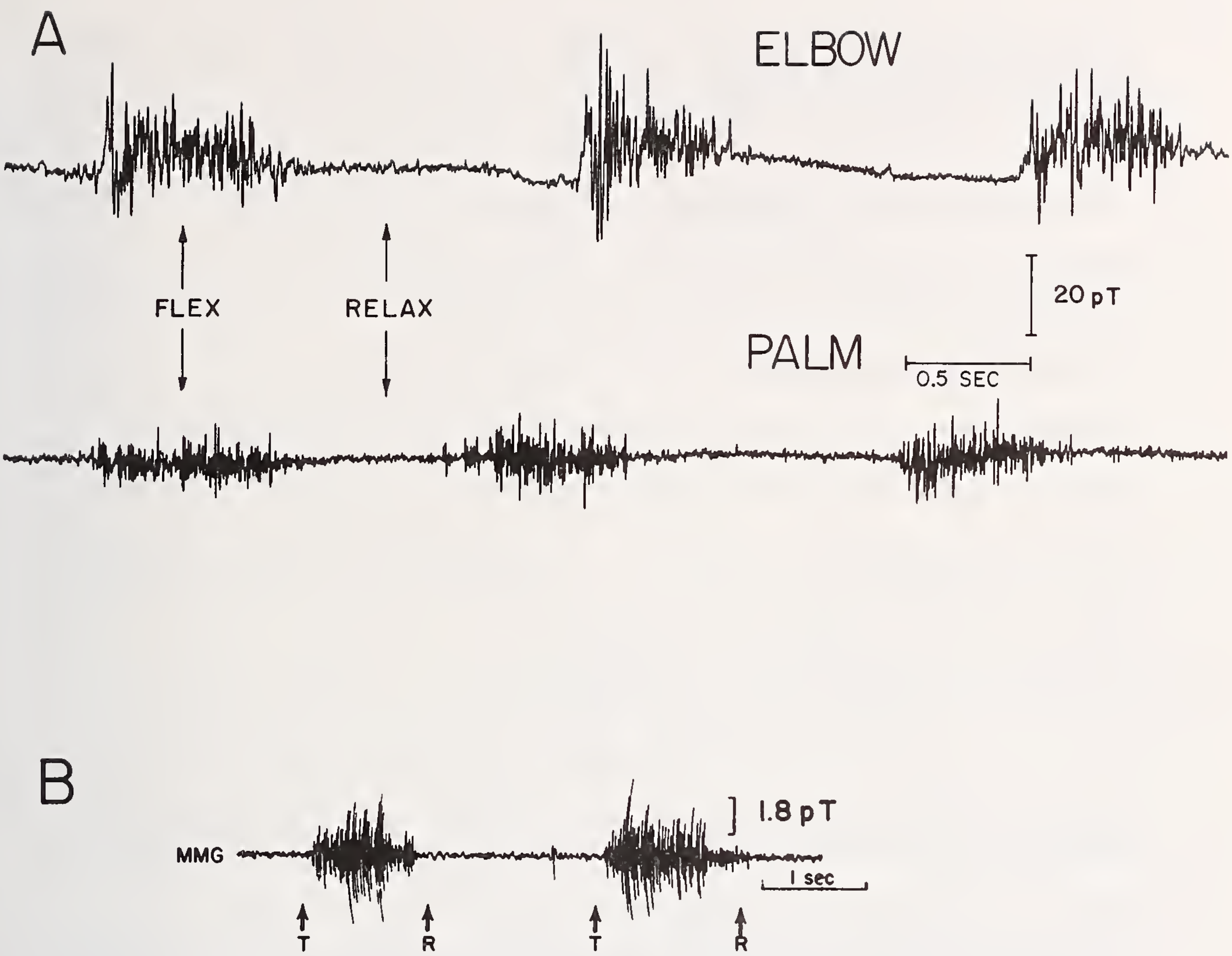

Figure 16. A: Magnetomyogram measured in the M.I.T. shielded room with the detection coil positioned near the elbow and palm. The bandwidth is 0-150 Hz. From reference 54. B: A.C. Magnetomyogram from the forearm with muscle tensed (T) and relaxed (R) as measured in the N.B.S. shielded room. From reference 43.

[1] Williamson, S.J., Kaufman, L., and Brenner, D., "Biomagnetism" in Superconductor Applications: SQUIDS and Machines, Schwartz, B.B., and Foner, S., Eds. (Plenum Publishing Corporation, New York, 1977), pp. 355-402.

[2] Fraser-Smith, A.C., and Buxton, J.L., J. Geophys. Res. 80, 3141 (1975).

[3] Cohen, D., Rev. de Phys. Appliquée 5, 53 (1970).

[4] Zimmerman, J.E., J. Appl. Phys. 48, 702 (1977).

[5] Baule, G.M., and McFee, R., Am. Heart J. 66, 95 (1963).

[6] Zimmerman, J.E., J. Appl. Phys. 42, 4483 (1971).

[7] Zimmerman, J.E., and Frederick, N.V., Appl. Phys. Letters 19, 16 (1971).

[8] Opfer, J.E., Yeo, Y.K., Pierce, J.M., and Rorden, L.H., IEEE Trans. Magn. 9, 536 (1974).

[9] Ketchen, M.B., Goubau, W.M., Clarke, J., and Donaldson, G.B., IEEE Trans. Magn. MAG-13, 372 (1977).

[10] Claassen, J.H., J. Appl. Phys. 46, 2268 (1975).

[11] Brenner, D., Williamson, S.J., and Kaufman, L., Science 190, 480 (1975).

[12] Brenner, D., Kaufman, L., and Williamson, S.J., IEEE Trans. Magn. MAG-13, 365 (1977).

[13] Widrow, B., Glover, J.R. Jr., McCool, J.M., Kaunitz, J., Williams, C.S., Hearn, R.H., Zeidler, J.R., Dong, E. Jr., and Goodlin, R.C., Proc. IEEE 63, 1692 (1975).

[14] Cohen, D., Edelsack, E.A., and Zimmerman, J.E., Appl. Phys. Letters 16, 278 (1970).

[15] Cohen, D., and Lepeschkin, E., "Review of Magnetocardiology" in The Electrical Field of the Heart, Rijlant, P., et.al., Eds. (Presses Académiques Européennes, Brussels, 1972), p. 91.

[16] Cohen, D., Lepeschkin, E., Hosaka, H., Massell, B.F., and Myers, G., J. of Electrocardiology 9, 398 (1976).

[17] Saarinen, M., Karp, P.J., Katila, T.E., and Siltanen, P., Cardiovascular Research 8, 820 (1974).

[18] Wikswo, J.P. Jr., Malmivuo, J.A.V., Barry, W.H., Leifer, M.C., and Fairbank, W.M., "The Theory and Application of Magnetocardiography", in Cardiovascular Physics, Ghista, D.N., van Vollenhoven, E., and Yang, W., Eds. (S. Karger, Basil, 1977).

[19] Rosen, A., and Inouye, G.T., IEEE Trans. Bio. Med. Eng. 22, 167 (1975).

[20] Matelin, D., Thesis, Université Scientifique et Médicale de Grenoble, Grenoble, 1974, unpublished.

[21] Denis, B., Matelin, C., Favier, C., and Martin-Noel, P., J. Physiol. (Paris) 69, 179 (1974).

[22] Denis, B., Matelin, D., Favier, C., Tanche, M., and Martin-Noel, P., Arch. Mal. Coeur 69, 299 (1976).

[23] Cohen, D., and McCaughan, D., Am. J. Cardiol. 29, 678 (1972).

[24] Hosaka, H., and Cohen, D., J. of Electrocardiology 9, 426 (1976).

[25] Wikswo, J.P. Jr., Ph.D. Thesis, Department of Physics, Stanford University, 1975, unpublished.

[26] Barry, W.H., Fairbank, W.M., Harrison, D.C., Lehrman, K.L., Malmivuo, J.A.V., and Wikswo, J.P. Jr., Science, in press.

[27] Malmivuo, J., Acta Polytechnica Scandinavica, Electrical Engineering Series No. 39, Helsinki, The Finnish Academy of Technical Sciences (1976).

[28] Saarinen, M., Karp, P.J., Katila, T.E., and Siltanen, P., Cardiovasc. Res. 8, 820 (1974).

[29] Karp, P.J., Katila, T.E., Saarinen, M., Siltanen, P. and Varpula, T.T., Ann. de Cardiologie et d'Angiologie, in press.

[30] McFee, R., and Baule, G., Proc. IEEE 60, 290 (1972).

[31] Geselowitz, D., J. Franklin Inst. 296, 379 (1973).

[32] Brody, D.A., Circ. Res. 4, 731 (1956).

[33] Malmivuo, J.A.V., and Wikswo, J.P. Jr., Proc. IEEE, in press.

[34] Wikswo, J.P. Jr., Opfer, J.E., and Fairbank, W.M., AIP Conference Proc. 18, 1335 (1974).

[35] Cohen, D., and Kaufman, L.A., Circulation Res. 36, 414 (1975).

[36] Cohen, D., Science 180, 745 (1973).

[37] Kalliomäki, P.-L., Karp, P.J., Katila, T., Mäkipää, P., Saar, P., and Tossavainen, A., Scand. J. Work Environ. and Health 4, 232-239 (1976).

[38] Albert, R.E., Lippmann, M., Spiegelman, J., Strehlow, C., Briscol, W., Wolfson, P., and Nelson, N., "The clearance of radioactive particles from the human lung", in Inhaled Particles and Vapors II, Davies, C.N., Ed. (Pergamon Press, London, 1966) pp. 361-378.

[39] Cohen, D., IEEE Trans. Magn. MAG-11, 694 (1975).

[40] Cohen, D., Science 161, 784 (1968).

[41] Cohen, D., Science 175, 664 (1972).

[42] Ahopelto, J., Karp, P.J., Katila, T.E., Lukander, R., and Mäkipää, P., International Conference on Biomedical Transducers (Biocapt. 75, Paris, 1975), Vol. 1, p. 347.

[43] Reite, M., Zimmerman, J.E., Edrich, J., and Zimmerman, J., Electroenceph. Clin. Neurophysiol. 40, 59 (1976).

[44] Hughes, J.R., Hendrix, D.E., Cohen, J., Duffy, F.H., Mayman, C.I., Scholl, M.L., and Cuffin, B.N., Electroenceph. Clin. Neurophysiol. 40, 261 (1976).

[45] Teyler, T.J., Cuffin, B.N., and Cohen, D., Life Sci. 15, 683 (1975).

[46] Williamson, S.J., Kaufman, L., and Brenner, D., Vision Research, in press.

[47] Breitmeyer, B.G., Vision Res. 15, 1411 (1975).

[48] Penfield, W., and Rasmussen, T., The Cerebral Cortex in Man (Macmillan, New York, 1950), p. 21.

[49] Brenner, D., Lipton, J., Kaufman, L., and Williamson, S.J., Science, in press.

[50] Kariniemi, V., Ahopelto, J., Karp, P.J., and Katila, T.E., J. Perinat. Med. 2, 214 (1974).

[51] Ahopelto, J., Hukkinen, K., Katila, T.E., Laine, H., and Kariniemi, V., Ann. Chir. Gyn. Fenn. 64, 152 (1975).

[52] Hukkinen, K., Katila, T.E., Laine, H., Lukander, R., Mäkipää, P., and Kariniemi, V., Am. J. Obstetrics and Gynecology, in press, 1976.

[53] Karp, P.J., Katila, T.E., Mäkipää, P., and Saar, P., Proc. Second International Conference on Medical and Biological Engr., Ottawa, Canada, Aug. 1976.

[54] Cohen, D., and Givler, E., Appl. Phys. Lett. 21, 114 (1972).

Cryogenic Techniques and Geophysical Measurements

W. D. Stanley
U.S. Geological Survey

Cryogenic techniques have begun to play a large role in geophysical measurements, particularly in measurement of the earth's magnetic field and remnant magnetization of rock samples. Superconducting quantum interference devices (SQUIDs) are now being used in the application of a technique known as magnetotelluric sounding.[1] In this method three cartesian components of the earth's magnetic micropulsation field[2] are measured in conjunction with the corresponding horizontal electric fields. The measured fields are H_x, H_y, H_z, and the electric fields are E_x and E_y where x and y are in the horizontal plane and z is vertical. An assumption is generally made that the transfer function relating the E's and H's at the surface of the earth is a rank two tensor:[3]

$$\begin{bmatrix} E_x \\ E_y \end{bmatrix} = \begin{bmatrix} Z_{xx} & Z_{xy} \\ Z_{yx} & Z_{yy} \end{bmatrix} \begin{bmatrix} H_x \\ H_y \end{bmatrix} = Z_{ij}H_j = E_i$$

Where the H's and E's now represent frequency domain variable and Z_{ij} is the impedance tensor. For a simple horizontally layered earth the coupling between E_x and H_x and between E_y and H_y is non-existent for the assumed planar incident fields and the tensor elements Z_{xx} and Z_{yy} are zero; in addition, $Z_{xy} = -Z_{yx}$. For an earth conductivity distribution that varies according to a function which can be defined by a function in a vertical plane (two-dimensional) or which consists of anisotropic horizontal layers (with anisotropy in x and y direction only) Z_{xy} and Z_{yx} will not be equal; in addition, for all measuring azimuths except one Z_{xx} and Z_{yy} are not zero. However, the impedance tensor can be mathematically rotated so that Z_{xx} and Z_{yy} vanish and either Z_{xy} or Z_{yx} becomes a maximum and the other a minimum. These are the principal directions for the tensor and are related directly to the direction of constant conductivity distribution for a structural geometry, or what is termed the "strike" direction in geology. This would be the trend direction for a lineated geologic feature such as a fault, for instance. For a layered anisotropic earth such an easy interpretation is not available, but asymptotic behavior at certain frequency ranges can provide quantitative determination of the anistropy of thick layers. The field data are usually presented in terms of principal resistivity and phase values, where the resistivities are:

$$\rho_{ij} = (0.2/f)|Z_{ij}|^2 \qquad f = \text{frequency}$$

and the phases are:

$$\varphi_{ij} = \tan^{-1} \frac{\text{real}(Z_{ij})}{\text{imag}(Z_{ij})}$$

The impedance tensor is derived from the 4 horizontal-field time-series using standard multiple input-multiple output transfer function analysis. The vertical magnetic field information is used to determine the proper quadrant for the tensor rotation. Interpretation of the derived resistivity-phase data is done either by a generalized least-squares inversion of the data (restricted to the layered earth approximation) or by trial and error fitting to finite difference models of a more complex conductivity distribution.

Conductivities in the earth at depths of 0-20 km are influenced by several conduction components including semiconduction, ionic conduction through pore fluids and in molten rock, and ordinary ohmic conduction through rock fabric. Temperature is either directly or indirectly a major factor in determining the magnitude of rock conductivity, particularly at depths exceeding 5 km. It is for this reason that a study of the earth's conductivity structure has been important in the exploration for geothermal resources in the last few years.[4] Because the earth's micropulsation field has abundant energy over wide frequency bands, with typically a reciprocal frequency power spectrum from 10^{-4} Hz to 1 Hz, it is a suitable source of excitation with plane waves for determining the conductivity structure of the earth from depths of several to several tens of kilometers.

Measurements of the earth's field for magnetotelluric sounding have been most commonly made using large induction coils cored with ferrite or mu-metal. Typical sensitivities of coils in useage are 150 $\text{uv/nT}\sqrt{\text{Hz}}$ and noise voltages are about 1-3 $\text{uv}/\sqrt{\text{Hz}}$ when coupled with suitable amplifiers. Typical SQUID magnetometers suitable for field recording of micropulsation activity have a noise figure of around .5 x 10^{-4}nT. Taking into consideration the 1/f characteristics of SQUID noise, the latter offer 10 to 100 times better noise figure than the induction coils. This can be even larger if other noise problems in the coils are not treated properly. For instance, magnetic domain noise in the coil cores and thermal effects require that the coils be allowed to stabilize for several hours after being buried in the earth to provide thermal and vibrational stability. A typical set of induction coils is made up of three separate sensors consisting of 30-100,000 turns of wire surrounding a multi-rod flux concentrating core, usually made of mu-metal, with each coil weighing about 40 kg and being about 2 m in length and 10 cm in diameter. A SQUID magnetometer in a 5 liter fiberglass DeWar set up for measuring three components weighs around 10 kg and can be ready for field measurements within a few minutes after installation. In addition, the multipole transfer function of the induction coils with their limited frequency response means that often two separate sets of coils may be required for wide bandwidth measurements; this is not a problem with SQUIDs.

Subsequent to early application of SQUIDs for magnetotelluric sounding, many investigators are now using SQUIDs for magnetotelluric measurements instead of induction coils.[5] Handling of liquid helium under field conditions has proved to not be an obstacle; however, a SQUID magnetometer operating with a compact, low power refrigeration unit would guarantee that SQUIDs would be used almost exclusively for this application and other wideband geophysical magnetic measurements. The magnetotelluric method has been used most often during the last 5 years for geothermal exploration, but is also applied in petroleum and mineral exploration as well as in academic studies of the earth's crust and upper mantle. Other geophysical studies utilizing measurements of the earth's magnetic fields could benefit from the advantages offered by SQUIDs, particularly combined with a magnetically quiet, low power refrigeration scheme. For instance, measurement of small peizomagnetic field changes or secondary fields due to conductivity changes in the vicinity of active stress regions may offer a tool for earthquake prediction.[6] Such measurements require an ultrasensitive array of long baseline horizontal gradiometers. Since stress fields around earthquake zones have time constants of interest in the several month range, it would be desirable to gain freedom from periodic filling with liquid helium. The same can be said of deployment of cryogenic gravity meters which are also needed in research and which use SQUIDs in a levitated-mass servo arrangement.[7]

References

[1] Frederick N. V., W. D. Stanley, J. E. Zimmerman, and R. J. Dinger, An application of superconducting quantum interference magnetometers to geophysical prospecting, IEEE Trans. Geoscience Electronics, GE-12, no. 3, p. 103 (1974).

[2] Jacobs, J. A., Geomagnetic micropulsations (Springer-Verlag, New York, 1970).

[3] Sims, W. E., and F. X. Bostick, Jr., Methods of magnetotelluric analysis, Tech. Rep. 58, Elec. Eng. Res. Lab., Univ. of Texas, Austin (1969).

[4] Stanley, W. D., J. E. Boehl, F. X. Bostick, and H. W. Smith, Geothermal significance of magnetotelluric sounding in the eastern Snake River Plain-Yellowstone region, Jour. of Geophys. Res., 82, no. 17, pp. 2501-2514 (1977).

[5] The number of commercial contractors and universities using SQUIDs for magnetotelluric measurements is growing. A relatively current list of groups using SQUIDs in this application is:

Colo. School of Mines, Golden, CO.
Group Seven, Inc., Golden, CO.
Argonaut Enterprises, Golden, CO.
Geonomics,Inc., San Francisco, CA.
Terraphysics Co., Oakland, CA.
Senturion Sciences, Tulsa, OK.
Mobil Research Labs, Dallas, TX.
Univ. of Calif., Berkeley, CA.
U.S. Geological Survey, Denver, CO.
Univ. of Hawaii, Honolulu, HI.

[6] Rikitake, T., Earthquake Prediction (Chapter 10, Geomagnetic and Geoelectric effects), 357 p. (Elsevier Publishing Co., New York, 1976).

[7] Warburton, R. J., Beaumont, C., and Goodkind, J. M., The effect of ocean tide loading on tides of the solid earth observed with the superconducting gravimeter, Geophys. Jour. Royal Astr. Soc., 43, p. 707-720 (1975).

Cryocoolers for Use with Superconducting Instruments: Some Estimates of Requirements

Michael B. Simmonds
S.H.E. Corporation, San Diego, California 92121

The cooling requirements for several types of commercial superconducting instruments are analyzed. The purpose is to obtain operational specifications for cryocoolers for use with these instruments. The specifications which have been considered include cooling time, cooling power, operating temperature, vibration, magnetic noise, and operating time between service.

Key words: Cryocooler; mechanical refrigeration; superconducting instrument.

1. Introduction

There has been a recent awakening of interest in the possibilities of cooling superconducting instruments by means of small mechanical refrigerators. The possibilities of doing this have not been opened up by any major technological advance in either the field of superconductivity or refrigeration, but rather because of a better awareness within each field of the capabilities and requirements of the other. To further this exchange, we would like to examine the special cooling requirements of various superconducting instruments which have commercial or military importance.

As we looked at the possibilities for mating our own instruments to some type of cryocooler, we realized that this is much more complex than simply cooling a piece of Nb_3Sn below its transition temperature. Each type of instrument seems to impose one or more challenging requirements on any proposed cooling system. Moreover, to be of commercial or military interest, these instruments must have high enough performance (compared to their conventionally cooled counterparts) that they are not disqualified in spite of their added convenience.

In this paper we will consider the cooling requirements for ELF/VLF antennas, geophysical magnetometers, biomedical gradiometers, rock magnetometers, susceptometers, and Josephson voltage standards. For these instruments, the specifications which will involve the cryocooler are: cooldown time, operating temperature, steady state heat load, vibration in the bandwidth of interest, magnetic noise level in the bandwidth of interest, and operating time between service. We will make estimates of performance requirements for the various types of instruments, then see how these requirements translate into specifications for the cryocooler itself. These requirements and specifications will be summarized in Table I.

Mechanically cooled thermal shields have proven very useful for reducing the liquid helium evaporation rate in conventional versions of some of the above instruments. However, in the following discussion we will only consider designs in which the cryocooler is the sole means of refrigeration.

2. Cooldown Time

The mass which must be cooled in these instruments can range from about 0.5 Kg for a typical geophysical magnetometer to 15 Kg or more for a high field susceptometer. Although this mass would be mostly dielectric support structure in the case of the magnetometer and mostly superconducting magnet wire in the case of the susceptometer, we can use a typical value of 100 J/g as the heat content at room temperature. The fact that more of this heat content is distributed at low temperature in metallic components makes it more difficult to remove the same quantity of heat. The magnitude of this bias will depend on the cooling power vs. temperature characteristics of the refrigerator's last stage, but this is not expected to be a large effect since the cryocooler can maintain its cooling power down to within a few degrees of its operating temperature. Our estimates of total mass to be cooled, and heat to be removed for the various instruments are given in the Table.

It is difficult to predict how long a user could be expected to wait for an instrument to cool down. If the refrigerator is reliable and permits long term continuous operation, then a one day delay should be acceptable. Some instruments, however, would only be used for a few days at a time. Under these conditions, half a workday would seem to be a reasonable maximum. Where the instrument is needed only for a short set of measurements or calibrations, it would be desirable to reach operating temperature in about one hour to remain competitive with the speed of using liquid helium. The Josephson voltage standard and the biomedical gradiometer in clinical use would fall into this last category.

3. Operating Temperature

Although standard superconductors are available with critical temperatures up to about 17 K, any instrument which requires close to ultimate performance from a Josephson junction or SQUID would need to be cooled well below this temperature. The use of Nb_3Sn or NbN SQUIDs appears, at first glance, to be a perfect way to relax the operating temperature specification for an instrument. However, with these devices it may not be possible to obtain even close to the energy sensitivity, bandwidth and dynamic range that is commercially available from "4 K" SQUIDs. There is a vast difference between making a SQUID which will show quantum interference behavior and building a complete SQUID-based instrument. There are problems such as fabricating highly accurate pickup loops, making shields for leads and sensors, building coupling transformers, and providing superconducting terminal boards. At above 9 K, these problems must be solved using exotic and extremely brittle materials. These difficult design problems can be vastly simplified if Nb or NbTi can be used for any superconducting parts. This requires that the cryocooler must be capable of reaching about 8K.

One of the instruments under consideration has an even more stringent temperature requirement. The Josephson voltage standards used by the National Bureau of Standards are normally operated in a pumped bath at 2 K to improve the voltage step characteristics. With the lead junctions presently in use, performance is marginal at 4 K.

The susceptometer is another instrument which derives some special benefit from a lower operating temperature. For samples in which the low temperature Curie Law behavior is of interest, one obtains an extra factor of two in temperature range by being able to reach 4 K instead of 8 K.

4. Steady State Heat Load

We can separate the cryocooler's last stage heat load into three categories. First is thermal radiation coming from the thermal shield connected to the previous stage. If superinsulation is used, part of this "radiation" load may technically be conduction, but functionally it will still depend on the total surface area of the low temperature assembly. If we assume that the second stage reaches 70 K and the separation distance is 2 cm, then we can expect a heat load of about $2.5 \mu w/cm^2$. This value could be obtained by using either moderately shiny surfaces or a few layers of superinsulation. Estimated sizes and surface areas for the instruments are given in the Table.

The second contribution to the heat load is conduction through support rods, electrical leads, and any other tubes or cables which run to the last stage. Generally these items can be thermally lagged to the previous stage, so we are only concerned with their conductivity between 70 K (to follow our example) and about 8K. If the vibration and motion of the cryocooler's last stage can be tolerated, the superconducting elements could be mounted directly to this stage and no additional support rods would be necessary. This is not the case for the ELF antenna and the geophysical magnetometer. The ELF antenna, in particular, would have a rather large superconducting pickup coil structure (10^4 cm^3) requiring extremely rigid support. Our estimated contributions from these supports are based on a thermal path length of 20 cm between the 70 K and the 8 K stages, and the use of a material such as fiberglass/epoxy (G-10). The other instruments are somewhat desensitized to motion in the earth's field either by magnetic shielding or by internal balancing against uniform fields.

Signal and heater leads can generally be designed to cause a negligible heat leak, but this is not the case for the current leads to a high field superconducting magnet. The requirement here is that the sum of direct conduction and Joule heat reaching the magnet while it is being energized must not raise any part of the magnet above its maximum operating temperature. We can gain a significant advantage by thermally lagging these leads to our canonical 70 K stage, and with the optimum choice of lead diameter, one gets a heat load of 8 mW/A. Charging a 5 Tesla susceptometer magnet would typically require 50 A and thus generate an additional 400 mW of heat. The use of a Nb_3Sn magnet would be almost inescapable in this situation, since the termperature could be allowed to rise to about 14 K. This is to be compared with a 5 K limit for a NbTi magnet.

The third category of heat load covers energy which is injected directly into the low temperature region from an external source. It is unaffected by shielding or lagging at any intermediate temperatures. The primary example in our present list of instruments is the 10 mW of microwave power which must be shined onto the junctions in the Josephson voltage standard. Another example is the power which must be used to heat superconducting shields or switches above their transition temperature, as in the susceptometer.

5. Vibration

The severity of this problem is critically dependent on the way the instrument is engineered and interfaced to the cryocooler. For this reason, it will not be possible to quantify any requirements on the cryocooler itself.

The angular motion of superconducting pickup coils is the crux of this problem. When the support structure is flexed so that a magnetometer pickup loop rotates slightly in the earth's field, then a spurious signal as large as 10^{-2} Gauss/degree can be generated. If the frequency of this flexing is within the bandwidth of the desired signals, then simple filtering will not be useful. However, we know that the vast majority of the mechanical disturbance from the cryocooler is perfectly periodic and predictable. That allows us, in principle, to determine and subtract this periodic signal from the instrument's output. As long as these synchronous disturbances are not so large as to cause non-linearities or overloads in the SQUID system, then this technique should be capable of giving at least a 40 dB improvement in noise. From the instrument designer's standpoint, it is therefore more important to have tight specifications on the non-reproducible component of the cryocooler's motion. The only defense against this random motion is to design sufficient mechanical isolation into the instrument. In Table 1 we have made estimates of how much non-synchronous motion could be tolerated in the pickup coil regions of the various instruments. Typical signal bandwidths are also given. For instruments which have inherent shielding or balancing against motion in the earth's field, these motion limitations are more dependent on internal flexing between the coils and shields. Our estimates in these cases are based on the degree of rigidity which we have observed in conventionally cooled versions of the same instruments.

6. Magnetic Noise

Except in the fully shielded instruments such as the susceptometer or rock magnetometer, the magnetic disturbance caused by the cryocooler is likely to be an extremely severe problem. These magnetic fields are locally generated and will be very non-uniform in the region of the pickup coils. Therefore the balancing scheme used in instruments such as the biomedical gradiometer will not be effective in rejecting them.

This is an area where some initial care on the part of the cryocooler manufacturer could save the instrument designer a tremendous amount of effort later. Nominally non-magnetic materials such as stainless steel should be used for any moving parts within several meters of an unshielded SQUID pickup loop. Parts such as the displacer and its supporting structure which are both cold and close to the pickup coils must be scrupulously non-magnetic. It would be even better if they were also non-metallic and had low paramagnetic susceptibility.

The effectiveness of ferromagnetic or superconducting shields for reducing the cryocooler's magnetic noise is limited. This is because such shields also distort and shield the fields which the geophysicist or medical researcher is trying to measure. We can, however, use the same technique of synchronous noise rejection which was proposed for vibration rejection. In practice one might not even distinguish between noise from motion and noise from direct magnetic pickup. Our estimates of maximum permissible magnetic noise refer to non-synchronous fields which are in the instrument's signal bandwidth.

7. Operating Time Between Service

This is probably the most subjective of our proposed requirements. Let us consider the instruments one at a time to see how we arrived at the times listed in Table 1.

The ELF/VLF antenna would presumably be towed behind a submarine. If any dismantling or repairing of the cryocooler was required during a routine cruise, this could well make the instrument design unacceptable to the military. A very large fraction of the instrument's cost should be devoted to obtaining an extremely reliable and long lived cryocooler, because unexpected mechanical failures could cause serious communication problems. Since a cruise would typically last 6 months, this period of continuous maintenance free operation should be the minimum specification.

The Josephson voltage standard would probably be used for a few hours at a time to do periodic calibration of secondary standards. We feel that a six month interval between factory servicing would be about the minimum acceptable. Based on one working day a week of use this would imply 200 operating hours. The convenience of not having to maintain a liquid helium supply would certainly outweigh the inconvenience and cost of the twice yearly service.

The rock magnetometer might be used for several days at a time, then be idle for several days. At a 50% duty cycle we would have to require about 2000 hours of unmaintained operation to obtain a twice yearly service schedule.

We expect the use pattern of the susceptometer to be similar to that of the rock magnetometer. However, the susceptometer is a larger, more complex instrument which would certainly have to be serviced in the field. It would therefore be desirable if scheduled maintenance of a major nature did not have to be done more often than once a year.

Geophysical magnetometers are usually taken into the field for surveys lasting only one or two months, and the use of cryocooled instruments could be more than a matter of convenience if the survey were being done in a remote area where liquid helium is not available. On the other hand, continuous and maintenance free operation would be absolutely necessary for the duration of the expedition. Between each survey we expect that complete maintenance would be performed.

The biomedical gradiometer, as used in a clinical environment, would probably be cooled only when required: it might be operated for one or two days each week. Under these conditions, and with an assumed service period of six months, we would require about 1000 hours of operation, on an intermittent basis.

Conclusion

Some of the demands which we have made on cryocooler performance in this paper are certainly beyond what is available in commercial or even in experimental machines. This is not meant to discourage development work on cryocooled superconducting instruments.

We do want to emphasize, however, that at this time, the task of designing a commercially viable system would be extremely difficult. A liquid helium bath is mechanically and magnetically quiet, thermally stable in the face of large heat loads, and not prone to mechanical breakdown. It will not be easy to make it obsolete, although we would certainly like to do so.

Table 1
Operating Specifications for Cryocooled Instruments

	VLF/ELF Antenna	Josephson Voltage Standard	Rock Magnetometer	Susceptometer	Geophysical Magnetometer	Biomedical Gradiometer
Cooled Mass (Kg)	2	0.5	2	15	0.5	1
Total Heat Content (Joules)	2×10^{5}	5×10^{4}	2×10^{5}	1.5×10^{6}	5×10^{4}	10^{5}
Required Cool Down Time (Hrs.)	24	1	4	24	24	1
Operating Temperature (K)	<8	2	<8	4	<15	<8
Expected Heat Load						
1) Radiation (mw)	5	1	5	10	1	20
2) Supports and Leads (mw)	7	0	0	400	2	0
3) Direct Heating (mw)	0	10	0	5	0	0
4) Total (mw)	12	11	5	415	3	20
Bandwidth of Interest (Hz)	$10^{2}-10^{3}$	<1	<10	<10	$10^{-4}-10^{2}$	$10^{-1}-10^{2}$
Maximum in Band Motion of Superconducting Parts (Non-Synchronous) (degrees)	10^{-9}	10^{-1}	10^{-1}	10^{-3}	10^{-7}	10^{-2}
Maximum In Band Magnetic Field at Superconducting Loops (Non-Synchronous) (Gauss)	10^{-11}	10^{-1}	10^{-1}	10^{-1}	10^{-9}	10^{-10}
Required Operating Time Between Service (Hours)	5×10^{3}	2×10^{2}	2×10^{3}	4×10^{3}	2×10^{3}	10^{3}

hig
tem
req
and

Key

4.2
hig
sig
the
sho
pow
com
are
pow
tha

the
thu
rem
ext
The
vol
lev
the
the
Tec
vol
per

for
tir
ins
37
has
pro
cor
(1
in
or
du
im
of

Refrigerator Requirements for Potential

Josephson Data Processing Systems

B. J. C. van der Hoeven, Jr. and W. Anacker

IBM Thomas J. Watson Research Center

Yorktown Heights, N. Y.

Josephson Technology offers the potential for data processing systems with ultra-high performance. Such a system would operate in a cyrogenic environment at liquid helium temperature. The basic operation of Josephson computer circuits and refrigerator requirements for such a processor are described, with emphasis on cost, size, reliability and power.

Key words: Josephson, Data Processing, Cryogenics, Refrigerators, I.O.

I. Introduction

Logic and memory circuits employing Josephson junctions operating at 4.2°K are promising candidates for data processing systems with ultra-high performance. [1, 2] They offer the potential of ultimate system performance significantly faster than that presently achieved with Si technology due to the fact that they combine very fast switching times (tens of picoseconds), short staged logic delays (∿100 picoseconds), and extremely low power dissipation (microwatts/circuit) for circuits with dimensions comparable to todays Si technology. Typically delays for Josephson circuits are approximately one order of magnitude less than Si circuit delays and power dissipation per circuit about three to four orders of magnitude less than Si.

A limiting factor in the performance of processors using Si technology is their physical size. Despite the miniaturization of devices on a chip, and thus the power dissipation per circuit, power density on a chip tends to remain constant or even go up. In order to extract this dissipated power, extensive structural hardware is necessary to diffuse and extract the heat. The space necessary for the heat removal hardware tends to keep the volumetric packaging density and thus physical size constant at the system level. As circuit speed increases, the propagation delay between circuits then becomes the limiting factor in overall system performance. Thus the combination of fast circuits and low power dissipation of Josephson Technology permits the design of high performance systems in a very dense, volumetric package, reducing the intercircuit distances and delays and permitting full utilization of the fast switching of the devices.

Figure 1 illustrates this comparison of circuit density at the system level for Josephson and Si, and also indicates the major contributors to the cycle time of a processor which ultimately determines the number of programming instructions a machine can process per unit time. For example, the IBM 370/168 can process about 3.5 million instructions per sec (3.5 MIPS) and has a cycle time of ∿70 nsec. (∿ 4 cycles/instruction). The central processing unit (CPU) of a large processing system such as the 370/168 contains typically about 200K logic circuits and several megabytes (1 byte = 8 data + 1 error detection bits) of memory. Systems of this size in Josephson Technology might occupy a volume equivalent to a cube on the order of 5-10 cm on a side and dissipate ∿ 1-5 watts, including dissipation due to heat leaks thru input/output cables. Such a processor would be immersed in liquid He, the power density on the chip being a few percent of the nucleate boiling limit for liquid He. Thus cooling is accomplished

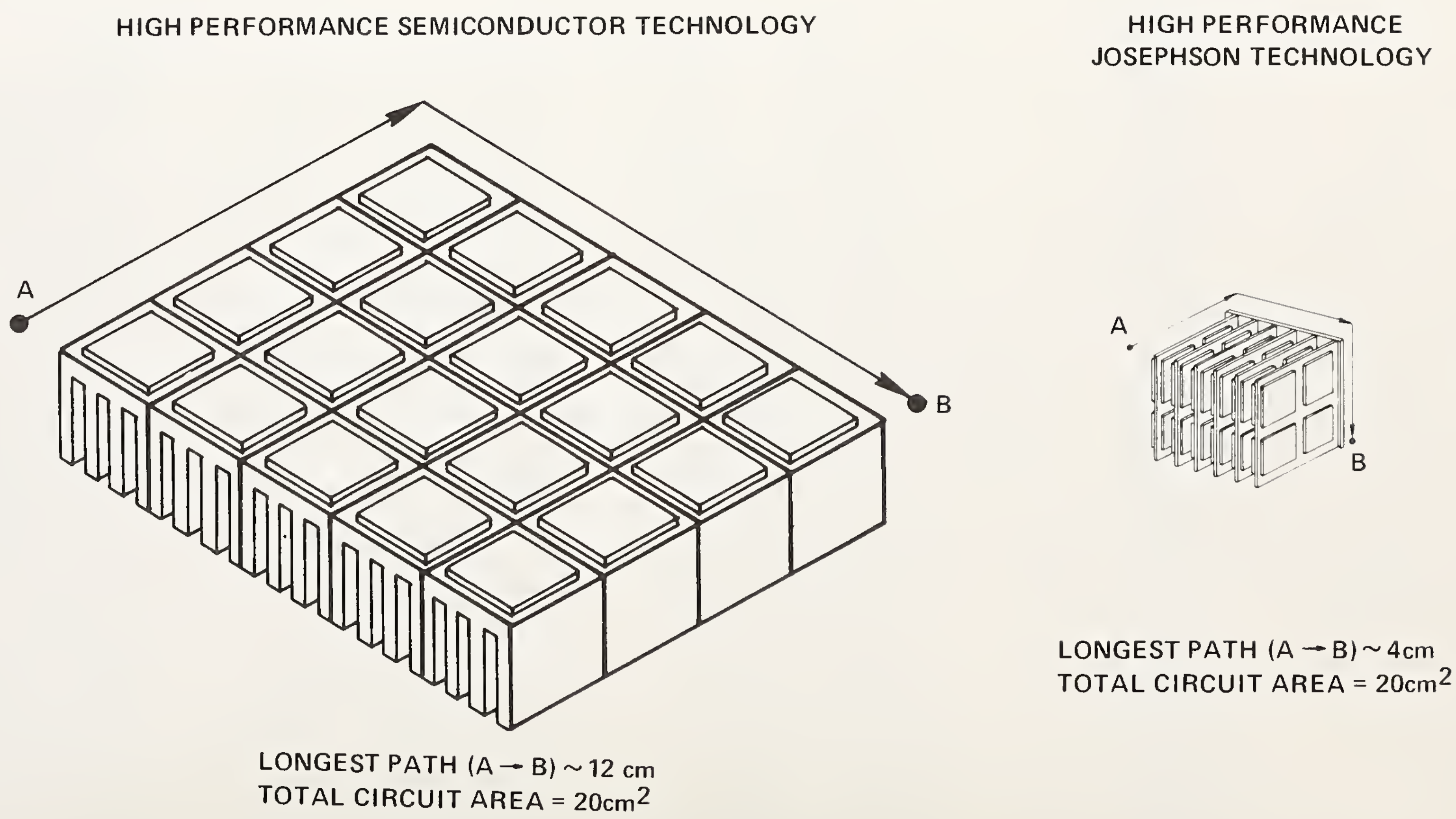

$$T_{CYCLE} = T_{LOGIC} + T_{PKG.\ INTERFACES} + T_{PROPAGATION}$$

Figure 1 Comparison of Packaging Densities of Semiconductor vs Josephson Technologies by convection of liquid He over the chips.

This paper will describe basic operation of Josephson computer circuits and refrigerator requirements for such a processor, taking into consideration cost, size, reliability and power.

II. Josephson Tunneling Devices & Circuits

The operation of switching devices used in Josephson Technology depends on two quantum-mechanical phenomena: superconductivity and electron tunneling. A Josephson tunnel junction consists of two films of superconducting metal separated by a layer of insulating oxide that is thin enough ($\sim$50Å) to permit electron tunneling [3]. The tunneling occurs in two quite different ways.

The BCS [4] theory of superconductivity postulates that superconducting electrons are associated in pairs since the energy of pairs is lower than the energies of the individual electrons, and that the waves associated with the pairs are all in step, or in phase, throughout the superconductor. The single electrons condensing into pairs leave behind a "forbidden energy gap" in the density of states vs. energy diagram. As a consequence, single electrons can not readily tunnel through an insulator as long as they are facing forbidden energy states in the metal electrodes. Only if they are given sufficient energy to tunnel into energy states above the energy gap does tunneling actually take place. This energy is supplied simply by establishing a voltage, typically of a few millivolts, across the insulator.

This prediction of the BCS theory was verified by I. Giaever [5] of General Electric in the early 1960's. Shortly thereafter, B. Josephson [6] of Cambridge University pointed out that if the insulating layer were thin enough, say about ten atom layers, the phase coherence of electron pairs could also extend through it. In this case, electron pairs can tunnel through the barrier, which behaves like a weak superconductor itself, and there is no voltage drop across it.

Thus we have two possible forms of tunneling. In one, single-electron tunneling, there is a voltage drop across the insulator typically of a few millivolts, and in paired tunneling there is no voltage drop at all. Josephson further showed that the pair tunneling could be influenced by a small magnetic field. The two types of tunneling, and the ability to switch from one to the other by applying a small magnetic field, provides the basis for the computer switching element.

In 1965, J. Matisoo [7] of the IBM Watson Research Center, Yorktown Heights, New York, built the first Josephson junction switching device for digital computer circuits. The basic switching device consists of a Josephson tunnel junction with an insulated control line above it. A small current in the control line generates a field which can switch the junction from the "no-voltage" state into the "voltage" state.

As soon as a voltage appears across the junction, the current through it will switch into another superconducting path if one is available. Current in the new path can then be used as control current for subsequent junctions. An array of such circuits thus can perform computer logic and arithmetic. For memory, the devices are placed in a superconducting loop in such a way that a persistent current can be established in either a clockwise or counter-clockwise sense. The direction of the current then represents binary information, a "1" or an "0". As long as the loop remains superconducting the currents persist essentially forever. Theory predicted that Josephson junctions should show extremely fast switching action. Switching times of about 35 picoseconds have been measured at the IBM Zurich Laboratory, the measurement being limited by the slow response of the equipment. [8] Theoretical computations, supported by other measurements, indicate that the switching is expected to have taken place in only about 10 picoseconds.

More recent work at the IBM Research Center in Yorktown Heights, N. Y. has led to the successful fabrication and evaluation of logic and memory circuits with minimum fabrication line widths of 25 μm. A 4 bit multiplier [9] utilizing ∿ 50 devices on a 6.35mm X 6.35mm chip was successfully operated with a cycle time of 6.7 nsec and a full 4 bit by 4 bit multiplication time of 27 nsec, again limited by experimental measurement. Simulations indicated successful operation at a a 3 nsec cycle and 12 nsec multiplication. A 64 bit (8 X 8) fully decoded array [10] was successfully operated with a cycle time of 5 nsec.

III. Refrigerator Requirements

For a variety of machine sizes, the estimated power dissipation and thus refrigerator cooling requirements for Josephson processors operating in the temperature range from 4.2 to 3.6°K can vary between ∿ 100 milliwatts and 10 watts, with typical requirements of ∿ 1 watt. This includes the power dissipation due to the processor itself, including logic, memory and power supply as well as the heat leak due to input/output (I/O) lines and through the cryostat walls into the liquid He. Such a system may require several hundred I/O lines between room temperature and 4.2°K in order to carry data to and from I/O devices (e.g. magnetic disc storage, terminals, etc.) and power lines to supply the appropriate current levels for the Josephson devices. Voltage levels on the power supply lines would range from a few hundred millivolts to a few volts with current levels ranging from milliamperes to several hundred milliamperes. Signal levels on I/O lines are foreseen to be on the order of 10 millivolts and fractions of a milliampere. It is also important to arrive at a judicious choice between signal attenuation and distortion on one hand and minimum heat leak on the other with respect to thermal and electrical resistance. Short, well thermally engineered lines, with heat sinking to take maximum advantage of helium vapor cooling as well as refrigerator cold stages appear capable of reducing heat leak to several tenths of a milliwatt/line. As pointed out above, immersing of circuit chips in liquid He is the preferred mode of providing the appropriate thermal environment and of extracting the heat.

An additional important consideration is the environment for such systems. They will typically be placed in an office or computer center location, and should be small, quiet, easily serviceable and reliable. It is envisaged that for a small processor with power dissipation less than 100 milliwatts, an open cycle refrigeration system could be used. This would include a low cost helium reservoir/dewar with gas recovery system capable of compressing the helium gas to storage cylinder pressure as it is expelled from the dewar at a very low boil-off rate. Helium could be returned to and liquified at a central distribution location, servicing many such processors.

Larger systems would include processor, closed cycle refrigerator (excluding compressor) and liquid helium reserve. One envisions a system incorporating a three stage expansion engine, Joule-Thompson valve and liquid helium reservoir existing concentrically around a removable center column containing the processor itself and associated I/O interface unit, such that either can be removed for field servicing and maintenance. Compressor and helium gas storage would be remotely located. The liquid helium reserve should be capable of maintaining the system at 4.2°K during refrigerator maintenance periods and break down. Finally the refrigerator MTBF must be sufficiently high.

It has already been mentioned that the internal regulated power requirements for a Josephson processor are small, on the order of a few watts corresponding to an unregulated power requirement for external power supplied (utility power) of the order of 100 watts. To this must be added the unregulated power requirement for the refrigerator which lies in the range of 1.5 to 2.5 Kwatts per watt refrigeration capacity at 4.2°K. In contrast, todays large processing systems (e.g. 370/168) require nearly 70 Kwatts unregulated power for the CPU, including cooling requirements. A significant consideration in the total cost of a processing system is the overhead capital cost associated with cooling and power supplies for the system. Josephson processors offer a significant advantage over semiconductor systems in terms of capital investment for power supplies (greater than a factor of 10). However capital investment for refrigerators for Josephson systems is proportionally high, in contrast to semiconductor systems for which capital cost for cooling is relatively low. It is therefore extremely desirable that refrigerator cost be reduced.

IV <u>Commercially Available Refrigerators</u>

A survey [11] has been made of the commercially available refrigerators which would initially meet some of the requirements above. Typical systems make use of a three stage Gifford-McMahan cycle plus a Joule-Thompson expansion valve.

Typical characteristics are:

- 2 watts cooling at 4.2°K
- 5 Kwatts unregulated power
- Total system MTBF = $20{,}000^{+}$ hours (with annual maintenance) covering refrigerator, compressors, dewar, etc.
- 30" diameter X 4' height
- 8' X 8' compressor and helium gas storage area
- 1 year operation without helium gas (5 cylinders) replacement
- Cost $60K single units

Cost for multiple units should be significantly lower. It is hoped that optimization of small closed cycle refrigeration systems (including compressor, expansion engine, J-T valve, etc.) for use in applications such as with Josephson processors will further reduce this cost and increase reliability.

V Conclusion

Future data processing systems utilizing Josephson Tunneling Technology have the potential of overcoming the fundamental limits of Si technology for use in ultra-high performance machines. Essential for their use in the commercial environment are the availability of extremely reliable, small, well thermally engineered, easily serviced, low power consumption, low cost, closed cycle refrigerators or open cycle systems with refrigeration capacity of $\sim$ 100 milliwatts to 10 watts in the temperature range from 4.2 to 3.6°K. Some of these characteristics are available today, some are not. It is hoped that further work especially in the areas of compressor/ refrigerator design, efficiency, reliability and cost reduction will be encouraged.

REFERENCES

1. Anacker, W., Proc. of European Solid State Devices Research Conference, Munich, Germany (Sept. 1976)

2. Zappe, H. H., Proc. of 1976 International Conference on Solid State Devices, Tokyo, Japan (Sept. 1976)

3. Greiner, J. H., Journal of Applied Physics 45, 32 (Jan. 1974)

4. Bardeen, J., Cooper, L. N., and Schrieffer, J. R., Phys. Rev. 108 (Dec. 1957)

5. Giaever, I., Phys. Rev. Lett. 5, 147 (1960)

6. Josephson, B. D., Phys. Lett. 1, 251 (1962)

7. Matisoo, J., Proc. IEEE 55, 172 (1967)

8. Jutzi, W., Mohr, T., Gasser M., & Gschwind, M., Electronics Lett. 8, 589 (1972)

9. Herrell, D. J., IEEE J. of Solid State Circuits, SC-10, 360 (1975)

10. Henkels, W., and Zappe, H. H., IEEE J. of Solid State Circuits, to be submitted.

11. Harvell, J., CTI Cryogenics, and Rerig, R., Air Products, Personal Communication

LITERS, KILOGRAMS, WATTS AND SECONDS:
Design Goals for a Refrigerator for Use with Superconductive Systems

M. Nisenoff
Naval Research Laboratory
Washington, D. C. 20375

ABSTRACT

A set of design goal values for certain non-thermal characteristics of a closed cycle refrigerator for use with superconductive electronic systems is proposed. These parameters include weight, volume, electrical input power requirements and turn-on time. Other parameters, such as mechanical vibrations, electromagnetic and radio-frequency inteference, which are also crucial to the utility of cryocoolers are not considered here.

Key Words: cryogenics, superconductivity, superconductive devices, Super-Schottky devices, closed cycle refrigeration systems.

1. Introduction

A common feature of most detectors of electromagnetic radiation whose operation is based on the Superconductive Josephson Effect is the inherent low noise characteristic of these devices. In the past, many of the proponents of these devices have stressed this particular feature, sometimes at the expense of other equally critical electrical and mechanical parameters. In this communication a summary of selected characteristics of systems employing both Josephson and conventional sensors will be presented with particular attention directed toward certain parameters, such as volume, weight, turn-on time, and input electrical power requirements. Typical values for these parameters will be used to propose a set of design goals for certain characteristics -- other than the obvious thermal ones -- for a closed cycle refrigeration system to be used with superconductive electronic (SCE) circuit elements.

2. Low Frequency Magnetic Field Sensors

One (or more) Josephson Effect devices inserted into an otherwise totally superconducting loop will form a class of devices known as SQUIDs (Superconducting QUantum Interference Device) which can detect extremely small magnetic field changes in the frequency range from DC to several megahertz. A comparison of several operating parameters of SQUID systems and conventional systems is shown in Table I. The performance of the conventional systems is probably quite close to optimum while the SQUID performance in terms of instrument noise and signal bandwidth can probably be improved by several orders of magnitude.

If SQUIDs are to be operated with closed cycle refrigeration systems, design goals for such parameters of the cryrocooler as volume, weight, input power requirements, turn-on time, etc. probably should be comparable to those of the optically pumped helium vapor magnetometer, the AN/ASQ-81. Such constraints would be essential for airborne and mobile land-based operations, while they probably could be relaxed for shipboard and stationary land-based situations.

3. Microwave and Millimeter Wave Radiation Detectors

The low noise characteristics of Josephson devices and Super-Schottky diodes as detectors of microwave and millimeter wave radiation are achematically shown in Figure 1 along with the performance of several conventional detection systems. At frequencies below about 20 GHz, conventional technologies are very good and improving. Thus the use of superconducting detection systems would appear to have potential only for frequencies above 30 GHz, where conventional technologies will probably remain inferior to superconducting ones.

In certain operational situations,, the improvement in noise performance offered by the superconductive devices may be offset by other system constraints and requirements. For example, in some military applications, the very limited dynamic range and low saturation power levels of the superconductive devices may preclude their use. In other situations, such as airborne applications, where the device may possess all the required electrical parameters, the volume and weight associated with the required cryocooler may make the use of a superconductive unit less desirable. Thus the entire set of electrical and mechanical parameters of the combined superconductive device <u>and</u> cryocooler must be considered when the replacement of a conventional system by a superconductive one is being proposed.

4. Design Goals for a SCE Cryocooler

Without specifying a specific application, it is rather difficult to propose a set of design goals for the parameters of a SCE cryocooler. However, for a "typical" application, a set of values can be proposed for certain non-thermal characteristics of the cryocooler for use with the superconductive systems, viz,

Volume	- several liters (10^2 inch^3)
Weight	- several kilograms (pounds)
Electrical Input Power requirements	- tens of watts
Turn On Time	- seconds (at most minutes)
Mean Time Between Failures	- 1000 hours minimum

(For a specific application, reference should be made to the operating manuals of the conventional system that is to be replaced.) Other non-thermal parameters, such as mechanical vibrations, electromagnetic and radio-frequency interference, which must be kept sufficiently low so as not to degrade overall system performance, have not been considered in this communication but will probably be treated elsewhere in these proceedings.

If closed cycle refrigeration systems can be built which satisfy the obvious thermal requirements and are compatble with the non-thermal parameters described here, it is highly probable that superconductive electronic systems could become acceptable for widespread use in the field and in military applications.

This work is partially funded by Naval Electronics Systems Command.

TABLE I

LOW FREQUENCY MAGNETIC SENSING SYSTEMS

	Optically Pumped Vapor Magnetometer	Air-Core Induction Loop	Saturable Reactor "Fluxgate"	Single Axis SQUID Magnetometer
Frequency Range (Hz)	DC to 10^3	30-130	0.1 to $5x10^4$	DC to $5x10^4$
Operation Bandwidth (Hz)	0.01 - 2	1	Variable	Variable
Minimum Detectable Magnetic Field Change (Gamma rms $Hz^{-1/2}$)	0.02	10^{-4}	10^{-2}	10^{-5}
Volume of Sensor Assembly (liters)*	23 (15 cm OD x 130 cm long)	- 600 turns 2 m. dia.	0.2 (3 cm diam. 20 cm. long	0.01 (1.2 cm diam. 7 cm. long)
Weight of Sensor Assembly (kg)	8	70	0.2	0.1
Weight of Total System (kg)	25	90	12	5 (exclusive of cryocooler) #
Total Input Power (W)	150	10	3	10 (exclusive of cryocooler) #
Turn-On Time (sec)	90 (typ.) 300 (max.)	-	-	-
	Note 1	Note 2	Note 3	Note 4

Comments:

* Sensor assembly alone not including remotely located electronics and power supplies.
# Seven day hold-time vertical dewar for SQUID systems has volume of 90 liters (30 cm OD by 130 cm long) and weighs about 25 kilograms)
Note 1 - Airframe mounted AN/ASQ-81; (AN/ASQ-81, Magnetic Detection Set, Texas Instruments, Inc., Dallas, TX 78767; June 1973 brochure).
Note 2 - ELF Air-core Induction Loop, (R. J. Dinger and J. A. Goldstein, Naval Research Laboratory, Washington, D.C., private communication.)
Note 3 - Model 6640 Magnetic Field Intensity Meter; (Electro-Mechanics, Inc. Austin, TX, brochure).
Note 4 - Single Axis SQUID magnetometer system with 3 inch diam. field coil; (Superconducting Technology, Inc. Mountain View CA; SHE Corporation, San Diego, CA; unpublished brochures).

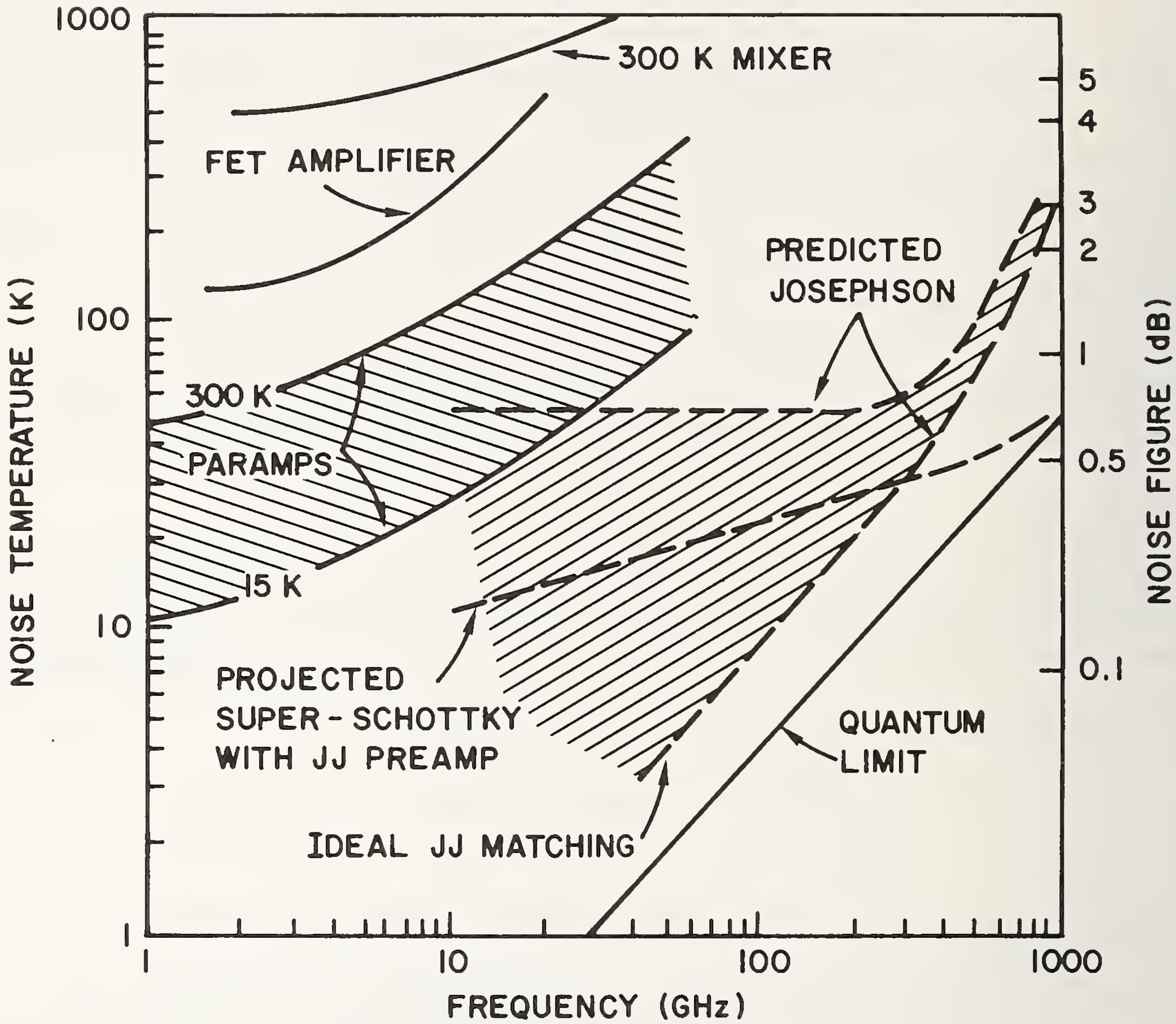

Figure 1. Comparison of the input noise characteristics of conventional and superconductive detection systems operating at microwave and milimeter wave frequencies.

TABLE II

MICROWAVE AND MILLIMETER WAVE DETECTION SYSTEMS

	GaAs FET Amplifier	Paramp	Paramp	Josephson Junction Amplifier
Frequency Range (GHz)	12-18	36	55-65	90-100
Bandwidth (GHz)	6	0.1	0.7	1.0
Noise Figure (dB)	8	3.8	5.8	0.5
Noise Temperature (K)	10^3	400	840	50
Small Signal Gain (dB)	30	18	14	1
P_{out} for 1 dB Compression (dBm)	+ 7	- 20	- 20	- 70
Dynamic Range (dB)	78	73	61	21
Volume (liters)	0.2	2.0	1.1	?
Weight (kilograms)	0.2	2.3	1.8	?
Prime Input Power (W)	3	10	5	10^{-3}
Heater Power (W)	0	40	10	?
Total Input Power (W)	3	50	15	?
Comments:	Note 1	Note 2	Note 3	Note 4

Note 1 - 12 VDC power supply not included (Model AMT 1800 series GaAs FET amplifiers built by Avantek, Inc. Santa Clara, CA, unpublished brochures).

Note 2 - Experimental model built by AIL, Inc. includes paraamp, downconverter, IF amplifier and DC power supply. (Microwave Journal, Feb. 1975, p 24).

Note 3 - Does not include 6 VDC power supply; (J. Wheleham, E. Kraemer and H. Paczkowski, Microwave Journal, Nov. 1973, p. 35).

Note 4 - Weight, volume and power requirements will be set by dewar or cryocooler to be used.

in
cry
whi
reg
rel
det

Key
res

The
on
re
to
cl
pu
li
ex

me
in
po
at
of
of
ma
te

ex
de

Potential Scientific Uses of Cryogenics in Space in the Temperature Range From 1 mK to 10K

E. Tward
Department of Physics and Astronomy
University of Regina
Regina, Saskatchewan
S4S OA2 Canada

and

P. V. Mason
Space Science Division
Jet Propulsion Laboratory
California Institute of Technology
Pasadena, California

In this paper we report the results of a survey of potential users of cryogenics in space. The survey was conducted informally in July, 1976, in order to determine the cryogenic needs of the scientific community for space experiments. The experiments which are described below are restricted to a temperature range extending from the mK region to liquid helium temperatures. Experimental areas identified are experimental relativity, He^3 and He^4 experiments, IR astronomy, microwave astronomy and cosmic ray detection.

Key words: Cryogenics for space; relativity in space; He^3 and He^4 in space; astronomical research in space.

I. INTRODUCTION

This paper reports the results of a survey of potential users of cryogens in space. The survey, conducted in July 1976, is intended for the determination of requirements on cryogenic systems in the foreseeable future with the intention of formulating a research plan to ensure that systems can be developed for space use in sufficient time to be available to users when required. This will allow their routine use on the wide classes of experiments which could benefit from low temperature techniques. For the purposes of the study the temperature range considered is 1 mK to 10K. The 1 mK lower limit is established by the temperatures which can be routinely reached in earth-based experiments.

Cryogenic devices have found wide use in earth-based research chiefly due to improvements attainable through reduction of thermal fluctuations in these devices. This results in the production of amplifiers and detectors of unprecedented sensitivity and low noise powers. Examples of this are the SQUID amplifier with an equivalent noise temperature at the input of ~ 10^{-6}K and superconducting IR detectors with a figure of merit an order of magnitude better than those currently in use. In addition, there exist a number of devices which make use of superconductivity (e.g., superconducting digital circuits, magnets, e-m shields, magnetic bearings) which can only be constructed at cryogenic temperatures.

The major experimental areas identified in this study are experimental relativity, experiments in He^3 and He^4, IR, microwave and gravitational astronomy, and cosmic ray detection.

Development of cryogenic techniques for space could in addition provide the opportunity to use devices of general utility in space. These include gryoscopes for guidance, superconducting bearings, low noise microwave receivers for communications and superconducting motors.

2. RELATIVITY EXPERIMENTS

Experimental relativity benefits greatly by the use of cryogenic temperatures.[1, 2] Many experiments can only be performed at these temperatures, due to the weakness of gravitational forces. For example, the ratio of gravitational to electric forces between a proton and an electron is:

$$\frac{Fg}{Fe} = \frac{Gm_p m_e}{e^2} = 4.4 \times 10^{-40}.$$

Since the motion of the objects responding to these forces is so small, it is often imperative that the background thermal vibration against which these motions are measured be reduced to a minimum. This can only be achieved by the reduction in thermal energy. Because the effects to be measured are so small, experiments in this field are extremely carefully thought out before they are attempted. In particular, disturbing extraneous forces must be carefully considered and eliminated by very careful experimental design and, if required, in reduction of the data. An example of this is the Stanford gyro experiment which has been 15 years in design and construction. The subtlety of the experiments and their implications for cosmology and the study of evolution of our universe and astronomical sources makes research in this field challenging and rewarding.

Three experiments are being actively developed at present (gravitational radiation detection, Stanford gyro, and equivalence). In addition a number of experiments which require cryogenics to reduce dissipation and a space location to produce a quiet environment have been proposed [3].

2.1 Gravitational Radiation Detection

These experiments have great implications for general relativity, cosmology and astronomy. If successful, they will confirm that gravitational radiation exists, as predicted by all gravitational theories except the Newtonian one. Detection of the radiation will shed some light on the validity of competing gravitational theories. Most important, perhaps, is that discovery of gravitational radiation will open a new window on the universe, mitigating the limits to our knowledge imposed by our previous restriction to the e-m spectrum and particle detection. Sensitive enough antennae could detect gravitational radiation emitted by a large variety of proposed sources, including quasars, stellar collapse into a black hole, supernova explosions, binary star systems, dying binary systems, pulsars and birth of new pulsars. Antennae now being constructed are reaching the sensitivities which theoreticians suggest are required to detect expected radiation fluxes [4].

The Weber detector will certainly require cooling [5] This detector consists of an antenna in the form of a cylinder. Under the action of gravitational radiation the antenna would be set into the vibration. With a transducer sensitive to vibrations at a normal mode of the bar (usually the first longitudinal mode), the gravitational radiation could be detected. To date an antenna of this type 1.5 meters long, operated at room temprature, has been able to detect vibrational amplitudes of 10^{-16} to 10^{-17} m (one hundredth the dimension of a nucleus). The limit on this sensitivity has been imposed by the thermal vibrational of the antenna itself. A number of groups are now attempting to cool antennae in order to improve their sensitivity by many orders of magnitude.

Cryogenics are required basically for the following reasons: reduction of thermal noise level in antennas; use of low noise amplifiers (probably SQUIDS); e-m shielding available with superconducting shields, and vibration thermal isolation available with a magnetically levitated antenna. That the lowest achievable temperatures will undoubtedly be required for a flyable antenna is suggested by the fact that a number of groups are now constructing antennae for operation on earth in the mK temperature region.

The choice of a space environment benefits the experiment since vibration isolation becomes increasingly difficult on Earth, especially if the antenna operates at low frequency. The most attractive cryogenic experiment for space is the detection of gravitational radiation from the Crab Nebula at 60 Hz as proposed by Weber [6]. Also, the possibility of long baselines between two or more antennae, which is necessary for spatial resolution, is available in space.

Preliminary estimates for the cryogenics required are given in Table I.

Table I - Relativity Experiments

Experiments	Temperature	Temperature Stability	Cooled Volume	Cooled Mass	Lifetime of Experiment	Ref.
Gyroscope	<2.2K	-	cylinder 0.4 m diameter x 1.5 m long	50 kg	1-2 years	[7]
Gravitational Wave Detector	<2.2K	<0.1K/week	cylinder 0.3 m diameter x 3.5 m long	300 kg	7 days	[5]
	10^{-2}K	$<10^{-3}$K/week	"	"	"	
Equivalence	<2.2K	-	20 litres	10 kg	1 day-1 year	[10]
Gravitational Spin-Spin Coupling	<0.1K	10^{-2}K/week	10 litres	5 kg	12 days	[3]
$\frac{\dot{G}}{G}$	1K	10^{-2}K/week	cylinder 0.4 m diamter x 0.4 m long	200 kg	1 week	[3]

2.2 Stanford Gyro Experiment

This experiment [7, 8], which has been funded since 1963 and is under active development, will probably be the first relativity experiments to be flown. The experiment tests Einstein's general theory of relativity by measuring the precession rate of one or more gyroscopes with respect to the axis of a telescope pointing at a suitable fixed star. In particular, the relativistic precession rate of a gyroscope in free fall about a rotating massive sphere (the earth), which was calculated by Schiff [9], is measured.

The experiment must be done in space in order to take advantage of the large mass and moment of inertia of the earth, the reduction of suspension forces and torques achievable on a gyro in space and the capability to utilize a drag-free satellite to reduce g.

It is proposed to develop a satellite which is essentially a free-flying dewar incorporating a drag-free controller. The cryogenic package is also a He dewar constructed totally of non-magnetic materials. It is first precooled in a low magnetic field facility and then inserted into the main flight dewar. Contained in the inner dewar are 4 gyroscopes, a zero g proofmass for the drag-free controller and a telescope used to orient the apparatus. Temperature required is < 2.2 K and is provided by superfluid He. Temperature stability provided by the He film is sufficient. An additional rationale for using superfluid is that this will eliminate bump boiling of the He which would send vibrations through the apparatus. Cryogenic estimates are given in Table I.

2.3 Equivalence Experiment

This proposed experiment [10] tests the weak equivalence principle, which states that the ratio of gravitational mass to inertial mass is the same for all bodies, irrespective of their composition. To date, earth-bound experiments have tested this hypothesis to at best 1 part in 10^{12}. Using cryogenic techniques in space it is hoped to improve these measurements to 1 part in 10^{17}. An experiment of this precision would allow one to test this fundamental postulate of gravitational theory.

The experiment consists of measuring the relative accelerations of two masses whose centers of mass are nearly coincident. The two masses are superconducting coaxial cylinders whose positions are sensed by superconducting coils. A feedback circuit drives the masses back to their equilibrium positions. Currents in the feedback circuit constitute the signal determining the motions of the cylinders which are being measured.

The two chief motivations for a space experiment are: firstly that disturbing forces are smaller in space. On earth the experiments would be limited by seismic noise to a precision of at best 1 part in 10^{13}; secondly, the driving acceleration in space may be the full gravitational attraction of the earth ~ 950 cm/sec^2. On earth the driving accelerations are derived from the sun or the earth's rotation and are three orders of magnitude smaller.

One is driven to the use of cryogenic techniques at this sensitivity by the following considerations. Gravity gradient effects on the test masses restrict the distance between the centers of mass to 10^{-8} cm or less. This forces abandonment of the traditional torsion balance technique and requires large improvements in sensitivity and stability. Using cryogenic techniques to measure the relative acceleration of two coaxial cylinders, this sensitivity may be achieved. Cooling the apparatus reduces the thermal noise, allows the use of superconducting magnetic shields and allows superconducting position sensors using SQUID amplifiers.

Many of the necessary techniques have already been developed for this and associated projects. It is hoped that the earth-based experiment will eventually yield sensitivities of ~ 1 part in 10^{13}. A satellite experiment as proposed tests the theory to 10^{-17} in an experiment lasting an hour and 10^{-19} in a year. If the system were increased to m = 100 kg as appears feasible and T reduced to 10^{-2}K, the equivalence principle would be tested to 10^{-22} at best. Given that the experiment must be done at cryogenic temperatures, it is apparent that reduction of temperature from the 2 K region to the 0.01 K region would give either the same resolution in 100th the time or 10 times the resolution with the same integration time.

The unprecedented sensitivity of this experiment would require a cryogenic system with the properties outlined in Table I

3. He EXPERIMENTS

These experiments are important not only for their intrinsic scientific interest but for their impact on future engineering of cryogenic systems in space as well. Measurements near the transition temperature where He^4 becomes a superfluid (λ-point) will contribute to our understanding of the theories of cooperative transitions in a wide variety of systems. Since cooperative transitions occur in solids as well as in phase changes from liquids to gases, study of the λ-point contributes to an understanding of these other systems as well. Experiments on superfluid films are of intrinsic scientific interest and as well are required for an engineering understanding of heat transfer mechanisms to a superfluid cryogen bath. Experiments on bulk superfluids are necessary for engineering purposes if superfluid He is used as a cryogen. Studies of the liquid-gas interface in He under zero-g conditions will contribute to the theory of these interfaces in all such systems. He^3 -He^4 mixture experiments in a zero-g environment will allow one to engineer the next generation of flyable refrigerators operating at temperatures substantially below 1 K.

3.1 Specific Heat near the λ-Point

λ-point experiments on helium provide information on the nature of the theories of all cooperative transitions. Of all cooperative transitions, study of the λ-point is the one most accessible to precise experimental measurements close to the transition temperature. This results from the intrinsic properties of helium for which the experimentally measured properties are not smeared by crystal structure defects, impurities, strains, etc., as in solids nor by the divergence of the compressibility and thermal relaxation time which makes measurements near the gas-liquid critical point difficult. Historically, whenever more precise specific heat measurements near the λ-point have been made in helium, great activity has been generated in study of phase transitions in a wide variety of other systems.

The experiment is of necessity cryogenic since the λ-point is at a temperature of $T_\lambda \sim 2.2$ K. To date, earth-bound experiments have approached T_λ to a temperature T given by:

$$\varepsilon = \frac{T}{T_\lambda} - 1 \simeq 10^{-6} .$$

In a finite sample on earth, this is just about the limit one can attain before the transition temperature is smeared by density gradient effects resulting from the earth's gravitational field. In a low-g environment the measurements can be improved to:

$$\varepsilon \simeq 2 \times 10^{-10} \text{ [11].}$$

Near T_λ, the coherence length, r diverges as $r \sim 2 \times 10^{-8} |\varepsilon|^{-2/3}$ cm. For a space experiment with $g/g_o = 10^{-3}$, a minimum temperature resolution $\varepsilon_o = 8 \times 10^{-10}$, an optimum sample height $h_o = 1.40$ cm and 4 days measuring time, the specific heat could be measured to 1%. With $g/g_o = 10^{-4}$, $\varepsilon_o = 2 \times 10^{-10}$, and $h_o = 3.5$ cm, a 1% measurement could be made in 18 days.

Cryogenic requirements on the temperature stability and thermometry are very stringent. the system to be cooled would have the representative properties listed in Table II.

Table II He Experiments

Experiment	Temperature	Temperature Stability	Thermometric Resolution	Size of Experiment Cooled	Exper-imental Time	Reference
Specific Heat	2.2K	10^{-12}K/sec	10^{-12}K	5 kg	4 days	[13]
Velocity of Sound near λ-point	2.2K	10^{-12}K/sec	10^{-12}K	5 kg	4 days	[14]
Liquid Gas Interface in Helium Near Its Critical Point	He^4 5.2K He^3 3.2K	10^{-3}K/sec	$<10^{-3}$K	5 kg	1 day	[15]
He^3-He^4 Mixtures	0.1K-2.2K	10^{-7}K/sec short term 10^{-12}K/sec long	$<10^{-7}$K	5 kg	1 week	[16]
Dynamics of Bulk Super-fluid Helium and Dynamics of Thick Superfluid Films	<2.2K	Measured		sphere 30 cm diameter 9 Kg	2 days	[18]

3.2 Velocity of Sound Near the λ-point

This experiment [12] is very similar to the specific heat measurements and could perhaps be done at the same time. The experiment proposes to measure the velocity of first sound, u, as close to the λ-point as feasible. u is given by:

$$u-u_\lambda = \frac{12 \times 10^9}{C_p}$$

where u_λ is velocity of sound at T and C_p is the specific heat. Therefore, measurements of u could give essentially the same information as specific heat experiments and is considered here because of the ease with which it can be measured.

Experimental cryogenic requirements would be similar to those for the heat capacity measurements listed in the previous section.

3.3 Liquid-Gas Interface in Helium Near Its Critical Point

The suggested experiment [13] aims at elucidating the behavior of the interfacial region between liquid and vapor phases of He in the critical region and thus contributes fundamentally to a theoretical understanding of the critical region. By measuring the surface tension σ and the density ρ (x), information for the use of either He^3 or He^4 cryogens in space could be obtained. A knowledge of σ and ρ would contribute to the modelling of the distribution of a liquid-gas system in a container under low g conditions.

The space environment is ideal for these measurements since on earth the gravitational forces establish a density gradient across the sample so that the sample is at a critical point only in a single plane perpendicular to g. Corrections which in principle can be made on earth-bound measurements are limited by knowledge of the equation of state, which is basically what one is attempting to measure. Surface properties will undoubtedly be affected by the reduction of g. Whether the thermodynamic properties associated with the interface will be modified in an essential way is an open question whose answer will have a significant effect on an understanding of the interfacial region. Experimentally, one is further helped by low g conditions since measurements of σ by a differential capillary rise method involving capacitive sensing is a method whose sensitivity is inverse to g.

3.4 He^3 - He^4 Mixtures

Study of He^3 - He^4 mixtures [14] could provide useful information on these systems. Study of the tricritical behavior where the λ-line meets the two-phase region would give information on the properties of this system in the transition region. Measurement of quantities such as heat capacity, vapor pressure and osmotic pressure, sound and second sound, and light scattering in a near zero-g environment would allow the tricitical point to be approached perhaps two to three orders of magnitude closer than is now possible on earth-bound experiments. On earth, experiments are limited by the earth's gravitational field which smears the transition temperature due to the very strong dependence of the concentration susceptibility $(\partial X/\partial \Delta)_{T,P}$ on the density of the fluid. Since the density on earth is height dependent, this imposes a severe restriction on the nearness of approach to T_λ. This is partially overcome in earth based experiments by reducing the height h of the sample and hence the temperature difference between the top and bottom of the container. On earth with:

$$\left(\frac{\partial X}{\partial \Delta}\right)_{T,\rho} \sim \frac{10^{16}}{|T-T_\lambda|} \text{ ergs}^{-1}$$

we are limited to $|T-T_\lambda| \sim 10^{-3}$K, with $h \sim 10^{-2}$ cm. There are limits to reducing h since the mixtures have different properties in small containers from their behavior in the bulk fluid. Reducing g to 10^{-3} g_o, as in the Space Shuttle, would allow a reduction of $T-T_\lambda$ by three orders of magnitude and hence, a significant improvement in the study of this system near the critical point.

An important additional problem is the nucleation of phase separation in metastable mixtures. This is not only of intrinsic interest but is also critical for the use of He^3 - He^4 dilution refrigerators in space. These refrigerators are now the first choice on earth in the temperature region of 10^{-2} K to 0.8 K.

A system capable of doing these experiments would have the cryogenic requirements listed in Table II.

3.5 Superfluid Agglomerates

This study [15] would investigate the possibility of creating in zero-g a new class of superfluid structures consisting of phase agglomerates of superfluid He^4 and either liquid He^3 (emulsions) or He^3 - He^4 vapors (foams). If these systems can be made stable, they would allow cryogenic engineers to design with space filling materials with variable thermo-mechanical properties intermediate between superfluid helium and either normal helium gas or liquid. The stability of these systems has engineering significance for the construction of flyable He^3 - He^4 dilution refrigerators to operate in the temperature region of 10^{-2} K to 0.8 K. These refrigerators now depend on moving either He^3 or He^4 across a phase boundary between the two phases of the mixture produced below 0.8 K. On earth the two phases are separated because of their different densities and the presence of the earth's gravitational field.

In a zero-g environment one might expect that when the two phases are mixed, the emulsion produced could be made meta-stable, since gravitational separation could no longer be a dominant mechanism. This may allow significantly increased times for study of the "metastable" states and the properties associated with them.

Production of these systems in space would provide a new class of superfluid structures allowing simplified measurements of restricted geometry effects and magnification of surface properties. A study of transport properties in superfluids of this type would be of great theoretical interest. It is possible that vortex dynamics could be studied in systems of this type.

At the present time an experimental design is premature.

3.6 Dyanamics of Bulk Superfluid Helium

This experiment [16] studies the bulk low frequency sloshing frequencies, damping and temperature distributions in a volume of superfluid He where the helium is dominated by surface tension forces rather than gravitational forces. The experiment is of great significance for understanding the properties of the superfluid in space. This is especially important for spacecraft designers wishing to understand the mechanical and thermal effects of bulk HeII liquid motion under a zero-g environment.

The ratio of gravitational to surface tension forces on a liquid is described by the Bond number B_r

$$B_r = \frac{\Delta\rho L^2 g}{\sigma}$$

where $\Delta\rho$ is the density difference between liquid and vapor, σ is the surface tension, g the acceleration and L a characteristic length of the container. For a 10^{-4} g environment, $B_r \sim 10^{-1}$ to 10^{-2}; hence, surface tension effects dominate. Therefore, in a partially filled dewar, large amplitude, low frequency motions could be expected where driven by external accelerations. This may have important consequences on thermal stability in the bath, thermal contact to the bath and on the feedback attitude control system of small spacecraft.

It is proposed to measure the fluid distribution using many liquid-vapor sensors. From this the distribution of the cryogen and the frequency and damping of the oscillations could be determined. In addition, temperature sensors will give an indication of the maximum temperature deviation which can be expected. The experiment can be performed in conjunction with any other experiment which uses superfluid He as a cryogen simply by instrumenting the cryogen bath with liquid vapor sensors and thermometers. The sensors, already developed and used on a rocket experiment, will fill the available bath.

Typical cryogenic requirements for this are listed in Table II.

3.7 Dynamics of Thick Superfluid Films

This experiment [16] proposes the study of quantized surface waves in thick superfluid films. Because superfluid helium has no viscosity it flows readily and forms thin films on surfaces due to Van der Wall forces. Under zero-g conditions this film, expected to coat all internal dewar surfaces, will provide an efficient heat link to the cryogenic bath.

A unique wave mechanism existing in HeII film is third sound, the propagation of gravity waves on HeII films thinner than a viscosity length λ_n.

$\lambda n = \frac{2\eta_n}{\rho_n \omega}$ where η_n is the viscosity of the normal fluid, ρ_n its density and ω the frequency. In this regime, the normal fluid is clamped to the substrate by its viscosity so that all motions take place in the superfluid. The dispersion relation for the wave motion in clamped HeII is given by:

$$c^2 = \frac{(g + \alpha/d^n)}{k} + \frac{\sigma}{\rho} k \tanh kd$$

where c is the wave velocity, g is the acceleration due to gravity, k is the wave vector, σ is the surface tension, ρ the density and d the thickness of the liquid film. The gravitational and Van der Wall's forces give the $\frac{g + \alpha/d^n}{k}$ term. For long λ and low frequencies, the g/k term dominates and the waves are gravitational. For short λ and high frequencies, the surface tension dominates and the waves are described as capillary. In a zero-g environment, capillary waves at frequencies at low as 1 Hz could be studied in films as thick as 10 μm. Measurements will allow extension of experiment and the theory of capillary waves to this frequency region in these thick films.

Study of capillary waves in a 1 g environment, even at higher frequencies, is impossible because of attenuation, how thin the films must be to meet the damping condition, and inability to maintain film uniformity. It is proposed to carry out this experiment in an integrated package with the bulk superfluid experiment.

Cryogenic estimates are given in Table II.

4. ASTRONOMICAL EXPERIMENTS

These experiments make use of space in order to eliminate obscuring effects due to the earth's atmosphere. The experiments can be categorized into three types. First are the detectors of e-m radiation, i. e., telescopes for IR and microwave regions of the e-m spectrum. Second are particle detectors of various types. Third is an experiment previously described to detect gravitational radiation.

Telescopes are now being designed for flight. These are chiefly for observation in the IR region of the spectrum, for example, the IR Astronomy Satellite. Additional IR facilities and microwave receivers are now under active consideration and are in early design and proposal stages. The IR telescopes all use cryogenic techniques. Microwave "telescopes" in space will make use of cryogenic techniques when the users can be assured that the lowest noise systems now available (maser amplifiers, [17, 18] cooled parametric amplifiers and super-Schottky microwave mixers [19] can be reliably flown with available cryogenic techniques. Amplifiers cooled to liquid He temperatures have noise temperatures at the input of 1.5 to 2 orders of magnitude lower than the best room temperature amplifiers [20]. Particle detectors under consideration would require superconducting magnets; hence, their inclusion in this study.

4.1 IR Telescopes

IR telescopes are cooled in order to reduce the infrared radiation emitted by the telescope itself. This improves the sensitivity of the telescopes since the instrument noise is reduced. The ultimate limit to the required cooling is imposed by the cosmic background radiation which is inescapable and is due to black-body radiation at 2.7 K. In addition, various types of IR detectors must be cooled in order to achieve required performance. (Missions involving IR telescopes or facilities include IRAS, Space Telescope, and Shuttle IR Telescope Facility.)

Interest in studying astronomical sources of infrared radiation is motiviated by attempts to understand both galactic and extragalactic sources. Because of obscuration by the earth's atmosphere, these measurements can best be done from a space environment. For galactic sources, the origin, constitution and replenishment of interstellar matter, the problem of star formation and the energy balance in HeII regions and molecular clouds can be studied by looking at the IR spectral region. For extragalactic sources, many of which emit mainly in the IR, an understanding of their luminosity in this region of the spectrum is a major astrophysical problem.

A. IRAS. With this Infrared Astronomy Satellite (IRAS) satellite, it is proposed [21] to undertake an all-sky survey to measure the IR flux in four wavelength bands centered at 10, 20, 50, and 100 μm. Since the aim of IRAS is to produce an all sky survey with unprecedented sensitivity, it is likely that a large number of new sources will be detected which will warrant further study. Part of this can be done with IRAS since 50 percent of the available time is reserved to special observational programs. Additional special studies would probably be performed using more higher resolution systems such as the proposed SIRTF [22], discussed below. The baseline IRAS system is capable of detecting sources similar to those already known to distances up to 3 orders of magnitude greater than the distances to known sources. Design of this system is well advanced and therefore will not be reproduced in this study.

The cryogenic design is driven by the requirement to reduce flux from the telescope itself and to cool the detectors. Cryogenic temperatures in the 1 - 4 K region are essential. As now proposed, the telescope is likely to be cooled by the gas evolving from a superfluid He cryogen bath. The telescope will be maintained at a temperature less than 10 K. The telescope baffles will be cooled to less than 16 K. The focal plane assembly, including the IR detectors, will be cooled to ~3 K. In addition, a cryogenic removable cover operating between 5.3 and 10 K will be used to protect the telescope optics from contamination during and after launch. Projected heat loads are 10 mW for the detectors at 3 K and 6 mW for the telescope at 5 - 10 K and 50 mW for those parts (baffling supports, etc.) cooled to 5.2 - 16 K. Extensive details are given in [21].

B. SIRTF. The shuttle infrared telescope facility (SIRTF) as proposed [22] is intended to be a man-operated astronomical observatory to perform infrared observations from the shuttle. An observatory of this type will allow extended observation of astronomical sources leading to a better understanding of galactic and extra-galactic sources of infrared radiation.

In order to obtain sensitivity in a space observatory in which incoming IR flux is not obscured by the earth's atmosphere, cooling of the telescope and detectors is required. Accordingly, it is proposed that a 1.0 meter class cryogenically cooled IR telescope will be provided with the capability to couple on a time sharing basis to a variety of IR instruments. Specifications for such a telescope facility have been written [22]. The proposed telescope barrel will be a large aperture dewar with sufficient cryogen stored to give a 30 day running time. The telescope will be ~ 1 meter in diameter and be cooled to 30 K or less. A cryogenic removable cover would be installed to allow cryopumping of contaminants during launch and while initially in flight. A multiple instrument chamber (MIC) will incorporate provisions for various instruments such as photometers, photoconductor detectors, Fourier spectrometers, polarimeters and grating spectrometers. Most of these will require cooling to liquid He temperatures. The cryogen is suggested to be superfluid He at ~ 2 K. Any instrument which requires cooling to He temperatures will be expected to use the 2 K reservoir as a heat sink.

A cryogenic design for such a telescope facility could have a number of features in common with that now being designed for IRAS. They include a similar cooling scheme and a similar contaminant control scheme.

4.2 Cosmic Background Studies

Cryogenics are chiefly required in order to realize the low noise performance of cooled amplifiers [20]. For the cosmic background experiments described herein this is crucial in one case. For the survey of cosmic background in the millimeter wavelength region the bolometers which are being suggested must be cooled. For cosmic background anisotropy experiments, cryogenic amplifiers would be useful but certainly not essential.

Study of the cosmic background microwave radiation provides a unique opportunity for study of the early pregalactic plasma stage of our universe. The radiation, characteristic of a black body of temperature 2.7 K, provides a window on the early history of the universe and its subsequent expansion and as such provides a test of the various proposed cosmologies. From previous study of cosmic background radiation and other astronomical evidence it would appear that the universe has evolved from an initial singular state or "big bang" as predicted using Einsteins's theory of general relativity. Since the photons of the radiation have not directly interacted with matter for almost all the history of cosmic evolution, study of this radiation provides a unique opportunity for gaining insight into the surface of the primordial hot plasma and inferring from small scale structure of that surface much of the early inhomogeneities which have lead to clumping and galaxy formation. A brief review of the scientific rationale for this study can be found in [20].

Two allied experiments are now under consideration for flight in the same cryogenic package.

A. Cosmic Background at Millimeter Wavelengths. The first is an experiment to measure the cosmic background radiation in the far infrared (or microwave) regions of the e-m spectrum for wavelengths between 0.5 to 3 mm.

The antenna would likely consist of an exponentially shaped horn of dimensions 1 m long and 30 cm aperture and would use bolometers as detectors. The spectrometer and cone would be cooled to temperatures ~2.7 K. Consideration is being given to developing bolometers to operate at 0.3 K in order to reduce the noise equivalent power (NEP) of the bolometer and hence increase their sensitivity.

B. Anisotropy of Cosmic Background. The second experiment proposes to survey the large scale anisotropy of the radiation [20]. The objective is to determine to high precision the dipole, quadrupole and higher order spherical harmonics of the cosmic background radiation field at frequencies in the range 18 - 90 GHZ. Determination of these forms of anistropy is an important problem of experimental cosmology bearing directly on the evolutionary history of the universe.

Earth based measurements have been dominated by problems due to variable atmospheric emission, hence the motivation for placing a system in orbit. This could be accomplished by mapping the microwave emission at several frequencies to a relative accuracy of 0.3 mK and an angular resolution of 15° over the entire celestial sphere. As initially proposed cryogenic techniques would not be required. However, should this experiment continue to be allied with the previous one, an opportunity would exist to use a cryogenically cooled amplifier having a sensitivity 2 orders of magnitude greater than those available at room temperature. This improvement could be used to reduce the time require to perform the experiment, to increase the relative accuracy, or to increase the angular resolution.

4.3 Cosmic Ray Detection

Study of high energy particles or cosmic rays incident on the earth is a subject with implications on cosmology. Identifying the incoming particles, their masses and energies can contribute to an understanding of galactic energy storage mechanisms, the 2.7 K cosmic background radiation through its influence on the electron spectrum, characteristics of the cosmic ray sources and the possible existence of primordial matter.

Magnetic spectrometers [23] incorporating cryogenically cooled superconducting magnets contribute to this study in the measurement of particle rigidities which are related to the particle momenta and charge. Since the spectrometer does not disturb the particle other than to change its flight direction, use of other available detection techniques in conjunction with the spectrometer would allow the particle to be separately identified as electrons, protons or individual nucleides and would distinguish between particles and anti-particles.

Cosmic ray particles can as well be used for studies in high energy physics. The highest energy particles avaiable to high energy physicists are not produced in large accelerators but rather arrive as cosmic rays.

Magnetic spectrometers using superconducting magnets have been successfully flown in balloons. The advantage to be gained by going to space comes from the fact that cosmic rays interact strongly with the atmosphere. An experiment above the earth's atmosphere would allow a study of the primary cosmic rays with potentially increased fluxes.

A cryogenic system suitable for space flight is similar to those already used for balloon-borne spectrometers. Typically it would consist of a dewar containing two large superconducting magnet coils. Two coils with opposing fields are required in order not to orient a spacecraft in the earth's magnetic field. Typical dewar dimensions are a cylinder 0.6 m long by 0.6 m diameter. The cryogen bath could be held anywhere in the temperature region of 1 - 5 K with no requirement on temperature stability. A suitable running time for a typical experiment would be a few days.

5. OTHER EXPERIMENTAL AREAS

Studies of the earth's atmosphere and cloud parameters might benefit from use of the very far infrared cooled detectors which are now being developed. At present, however, no definite proposals could be identified. It is to be expected that once these detectors have been developed for astronomical use and become generally available, use of these devices will become widespread in atmospheric physics research.

6. CONCLUSIONS

A number of research areas requiring flyable cryogenic systems at temperatures below 4 K have been identified. Systems requiring temperatures of 2 K for periods of a year or more now under active development for flight before 1980. Experiments operating to the mK temperature region are now being proposed. Provision of temperatures down to 1 K for extended periods now appears to be feasible. Considerable effort is, however, required for the development of flyable cooling systems working at temperatures below 1 K. A number of possible techniques are suggested in [24].

References

[1] Fairbank, W. M., "The Use of Low Temperature Technology in Gravitational Experiments," Proc. of the International School of Physics "Enrico Fermi" Course LVI, ed. B. Bertotti, Academic Press, New York (1974).

[2] Everitt, C. W. F., "Gravitation, Relativity and Precise Experimentation," in Marcel Grossman Proc. ed. R. Ruffini, Trieste, July 7 - 12, 1975, North Holland Press.

[3] Braginsky, V. B., Caves, C. M., and Thorne, K. S., Phys. Rev. D, 15, 2047 (1977).

[4] Rosi, L. A. and Zimmerman, R. L., "A Maximal Background Spectrum of Gravitational Radiation," Astrophys. & Space Sci. (Netherlands) 45, 447 (December 1976).

[5] Weber, J., General Relativity and Gravitational Radiation, New York Interscience, (1961).

[6] Weber, J., "Gravitational Radiation Experiments at Moderate and Low Temperatures," (in press), Proceedings of the Academia Nazionale dei Lincei International Symposium on Experimental Gravitation, Pavia, Italy, Sept. 17 - 20, 1976.

[7] Everitt, C. W. F., "The Gyroscope Experiment I, " Proc. of the International School of Physics "Enrico Fermi" Course LVI, ed. B. Bertotti, Academic Press, New York (1974).

[8] Lipa, J. A., Fairbank, W. M. and Everitt, C. W. F., "The Gyroscope Experiment II" in Proc. of the International School of Physics "Enrico Fermi" Crouse LVI, ed. B. Bertotti, Academic Press, New York (1974).

[9] Shiff, L. I., Proc. Nat. Aca. Sci., 46, 871 (1960).

[10] Worden, P. W., Jr., and Everitt, C. W. F., "The Gyroscope Experiment III, Tests of the Equivalence of Gravitational and Inertial Mass Based on Cryogenic Techniques," Proc. of the International School of Physics "Enrico Fermi" Course LVI, ed. B. Bertotti, Academic Press, New York (1974).

[11] Fairbank, W. M., Van Kann, F. J., and Lipa, J. A., "The Possibility of Performing in Space an Improved Measurement of the Lambda Point Heat Capacity Singularity" Proceedings Summary of the Conference on Quantum Fluids in Space, Eugene, Oregon, July 1, 2, 1975, ed. R. J. Donnelly and P. Kittel, p. 35.

[12] Rudnick, I., "Preliminary Feasibility Study for Lambda Point Experiment on Liquid Helium," ibid, p. 26.

[13] Northby, J. A. and Hallock, R. B., "The Liquid-Gas Interface in Helium Near its Critical Point," ibid, p. 16.

[14] Cole, M. W., Goldman, A. M., and Saam, W. F., "Possible Cryogenic Mixture Experiments in Two Component Systems in Space," ibid, p. 6.

[15] Campbell, L. J., "Proposal of STudy of Superfluid Dispersion," LASLP77, Los Alamos Scientific Library.

[16] Mason, P. V., "Dynamics of Bulk and Thick Film Superfluid Helium," Proposal to NASA, Investigation and Technical Plan, JPL Internal Document No. 750-86, June 11, 1976.

[17] Clauss, R. C. and Wiebe, E., "The Deep Space Network Progress Report for Jan. & Feb., 1973," JPL Technical Report 32-1526 Vol. XIX, April 15, 1973.

[18] Reid, M. S., Clauss, R. C., Bathker, D. A. and Stelzried, C. T., Proc. of the IEEE, 61, 1330 (1973)

[19] McColl, M., Milea, M. F., Silver, A. H., Bottjer, M. F., Pedersen, R. M., and Vernon, F. L., Jr., "The Super-Schottky Microwave Mixer," 1976 Applied Superconductivity Conference, Stanford University, Aug. 17 - 20, 1976, paper G1.

[20] Interim Study Report for Cosmic Background Explorer, Feb. 1, 1977, Goddard Space Flight Center, Greenbelt, Maryland.

[21] IRAS, "Report of the Joint Scientific Mission Definition Team for an Infrared Astronomical Satellite," May 1976.

[22] "Preliminary Design Study for Space Shuttle Infrared Telescope Facility Final Report," August 1976, NASA Ames Research Center, Moffett Field, California.

[23] Golden, R. L., and Badhwar, G. D., "Superconducting Magnets for Spaceflight," presentation to Research Goals for Cosmic Ray Astrophysics in the 1980's ESRIN, Frascati, Italy, October 24, 1974.

[24] Tward, E., "Refrigeration Below 1 K," Report to JPL/NASA, JPL Internal Document No. 900-756, August 1976.

vol
tio
vol
whe
Nat
tha

an
tio
sta
the
mai
sin
and
sec
Ele
or
whi
rf
wit
ing

cir
and
wer
des
The

Ins
jun
can
Mor
the
mat
of
to
pot
ope

Pe
Mon

Josephson Voltage Standards - An Application for Cryocoolers?

L. B. Holdeman and C. C. Chang†
Electricity Division, Institute for Basic Standards,
National Bureau of Standards, Washington, D.C. 20234

A Josephson-effect voltage-standard instrument, similar to but less accurate than the instrument used to maintain the U.S. legal volt, has been developed by the Electricity Division of the National Bureau of Standards. The Josephson device incorporated into this instrument operates with a combined rf and dc power input of less than one milliwatt. Microwave radiation is brought to the Josephson device via a small-diameter stainless-steel coaxial cable, so that the thermal load on the cryostat due to heat leaks is minimal.

Key Words: ac Josephson effect; Josephson junction; low temperature; superconductivity; voltage calibration; voltage standard.

When a Josephson junction is irradiated with microwaves of frequency ν, constant-voltage steps are induced in the I-V characteristic of the junction at voltages proportional to ν [1,2], and thus a Josephson junction can be used as a precision frequency-to-voltage converter [3]. The constant-voltage steps occur at integral multiples of $(h/2e)\nu$, where h is Planck's constant and e is the charge on an electron. On July 1, 1972, the National Bureau of Standards adopted the value $2e/h = 483593.420$ GHz/V_{NBS} [4], and since that date the U.S. volt has been maintained via the ac Josephson effect [5].

It has been estimated that more than six thousand laboratories in the U.S. maintain an "in-house" dc voltage reference [6]. Over three hundred of these utilize the calibration services of NBS, which require the transportation of Weston-type cadmium-sulfate standard cells to and from the NBS volt facility at Gaithersburg, Maryland. However, with the volt defined in terms of frequency through 2e/h, it is now possible for laboratories to maintain a unit of emf traceable to NBS without having to transport electrochemical cells, since frequency standards are broadcast throughout the U.S. by NBS on radio stations WWV and WWVH. A prototype Josephson-effect voltage-standard instrument, designed to be used by secondary standards laboratories to calibrate standard cells, has been developed in the Electricity Division of NBS [7-9]. The instrument has an overall accuracy (2σ) of 0.4 ppm or better [8], and will be commercially available [10]. The feature of the instrument which is perhaps most pertinent for cryocooler considerations is that the combined dc and rf power input required for the Josephson junction is less than one milliwatt, as compared with tens to hundreds of milliwatts for "conventional" Josephson voltage standards operating on the same voltage step.

The system consists of four major parts: a Josephson junction-microwave integrated circuit package (MIC), a microwave source and dc current supply for the junction, a dewar and probe, and a potentiometer system. The room temperature components of the instrument were developed by B. F. Field of the Electricity Division staff. The dewar probe was designed by V. W. Hesterman, an NBS Research Associate from Superconducting Technology, Inc. The MIC used in the instrument was developed by the authors [9].

The design of the potentiometer system makes the instrument extremely simple to use. Instead of the usual procedure of adjusting the microwave frequency to "fine-tune" the junction voltage to match the potentiometer output, the potentiometer ratio is adjusted and can be varied sufficiently to accomodate both saturated and unsaturated standard cells. Moreover, the Josephson junction need not be employed for each and every cell measurement: the potentiometer incorporates a constant current source which is "standardized" by matching the potential drop across the resistor network to the junction voltage. The drift of the current source is less than 0.2 ppm/hr. Thus the Josephson junction is needed only to determine the initial potentiometer current setting and for periodic readjustment of the potentiometer current to compensate for drift; i.e. for less than five minutes per hour of operation.

†Permanent address: Department of Electronics, The Chinese University of Hong Kong, Shatin, Hong Kong.

Except for the MIC, the major parts of the instrument are described in detail elsewhere [8] and will not be described further in this paper.

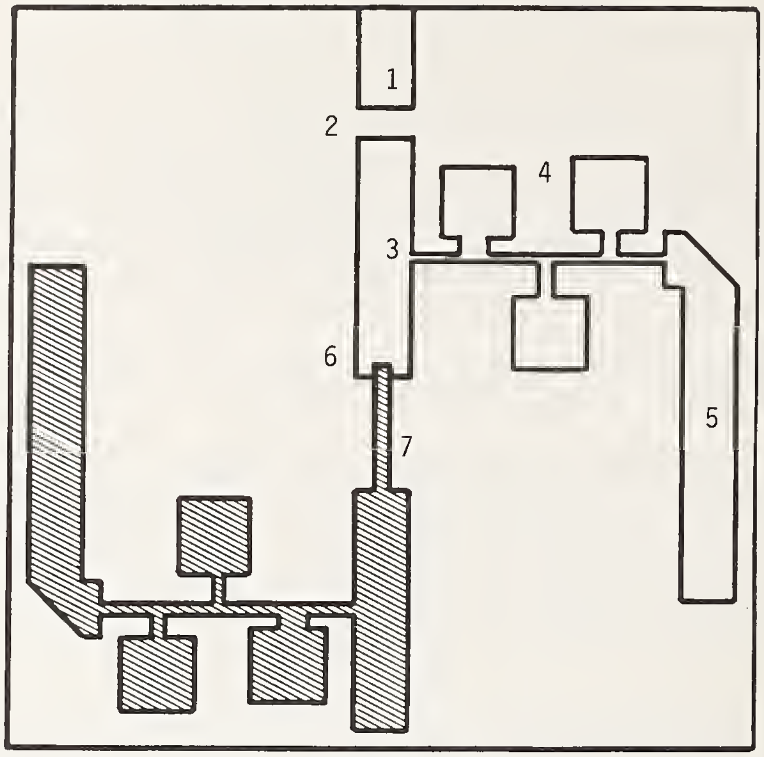

Figure 1: Josephson junction-microwave integrated circuit developed for the one-ppm 2e/h voltage standard: (1) Section of 50 Ω microstrip transmission line for contact to coax-to-microstrip launcher, end-coupled to one of two microstrip resonators; (2) Gap between launch pad and resonator determines the loaded Q of the coupled resonators; (3) Half-wavelength microstrip resonator; (4) DC lead incorporating an elliptic-function low-pass filter (5) Section of 50 Ω microstrip transmission line terminating the low-pass filter and forming a contact pad for attaching external dc leads (6) Josephson tunnel junction formed at the overlap of the two superconducting films; (7) Section of high-impedance microstrip transmission line coupling the two microstrip resonators.

The geometry of the MIC is shown in Fig. 1. The circuit is produced by evaporating Pb films through stencil masks onto 25 mm x 25 mm x 0.8 mm glass substrates; the shaded and unshaded parts of the circuit are evaporated separately. An oxidation process is carried out between evaporations so that a Josephson tunnel junction is formed where the two films overlap. The Pb films are made thin (thickness $\lesssim$ 200 nm) so that the $Pb/PbO_xO_y/Pb$ tunnel junction can be cycled several times between room and liquid helium temperatures; $Pb/Pb_xO_y/Pb$ tunnel junctions can be stored indefinitely at 77 K.

The circuit is mounted in an enclosed MIC package with an aluminum ground plane beneath the substrate; thus, except for the Josephson junction, the circuit is composed of sections of microstrip transmission line which are combined to form resonators, low-pass filters, coupling elements, and filter terminations and contact pads for external dc leads.

Microwave power is brought into the cryogenic environment via a small diameter stainless steel 50 Ω coaxial cable and into the MIC package through a commercial coax-to-microstrip adaptor to a short section of 50 Ω microstrip transmission line. This section of microstrip line is end-coupled to a "half-wavelength" microstrip resonator, which in turn is coupled to a second microstrip resonator through the junction impedance and a short section of high impedance microstrip line. This "double-resonator" configuration results in excellent coupling of the microwave radiation to the Josephson junction.

The MIC operates at 4.2 K and 9 GHz on a constant voltage step at approximately 5.2 mV [7]; the exact rf power required depends on the junction resistance. Junction resistances can be between 0.4 and 1.0 Ω (the lower limit is set by junction self-heating and the upper limit by the minimum acceptable height of the current steps); the corresponding rf power inputs required for steps at 5.2 mV are 0.9 and 0.25 mW respectively (measured at the top of the cryostat). For 0.9 mW power input the reflected rf power was 0.1 mW. Junction dimensions are approximately 75 μm x 125 μm. A more detailed description of the MIC and its development is given in another publication [9].

In addition to the support structure and stainless steel coaxial rf cable, other necessary heat leaks are due to six dc leads and a hollow fiberglass tube to actuate a superconducting mechanical switch. In the prototype instrument, there are four 0.13 mm diameter (#36 AWG) wires of SiCu alloy for junction current and voltage leads, and two 0.16 mm diameter (#34 AWG) copper leads connecting the junction to the potentiometer. The superconducting switch is a shorting-type switch that is used to null thermal emf's in the potentiometer leads, and could be eliminated for cryocooler applications by attaching the potentiometer leads directly to the junction contact pads with superconducting solder, or by a modification of the measurement procedures.

In conclusion, a prototype Josephson-effect voltage-standard instrument has been constructed and operated. The Josephson device developed for the instrument requires less than one milliwatt of power for operation, and the heat leak to the cryogenic environment through dc and rf connections to the device is very small. Our future R & D plans include producing the MIC from more durable materials, producing the MIC from higher-T_c materials, and investigating MIC's incorporating Josephson junctions of different types.

Development of the prototype Josephson-effect voltage-standard instrument was supported in part by the Calibration Coordination Group of the Department of Defense. Additional partial support for the MIC development was provided by NASA through GO# H-27908B. The authors would like to thank Jaan Toots for his untiring assistance, especially in junction fabrication, and to thank B. F. Field and T. F. Finnegan for many valuable discussions. One of us (CCC) acknowledges with appreciation a travel grant from the Ford foundation.

References

[1] Josephson, B. D., Phys. Lett. 1, 251 (1962).

[2] Shapiro, S., Phys. Rev. Lett. 11, 80 (1963).

[3] Langenberg, D. N., Parker, W. H., and Taylor, B. N., Phys. Rev. 150, 186 (1966).

[4] NBS Tech. News Bull. 56, 159 (1972).

[5] Field, B. F., Finnegan, T. F., and Toots, J., Metrologia 9, 155 (1973).

[6] Belecki, N. B. (Chief, Electrical Reference Standards Section, Electricity Division, NBS), private communication.

[7] Field, B. F. and Hesterman, V. W., in Fifth Cal Poly Measurement Science Conference Proceedings, (held Dec. 5-6, 1975, at California Polytechnic State University, San Luis Obispo, California), Session 75-1, p. 1.

[8] Field, B. F. and Hesterman, V. W., IEEE Trans. Instrum. Meas. IM-25, 509 (1976).

[9] Chang, C. C., Holdeman, L. B., and Toots, J. (to be published).

[10] The Josephson-effect voltage-standard instrument will be marketed by Superconducting Technology, Inc., of Mountain View, Calif. This information is included for the convenience of the reader and should not be construed as an endorsement or recommendation by the National Bureau of Standards. Technology developed by NBS is in the public domain.

Photograph of Delegates

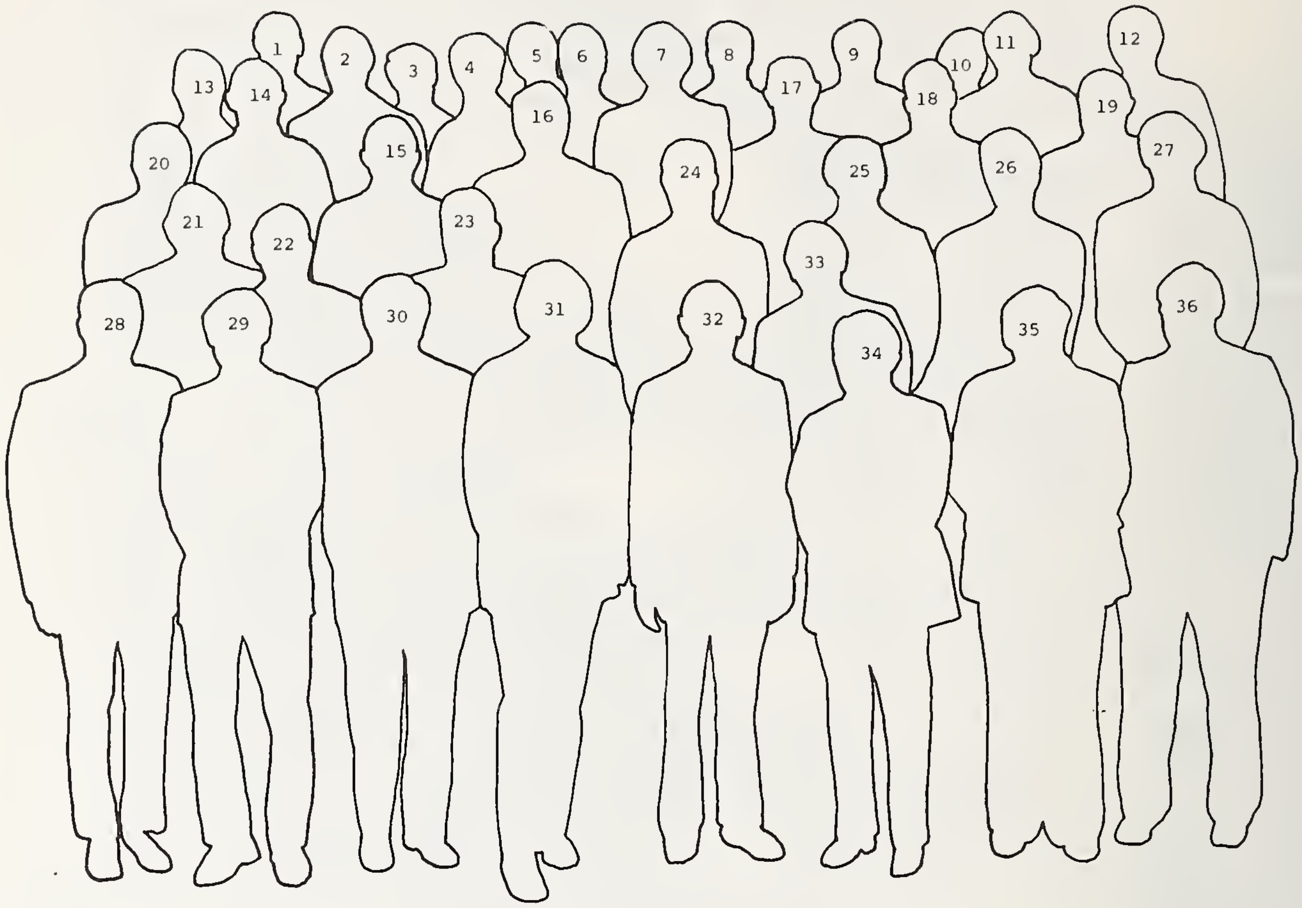

IDENTIFICATION OF PHOTOGRAPH

1. P. Durenec
2. R. Brandt
3. L. Holdeman
4. J. Goodkind
5. D. Sullivan
6. S. Williamson
7. W. Steyert
8. M. Simmonds
9. B. van der Hoeven
10. G. Karr
11. W. Little
12. J. Hummeldorf
13. L. Ishol
14. D. McDonald
15. W. Hartwig
16. A. Silver
17.
18. B. Renyer
19. J. Cox
20. J. Harvell
21. M. Nisenoff
22. F. Chellis
23. W. Gifford
24. J. Edrich
25. W. Goree
26. J. Zimmerman
27. M. Beasley
28. S. Horn
29. R. Radebaugh
30. R. Longsworth
31. J. Vorreiter
32. R. Guernsey, Jr.
33. B. Troutman
34. W. Higa
35. M. Tward
36. P. Mason

ATTENDANCE LIST

CRYOCOOLER APPLICATIONS CONFERENCE
October 3 & 4, 1977

John Vorreiter
Research Scientist
244-7
NASA Ames Research Center
Moffett Field, California 94035
415-965-6525

Peter Mason
183-401
Jet Propulsion Lab
Pasadena, California 91103
213-354-4056

Walter Higa
238-528
Jet Propulsion Lab
Pasadena, California 91103
213-354-4240

Fred Chellis
CTI Cryogenics
266 Second Ave.
Waltham, MA 02154
617-890-9400

John Goodkind
Dept. of Physics B-019
University of California, San Diego
La Jolla, California 92093
714-452-3666

Bill Gifford
Syracuse University
Syracuse, New York 13210
315-423-3235

W. H. Hartwig
Electronic Materials Research Lab
Engineering Science Bldg. 439
University of Texas
Austin, Texas 78712
512-471-1754

Thomas M. Flynn
NBS - Cryogenics Division
Boulder, Colorado 80303
303-499-1000, ext. 4108

M. R. Beasley
Department of Applied Physics
Stanford University
Stanford, California 94305
415-497-1196

Ralph C. Longsworth
Air Products & Chemicals, Inc.
Advanced Products Department
1919 Vultee Street
Allentown, Pennsylvania 18103
215-398-8357

J. L. Hummeldorf
Actus, Inc.
7370 Industrial Road
Florence, Kentucky 41042

P. Durenec
U.S. Army Night Vision Lab
DRSEL-NV-SD
Ft. Belvoir, Virginia 22060
202-274-8331

S. Horn
U.S. Army Night Vision Lab
DRSEL-NV-SD
Ft. Belvoir, Virginia 22060
202-274-8321

Gerald R. Karr
University of Alabama, Huntsville
P.O. Box 1247
Huntsville, Alabama 35805
205-895-6330

Bryan Troutman
IBM
18100 Frederick
Gaithersburg, Maryland 20760
301-840-7228

Robert W. Guernsey, Jr.
IBM - Watson Res. Center
Yorktown Heights, New York 10598
914-945-2639

Bernard J. van der Hoeven
IBM - Watson Res. Center
Yorktown Heights, New York 10598
914-945-1593

John T. Harvell
CTI Cryogenics
266 Second Ave.
Waltham, MA 02154
617-890-9400

William A. Little
Physics Department
Stanford University
Stanford, California 94305
415-497-4233

W. D. Stanley
U.S. Geological Survey
Bldg. 25, Room 2294
Denver Federal Center
Denver, Colorado 80225
303-234-4091

Lyle M. Ishol
Code 792
Naval Coastal Systems Lab.
Panama City, Florida 32405
904-234-4142

D. Ashley Vincent
Department of Physics
University of South Florida
Tampa, Florida 33620
813-254-9581

William L. Goodman
Applied Physics Systems
Palo Alto, California
415-494-8492

William S. Goree
Superconducting Technology
Mountain View, California 94043
415-969-9400

Arnold H. Silver
Aerospace Corp.
Box 92957
Los Angeles, California 90009
213-648-5840

David E. Daney
NBS, Cryogenics Division
Boulder, Colorado 80303
303-499-1000, ext. 3595

Roland O. Voth
NBS, Cryogenics Division
Boulder, Colorado 80303
303-499-1000, ext. 3632

Louis B. Holdeman
Electricity Division (211.07)
National Bureau of Standards
Washington, D.C. 20234
301-921-3806

Viri Vrba
CTF Systems, Inc.
Port Coquitlan, B.C.
604-941-8561

F. Consadori
CTF Systems, Inc.
Port Coquitlan, B.C.
604-941-8561

Richard E. Harris
NBS, Cryogenics Division
Boulder, Colorado 80303
303-499-1000, ext. 3776

Michael B. Simmonds
SHE Corporation
San Diego, California 92121
714-453-6300

Bernard L. Renyer
Hughes Aircraft
Culver City, California 90230
213-391-0711

Jochen Edrich
Denver Research Institute
University of Denver
Denver, Colorado 80210
303-753-2241

John E. Cox
Naval Research Lab
Code 6430
Washington, D.C. 20375
202-767-2793

Manny Tward
University of Regina
Regina, Saskatchewan
Canada
306-584-4274

Richard Brandt
Office of Naval Research
Pasadena Branch Office
1030 East Green Street
Pasadena, California 91106
213-795-5971

Samuel J. Williamson
Physics Department
New York University
4 Washington Place
New York, New York 10003
212-598-2867

William Steyert
Los Alamos Scientific Lab
Mail Stop 764
P.O. Box 1663
Los Alamos, New Mexico 87545
505-667-4935

M. Nisenoff
Naval Research Lab
Code 6430
Washington, D.C. 20375
202-767-3099

Ray Radebaugh
NBS, Cryogenics Division
Boulder, Colorado
303-499-1000, ext. 3710

NBS-114A (REV. 7-73)

U.S. DEPT. OF COMM. BIBLIOGRAPHIC DATA SHEET	1. PUBLICATION OR REPORT NO. NBS SP-508	2. Gov't Accession No.	3. Recipient's Accession No.
4. TITLE AND SUBTITLE Applications of Closed-Cycle Cryocoolers to Small Superconducting Devices Proceedings of a Conference Held at the National Bureau of Standards, Boulder, Colorado, October 3-4, 1977			5. Publication Date April 1978
			6. Performing Organization Code
7. AUTHOR(S) James E. Zimmerman and Thomas M. Flynn, Editors			8. Performing Organ. Report No.
9. PERFORMING ORGANIZATION NAME AND ADDRESS NATIONAL BUREAU OF STANDARDS DEPARTMENT OF COMMERCE WASHINGTON, D.C. 20234			10. Project/Task/Work Unit No. 2750187
			11. Contract/Grant No.
12. Sponsoring Organization Name and Complete Address *(Street, City, State, ZIP)* The National Bureau of Standards and The Office of Naval Research, Arlington, Virginia 22217			13. Type of Report & Period Covered
			14. Sponsoring Agency Code

15. SUPPLEMENTARY NOTES

Library of Congress Catalog Card Number: 78-606017

16. ABSTRACT *(A 200-word or less factual summary of most significant information. If document includes a significant bibliography or literature survey, mention it here.)*

This document contains the proceedings of a meeting of specialists in small superconducting devices and in small cryogenic refrigerators. Industry, Government, and academia were represented at the meeting held at the National Bureau of Standards (NBS) on October 3 and 4, 1977. The purpose of the meeting was to define the refrigerator requirements for small superconducting devices and to determine if small cryogenic refrigerators that are produced in relatively large quantities can be adapted or developed to replace liquid helium as the cooling medium for the superconducting devices. Because the focus was on small superconducting devices, the discussion was primarily limited to refrigerators with capacities from zero up to a watt or two in the temperature range of 2 to 20 K. The meeting was jointly sponsored by the Office of Naval Research (ONR) and NBS.

17. KEY WORDS *(six to twelve entries; alphabetical order; capitalize only the first letter of the first key word unless a proper name; separated by semicolons)*

Cryocoolers; Refrigeration; Superconducting devices

18. AVAILABILITY [X] Unlimited	19. SECURITY CLASS (THIS REPORT) UNCLASSIFIED	21. NO. OF PAGES 238
[ ] For Official Distribution. Do Not Release to NTIS		
[X] Order From Sup. of Doc., U.S. Government Printing Office Washington, D.C. 20402, SD Stock No. SN003-003 -	20. SECURITY CLASS (THIS PAGE) UNCLASSIFIED	22. Price $4.25
[ ] Order From National Technical Information Service (NTIS) Springfield, Virginia 22151		

USCOMM-DC 29042-P74

☆ U. S. GOVERNMENT PRINTING OFFICE : 1978 261-238/63

NBS TECHNICAL PUBLICATIONS

PERIODICALS

JOURNAL OF RESEARCH—The Journal of Research of the National Bureau of Standards reports NBS research and development in those disciplines of the physical and engineering sciences in which the Bureau is active. These include physics, chemistry, engineering, mathematics, and computer sciences. Papers cover a broad range of subjects, with major emphasis on measurement methodology, and the basic technology underlying standardization. Also included from time to time are survey articles on topics closely related to the Bureau's technical and scientific programs. As a special service to subscribers each issue contains complete citations to all recent NBS publications in NBS and non-NBS media. Issued six times a year. Annual subscription: domestic $17.00; foreign $21.25. Single copy, $3.00 domestic; $3.75 foreign.

Note: The Journal was formerly published in two sections: Section A "Physics and Chemistry" and Section B "Mathematical Sciences."

DIMENSIONS/NBS (formerly Technical News Bulletin)—This monthly magazine is published to inform scientists, engineers, businessmen, industry, teachers, students, and consumers of the latest advances in science and technology, with primary emphasis on the work at NBS. The magazine highlights and reviews such issues as energy research, fire protection, building technology, metric conversion, pollution abatement, health and safety, and consumer product performance. In addition, it reports the results of Bureau programs in measurement standards and techniques, properties of matter and materials, engineering standards and services, instrumentation, and automatic data processing.

Annual subscription: Domestic, $12.50; Foreign $15.65.

NONPERIODICALS

Monographs—Major contributions to the technical literature on various subjects related to the Bureau's scientific and technical activities.

Handbooks—Recommended codes of engineering and industrial practice (including safety codes) developed in cooperation with interested industries, professional organizations, and regulatory bodies.

Special Publications—Include proceedings of conferences sponsored by NBS, NBS annual reports, and other special publications appropriate to this grouping such as wall charts, pocket cards, and bibliographies.

Applied Mathematics Series—Mathematical tables, manuals, and studies of special interest to physicists, engineers, chemists, biologists, mathematicians, computer programmers, and others engaged in scientific and technical work.

National Standard Reference Data Series—Provides quantitative data on the physical and chemical properties of materials, compiled from the world's literature and critically evaluated. Developed under a world-wide program coordinated by NBS. Program under authority of National Standard Data Act (Public Law 90-396).

NOTE: At present the principal publication outlet for these data is the Journal of Physical and Chemical Reference Data (JPCRD) published quarterly for NBS by the American Chemical Society (ACS) and the American Institute of Physics (AIP). Subscriptions, reprints, and supplements available from ACS, 1155 Sixteenth St. N.W., Wash., D.C. 20056.

Building Science Series—Disseminates technical information developed at the Bureau on building materials, components, systems, and whole structures. The series presents research results, test methods, and performance criteria related to the structural and environmental functions and the durability and safety characteristics of building elements and systems.

Technical Notes—Studies or reports which are complete in themselves but restrictive in their treatment of a subject. Analogous to monographs but not so comprehensive in scope or definitive in treatment of the subject area. Often serve as a vehicle for final reports of work performed at NBS under the sponsorship of other government agencies.

Voluntary Product Standards—Developed under procedures published by the Department of Commerce in Part 10, Title 15, of the Code of Federal Regulations. The purpose of the standards is to establish nationally recognized requirements for products, and to provide all concerned interests with a basis for common understanding of the characteristics of the products. NBS administers this program as a supplement to the activities of the private sector standardizing organizations.

Consumer Information Series—Practical information, based on NBS research and experience, covering areas of interest to the consumer. Easily understandable language and illustrations provide useful background knowledge for shopping in today's technological marketplace.

Order **above** *NBS publications from: Superintendent of Documents, Government Printing Office, Washington, D.C. 20402.*

Order **following** *NBS publications—NBSIR's and FIPS from the National Technical Information Services, Springfield, Va. 22161.*

Federal Information Processing Standards Publications (FIPS PUB)—Publications in this series collectively constitute the Federal Information Processing Standards Register. Register serves as the official source of information in the Federal Government regarding standards issued by NBS pursuant to the Federal Property and Administrative Services Act of 1949 as amended, Public Law 89-306 (79 Stat. 1127), and as implemented by Executive Order 11717 (38 FR 12315, dated May 11, 1973) and Part 6 of Title 15 CFR (Code of Federal Regulations).

NBS Interagency Reports (NBSIR)—A special series of interim or final reports on work performed by NBS for outside sponsors (both government and non-government). In general, initial distribution is handled by the sponsor; public distribution is by the National Technical Information Services (Springfield, Va. 22161) in paper copy or microfiche form.

BIBLIOGRAPHIC SUBSCRIPTION SERVICES

The following current-awareness and literature-survey bibliographies are issued periodically by the Bureau:

Cryogenic Data Center Current Awareness Service. A literature survey issued biweekly. Annual subscription: Domestic, $25.00; Foreign, $30.00.

Liquified Natural Gas. A literature survey issued quarterly. Annual subscription: $20.00.

Superconducting Devices and Materials. A literature survey issued quarterly. Annual subscription: $30.00. Send subscription orders and remittances for the preceding bibliographic services to National Bureau of Standards, Cryogenic Data Center (275.02) Boulder, Colorado 80302.

U.S. DEPARTMENT OF COMMERCE
National Bureau of Standards
Washington, D.C. 20234

OFFICIAL BUSINESS

Penalty for Private Use, $300

POSTAGE AND FEES PAID
U.S. DEPARTMENT OF COMMERCE
COM-215

U.S.MAIL

SPECIAL FOURTH-CLASS RATE
BOOK